Heat Transport in Structured Catalytic Reactors for Gas-Phase Reactions

Vom Fachbereich Produktionstechnik
der
UNIVERSITÄT BREMEN

zur Erlangung des Grades
Doktor-Ingenieur
genehmigte

Dissertation
von
M.Sc. Christoph Sinn

Gutachter:
Prof. Dr.-Ing. Jorg Thöming
Prof. Dr.-Ing. habil. Udo Fritsching

Tag der mündlichen Prüfung: 20.07.2021

Zusammenfassung

Es ist seit langem bekannt, dass das Management des Wärmetransports ein entscheidender Faktor für die Leistungsfähigkeit katalytischer Reaktoren ist. Diese werden beispielweise für stark exo- und endotherme Gasphasenreaktionen eingesetzt. Offenzellige feste Schäume (oder auch Schwämme) kombinieren einen geringen Druckabfall mit bemerkenswerten Wärmetransporteigenschaften und bieten damit eine Kombination, die sie zu einer äußerst attraktiven Option als monolithische Katalysatorträger macht. Für kleinvolumige dynamisch betriebene Reaktoren (zum Beispiel für die Methanisierung von CO_2) haben offenzellige Schäume gegenüber herkömmlichen Pelletkatalysatoren vorteilhafte Wärmetransporteigenschaften gezeigt. Dies gilt solange die Wärme hauptsächlich radial über Konduktion abgeführt wird. Um effiziente und sichere strukturierte Schwammreaktoren zu entwerfen und außerdem zuverlässige technische Modelle zu entwickeln, ist ein gründliches Verständnis der drei Wärmetransportmechanismen, Konduktion, Konvektion und Wärmestrahlung, erforderlich. Das gekoppelte thermische Verhalten von Schäumen und Gasen während der Wärmeerzeugung, z.B. durch exotherme chemische Reaktionen, wurde trotz ihres Potenzials zur Optimierung der Temperaturregelung in Festbettreaktoren immer noch nicht gründlich beschrieben. Ziel dieser Arbeit ist es daher, einen tieferen Einblick in die gekoppelte konjugierte Wärmeübertragung und Wärmeerzeugung in offenzelligen Schäumen zu erhalten, welche in Rohrreaktoren (d.h. strukturierten Schaumreaktoren) verwendet werden.
Mithilfe von 3D Strömungssimulationen (engl.: computational fluid dynamics, CFD) im Porenmaßstab können Wärmeflüsse und Temperaturen von Gasen und Feststoffen gründlich untersucht werden. CFD Simulationen vollständig aufgelöster chemischer Reaktionen sind rechenintensiv und erfordern außerdem viele detaillierte Kenntnisse über die Reaktionskinetik. Darüber hinaus existieren nur wenige CFD Studien zu reaktiven Schäumen, welche sich meist nicht explizit mit dem Wärmetransport befassen. Um die Reaktionswärme während einer exothermen chemischen Reaktion abzubilden und um den Rechenaufwand zu reduzieren, werden volumetrische Wärmequellen homogen in den festen Schaum implementiert. Die Vereinfachung der Wärmequelle ermöglicht es, die Auswirkung der Wärmeerzeugung im Reaktor auf die Wärmeübertragung zu untersuchen. Auf diese Weise kann der Wärmetransport von der chemischen Reaktion isoliert untersucht werden.
Zunächst wird ein konjugiertes Wärmeübertragungsmodell vorgestellt, das auf einem durch Luft durchflossenen Schwamm basiert. Die Geometrieinformation des Modells stammt aus Röntgenscans. Das Simulationsmodell wird gegen Druckabfall- und Wärmeübertragungskoeffizienten aus der Literatur verifiziert bzw. validiert. Der Einfluss der Intensitäten der Wärmequellen auf Wärmeflüsse und Temperaturfelder fester und fluider Phasen wird untersucht. Die ersten Ergebnisse präsentieren das Konzept, Wärmequellen zur Untersuchung von Schaumreaktoren zu verwenden und analysieren das thermische Verhalten der Wärmequellen. Um die Vereinfachung der Wärmequelle mit einer tatsächlichen exothermen Reaktion zu vergleichen, wird die CO Oxidation als Modellreaktion implementiert. Das reaktive Modell kann Literaturdaten reproduzieren. Der Vergleich zwischen Wärmequellen und der Reaktion zeigt eine hohe Übereinstimmung für integrale Wärmeströme und mittlere Temperaturerhöhungen. Genaue Hot-Spot-Positionen und lokale Temperaturgradienten können jedoch nicht aufgelöst werden. Der erste Teil dieser Arbeit sowie der größte Teil der Literatur führen CFD basierte Wärmetransportanalysen von Schäumen hauptsächlich für Luft bei 1 bar Ausgangsdruck durch und vernachlässigen zusätzlich die Gravitationsbeschleunigung. Diese Bedingungen können während

tatsächlicher Reaktionen stark abweichen. Um reale Bedingungen besser abbilden zu können wird der Wärmequellenansatz deshalb auf einen erhöhten Druckbereich (1-10 bar), um andere Gasarten (z.B. Methan), um den Einfluss von Schwerkraft und erhöhte Geschwindigkeiten (einschließlich Turbulenzmodellierung) erweitert. Anschließend wird der Wärmequellenansatz angewendet, um den Einfluss von Wärmestrahlung auf den Wärmetransport in Schaumreaktoren für verschiedene Leerrohrgeschwindigkeiten, Wärmeleitfähigkeiten, Feststoffemissionsgrade und Temperaturniveaus zu untersuchen und zu quantifizieren. Die untersuchten Temperaturniveaus entsprechen dabei einer Reihe exothermer Reaktionen. Zuletzt werden fünf verschiedene periodische offenzellige Strukturen verwendet, um eine Analyse des Struktureinflusses auf den Wärmetransport durchzuführen. Die Verwendung von Wärmequellen in mehr als 100 Simulationen ergibt, dass die Feststoff Wärmeleitfähigkeit und der Stegdurchmesser die dominierenden Parameter sind, die die radiale Wärmeabfuhr in Schäumen bestimmen.
Die Ergebnisse dieser Arbeit quantifizieren dominante Wärmetransportmechanismen in Schaumreaktoren, etablieren Wärmequellen als Instrument zur Untersuchung des Wärmetransports in strukturierten Reaktoren und geben Designrichtlinien für die Auslegung von Reaktoren und deren Katalysatorträgern bei hoch exo- oder endothermen Reaktionen.

Abstract

It has been long known, that the management of heat transport is crucial for the overall performance of catalytic reactors. This is especially important for strongly exo- and endothermal gas-phase reactions. Combining low pressure drop and remarkable heat transport properties, open-cell foams offer a combination that make them a highly attractive option as monolithic catalyst carriers. For small-scale dynamically operated reactors (for instance for the methanation of CO_2), open-cell foams have shown advantageous heat transport characteristics over conventional pellet catalyst carriers, as long as produced heat is mainly removed radially via conduction. To design efficient and safe foam reactors as well as to deploy reliable engineering models, a thorough understanding of the three heat transport mechanisms, i.e., conduction, convection, and thermal radiation, is needed. The coupled thermal behavior of foams and fluids during heat production, e.g., during exothermal chemical reactions, is still not thoroughly described despite of the potential of foams to optimize temperature control in fixed-bed reactors. Hence, the aim of this thesis is to get deeper insight into coupled conjugate heat transfer and heat production in open-cell foams used in a tubular reactors (i.e, structured foam reactors).
Using pore-scale 3D computational fluid dynamics (CFD) simulations, heat flows and temperature of fluid and solid phases can be investigated thoroughly. CFD simulations of fully resolved chemical reactions are computational costly and further require detailed knowledge on kinetics. Furthermore, only a few CFD studies on reactive foams exist. None of them deal explicitly with heat transport. In order to mimic the heat of reaction during an exothermal chemical reaction and reduce computational cost, volumetric heat sources are implemented homogeneously in the solid foam. The heat source simplification allows to study the effect of heat production on heat transfer separated from actual chemistry.
A conjugate heat transfer model based on a X-Ray foam scan which is flown through by air is presented, validated, and verified against pressure drop and heat transfer coefficients from literature. Heat source intensities that correspond to exothermal gas-phase reactions are implemented in the solid foam. The impact of these heat source intensities on heat flows and temperature fields of solid and fluid phases is investigated. The first results of this work present the concept of using heat sources to study foam reactors and analyze the thermal behavior of the heat sources. To compare the heat source simplification with an actual exothermal reaction, the CO oxidation is implemented as model reaction with good resemblance of literature data. Integral heat flows and mean temperature increases of the heat source are in very good agreement with the simulated chemical reaction. Exact hot-spot locations and local temperature gradients, however, cannot be resolved using the simplification. The first part of this work and most of the literature mainly investigate foams using air at 1 bar outlet pressure and neglect gravitational acceleration; conditions that might differ severely from actual reactions. Hence, the heat source approach is extended to an increased pressure range (1-10 bar), fluid material (e.g., methane), gravity and elevated velocities (including turbulence modeling). Eventually, the heat sources approach is applied to study and quantify the impact of thermal radiation on heat transport in foam reactors for several superficial velocities, thermal conductivities, solid emissivities, and temperatures levels that correspond to a range of exothermal reactions. Lastly, five different periodic open-cell structures are used to conduct a structure-heat transport analysis. The utilization of heat sources, applied in more than 100 simulations, reveals that the solid thermal conductivity and the strut diameter are the dominant properties determining the radial heat removal in foams.

The results of this work quantify dominant heat transport mechanisms in foam reactors, elaborate heat sources as tool to study heat transport in structured reactors and give design guidelines for ensuring proper heat removal.

Acknowledgements

Meine Dissertation und ganz besonders die schöne lehrreiche Zeit sind vor allem das Ergebnis der Einflüsse vieler Menschen auf mich. Deswegen möchte ich mich bei all denen Bedanken, die mich in dieser Zeit ganz besonders unterstützt haben.
Zunächst geht mein besonderer Dank an Herrn Thöming, der mir die Chance gab, mich an diesem interessanten Thema zu versuchen. Er hat mir außerdem stets die Freiheit gelassen, dass Thema nach meinen Wünschen und Interessen zu untersuchen und die Arbeit zu gestalten.
Vielen Dank möchte ich auch Herrn Fritsching sagen, der spontan die Rolle des Zweitgutachters eingenommen hat und sofort dem Thema interessiert gegenüberstand.
Großer Dank gilt auch Georg Pesch, der als Post-Doc der Reaktionstechnik meine Forschung stets gefördert hat und immer zuverlässig ansprechbar war.
Mein weiterer Dank geht an Lars Kiewidt, der mir mit seinem stets hilfreichen Input sehr geholfen hat, Fuß im Thema zu fassen sowie mein Dissertationsthema zu schärfen.
Ein herzliches Dankeschön möchte ich außerdem an Harm, Jonas und Jasper richten, mit denen ich seit Studienzeiten über alles sprechen kann. Also daher: Danke für unzählige Kafferunden, Diskussionen, therapeutische Rennradfahrten, Partys, Kneipenabende und alles andere.
Vieles des gerade genannten trifft auch auf die AG Thöming zu, die der Hauptgrund ist, dass ich an der Uni geblieben bin. Danke daher auch an alle Kollegen/Freunde der AG Thöming, die ich jetzt hier leider nicht alle erwähnen kann. Stellvertretend möchte ich mich noch bei Michael Baune bedanken, der mit seiner Offenheit Menschen, Projekte und Ideen in die AG integriert.
Außerhalb der AG gilt mein Dank vor allem Jan Ilsemann für unzählige Kaffeerunden und Diskussionen über Katalyse.
Vielen Dank an auch an meine Eltern, Ilse und Peter, die mich immer unterstützt haben und nie Zweifel hatten an dem, was ich tue.
Zuletzt möchte ich mich bei dir bedanken, Caterina. Dafür, dass du trotz der vielen Zeit, die ich in diese Arbeit gesteckt habe, mich stets aufbaust, mich zwingst nicht am Wochenende zu arbeiten und immer zu mir hältst.
Danke!

List of Publications

- Sinn, C.; Pesch, G.R.; Thöming, J.; Kiewidt, L. Coupled conjugate heat transfer and heat production in open-cell ceramic foams investigated using CFD. International Journal of Heat and Mass Transfer, 2019, 139, 600–612.
- Sinn, C.; Kranz, F.; Wentrup, J.; Thöming, J.; Wehinger, G.D.; Pesch, G.R. CFD Simulations of Radiative Heat Transport in Open-Cell Foam Catalytic Reactors. Catalysts, 2020, 10, 716.
- Sinn, C.; Wentrup, J.; Thöming, J.; Pesch, G.R., Influence of Pressure, Velocity and Fluid Material on Heat Transport in Structured Open-Cell Foam Reactors Investigated Using CFD Simulations, ChemEngineering, 2020, 4, 61.
- Sinn, C.; Wentrup, J.; Pesch, G.R.; Thöming, J.; Kiewidt, L. Structure-heat transport analysis of periodic open-cell foams to be used as catalyst carriers, Chemical Engineering Research and Design, 2021, 166, 209–219.
- Sinn, C.; Wentrup, J.; Pesch, G.R.; Thöming, J. Heat Transport in Open-Cell Foams: CFD Analysis of Artificial Heat Sources vs Fully Resolved Exothermal Reactions, Industrial and Engineering Chemistry Research, 2021, 60, 4542–4551.

Contents

Chapter 1

Introduction

1.1 Motivation and Objective

A great quantity of products of our modern society are based on catalytic processes. Common examples are the refinement of crude oil and the general industrial production of base chemicals. Generally, catalytic processes can be distinguished into homogeneous and heterogeneous catalysis. While the catalyst and reactants share the same phase in homogeneous catalysis, they differ in phase in heterogeneous processes. Not only are industrial (catalytic) processes accountable for considerable energy usage but also for major CO_2 emissions. Efficient chemical processes are crucial for the reduction of carbon emissions. An example for a heterogeneous exothermal catalytic reaction is the CO_2 methanation or also called Sabatier process (Rönsch et al., 2016)

$$CO_2 + 4H_2 \leftrightarrows CH_4 + 2H_2O,\ \Delta_R H^0 = -164\,\mathrm{kJ\,mol^{-1}}. \tag{1.1}$$

This reaction currently attracts a lot of attention as it offers the possibility to chemically store electrical energy. In the so-called Power-to-Methane (PtM) concept, the renewable surplus energy (e.g, wind or solar power) is used to generate hydrogen via electrolysis of water. Thereafter, the hydrogen reacts to methane and can be stored in the already available natural gas grid.
In the future, small-scale dynamically operated reactors are needed for the PtM or Power-to-Gas (PtG) processes (Kalz et al., 2017). Usually, active pellets are used for catalytic gas-phase reactions. The thermal management during catalytic reactions is crucial in process control to obtain optimal temperature profiles in terms of yield and to avoid potentially catalyst-harming hot-spot formation (Kiewidt and Thöming, 2015; Gräf, Ladenburger, and Kraushaar-Czarnetzki, 2016 and Chapter 2). Catalyst carriers competing with conventional pellets are cellular and interconnected open-cell foam structures. Their potential for the intensification of strongly exo- and endothermic catalytic reactions is based on their outstanding radial heat transport, high radial mixing, and low pressure loss (Bianchi et al., 2012; Gräf, Rühl, and Kraushaar-Czarnetzki, 2014). For low flow rates, monolithic catalyst carriers such as open-cell foams provide resilient heat transport and can outperform conventional pellets with respect to suppression of hot-spots (Kiewidt and Thöming, 2019b; Busse, Freund, and Schwieger, 2018). Open-cell foam structures provide a remarkable potential for process intensification in, among others, solar receivers, pore burners, and catalytic reactors (Wu and Wang, 2013; Gao et al., 2014; Kiewidt and Thöming, 2019a). Although the use of open-cell foams in highly exothermic reactions, such as the CO_2 methanation in PtG applications, has been reported several times, they are not yet widely used in commercial applications (Kiewidt and

Thöming, 2019b; Montenegro Camacho et al., 2018). Reasons for that are the difficult mounting with proper wall coupling, especially for large multi-tubular fixed-bed reactors, as well as a lack of accurate heat and mass transport models (Reitzmann, Patcas, and Kraushaar-Czarnetzki, 2006; Tronconi, Groppi, and Visconti, 2014). A more thorough understanding of the structure-transport relations is thus, fundamental to the development of structured foam reactors with robust heat transport and parametric stability.

Among other methods, full-field three-dimensional computational fluid dynamics (CFD) simulations of open-cell foams proved to be valuable in getting insight into the three heat transport mechanisms: thermal conduction, convection, and thermal radiation. The simulations can be performed without prior knowledge (i.e., no engineering correlations are needed). Moreover, CFD was successfully applied to study the influence of geometry, material, velocity, and wall coupling on heat transport in foam structures (Zafari et al., 2015; Bianchi et al., 2015; Della Torre et al., 2015; Razza et al., 2016). Nevertheless, CFD studies dealing with full-field exothermal reactions in open-cell foams are scarce. This is due to the high computational cost and modeling effort of full-field catalytic surface reactions in open-cell foams (Della Torre et al., 2016; Wehinger, Heitmann, and Kraume, 2016; Dong et al., 2018). Therefore in this work, it is proposed to mimic the heat production in the solid foam (that is caused by exothermicity) using artificial volumetric heat sources (Chapter 4). This way, thermal effects in the structured reactor can be studied decoupled from chemistry. In order to derive design guidelines for catalyst carriers from this approach, the validity and applicability of this approach needs to be tested. Hence, heat flows and temperature fields of an actual exothermic reaction are compared with artificial heat production in the solid (Chapter 5). This is followed by an extension of the heat transport analysis with an focus on the fluid properties (Chapter 6). Eventually, the artificial heat source approach is used to study the influence of thermal radiation under reaction conditions (Chapter 7) and to conduct a structure-heat transport analysis (Chapter 8). None of these mentioned targeted studies, have been reported yet.

The approach of this work is to use 3D pore-scale CFD simulations to get insight into the heat transport phenomena in structured catalytic reactors. The main methodical challenges can generally be listed as meshing, modeling and validation. First of all, fluid (e.g., air or methane) and solid (i.e., ceramic foam) require to be discretized in a way that energy can be exchanged between the phases. Hence, multi-region meshes are created where nodes of both regions collapse and form conjugate heat transfer interfaces. Furthermore, scans of irregular foams are used as input for the simulation and are quite challenging for the overall mesh generation (see Figure 1.1). Here, the problem is not only to generate an arbitrary multi-region mesh but to generate a mesh that is suitable for resolving surface reactions, turbulence and thermal radiation in order to be able to study the heat transport in structured reactors. Secondly, modeling itself is a challenge throughout this work as the model should have minimal complexity. Therefore, several parameters of fluid and solid regions (e.g., diffusion models, thermal dependent material properties, kinetics) as well as numerical parameters (e.g., solver and solution scheme) are adapted for the targeted parameter range. Lastly, the deployed models are verified and validated against models, correlations and experimental data from literature. Here, intermediate steps of the model are compared against corresponding simulation data or experiments (e.g., pressure drop: Dietrich, 2012; Inayat et al., 2016 ; heat transfer: Meinicke, Wetzel, and Dietrich, 2017; Giani, Groppi, and Tronconi, 2005a; Gancarczyk et al., 2018; concentration profiles: Wehinger, Heitmann, and Kraume, 2016; Dong et al., 2018).

To sum up, the model developed in this thesis is able to compute 3D structured reactors with

- irregular foams from scans (see Figure 1.1) and regular foams designed with software,
- catalytic reactions (micro-kinetics)
- or an artificial heat source in the solid,
- thermal radiation and
- turbulence.

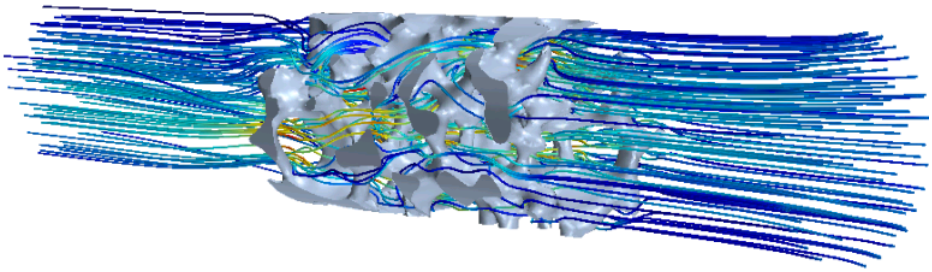

FIGURE 1.1: Streamlines in a structured foam reactor (10 ppi alumina foam). The direction of flow is from left to right.

With the aid of a verified and validated 3D CFD model, the goals of this work are:

1. Understanding heat transport mechanisms and their contributions in structured reactors for process conditions relevant in heterogeneous catalysis (pressure, temperature level, heat of reaction, solid material, superficial velocity, etc.).
2. Establishing and elaborating artificial heat sources as a tool for studying catalyst carriers and improving existing or deriving new models.
3. Deploying design and modeling guidelines for structured catalyst carriers.

This thesis aims to contribute to the understanding and design of open-cell foams to be used as catalyst carriers in gas-phase reactions. Two current knowledge gaps or challenges are addressed here. Firstly, there is a need for simplifying the complex transport phenomena through deriving easy-to-handle engineering correlations (Tronconi, Groppi, and Visconti, 2014) and conduct suitable CFD model reductions (Jurtz, Kraume, and Wehinger, 2019). Secondly, for establishing foams in industrial applications, specifically tailored structures based on application should be implemented instead of the one-size fits all approach used previously (Kapteijn and Moulijn, 2020).

1.2 On the Structure of this Thesis

The system that is investigated in this thesis is a structured tubular reactor (Figure 1.2). Generally, this thesis consists of five published manuscripts as well as additional unpublished results. **Chapter 2: Background and State of Literature** introduces the reader to the general context of this work such as catalysis and chemical

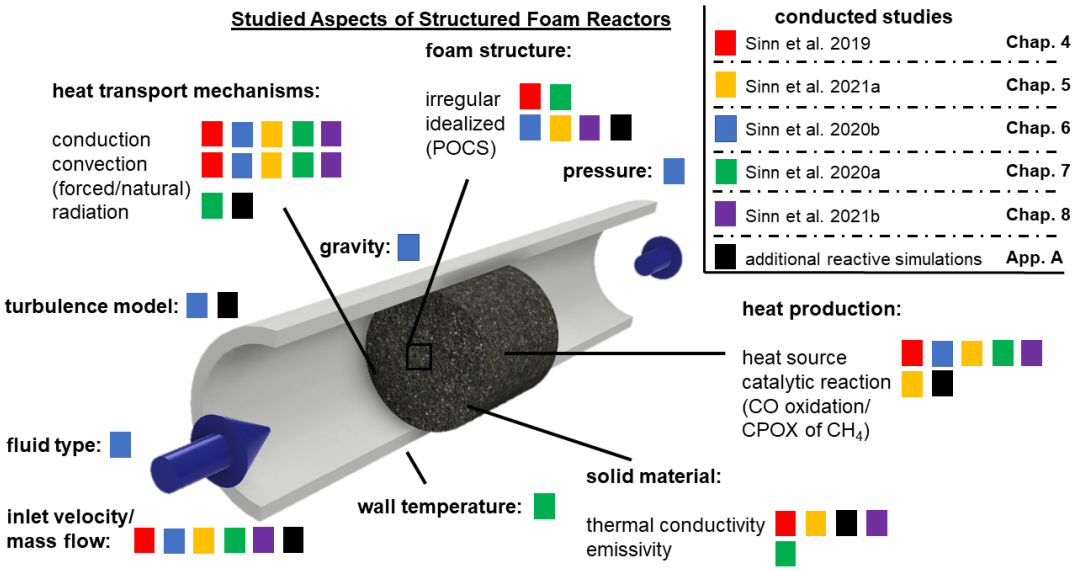

FIGURE 1.2: General structure of the thesis and and investigated properties. The field of investigation of this study is a tubular reactor that contains open-cell foams as catalyst carriers. Investigated properties of the tubular foam reactor system are highlighted in colors corresponding to the individual chapters or manuscripts composing this thesis.

energy storage as concepts for reducing carbon dioxide emissions. The chapter also contains a literature review on (catalytic) open-cell foams with an emphasis on transport phenomena relevant for heterogeneous catalysis. The background is eventually rounded up by the description of the main methods of this thesis (i.e., CFD) and its application in heterogeneous catalysis. Herein again, especially literature regarding open-cell foam reactors and transport phenomena is discussed and presented. In **Chapter 3: Methodology and Description of CFD Reactor Model**, the actual model and its features are presented. The results part consists of three chapters which include several aspects of heat transport in open-cell foam reactors (Figure 1.2). The **Chapter 4: Heat Sources — Concept and Thermal Behavior** introduces, verifies and validates the conjugate heat transfer model of a structured reactor. It essentially describes what happens thermally in foam reactors with heat production in the solid. The investigation is followed by the comparison of the heat source approach against an actual exothermal reaction (model reaction: CO oxidation). These aspects are covered in **Chapter 5: Validity of Heat Sources**. The next step is to extend the investigated parameter range by pressure, velocity (and turbulence), fluid material and the influence of gravity to check which effects need to be accounted for. This is conducted in **Chapter 6: Heat Sources — Influence of the Fluid Properties**. The heat source approach in the verified and validated model is then applied to quantify the impact of radiation on the overall heat transport. This investigation is done in **Chapter 7: Application of Heat Sources I — Thermal Radiation**. The last investigation in **Chapter 8: Application of Heat Sources II — Structure-Heat Transport Analysis** demonstrates the benefit of the simplification by relating structural foam parameters with heat-transport behavior of foams. Even though all manuscripts contain own conclusions and outlook chapters, there is an overall conclusion at the end of the document in **Chapter 9: Conclusion and Outlook**.

Chapter 2

Background and State of Literature

2.1 Sustainability, Power-to-Gas and Heterogeneous Catalysis

2.1.1 Climate Crisis and the Role of the Chemical Industry

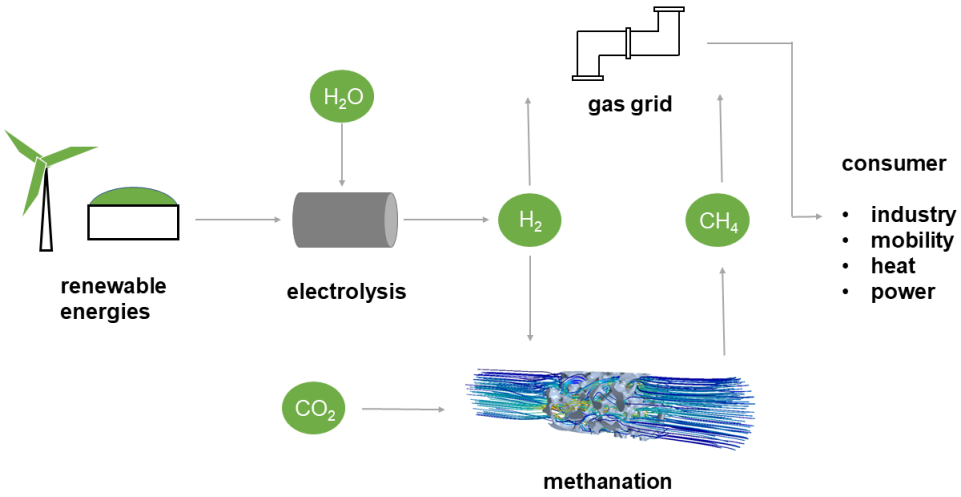

FIGURE 2.1: The power-to-methane (PtM) concept including the strongly exothermal methanation reaction.

The climate on our planet has changed drastically due to anthropogenic emissions of greenhouse gases such as carbon dioxide or methane. The majority of these emissions are based on the combustion of fossil energies supply such as oil or coal (Jackson et al., 2017). As the world population continues to grow and developing countries increase their living standard, a decline in energy demand cannot be expected (Semieniuk et al., 2021). In order to reduce global warming, more renewable energies are needed in the future. For instance, this can be achieved through expanding plants of windmills or photovoltaics. Unfortunately, the renewable energies with the highest potential (photovoltaic and windmills) highly fluctuate due to natural changes in wind and sunlight (e.g., day and night or clouds). Moreover, the majority of energy that we use is not electrical but thermal or chemical. Only by using so-called sector coupling, renewable energies can be optimally used and integrated. This is especially important as the power supply and demand need to be balanced on different time scales (minutes, hours and days) (Zhang et al., 2017). In

order to buffer fluctuations and achieve sector coupling (i.e., transformation of electrical renewable energy into other energy carriers), energy needs to be stored. Here, chemical energy storage can be a key technology for transforming the current, still fossil-based energy sector to a fully sustainable and renewable one (Robinius et al., 2017).
The field of chemical engineering can contribute to the development of chemical energy storage in two ways which are either process intensification of existing processes, or the development of new innovative reaction systems. A chemical reaction potentially important for chemical energy storage is the Sabatier reaction (Equation 1.1) which is part of the so called Power-to-Methane (or Power-to-Gas) concept (see Figure 2.1). In this concept, excess energy (from renewable sources) is converted into hydrogen via electrolysis of water. In the Sabatier reaction, the hydrogen then reacts with carbon dioxide to methane. This process can be easily implemented into the existing infrastructure by using the natural gas grid (Vogt et al., 2019). From a technical point of view, it is thus considered to be rapidly realizable (Schnuelle et al., 2019). Furthermore, pure hydrogen can also be added to the German natural gas grid in small percentages. However, the currently estimated cost for methane produced from the Sabatier process is significantly higher than using conventional natural gas from fossil sources (Schnuelle et al., 2019). To reduce the cost of sustainable methane, it is thus very important to achieve high reaction yields to be able to deliver directly into the gas grid and save on expensive downstream purification (Rönsch et al., 2016). Another cost factor of renewable methane is the energy demand of the overall reaction process (from supply of CO_2 to usable CH_4) (Schnuelle et al., 2019). Here again, proper heat management of the reactor system is crucial to further reduce the cost of the product and make it competitive.
The CO_2 methanation is only one example for many more strongly catalytic endo- and exothermal reactions that are industrially relevant or might play a role in the context of chemical energy storage. For instance the CO methanation, where CO replaces CO_2 as reactant, is a chemical energy storage process and interesting for CO-emitting industries such as the steal or concrete production industry:

$$CO + H_2 \leftrightarrows CH_4 + H_2O,\ \Delta_R H^0 = -206\,\mathrm{kJ\,mol^{-1}}. \tag{2.1}$$

The reverse reaction —the endothermal methane steam reforming— is responsible for approximately 50 % of the world's produced hydrogen (Iulianelli et al., 2016),

$$CH_4 + H_2O \leftrightarrows CO + 3H_2,\ \Delta_R H^0 = +206\,\mathrm{kJ\,mol^{-1}}. \tag{2.2}$$

Other hydrogen or syngas (CO + H_2) production routes are the catalytic partial oxidation of methane (Schwiedernoch et al., 2003)

$$2CH_4 + O_2 \leftrightarrows 2CO + 4H_2,\ \Delta_R H^0 = -71\,\mathrm{kJ\,mol^{-1}}, \tag{2.3}$$

and the dry reforming of methane (Jang et al., 2019)

$$CO_2 + CH_4 \leftrightarrows 2CO + 2H_2,\ \Delta_R H^0 = +247.3\,\mathrm{kJ\,mol^{-1}}. \tag{2.4}$$

Prominent strongly exothermal reactions are also the methanol synthesis as well as the Fischer-Tropsch synthesis. Those two reactions produce liquid fuels and base chemicals. They consequently might also be a cornerstone in the sustainable transition of the energy sector.

2.1.2 Significance of Temperature and Heat Management

Many relevant heterogeneous gas-phase reactions, such as the CO_2 methanation, are strongly exothermal, which means that heat is released during the product formation. In the following, the significance of heat and temperature management is introduced and explained using the methanation as example.
According to the principle of Le Chatelier and thermodynamic analyses, low temperatures and high pressures are favorable to achieve maximum conversion (Kiewidt and Thöming, 2015; Sahebdelfar and Takht Ravanchi, 2015). In contrast, the rate of methane formation (i.e., the kinetics) significantly increases with temperature. Therefore, the methanation reaction is usually operated around 350 °C as a result of the trade-off between maximum conversion and formation rate. Prospectively, improved catalysts could reduce the required temperature even further. For the CO_2 methanation reaction, usually catalysts (e.g., Ni, Ru or Co) are needed to lower the activation energy and enable the process to take place at conditions around 4 – 10 bar (Rönsch et al., 2016).
The temperature control within the reactor is of utmost importance for the interplay of thermodynamic and kinetic limitations to reach maximum efficiency. Potential harm of the catalyst is also linked to the temperature inside the reactor. At certain temperature levels, active catalyst particles might sinter and lose their active surface area. Which side reactions actually occur, as well as the selectivity of many catalysts also is temperature dependent. For instance, coking (blocking of active catalyst sites) might occur at certain temperatures. Another reason for the importance of temperature management in catalytic reactors is thus the robust and safe (e.g., avoid unwanted toxic side products) operation.
A current state of research for the CO_2 methanation is the dynamic operation which refers to sudden changes in load, working pressure, gas composition or even gas type (Mutschler et al., 2020; Kreitz, Wehinger, and Turek, 2019). Developing and using robust processes for dynamics can lead to a decrease of 8 % of the total invest of a PtM plant (Theurich, Rönsch, and Güttel, 2020). However, the dynamic operation of the reaction can result in undesired or uncontrollable temperature increases. When designed poorly, the continuously produced heat cannot be removed sufficiently. The resulting temperature increase in the reactor might lead to a self-amplifying behavior due to the temperature dependent kinetics and might result in a thermal runaway (Kapteijn and Moulijn, 2020).
In order to achieve a proper heat removal during the CO_2 methanation reaction (or other gas-phase reactions), competing strategies exits. This work deals with structured catalyst carriers (open-cell foams) which are presented in more detail in the next chapters. In order to optimize heat removal, Pfeiffer and colleagues utilized several micro channels (i.e., micro reactors) with a high surface to volume ratio of the channels (Belimov, Metzger, and Pfeifer, 2017). Another concept is the utilization of slurry-bubble reactors where the presence of a fluid phase facilitates heat removal (Lefebvre et al., 2015). Furthermore, researchers are researching for more sophisticated catalysts, that work sufficiently well even under 300 °C and enable other reactor concepts (Sahebdelfar and Takht Ravanchi, 2015).
To sum up, heat and temperature control for strongly exo- and endothermal gas-phase reactions is crucial to:

1. increasing the yield,
2. increasing the selectivity,
3. ensuring safety,

4. ensuring catalyst protection, as well as
5. a robust and flexible reactor operation.

Hence, by tailoring temperature profiles inside the chemical reactors, the overall technical reaction process can be optimized.

2.2 Open-Cell Foams and Structured Reactors

Structured reactors are currently widely discussed in the context of designing efficient, heat transport managing reactors for strongly exo- or endothermal reactions (Kapteijn and Moulijn, 2020; Wan et al., 2021). In this chapter, structured reactors and especially open-cell foams are introduced. It is then explained how pressure drop, heat and mass transport can be described and expressed through easy-to-handle engineering correlations. The advantages and disadvantages of foam reactors compared to conventional pellet fixed-bed reactors are also discussed. Finally, studies that apply structured foam reactors on gas-phase reactions are reviewed. This chapter should guide the reader into the key topic of this thesis, that being the heat transport in foam reactors. It is also analyzed, why there is a need to overcome the one-size fits all solution for foams as catalyst carriers.

2.2.1 Introduction to Open-Cell Foams and Structured Reactors

Open-cell foams can be described as interconnected cellular (i.e., porous) materials with voids that allow for fluid flow. Their characteristics are low pressure drop, high surface areas, and excellent radial heat transport which makes them promising catalyst carriers (Reitzmann, Patcas, and Kraushaar-Czarnetzki, 2006). Their counterpart, closed-cell foams, are obviously of minor interest for the chemical engineering community as they prevent fluid flow and are more suitable for usage as insulation material (neoprene is a common example). Open-cell foams inserted in tubes or ducts are called structured foam reactors. In general, structured reactors can also refer to other structured catalyst carriers such as honeycombs (Groppi et al., 2012), wire meshes (Sheng et al., 2011), or even to a structured catalyst material (Schwieger et al., 2016). In this thesis, however, structured reactor or structured foam reactor always corresponds to open-cell foams to be used as catalyst carriers (i.e., in the macro scale). Open-cell foams are not only interesting for chemical engineers in the context of catalyst carriers, but for many more engineering disciplines. Originally designed for filtering molten metals (Taslicukur, Balaban, and Kuskonmaz, 2007), their characteristics are also desirable when used as heat exchangers (Sommers et al., 2010), cooling devices for lithium ion batteries (Saw et al., 2017), solar receivers (Chen et al., 2015; Mey-Cloutier et al., 2016), sound barriers and weapon silencers (Wan et al., 2021), and filter base for dielectrophoresis (Lorenz et al., 2020). Obviously, many more applications are also likely. Consequently, the findings of this thesis are not limited to the field of catalysis and chemical reaction engineering but might apply to other fields of research, too. However, the emphasis of this thesis is undoubtedly on foams to be used as catalyst carriers. Therefore, the application of foams in catalysis is reviewed in much more detail later in this chapter.

2.2.2 Geometrical Properties and Fabrication

Open-cell foams occur in all kinds of forms and materials ranging from metals such as aluminum or copper over ceramics to carbon and glass (Reitzmann, Patcas, and

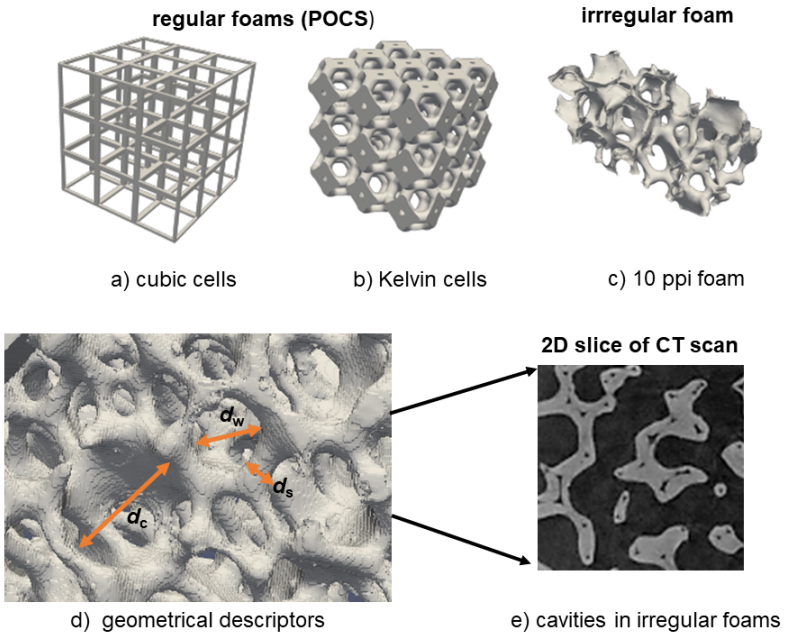

FIGURE 2.2: Geometrical foam characteristics. a) - c) Two major types of foams: irregular and regular; d) principal geometrical descriptors: strut diameter (d_s), window diameter (d_w), cell diameter (d_c); e) 2D scan of foam for elucidating cavities.

Kraushaar-Czarnetzki, 2006; Gancarczyk et al., 2018; Meinicke et al., 2017). The easiest way to classify open-cell foams is to distinguish between regular (Figure 2.2 a) and b)) and irregular foams (Figure 2.2 c)). Regular foams usually consist of some sort of unit cells (or even different, combined cells) that are repeated in the three spatial directions to form a perfectly ordered foam lattice. An other frequent name for regular foams is periodic open-cell structures (POCS). Very common shapes of cells in the literature are, among others, cubic cells (Figure 2.2 a), Kelvin cells (Figure 2.2 b) and diamond cells (see for instance Horneber, Rauh, and Delgado, 2014). In principle, many more cells are imaginable leading to a huge design space for adapting to specific process requirements.

Generally, the five geometrical descriptors window diameter d_w, cell diameter d_c, strut diameter d_s, specific surface area S_v, and the open porosity ε_o are used to describe and compare regular and irregular foams (Reitzmann, Patcas, and Kraushaar-Czarnetzki, 2006). The open porosity is widely used, although for irregular foams total and hydrodynamic porosities ε_t exist as well. This anomaly is based on the fabrication process. Irregular ceramic foams can be produced through replica processes, where a polyurethane (PU) foam template is coated (for instance with metal or ceramic powder slurries). During sintering, the pyrolyzed PU evaporates and leaves cavities (see Figure 2.2 e)). Hence, the total porosity ε_t of irregular foams with cavities usually differs about 5 % from the open porosity (Dietrich, 2012).

For conventional irregular foams, the geometrical properties d_w, d_c and d_s are distributions and hence, might vary tremendously for a single foam structure (Inayat et al., 2011). In contrast, characteristic diameters of POCS (and irregular foams that are created through algorithms, e.g., tessellations (Bracconi et al., 2017)) can be described sufficiently with single values rather than distributions.

The geometrical descriptors of foams generally depend on each other. When only some descriptors are known (i.e., d_s and d_c) the other dependent descriptors can be

obtained through correlations. These are available for irregular and regular foams. One example is the correlation from Lucci and colleagues for Kelvin cell lattices (Lucci et al., 2014)

$$\varepsilon_o = 1 - \frac{3\pi}{\sqrt{2}} \left(\frac{d_s}{d_c + d_s} \right)^2 + 7.54 \left(\frac{d_s}{d_c + d_s} \right)^3, \tag{2.5}$$

$$S_v = 10.33 \frac{\sqrt{1-\varepsilon_o}}{d_c + d_s} - 5.8 \frac{1-\varepsilon_o}{d_c + d_s}. \tag{2.6}$$

Open-cell foams are also sometimes characterized by their pore count or ppi number (pores per square inch). This is easy to use as it narrows down the porous morphology of the foam to a single number. However, it is also highly inaccurate. Firstly, often the ppi number is related to the original PU template and thus, might be different for the actual irregular foam. Secondly, combinations with very different values in the other describing parameters can lead to the same ppi number (Kiewidt, 2017). This is the case for both, regular and irregular foams. Therefore, the ppi number cannot be used to reliably relate to a certain foam morphology.
The strut shapes are another degree of design freedom. These can be, for instance, triangular or circular (Inayat et al., 2011). Regular foams (or POCS) can easily be designed in computers. Due to the significant advances and increased availability of additive manufacturing technologies, they can nowadays be produced in all kinds of shapes and materials (Li et al., 2018; Parra-Cabrera et al., 2018; Zhou and Liu, 2017). This way, foams optimized for their usage in terms of geometry and material will become more and more common. To sum up, foams can have a regular or irregular structure. Irregular foams have been used in the past frequently, but due to the rise of CAD and additive manufacturing tailored regular foams are becoming increasingly popular.

2.2.3 Modeling Pressure Loss Along Foams

Knowing the integral pressure drop caused by open-cell foams (regular and irregular) is crucial as it adds significantly to operating costs of the actual process. Moreover, the integral pressure drop is easy to measure and thus a comparable quantity which has been subject to multiple studies, both experimental (Dietrich et al., 2009; Lacroix et al., 2007) and simulative (Regulski et al., 2015; Bai and Chung, 2011; Skibinski et al., 2015).
Generally, the pressure drop of porous media Δp per length ΔL can be expressed through the well-known Darcy-Forchheimer equation (Edouard et al., 2008)

$$\frac{\Delta p}{\Delta L} = \frac{\mu_f}{k_1} \cdot v + \frac{\rho_f}{k_2} \cdot v^2, \tag{2.7}$$

with μ_f denoting the dynamic viscosity of the fluid, v denoting the superficial velocity, ρ_f denoting the density of the fluid, k_1 denoting the permeability coefficient and k_2 denoting the Forchheimer coefficient. Usually, k_1 and k_2 depend on structural characteristics of the porous media and are therefore fitted to experimental data. For fixed beds, a well-known adaption is the so-called Ergun equation

$$k_1 = 150 \cdot \frac{(1-\varepsilon_h)^2}{\varepsilon_h^3} \cdot \frac{1}{d_p^2}, \; k_2 = 1.75 \cdot \frac{(1-\varepsilon_h)}{\varepsilon_h^3} \cdot \frac{1}{d_p}, \tag{2.8}$$

where ε_h is the porosity of the bed and d_p the particle diameter of the bed. It was shown that a direct application of the Ergun equation (i.e., inserting the cell diameter d_c for d_p as well as the open porosity of the foam) to foams deviated from

experiments by 50 % (Innocentini et al., 1999). They concluded that a direct utilization of the Ergun equation is not rational. Other researchers fitted the Ergun equation to fluid flow data of foams (Dietrich et al., 2009; Lacroix et al., 2007; Moreira, Innocentini, and Coury, 2004; Woudberg and Du Plessis, 2016). These specific adjustments seem not capable to sufficiently describe pressure drop behavior of foams over a wide range of geometrical properties. In 2012, Dietrich could reproduce 2500 data points from literature within ± 40 % accuracy (Dietrich, 2012). The Darcy-Forchheimer equation was specifically fitted to open-cell foams with reported deviations from literature below 8 % (Kumar and Topin, 2017). A correlation that is completely based on theoretical grounds (i.e., no fitting) was proposed in the literature (Inayat et al., 2016):

$$k_1 = \frac{\varepsilon_o \cdot d_h^2}{32 \cdot \tau_{foam}^2}\,,\; k_2 = \frac{2 \cdot \varepsilon_o^2 \cdot d_h}{\tau_{foam}^3}\,,\; \tau_{foam} = 1 + \frac{S_V d_w}{4\varepsilon_o}, \tag{2.9}$$

with d_h being the hydraulic diameter and τ_{foam} being the tortuosity of the foam. With a reported error of max. 10 %, this correlation is currently the most accurate.

2.2.4 Modeling Heat Transport

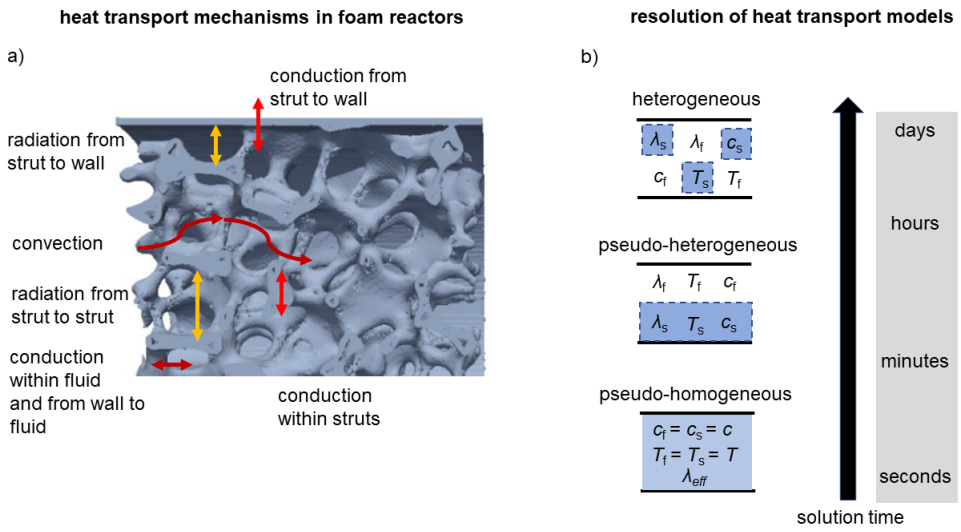

FIGURE 2.3: Heat transport in open-cell foams. a) Possible heat transport mechanisms for open-cell foam reactors (adapted from Wehinger, 2016); b) resolution of heat transport models (adapted from Kiewidt, 2017).

During strongly exo- or endothermal gas-phase reactions, several heat transport phenomena might occur within structured foam reactors (see Figure 2.3 a)). To begin with, heat is produced (or consumed) at the catalytic active surface. The thermal energy can then be transported via thermal conduction through the solid matrix. It could also be emitted from the hot solid surface and eventually be absorbed by either another part of the solid or even the fluid. Furthermore, thermal energy can be transferred between solid foam and the fluid in the voids via convection. Hence, all three main heat transport mechanisms potentially contribute to the overall heat transport in foams and thus foam reactors.
To describe or model the heat transport in structured reactors, different approaches

exist. They differ in terms of accuracy and resolution and consequently, required solution time (see Figure 2.3 b)). The models that can be solved the fastest are the so-called pseudo-homogeneous approaches. These approaches do not distinguish between solid and fluid phases. Instead, the foam and fluid are treated as one with an effective transport property, which is the so-called effective (or two-phase) thermal conductivity $\lambda^{(\mathrm{eff})}$. The main advantage is the reduction of computational cost while still delivering an acceptable level of accuracy. The effective thermal conductivity exists in axial $\lambda_{\mathrm{ax}}^{(\mathrm{eff})}$ and radial direction $\lambda_{\mathrm{r}}^{(\mathrm{eff})}$. Axial and radial transport properties again consist of a stagnant and a dispersive (i.e., flow depending) contribution

$$\lambda_{\mathrm{ax}}^{(\mathrm{eff})} = \lambda_{\mathrm{stg}}^{(\mathrm{eff})} + \lambda_{\mathrm{disp,ax}}^{(\mathrm{eff})}, \tag{2.10}$$

$$\lambda_{\mathrm{r}}^{(\mathrm{eff})} = \lambda_{\mathrm{stg}}^{(\mathrm{eff})} + \lambda_{\mathrm{disp,r}}^{(\mathrm{eff})}. \tag{2.11}$$

The stagnant part of the effective thermal conductivity consists of a conductive part $\lambda_{\mathrm{cond}}^{(\mathrm{eff})}$ and a radiative part $\lambda_{\mathrm{rad}}^{(\mathrm{eff})}$,

$$\lambda_{\mathrm{stg}}^{(\mathrm{eff})} = \lambda_{\mathrm{cond}}^{(\mathrm{eff})} + \lambda_{\mathrm{rad}}^{(\mathrm{eff})}. \tag{2.12}$$

Pseudo-homogeneous models are usually derived from experiments or models and simulations that have a higher level of resolution (Kiewidt, 2017) and are therefore only valid in a certain parameter range of foam morphologies and operating conditions (e.g., pressure and temperature level). The models thus might make errors in the range of $\pm$ 40 % (Wallenstein, Kind, and Dietrich, 2014; Fischedick, Kind, and Dietrich, 2015; Fischedick, Kind, and Dietrich, 2017; Ranut, 2016).
Another commonly used approach is the pseudo-heterogeneous one. This simplification distinguishes between fluid and solid phases, but does take the detailed solid morphology into account. Pseudo-heterogeneous models resolve heat transfer between the phases and mostly follow the general form of

$$Nu = \mathrm{C_h} \cdot Re^{m} \cdot Pr^{\frac{1}{3}}, \tag{2.13}$$

where the dimensionless numbers (Nu = Nusselt, Re = Reynolds and Pr = Prandtl) can be expressed as

$$Nu = \frac{\alpha \cdot d_{\mathrm{char}}}{\lambda_{\mathrm{f}}},\ Re = \frac{\rho_{\mathrm{f}} \cdot v \cdot d_{\mathrm{char}}}{\mu_{\mathrm{f}}},\ Pr = \frac{\mu_{\mathrm{f}} \cdot c_{\mathrm{p,f}}}{\lambda_{\mathrm{f}}}. \tag{2.14}$$

Here, α is the heat transfer coefficient, d_{char} the characteristic diameter, λ_{f} the thermal conductivity of the fluid, ρ_{f} the density of the fluid, v the superficial velocity, μ_{f} the dynamic viscosity of the fluid and $c_{\mathrm{p,f}}$ the isobaric heat capacity of the fluid. Several correlations for Nu are available in literature and are based on simulations (Zafari et al., 2015; Das, Deen, and Kuipers, 2016) and experiments (Giani, Groppi, and Tronconi, 2005a; Bastos Rebelo et al., 2018)). Dietrich deployed a Nu correlation and used the data of irregular foams with all kinds of geometries and ceramic materials and reported an maximum error of 40 % between experimental and correlated data (Dietrich, 2013). Currently, the most accurate correlation is one reported by Gancarczyk and colleagues with a stated error of 25 % (Gancarczyk et al., 2018). The basis of their correlation are own experiments with highly conducting materials (ceramics and metals) as well as a literature data

$$Nu = Pr^{\frac{1}{3}} \cdot 0.4038[21.33Re\frac{D_{\mathrm{ganc}}}{l_{\mathrm{ganc}}}(1 + \frac{0.045D_{\mathrm{ganc}}Re}{l_{\mathrm{ganc}}})^{0.5}]^{\frac{1}{3}}. \tag{2.15}$$

In this equation, D_{ganc} and l_{ganc} are characteristic diameters.
The several pseudo-homogeneous and pseudo-heterogeneous heat-transport models can be used to rapidly calculate heat-transport related properties and thus accelerate reactor model simulations (see for instance Gräf, Ladenburger, and Kraushaar-Czarnetzki, 2016; Kiewidt and Thöming, 2019a). However, many of these engineering correlations still lack accuracy for several foam parameters and shapes. Thermal radiation, for instance, is not yet available in pseudo-heterogeneous foam models. To capture and understand heat transport in foams as well as individual mechanistic contributions, more detailed modeling is needed. Heterogeneous models, which can be solved by CFD simulations, capture detailed foam morphologies and describe both phases separately. The level of accuracy is therefore the highest with obviously the highest needed solution time. Eventually, these detailed heterogeneous models can be used (alongside experiments) to derive improved pseudo-heterogeneous and pseudo-homogeneous models.

2.2.5 Modeling Mass Transport

In contrast to pressure drop, flowing behavior, and heat transport, mass transport in foams was studied significantly less thoroughly (Giani, Groppi, and Tronconi, 2005b; Incera Garrido and Kraushaar-Czarnetzki, 2010; Lucci et al., 2014). The description of mass transport in foam reactors (or foams) can be done analogously to the heat transport. The principal mechanisms (diffusion/conduction and convection) of heat and mass transport are similar (except for radiation). This was also reported by Incera Garrido and co-workers who compared correlations of heat and mass transfer and observed the Chilton-Colburn analogy (Incera Garrido et al., 2008)

$$\frac{Nu}{Pr^{\frac{1}{3}}} = \frac{Sh}{Sc^{\frac{1}{3}}}, \tag{2.16}$$

where the mass transport is characterized through the Schmidt (Sc) and Sherwood numbers (Sh). Hence, the developed correlations follow the form

$$Sh = C_{\text{m}} Re^{\text{M}} Sc^{\frac{1}{3}}, \tag{2.17}$$

with

$$Sh = \frac{\beta d_{\text{char}}}{D},\ Sc = \frac{\mu_{\text{f}}}{\rho_{\text{f}} D}. \tag{2.18}$$

Here, D is the diffusion coefficient and β is the mass transfer coefficient. One of the best correlations reached a maximum deviation of 15 % (Bracconi et al., 2018b). However, the amount of samples and literature data is particularly small, so that more research is surely needed. Concluding, studying and understanding heat transport can potentially bring light into mass transport phenomena.

2.2.6 Foams Compared to Other Catalyst Carriers

In the sections above, it is described that open-cell foams stand out due to their combination of low pressure drop as well as excellent heat and mass transport. With respect to these characteristics, essential relations and correlations are introduced. However, foams to be used as catalyst carriers compete against established systems. Sound and suitable operating ranges of foams in production scale are needed for the transition from research to actual application. Therefore in the following, the performance of catalytic foams is reviewed in comparison with the performance of the

	randomly packed bed	irregular open-cell foam	periodic open-cell foam (POCS)	honeycomb
state	state-of-the-art	development	research	state-of-the-art
			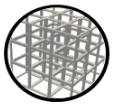	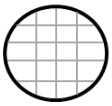
flow pattern	crossmixed	crossmixed	crossmixed	no crossmixing
radial transport				
- **mass**	high	high	high	none
- **heat**	low	high	high	high
pressure drop	high	low	low	low
morphology	irregular	irregular	regular	regular
design freedom	barely	barely	high	barely

FIGURE 2.4: Catalyst carriers suitable for catalytic gas-phase reactions (adapted from Schwieger et al., 2016; Busse, Freund, and Schwieger, 2018). Note that the characteristics only serve as rough overview and are not universal.

main competitors: pellets (or fixed beds) and honeycombs.
In chemical reactors, the active catalyst material can be dispersed on different catalyst carriers (Figure 2.4). Active compounds (for instance active metallic nanoparticles) can be applied on the surface and interact with the support material (Tronconi, Groppi, and Visconti, 2014). This is commonly done for conventional pellet or fixed-bed reactors. In contrast, structured reactors, such as honeycomb or foam reactors, are often washcoated (Twigg and Richardson, 2007). A washcoat contains the active catalytic material (e.g, Ni or Ru for the CO_2 methanation) and a support material (e.g., Al_2O_3 or TiO_2) that enhances the overall catalyst performance (see for instance Stiegler et al., 2019). If washcoats are utilized, the catalyst carrier and the catalyst material itself can be designed and optimized separately. That means, foams enable the decoupling of catalyst activity and macroscopic heat and mass transport. Nevertheless, applying washcoats on foams (i.e., through dipcoating) can produce a lot of waste and might be challenging to be applied with constant thickness over an entire foam. Therefore, Wolf and colleagues recently proposed to activate periodic open-cell foams with a NaOH solution (Raney-copper catalysts) for using in methanol synthesis (Wolf et al., 2020). In contrast, impregnated pellets (i.e., pouring a solution of dissolved catalyst precursors over pellets) are generally more convenient. Furthermore, randomly packed beds are state-of-the art and widely used in the chemical industry. Hence, many more correlations and literature on transport phenomena are available in comparison with open-cell foams. The only frequently used structured reactors are honeycomb reactors. The straight channels allow for easy up-scaling, while still offering sufficient specific surface area (i.e., accessible catalyst material). On top of that, they usually provide the lowest pressure drop (Patcas, Garrido, and Kraushaar-Czarnetzki, 2007; Bracconi et al., 2019). The most common example is their application as automotive catalytic exhaust gas purifiers.
Irregular foams and POCS are currently under development and being researched

thoroughly. In order to be a rational alternative as catalyst carriers, foam reactors have to outperform conventional pellet fixed-bed reactors and structured honeycomb reactors in terms of heat management, pressure drop and chemical conversion for relevant reactions and process conditions.
In 2007, Patcas et al. compared the performance of honeycombs, beads (i.e., pellets) and foams during the strongly exothermal oxidation of CO in terms of pressure drop as well as heat and mass transfer (Patcas, Garrido, and Kraushaar-Czarnetzki, 2007). They investigated two foams, one honeycomb and two sets of beads and found the pressure loss increasing from honeycomb over foam to beads. Additionally, foams were superior over beads and honeycombs in overall reactor performance due to their combination of low pressure drop (advantage over beads) and good radial heat and mass transfer (advantage over pellets and honeycombs). In a different study, the ability of foams to reduce hot spots compared to pellets was shown for the hydrogenation of benzene into cyclohexane (Gräf, Rühl, and Kraushaar-Czarnetzki, 2014). The comparison of foams with each other in terms of temperature increase further demonstrated the great influence of the solid thermal conductivity on the heat removal. Again, this was only tested for two materials, three specific irregular foam samples, and one set of pellets. An increased methane selectivity was also reported for foams over pellets during the CO_2 methanation (Ho et al., 2020). The reason was rooted in the increased radial heat transfer of the foams compared to the pellets which lowered the overall temperature level.
Kiewidt and Thöming developed a multi-scale 2D pseudo-homogeneous foam reactor model (Kiewidt and Thöming, 2019a) and conducted a pareto optimization of the foam parameters with the target values high space-time yield, low pressure drop and low temperature increase. This was done also for the CO_2 methanation reaction as case study (Kiewidt and Thöming, 2019b). They formulated a design trilemma between low pressure drop (high window diameters, high porosity), high catalyst inventory (low window diameter) and high solid thermal conductivity (low porosity) and used a genetic algorithm to define optimal working ranges for foams and pellets. They clearly pointed out that at a certain velocity (i.e, volume flow) foams lose their advantage over pellets and thus foams are only beneficial at low superficial velocities. The reason for this lies in the different heat removal mechanisms. While loosely, randomly packed beds of pellets have a good heat transfer with the fluid, the heat transport through the solid pellets is limited. Thermal conduction between pellets means an additional heat transport resistance between every pellet. Therefore, thermal energy is mainly removed from the reactor axially and radially via convection. In contrast for foam reactors, the continuous solid network enables unhindered heat removal via conduction. As convective heat transport is highly dependent on the amount of transported mass, it becomes obvious that low velocities in the reactor favor the utilization of structured foam reactors. In contrast at elevated velocities, pellets remove heat axially via convection more efficiently than foams due to the increased mixing (Kiewidt, 2017). In 2018, it was also reported that foams have advantageous heat removal over pellets at low velocities (Busse, Freund, and Schwieger, 2018). Here, they focused solely on heat transport (i.e., no reaction) and compared irregular foams, POCS and honeycombs of the same specific surface area. The specific surface area very roughly corresponds to the applied catalyst material for honeycombs and foams. In a different study, three 3D-printed POCS (e.g., Tetrakaidecahedron and Weaire –Phelan) and a 3D-printed irregular foam where compared regarding pressure drop and heat transfer (Rezaei et al., 2020). Here, the POCS showed an increase of 50 % in heat transfer while suffering from a 2-3 times higher pressure loss compared to the

single irregular foam. A completely different approach was taken by Wehinger and co-workers, who used small metal foams (instead of pellets) and arranged them as a packed bed. When comparing conventional pellets with metal foam pellets they found similar heat transfer properties with lower pressure loss for the foam arrangement (Wehinger et al., 2019).
When comparing different catalyst carriers, it is always difficult to decide which geometrical parameters are kept constant (such as porosity or specific surface area). Common foams have porosities between 0.8–0.95, whereas pellet beds often have porosities around 0.4 (Twigg and Richardson, 2007). Thus, all comparisons need to be carefully reviewed since universally usable carriers do not exist or have not yet been described. Hence, optimal working ranges for the catalyst carriers need to be defined which are adapted to their specific field of utilization. The question thus arises, under what conditions are foams a reasonable alternative to honeycombs or pellets? To overcome the limiting catalyst loading of pure foam reactors (i.e., limiting specific surface area), Tronconi and co-workers proposed the utilization of packed foams. Here, the voids of an uncoated foam are filled with catalytic active pellets. This way, the continuous solid strut network can remove heat radially, while the pellet provide high catalyst inventory (Ambrosetti et al., 2020a; Ambrosetti et al., 2020b).
To sum up, honeycombs, foam structures, and pellets all have their advantages and disadvantages. At low flow rates, foams can provide respective conversion while ensuring excellent radial heat transport. The optimal working conditions for these reactors still need to be determined.

2.2.7 Foams Applied in Highly Exo- and Endothermal Reactions

So far, it was pointed out that foam reactors stand out when radial heat removal (or radial heating) is crucial. This is especially relevant for strongly exo- and endothermal gas-phase reactions that are the targeted application of this thesis. Many reactions potentially might benefit from open-cell foams as catalyst supports. In this thesis, however, only a few reactions are named or used as model reactions. Therefore, this section aims to give an overview of the several conducted studies that utilize foams as catalyst carriers to ensure a proper thermal management. Further, it is reviewed which geometrical types of foams and materials are used.
Generally, short contact time reactors (i.e., where the catalyst bed is quite short) are promising for foam applications (Wehinger, Heitmann, and Kraume, 2016). The reason lies in the smaller specific surface area of the foams in comparison with pellets. This way, high conversions are not limited by the limiting surface area. For instance, the catalytic partial oxidation of methane into syngas was performed on an irregular foam and reached high conversion (Horn et al., 2006). Other fast reactions that were experimentally tested in lab scale reactors are the CO oxidation on irregular ceramic foams coated with a Pt catalyst (Dong et al., 2018; Patcas, Garrido, and Kraushaar-Czarnetzki, 2007) as well as aluminum POCS coated with a Pd catalyst (Balzarotti et al., 2021). Further, foams were successfully applied for the methane combustion in lean conditions (Ercolino, Stelmachowski, and Specchia, 2017). The hydrogenation of benzene to cyclohexane was also used as model reaction in order to study the open-cell foam behavior under reacting conditions (Gräf, Ladenburger, and Kraushaar-Czarnetzki, 2016; Gräf, Rühl, and Kraushaar-Czarnetzki, 2014).
Lind et al. investigated the process intensification potential of cubic cell lattices (POCS) for the oxidation of NO in nitric acid plants (Lind et al., 2020). Instead of washcoating, they anodized the aluminum alloy foam for increasing the surface area

followed by Pt deposition. They also found increased heat transfer as well as conversion compared to conventional (pellet) systems.
Santoro et al. applied foams for the dry reforming of methane (Santoro et al., 2020). This reaction is interesting as it valorizes two climate gases (methane and carbon dioxide) into syngas and might find use in biogas plants.
It was also shown that foam reactors are ready to leave lab-scale and are at the edge of entering production scale for the hydrogen production from biogas (Montenegro Camacho et al., 2018). In this study, the efficient use of both POCS and irregular foams also in production/industrial scale was shown. They used SiC (silica carbide) as foam material due to the high solid thermal conductivity and mechanical strength.
Several studies also used irregular foams for the exothermal CO_2 methanation reaction (Kiewidt and Thöming, 2019a; Navarro et al., 2018) and the Fischer-Tropsch synthesis (Egana et al., 2018).
In order to improve the radial heat removal during the methanation, often metals were utilized as foam material (Dou et al., 2019; Danaci et al., 2016). For instance, Frey et al. used Al-based irregular foams and found the same conversion as for powder-based catalyst, but with a much lower temperature increase (Frey et al., 2017). The improved hot-spot control during the CO_2 methanation was also shown for metallic POCS (Danaci et al., 2018; Danaci et al., 2019).
Türks et al. defined structured fixed-bed reactors as deliberately ordering catalyst active material along the fixed beds for controlling temperature increases (Türks et al., 2017). They showed that temperature control can also be obtained using this simple method, which could also give foams another degree of design freedom.
Stiegler et al. designed a fully-integrated dynamically operated foam structured reactor for the methanation. The dynamic volume flow pattern mimicked varying hydrogen supply due to fluctuating renewable energies. The reactor contained printed metal POCS for ensuring proper radial heat removal (Stiegler et al., 2019). During operation, the temperature increase stayed below 15 °C showing that foam reactors can successfully control hot spots under dynamic conditions.
Recently, the concept of foams packed with active pellets (i.e., packed foams) was also applied on the highly exothermal Fischer-Tropsch synthesis for both, irregular packed foams (Fratalocchi et al., 2018) and packed POCS (Fratalocchi et al., 2020). Utilizing highly conductive metals (Cu), they compared the pure foams with packed foams and found stable operation over a wide range of temperatures for packed foams (and POCS) while washcoated foams (no pellets in the voids) where prone to thermal runaways. Furthermore, packed beds where not able to be operated at these conditions, whilst structured reactors enabled robust and safe operation.
The successful application of foam based reactors on the FTS shows that the process intensification potential of foam structured reactors is not limited on gas-phase reactions, since the Fischer-Tropsch synthesis is technically no pure gas-phase reaction (gases, liquids and waxes are produced). The potential of POCS for optimizing multi-phase reactions exemplified for a hydrodesulfurization plant was also discussed in the literature (Von Beyer, 2019).
Not only exothermal gas-phase reactions, but also endothermal reactions were tested using foam structured reactors. Endothermal reactions benefit from efficient heating (rather than cooling by exothermal reactions). The group of Tronconi and co-workers applied packed foams on the strongly endothermal steam reforming reaction and found less emphasized temperature cold-spots (Balzarotti et al., 2020) compared to a conventional packed bed. This underlines the broad possible application for foam-based catalyst carriers.

In conclusion, structured foams were successfully applied in several strongly exo- and endothermal reactions where heat management (or heat removal) is crucial. Most of the recent studies used metal foams (mostly Al or Cu based) due to their high solid thermal conductivities for enabling unhindered radial heat transport.

2.3 CFD in Heterogeneous Catalysis

In this chapter, firstly, the concept of computational fluid dynamics (CFD) in heterogeneous catalysis is introduced. Then, CFD studies regarding pressure drop, heat transport and catalytic reactions are reviewed as they are especially relevant for this thesis. The CFD models that are used in the published manuscripts are described in detail in Chapter 3.

2.3.1 What is CFD? Potentials and Limitations

Engineers and researchers want to get insight into transport phenomena to understand and optimize their processes. Experiments that deliver a high spatial resolution of transport phenomena are often either expensive or just not developed yet. Here, computer simulations in general can help out. Macroscopic transport phenomena in porous catalyst carriers (i.e., foams) are often difficult to study experimentally. For instance, temperature, velocity and concentration information are not easily accessible for optical systems as they are masked by the opacity of the solid media. Computational fluid dynamics are nowadays a well-established tool to tackle problems related to fluid flow in the fields of thermal and chemical engineering. As the computational power has risen tremendously over the last decades, more complex phenomena related to fluid flow can be simulated.
In the CFD methodology, conservation equations are numerically approximated since exact solution of the partial differential equations are hard to achieve or sometimes even not possible (Versteeg and Malasekera, 2007). The approximation (discretization) is done in certain spatial regions, the so-called control volumes (Deutschmann, 2015). The three major discretization methods are finite differences (FD), finite elements (FEM) and finite volume (FVM). FVM and FEM can be used for unstructured grids with an adaption to reactor specifics and are thus suitable for studying open-cell foams (Deutschmann, 2015). Due to the relatively low computational cost, the finite volume method is mostly used in literature for studying catalytic reactors through CFD (Jurtz, Kraume, and Wehinger, 2019; Deutschmann, 2015). The general form of the conservation equations for a quantity ϕ (e.g., enthalpy h) can be expressed as

$$\underbrace{\frac{\partial}{\partial t}(\rho\phi)}_{\text{time accumulation}} = - \underbrace{\nabla \cdot (\rho \vec{u} \phi)}_{\text{convective transport}} + \underbrace{\nabla \cdot (\vec{D} \nabla \phi)}_{\text{diffusive transport}} + \underbrace{S_\phi}_{\text{source terms}} . \tag{2.19}$$

These conservation equations (e.g., for energy) are discretized and solved for a geometry of interest, which are structured foam reactors in this work. The simulations can be carried out without a-priori knowledge, meaning that no engineering correlations are needed (Jurtz, Kraume, and Wehinger, 2019).
In order to solve the conservation equations, the geometry of the foam reactor needs to be divided into small numerically solvable volumes, so-called control volumes. These control volumes eventually form the irregular meshes that are used in this thesis. Generally, the digitally usable foam structure can be obtained through scans

(i.e., image-based, Habisreuther, Djordjevic, and Zarzalis, 2009), algorithms (e.g., tesselation, Nie, Lin, and Tong, 2017; Bracconi et al., 2017) or through computer aided design (CAD, Kopanidis et al., 2010). Irregular foams can be described, for instance, in more detail using image-based procedures such as μCT or MRI scans. In contrast, POCS can be designed easily in computers due to their periodic nature. In this work, image-based as well as CAD-based foam information will be utilized. Theoretically, it is also possible to express the foams with porous media equations (Meinicke, Wetzel, and Dietrich, 2017). In the order of magnitude of the relation from macro pores to tube diameter, these models do not yield accurate results. The detailed arrangement of the macropores determines heat and mass transport and thus needs to be resolved (Wehinger and Kraume, 2017).
CFD simulations are perfectly suited to understand the relationship between geometrical design and macroscopic heat transport phenomena such as thermal conduction, convection and thermal radiation. This is based on their ability to resolve 3D structures such as open-cell foams with a high level of detail and unravel unknown process intensification potential. As stated before, pure heat transport simulations of foam reactors can be done without a-priori knowledge. Here, only heat, mass and momentum conservation are solved. A need for validation or justification is essential for influential model assumptions such as neglecting transport phenomena (e.g, radiation) or assuming constant transport properties (e.g., constant fluid thermal conductivity). This is especially important when the impact of assumptions is not clear. Sweeping studies are a regular tool for checking impact of these assumptions (see for instance Wehinger and Flaischlen, 2019). Furthermore, a frequent problem when comparing CFD simulations with experiments are the unclear boundary conditions in the experiments. For instance, when insufficiently insulated tube reactors are used, the temperature boundary conditions can often only be estimated (see exemplary Dong et al., 2018).
CFD simulations are often used for detailed studies on certain geometries and boundary conditions with a high level of accuracy. In contrast, changing the geometry or even optimizing geometrical parameters automatically is cumbersome and often hard to realize. In a recent study, Daymo et al. coupled a catalytic surface chemistry solver (DuO) with an automated geometry generator of honeycombs and optimized the geometry in a fully-automized workflow (Daymo et al., 2019). This might be an alternative for foam reactor design in the future, too. Another limiting point of CFD models in heterogeneous catalysis is the need for detailed reaction kinetics of each individual catalyst. Kinetic mechanisms are often limited to certain temperature and pressure ranges and are valid for one specific catalyst with its very own characteristics. Getting robust and accurate kinetics for all kinds of catalysts is often difficult or time consuming as well as costly. CFD simulations are hence more suitable to study reactor performances or reactor systems in general. Catalytic insight can also be gathered but should always be interpreted according to the specific catalysts used. In reality catalysts might deactivate due to different mechanisms (e.g., coking or sintering for CO_2 methanation, Rönsch et al., 2016). Up to now, no universal kinetic models capturing all these assumptions are available. The kinetic modeling applied in this thesis is described in more detail in Chapter 3.
To sum up, CFD studies of foam reactors are suitable for investigating detailed transport phenomena. For multiple geometries and detailed catalytic mechanisms, however, they are limited in their application.

2.3.2 CFD Studies on Pressure Drop and Velocity Fields

Several studies exist in the literature that use CFD foam simulations on pressure drop as well as velocity and pressure fields (Bai and Chung, 2011; Habisreuther, Djordjevic, and Zarzalis, 2009). To clarify, multiple studies contain both, pressure drop and heat transport analysis, and can therefore not be clearly classified in either one.
Generally, the easier to model a certain transport phenomena, the more studies exist. For instance, pure single phase hydrodynamic studies require less cells in the discretized domain (i.e., computational mesh) in comparison to models were also the solid domain is discretized (e.g., in conjugate heat transfer cases. See next chapter). Furthermore, modeling single phase pressure drop through foams only requires two conservation equations. At low Mach numbers (*Ma*) and isothermal conditions, the fluid can even be treated as incompressible (Versteeg and Malasekera, 2007).
One of the first numerical studies regarding pressure drop in foams was conducted in 2003 (Boomsma, Poulikakos, and Ventikos, 2003). Computed and experimentally measured pressure drop agreed well in this study.
Later, it was shown that the pressure drop of a regular foam structure (Kelvin cell) was 20% lower than the one of a irregular foam showing that correlations for irregular foams do not necessarily work on POCS (Xu et al., 2008).
Furthermore, the usage of a single unit cell (e.g., a single Kelvin cell) does not provide the same pressure drop as a lattice due to wall effects (Horneber, Rauh, and Delgado, 2012). It is thus, necessary to simulate a certain count of unit cells to capture real reactor behavior.
As stated earlier, the pressure drop of foams can accurately be measured and compared with experiments. In the literature, numerical and experimentally obtained values agree quite well, showing that standard CFD code is very reliable capturing pressure loss (Diani et al., 2014; Regulski et al., 2015) and velocity fields (Meinicke et al., 2017; Sadeghi et al., 2020; Clarke et al., 2020) in porous foam media.
In a different study, higher porosity (i.e., less solid content) was linked to decreasing pressure drop (Zafari et al., 2015). Della Torre and co-workers compared laminar and turbulence models (DNS and steady-state RANS) and thus, the flow regime on pressure drop (Della Torre et al., 2014). For a wide range of Reynolds numbers (i.e., velocities), it was found that the consideration of turbulence models does not affect the pressure drop even in the fully turbulent regime. The authors concluded that at high Reynolds number, foam drag contributes more to the pressure loss than wall-shear stress. Turbulence models are therefore only needed if solver convergence needs to be assisted.
Transient CFD simulations were used with inserted tracer particles for determining dispersion coefficients (Parthasarathy, Habisreuther, and Zarzalis, 2013). In this study, it was further found that the Peclet number of foams approximately equals the one from fixed beds.
It was also studied that an increased surface roughness of a foam significantly influences the friction factor and thus, means more pressure loss (Horneber, Rauh, and Delgado, 2012).
From fluid flow analysis of different POCS (cubic, diamond and Kelvin cells), the same authors analyzed that different cell types favor different reaction types. They suggested that a reactor could contain locally varying cell types adapted to the local occurring reaction process (Horneber, Rauh, and Delgado, 2014).
Recently, Bracconi and co-workers extensively investigated the pressure loss of virtually constructed irregular foams (i.e., through tessellations) both, numerically and

experimentally with printed foams. Using 3D printing and CFD technology, they could close the gap from which many correlations from the last decade often suffered from: structural differences between adopted models and actual foams. Besides proposing an own correlation, they showed that using circular struts over triangular foams reduces the pressure drop. Using rational design, foams can even have lower pressure drop than honeycombs for $Re < 20$ (Bracconi et al., 2019). This again emphasizes that computer aided design of foams will become standard for foams in order to improve the understanding of transport phenomena and enable tailored foam design.

2.3.3 CFD Studies on Heat Transport in Foams

Equivalently to the pressure loss, different aspects of heat transport in foams have been investigated in the literature using both image-based techniques (Iasiello et al., 2020; Du et al., 2019; Fan et al., 2016; Das, Deen, and Kuipers, 2016) and computer aided design (Iasiello et al., 2017; Peng et al., 2017). Regarding heat transport mechanisms in foams, pure thermal conduction (Bracconi et al., 2018a) was studied the most, followed by forced convection (Diani et al., 2015).
Pure conductive studies usually aim to investigate the effective thermal conductivity (i.e., pseudo-homogeneous models (Ranut, 2016; Bracconi et al., 2020; Della Torre et al., 2015)). In these studies, a temperature gradient is usually imposed on one boundary side of the foam and the resulting heat flows or solid temperatures are analyzed (Ranut, Nobile, and Mancini, 2015). Multiple studies found that the effective thermal conductivity (which very roughly corresponds to the heat removal trough the wall) increases with decreasing porosity and with increasing solid thermal conductivity. In other words: more solid foam material and more conductive material improves the heat conduction to the wall (Ranut, 2016).
In heterogeneous catalysis, there are obviously fluids present that participate significantly in the overall heat transport. Hence, solely focusing on conductive heat transport helps to study a foam structure and material in an isolated manner but does not represent the actual reactor behavior. To get a broader picture, multiple researchers also studied single phase fluid heat transfer (Nie, Lin, and Tong, 2017; Ranut, Nobile, and Mancini, 2014; Diani et al., 2015; Zafari et al., 2015) as well as conjugate heat transfer (i.e., solid and fluid phase (Meinicke, Wetzel, and Dietrich, 2017; Kopanidis et al., 2010; Della Torre et al., 2015)). The single phase studies usually assume a constant solid boundary temperature when high conductive metal foams (i.e., Cu or Al) are investigated. When the solid domain is explicitly considered, the influence of the actual material (e.g., ceramic or metal) on the heat transport can be studied in the first place.
As experiments of heat flows and especially detailed temperature measurements are hard to perform or sometimes unavailable, the heat transport models are often validated against macroscopic values such as pressure drop and heat transfer coefficients (Wu et al., 2011).
In their study, Della Torre and colleagues compared three different μCT-based structures in conjugate and single heat transfer simulations (metal: Al, ceramics: SiC and cordierite, Della Torre et al., 2015). They found drastic difference between these real arbitrary structures in terms of conductive and convective heat transport which is difficult to pin down to general structure-transport relations.
In 2014, it was also shown that irregular foams cannot be described using regular foams in terms of convective heat transport. In this study, the Nusselt numbers of irregular and regular foams do not resemble for a range of Reynolds numbers (Iasiello

et al., 2014).
An effort to not only investigate arbitrary foams, but to correlate structural properties of foams with heat transport was done later by Ambrosio et al., 2016. In their study, the authors investigated the effect of the strut shape (convex, concave and triangular) in irregular metal foams on convection and found increased convective heat transfer for convex shaped struts.
In two different studies where pure conduction was simulated (i.e., no fluid present), the strut to node ratio was varied for both POCS (Bianchi, Schwieger, and Freund, 2016) and irregular foams (Bracconi et al., 2018a). The essence of these studies is, that the solid material (i.e, the porosity) needs to be evenly distributed over the reactor to ensure unhindered radial heat removal. This shows, that convex shaped struts (e.g., in irregular foams) are less effective than homogeneously shaped struts. Hence, low-diameter struts may hinder conductive radial heat removal.
Subsequently, Bracconi et al. compared foams with the same porosity and varied the solid material radially and axially (i.e., anistropic). When bigger struts pointed to the wall, they could increase radial heat removal by 40 % (Bracconi et al., 2020). Again, this was only shown so far for pure conduction and thus not under actual reaction conditions.
A very practical foam related issue, is the proper coupling of the monolith with the tube/reactor wall. Freund and co-workers investigated the effect by systematically varying the foam-wall contact area (Bianchi et al., 2013; Bianchi et al., 2015; Razza et al., 2016). They described the great influence of the foam structure on radial heat removal and found that 20 % of the struts need to be in contact with the wall to ensure almost unhindered radial heat removal. In practice, this can be realized by wrapping foams in highly conductive foil (Kiewidt and Thöming, 2019a) or by printing a so-called skin (Fratalocchi et al., 2021). Another practical related foam issue, was investigated by Peng et. al. who showed that the application of a washcoat can increase the heat transfer due to the change of surface morphology (Peng et al., 2017).
In 2014, it was also shown that irregular foams cannot be described using regular foams in terms of convective heat transport, as for instance Nusselt numbers do not necessarily resemble (Iasiello et al., 2014).
To speed up the computational costly simulations, Meinicke et al. proposed a hybrid approach between detailed conjugate pore-scale simulations and a general porous media model for the bigger scope (Meinicke, Wetzel, and Dietrich, 2017; Meinicke et al., 2020). They also showed, that detailed pore-scale simulations (as done in this study) are mandatory to fully capture heat transport mechanisms in foams.
In contrast to conduction and forced convection, the contribution of free convection and especially thermal radiation to the overall heat transport have not been investigated for conditions relevant in heterogeneous catalysis using CFD techniques. Free convection is driven by the gravitational acceleration resulting in temperature caused buoyancy.
First transient CFD studies were also published analyzing the local thermal equilibrium. For the design of catalyst carriers, this might helpful for studying the start-up behavior of dynamic operation (Wu and Wang, 2013; Lu et al., 2020). Wu et. al. for instance found for air in a solar receiver (i.e., ceramic foam) a reaction time to sudden heat flux changes (imposed as fluid/solid boundary) to be between 30 - 70 s (Wu and Wang, 2013).
When scanning the above presented heat transport literature, it appears that most of the studies used air as fluid and 1 bar absolute pressure. However, flexible small-scale plants might be subject to sudden drastic changes in pressure, fluid composition, and velocity as a result of dynamic (i.e., time-dependent) or changing load (i.e.,

multiple steady-states) operation. In this regard, only the effect of changes in superficial velocities on the foam heat transport have been addressed in the literature. Furthermore, heat transport studies in the literature are also limited in their transferability to heterogeneous catalysis due to their temperature boundary conditions. As stated earlier, studies impose thermal energies either through fixed temperatures on the boundaries (e.g., one heated and one cooled wall) or through fixed heat fluxes at the boundaries. This might be an accurate approach for studying heat exchangers. In actual reactions, however, the heat is produced at the fluid/solid interface, enabling different heat flow paths and thus affects the overall heat removal in the reactor differently.
To sum up, several aspects of heat transport in foams have been published. What is missing, are heat transport studies under reacting or close-to-reacting conditions (temperature level, complete reactor geometry, pressure, etc.). There is also a lack of studies about the impact of radiation and free convection and most importantly, thorough studies connecting heat transport mechanisms with structural foam parameters.

2.3.4 CFD Studies on Reactive Foams

In contrast to pressure drop, velocity field and heat transport studies, only a few studies exist dealing with actual catalytic reactions on foams. Most of the reactive foam studies deal with the strongly exothermal CO oxidation, which is a popular model reaction, due to its relatively simple nature (Rickenbach et al., 2015). The fast kinetics of the CO oxidation (e.g., for Pt (Deutschmann et al., 1996)) enable short catalyst beds (i.e., foam lengths) for reaching full conversion. Implementing kinetic behavior in CFD models can roughly be distinguished in three different concepts. The first assumes infinitely fast kinetics of heterogeneous reactions (Lucci et al., 2014; Bracconi et al., 2018b). This concept basically represents a boundary condition where the concentration of the mass-transfer limited reactant is set to zero. It can therefore only be used in the mass-transfer controlled regime and does not apply in the kinetically controlled one. The second kinetic method is the usage of rate determining step approaches (e.g., Langmuir-Hinshelwood kinetics (LH) (Della Torre et al., 2016)). The third and most detailed kinetic approach is the utilization of micro-kinetics (Wehinger, Heitmann, and Kraume, 2016; Dong et al., 2018).
Using infinitely fast kinetics in reactive foam models was mostly done for studying mass transport from gas to solid (Bracconi et al., 2018b; Lucci et al., 2014; Lucci et al., 2015; Lucci et al., 2017; Rickenbach et al., 2015; Aguirre et al., 2020). These studies cover the biggest proportion of reactive foam studies. Among these studies, Bracconi et al. extensively investigated the mass transfer behavior of several foams in a fundamental investigation (Bracconi et al., 2018b). They found that the porosity is the driving mass transfer property while cell and strut diameter have no direct influence.
In their study, Lucci et al. compared the mass transfer behaviour of POCS (Kelvin cells) with irregular foams (μCT), and found increased mass transfer coefficients for equivalent Kelvin cells over the irregular foams (Lucci et al., 2017).
In 2016, Della Torre and co-workers simulated the CO oxidation on a Kelvin cell lattice and could reproduce the typical light-off curve from experiments (Della Torre et al., 2016). More recently, the CO oxidation was simulated on a μCT-based irregular foam and validated against experiments on the very same foam. The temperature and concentration information in the experiment was obtained from a capillary that was moved through a circular hole in the center of the foam (Dong et al., 2018)).

Using artificially generated irregular foams, Wehinger et al. simulated the catalytic partial oxidation of methane (CPOX) and validated the model against an experiment from the literature (Wehinger, Heitmann, and Kraume, 2016; Horn et al., 2006; Dalle Nogare et al., 2008). This way, they proved the functionality of their artificial foam structure modeler.
Reactive studies on foams in general and entire structured foam reactors in particular are computationally costly and still often require the power of high performance clusters. Therefore, the published studies contain only a few reaction simulations. The problem of limited computational power in the field of CFD simulation on heterogeneous catalysis obviously is also a problem for the research on other catalyst carriers. With the ongoing increase in affordability and availability of computational power, more extensive reactive CFD studies on foams will be possible. For insight into CFD modeling and transport phenomena in foams, it is also helpful to include reactive studies of other catalyst carriers. For pellets and honeycombs more studies are generally available (see for instance Fernengel, Bolton, and Hinrichsen, 2019; Benzinger et al., 2019).
As the little amount of reactive foam studies implies, a lot of research is still to be done regarding this topic. For instance, studies about reactor performance especially with an emphasis on heat transport are, to the best of the author's knowledge, not available.

Chapter 3

Methodology and Description of CFD Reactor Model

3.1 Introduction

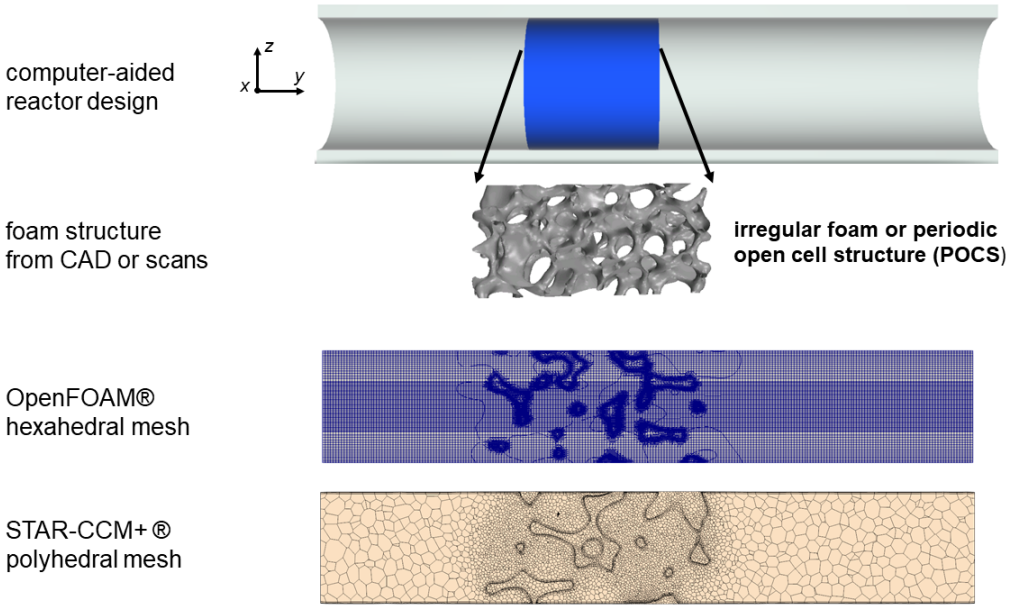

FIGURE 3.1: The tubular structured foam reactor as well as different mesh types.

Every published manuscript in the results part of this thesis contains an own methods part. Nevertheless, to get a better overview on different used models and assumptions, this chapter summarizes and explains the modeling work coherently. As the fully resolved modeling and simulation of exothermal catalytic gas-phase reactions is computational costly and often suffers from a lack of knowledge (e.g., about kinetics), this thesis follows the idea to mimic exothermicity through homogeneously distributed volumetric heat sources. This way, modeling and computational effort can be reduced significantly (see solution time in Appendix A).
To setup simulations of catalytic foam reactors, detailed information about the foam structure is needed. As described in the Chapter 2, the geometrical characterization of the porous foam structure can be obtained in several ways. In this work, the detailed structure information are obtained either through X-Ray scans (μCT, for irregular foams) or completely through computer aided design (for POCS) (see Figure 3.1). Both procedures result in digitally usable foam data, which can be placed in a

tube and thus, form a structured foam reactor. The setup and solving of CFD models can be easily done nowadays with both, open source and commercial software. In this thesis, the open source CFD toolbox OpenFOAM (Weller et al., 1998) is used as well as the commercial software STAR-CCM+ (PLM, 2021). Both software are based on the finite volume method in order to discretize the conservation equations. Currently, no heterogeneous reaction solver is available for OpenFOAM. Therefore, reactive simulations are completely performed using STAR-CCM+, while conjugate heat source simulations are computed with both software packages. Standard CFD software has proven to yield good results in the analysis of thermal behavior (Zafari et al., 2015; Meinicke, Wetzel, and Dietrich, 2017) and catalytic reactions with respect to open-cell foams (Wehinger, Heitmann, and Kraume, 2016; Dong et al., 2018; Della Torre et al., 2016) and is thus, used in this work.
The used reactor model and the simplifications are further developed or adapted to the requirements of each study throughout the results (i.e., manuscripts). Therefore, the model introduction in this chapter does not cover all model features. However, these are listed or mentioned in the corresponding results part. This chapter aims to present the majority of the model features in a combined way to provide the reader a better overview. Generally, all models solve steady-state conjugate heat transfer between a solid foam and one or multiple fluids.

3.2 Modeling Conjugate Heat Transfer with Volumetric Heat Sources

Since this thesis investigates conjugate heat transfer between fluid and solid, conservation equations for both phases are required [1]. For a Newtonian fluid (e.g., air) with neglected gravitational acceleration, the set of equations can be described as follows (Versteeg and Malasekera, 2007). The conservation of mass can be characterized with

$$\nabla \cdot (\rho_\mathrm{f} \vec{u}) = 0, \tag{3.1}$$

where ρ_f describes the density of the fluid and $\vec{u}$ the velocity field. The conservation of momentum is expressed as

$$\nabla \cdot (\rho_\mathrm{f} \vec{u} \otimes \vec{u}) + \nabla \cdot \boldsymbol{\tau} + \nabla p = 0, \tag{3.2}$$

with p denoting the pressure and $\boldsymbol{\tau}$ describing shear stress. Since air is a Newtonian fluid, the shear stress can be expressed as

$$\boldsymbol{\tau} = \mu_\mathrm{f}[\nabla \otimes \vec{u} + (\nabla \otimes \vec{u})^\mathrm{T}] - \frac{2}{3}\mu_\mathrm{f}(\nabla \cdot \vec{u})\mathbf{I}, \tag{3.3}$$

where μ_f is the viscosity of the fluid. The conservation of energy can be described as

$$\nabla \cdot (\rho_\mathrm{f} \vec{u} h) - \nabla \cdot (\lambda_\mathrm{f} \nabla T_\mathrm{f}) = 0, \tag{3.4}$$

where h denotes enthalpy, λ_f the thermal conductivity of the fluid, and T_f the temperature of the fluid. The compilation of equations for the fluid phase is completed by the ideal gas law

$$pV = nRT_\mathrm{f}. \tag{3.5}$$

Furthermore, the temperature dependency of the dynamic viscosity is expressed through the Sutherland equation (see Supplementary Material in Appendix B), whereas

[1] The model description is adapted from Sinn et al., 2019

the temperature dependency of the thermal conductivity of the fluid can be taken into account via the Eucken approximation (Poling, Prausnitz, and O'Connell, 2001). In contrast, the solid phase (i.e., the solid open-cell foam) is only described by the conservation of energy which diminishes the set of equations to

$$\lambda_s \cdot (\nabla^2 T_s) + S_{spec} = 0, \tag{3.6}$$

with λ_s denoting the thermal conductivity of the solid, S_{spec} denoting an artificial heat source (specified in $W\,m^{-3}$) and T_s denoting the temperature of the solid.
The applied boundary conditions also vary little from manuscript to manuscript. Generally, a fixed temperature and a fixed velocity were applied as inlet boundary condition, whereas at the outlet, a fixed pressure was set. At the pipe walls as well as at the surface of the foam the velocity is set to zero (no slip). Furthermore, the temperature at the tube walls (T_{wall}) is set to be constant. The open-cell foam, the fluid, and the tube are linked since the outer points of the regions collapse at their interfaces. This way energy can be passed from one region to another. At the interface, the regions are coupled through the continuous heat flux from both sides (Kopanidis et al., 2010)

$$\lambda_{region1} \frac{\partial T_{region1}}{\partial n} = \lambda_{region2} \frac{\partial T_{region2}}{\partial n} \tag{3.7}$$

and equal temperatures

$$T_{region1} = T_{region2}. \tag{3.8}$$

Here, n denotes the normal distance between region interface and the first mesh node. The mesh density and structure on both regions does not necessarily need to be equal (resulting in different n for the regions).

3.3 Modeling Actual Catalytic Reactions

3.3.1 Introduction to Modeling Catalytic Reactions

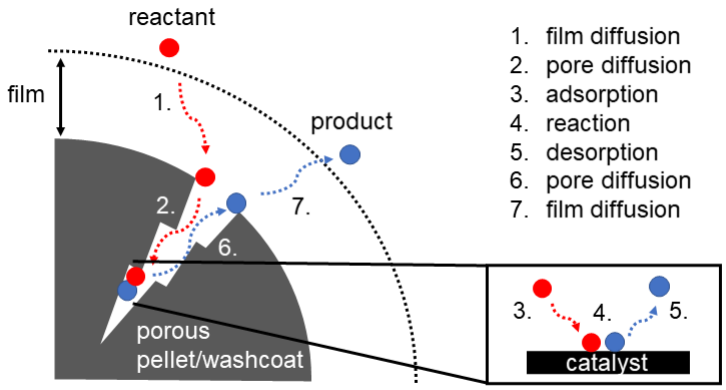

FIGURE 3.2: Principal molecular steps during heterogeneous catalysis (adapted from Jurtz, Kraume, and Wehinger, 2019).

So far, the non-reactive conjugate heat transfer model was introduced. For the modeling of actual heterogeneous catalytic reactions, the macroscopic transport inside the foam cells needs to be coupled with the surface processes. Principally in heterogeneous catalysis, the reactant(s) firstly needs to diffuse through a stagnant layer

TABLE 3.1: Methods for modeling kinetics in heterogeneous catalysis (adapted from Jurtz, Kraume, and Wehinger, 2019).

modeling method	simplification
ab initio calculation	most fundamental method
direct functional theory	using electron density for the N electron wave function
(kinetic) Monte Carlo	neglect details of dynamics
mean-field approximation	neglect details on adsorbate-adsorbate interactions
LHHW kinetics	require rate-determining step
power-law kinetics	neglect all mechanistic aspects

surrounding the pellet or washcoat (i.e., film diffusion; Figure 3.2). This process is followed by pore diffusion through the microporous network to reach the catalytic active sites. Here, the reactant(s) adsorb, react and desorb. Finally, the product(s) diffuse out of the pore network through the film back into the gas-bulk. Both, the diffusion or transport process (step 1, 2, 6 and 7) as well as the microkinetic process (steps 3-5) can be modeled with several methods differing in accuracy, availability and resulting computational cost. Since every single species (e.g., reactants, byproducts or intermediate products) might adsorb, desorb and diffuse inside the catalyst multiple times, the figure serves only as rough introduction (Deutschmann, 2015).
The methods for modeling rate expressions in heterogeneous catalysis are listed in Table 3.1. The most fundamental approaches are the quantum-mechanical models *ab initio* calculation and density functional theory which calculate first principle electron interactions. More simplified are kinetic Monte Carlo approaches with stochastically evaluated surface reaction rate expressions (Deutschmann, 2015). Nevertheless, these methods are often just too computationally costly and a lot of detailed knowledge about microscopic characterization is mandatory. Hence, these approaches are often not practical for simulations of foam reactors in particular and reaction engineering in general. With the aid of mean-field approximations, the catalyst surface is considered as uniform since mean values for all cells are used. This approach means a significant reduction of computational time while still achieving sufficient accuracy in CFD models (Deutschmann, 2015; Jurtz, Kraume, and Wehinger, 2019). When neglecting the surface coverage dependency of rate constants, the models can be further simplified. When the reaction rate is correlated with partial pressures from the gases, the assumption of a rate determining step leads to a Langmuir-Hinshelwood-Hougen-Watson (LHHW) mechanism (Jurtz, Kraume, and Wehinger, 2019). The most simplified methods are power-law approaches. As they completely neglect mechanistic aspects, they are mainly used for scale-up and black-box systems.
In this work, only approaches based on the mean-field approximation are used. Here, the surface is described using averaged values per cells which means that the actual catalyst surface is not resolved (e.g., no site defects). Instead, the chemical reaction is coupled with the gas-phase on the gas/solid interface via boundary conditions.

3.3.2 Reactive Foam Model

In this thesis, the numerical calculation of the reactive-flow simulation follows the general conservation of mass, momentum, species, and energy within the commercial STAR-CCM+ software package.[2] The steady-state model neglects gravitational forces (the influence is studied in detail in Chapter 6), as well as homogeneous gas-phase reactions. The conservation equations of mass and momentum are equivalent to the pure conjugate heat transfer case. The conservation of each species i is defined as

$$\nabla \cdot (\rho_\mathrm{f} Y_i \vec{u}) + \nabla \cdot \vec{j}_i = R_i^\mathrm{het}, \tag{3.9}$$

with the mass fraction of the species Y_i, the diffusion mass flux $\vec{j}_i$ and the net rate of the production of the species at the catalytic surface $\vec{j}_i$. The diffusion mass flux is calculated as

$$\vec{j}_i = -\rho_\mathrm{f} \frac{Y_i}{X_i} D_{i,\mathrm{m}} \nabla X_i, \tag{3.10}$$

where X_i is the mass fraction of species i. $D_{i,\mathrm{m}}$ is the mass-averaged diffusion coefficient

$$D_{i,\mathrm{m}} = \frac{1 - Y_i}{\sum_{j \neq i}^{N_\mathrm{s}} \left(X_j / D_{j,i} \right)}, \tag{3.11}$$

using the binary diffusion coefficients $D_{j,i}$ of species j and i in the mixture of N_s species. Energy conservation is expressed as

$$\nabla \cdot (\rho_\mathrm{f} \vec{u} h_\mathrm{f}) + \nabla \cdot \vec{j}_\mathrm{q} - \vec{u} \nabla p + \sum_i \left(h_i^0 \cdot R_i^\mathrm{het} \right) = 0 \tag{3.12}$$

with the enthalpy of the fluid mixture h_f, the diffusive heat flow $\vec{j}_\mathrm{q}$ and the heat production caused by chemical reactions $\sum_i \left(h_i^0 \cdot R_i^\mathrm{het} \right)$, where h_i^0 is the standard enthalpy of formation of the species. The diffusion heat flow is defined as

$$\vec{j}_\mathrm{q} = -\lambda_\mathrm{f} \nabla T + \sum_{i=1}^{N_\mathrm{s}} h_i \vec{j}_i. \tag{3.13}$$

with the thermal heat conductivity of the fluid λ_f. The species' enthalpies h_i and the mixture's enthalpy h_f are connected via

$$h_\mathrm{f} = \sum_{i=1}^{N_\mathrm{s}} Y_i h_i(T). \tag{3.14}$$

The ideal gas law completes the set of governing equations for the fluid phase

$$p = \frac{\rho R T}{\sum_{i=1}^{N_\mathrm{s}} X_i M_i} \tag{3.15}$$

where R is the universal gas constant and M_i the molar mass of species i. The solid phase is solely described by the conservation of energy

$$\lambda_\mathrm{s} \cdot (\nabla^2 T_\mathrm{s}) = 0, \tag{3.16}$$

with the solid thermal conductivity λ_s.
The fluid properties (e.g., λ_f, $D_{j,i}$ or $c_{\mathrm{p,f}}$) might depend on temperature, mixture

[2] The model description is adapted from Sinn et al., 2021a

or pressure. To account for these potential dependencies, the dynamic viscosity and binary diffusion coefficients are derived from the Chapman and Enskog theory. The thermal conductivity is calculated for each species using the kinetic theory with mass-weighted averaging if required. The isobaric heat capacity of the fluid mixture is determined using NASA polynomials for the individual species. Equivalently, the property is averaged by mass-weighting. This procedure is commonly accepted in the literature (Dong et al., 2018; Wehinger, Heitmann, and Kraume, 2016).
On the catalytic surface, species' production or consumption via chemical reaction is calculated by balancing the diffusive mass flux normal to the surface and the net rate of heterogeneous surface reactions

$$\vec{n} \cdot \vec{j}_i = \eta F_{\text{cat/geo}} M_i \dot{s}_i \tag{3.17}$$

where $\vec{n}$ is the unit vector, normal to the surface, η the effectiveness factor, $F_{\text{cat/geo}}$ the ratio of catalytically active surface and geometrical surface and $\dot{s}_i$ the species' molar surface reaction rate. Here, one could in principle also use 3D reaction-diffusion models for modeling potential diffusion limitations in the washcoat. However, in the literature it was shown that the effectiveness factor is sufficient for simulating the CO oxidation (Wehinger, Klippel, and Kraume, 2017).
The reaction rates for a set of R_s reactions are solved via elementary mass-action kinetics

$$\dot{s}_i = \sum_{k=1}^{R_\text{s}} \nu_{i,k} k_k \prod_{j=1}^{N_\text{s}} c_j^{\nu'_{j,k}}. \tag{3.18}$$

with the stoichiometric coefficients $\nu_{i,k}$, the rate constants k_k and the species' molar concentrations c_j. All rate constants follow the common Arrhenius dependency

$$k_k = A_k T^{\beta_k} \exp\left(-\frac{E_{\text{a}_k}}{RT}\right) \prod_{i=1}^{N_\text{s}} \theta_i^{\mu_{i_k}} \exp\left(\frac{\varepsilon_{i_k}\theta_i}{RT}\right). \tag{3.19}$$

where A_k is the pre-exponential factor, β_k the temperature exponent, and E_{a_k} the activation energy. Reaction order and activation energy are influenced by the number of occupied surface sites and corrected via the surface coverage of species i, θ_i, in combination with two correction terms μ_{i_k} and ε_{i_k}. The adsorption processes of O_2 and CO_2 are modeled via a sticking coefficient S_i

$$\dot{s}_i = \frac{S_i}{1 - 0.5 S_i} \sqrt{\frac{RT}{2\pi M_i}} c_i, \quad \text{with} \quad S_i = S_i^0 \prod_{j=1}^{N_\text{s}} \theta_j^{\nu_{j_k} + \mu_{j_k}}. \tag{3.20}$$

In this work, the reactive foam model uses the strongly exothermic CO oxidation as model reaction (Chapter 5). Using a one step formula, the CO oxidation can be expressed as

$$\text{CO} + \frac{1}{2}\text{O}_2 \leftrightarrows \text{CO}_2, \; \Delta_\text{R} H^0 = -283\,\text{kJ mol}^{-1}. \tag{3.21}$$

The principally equivalent model can also be used used for other catalytic reactions by simply changing the reaction mechanism and adapting the species (see Appendix A, for CPOX of methane). The elementary surface reaction mechanism for the CO oxidation over Pt from Deutschmann et al., 1996 is implemented as kinetic model, equivalent to the study by Dong et al., 2018. All reactions k are listed in Table 3.2. The applied boundary conditions in the reactive simulations are basically similar to the ones from the pure conjugate heat transfer cases (i.e., fixed temperature, velocity inlet and pressure outlet). However, all manuscripts and the additional reactive

TABLE 3.2: Kinetic mechanism used in this study: CO oxidation over Pt (adopted from Deutschmann et al., 1996).

No.	Reaction	A_k ($\mathrm{cm\,mol^{-1}\,s^{-1}}$)	β_k (-)	E_{a_k} ($\mathrm{kJ\,mol^{-1}}$)
R1	$CO + Pt(s) \rightarrow CO(s)$[a]	1.618×10^{20}	0.5	-
R2	$O_2 + 2\,Pt(s) \rightarrow 2\,O(s)$	0.023[b]	-	-
R3	$CO_2 + Pt(s) \rightarrow CO_2(s)$	0.005[b]	-	-
R4	$CO(s) + O(s) \rightarrow CO_2(s) + Pt(s)$	3.7×10^{21}	0	105.0
R5	$CO(s) + Pt(s) \rightarrow C(s) + O(s)$	1.0×10^{18}	0	184.0
R6	$C(s) + O(s) \rightarrow CO(s) + Pt(s)$	3.7×10^{21}	0	62.8
R7	$CO(s) \rightarrow CO + Pt(s)$	1.0×10^{13}	0	125.5
R8	$2\,O(s) \rightarrow O_2 + 2\,Pt(s)$	3.7×10^{21}	0	$213\text{-}60 \cdot \theta_{O(s)}$
R9	$CO_2(s) \rightarrow CO_2 + Pt(s)$	1.0×10^{13}	0	20.5

Surface site density $\Gamma = 2.72 \times 10^{-9}\,\mathrm{mol\,cm^{-2}}$

[a] Reaction order of Pt(s) is 2 for this step
[b] Sticking coefficient, S_i^0 / -

simulations from the Appendix contain a description of the applied boundary conditions.
Differences between the modeling of fully resolved exothermal reactions and the heat source simplification already become apparent. First of all, the origin of the heat source differs. While for the reaction, the heat evolves on the fluid side of the fluid/solid interface, the heat source simplification distributes the thermal energy homogeneously solely over the solid volume. Further, the heat source simplification can omit species conservation and thus, the need for mixture equations. The mandatory set of equations and assumptions is hence significantly reduced through the heat source approach.

3.4 Modeling Radiation

At high temperatures the effect of thermal radiation on the overall heat transport might be severe [3]. In contrast to conduction and convection, radiation does not need media to transport heat since electromagnetic waves can spread in vacuum. Further, heat transport by radiation does not only depend on the value of the temperature gradient, but also on the absolute temperature level. The maximum specific heat flow ($\mathrm{W\,m^{-2}}$), that a real solid body emits, can be expressed by the Stefan-Boltzman

[3] The model description is adapted from Sinn et al., 2020a

law extended by the surface emissivity ε_{ray}

$$\dot{q} = \sigma \varepsilon_{\text{ray}} T^4 \tag{3.22}$$

with $\sigma = 5.67 \times 10^{-8}\,\text{W m}^{-2}\,\text{K}^{-4}$ being the Stefan-Boltzmann constant. The surface emissivity is generally between 0 and 1 (colored or real body: $\varepsilon_{\text{ray}} = f(T)$; grey body: ε_{ray} = const.; black body: ε_{ray} = 1). When radiation hits a material, the energy can be reflected, absorbed or transmitted (depending on e.g., the wavelength or material):

$$\dot{q} = \gamma_{\text{ray}} \dot{q} + \alpha_{\text{ray}} \dot{q} + \tau_{\text{ray}} \dot{q} \tag{3.23}$$

with γ_{ray} denoting the degree of reflection, α_{ray} the degree of absorption and τ_{ray} the degree of transmission. Furthermore, the radiant intensity I is the specific radiant heat flux per unit solid angle ($\text{W m}^{-2}\,\text{sr}$):

$$I = \sigma \varepsilon_{\text{ray}} T^4 \frac{1}{\pi}. \tag{3.24}$$

Generally, radiation modeling in CFD codes can be distinguished in approaches with and without fluid participation. OpenFOAM contains the following three radiation models: viewFactor (no fluid participation), fvDOM (fluid participation; finite volume discrete ordinate model), and the P1 (fluid participation) model. In contrast, in STAR-CCM+ the S2S radiation models (surface-to-surface; similar to viewfactor) and DOM (discrete ordinate model; similar to fvDOM) are implemented.
The view factor approaches in OpenFOAM and STAR-CCM+ calculate a matrix of view factors for all solid surface cells via ray tracing prior to the actual simulation. These view factors are later used to compute the thermal energy exchange between the surfaces. The fluid phase is treated as a non-participating medium.
Additionally, the fluid participating approaches are frequently used as they have been successfully applied in literature for high temperature heat transfer and are also suitable for symmetry boundary conditions (Habibi, Merci, and Heynderickx, 2007; Wehinger, 2019; Wehinger and Flaischlen, 2019). In this study, the fluid participation is not expected to play a significant role for the model fluid (air) as well as the model conditions (i.e., atmospheric pressure, temperatures and geometrical dimensions) (Wehinger, 2019; Wehinger and Flaischlen, 2019). The fluid participating approaches basically solve the radiative transfer equation (RTE) that describes the change of the radiant intensity at any point along a path through a participating medium (fluid) depending on scattering, emission and adsorption effects (Modest, 2013). For further explanation and discussion the reader is referred to Modest, 2013 and Versteeg and Malasekera, 2007. Due to the lack of (soot) particles as well as relatively low distances, no scattering model is needed for this study (Hettel, Daymo, and Deutschmann, 2018). For a non-scattering medium, the RTE reads (Modest, 2013)

$$\frac{dI(r,s)}{ds} = \kappa I_{\text{b}} - \kappa I(r,s) \tag{3.25}$$

where r denotes the position vector, s the direction vector, κ the fluid's absorption coefficient, I_{b} denotes the black body intensity, and σ_{s} the scattering coefficient. The calculated radiative heat flows are eventually included in the energy conservation source term. In this thesis, the fvDOM (OpenFOAM) and DOM (STAR-CCM+, for verification) models as well as the S2S (STAR-CCM+) are used. In the literature, it was shown that using the DOM model and the S2S model yielded almost the

same temperature profiles in a fixed-bed reactor (Wehinger and Flaischlen, 2019; Wehinger, 2019). However, the DOM model was 35 % more costly than the S2S model for the simulation of the steam reforming reaction in a fixed-bed reactor (Wehinger and Flaischlen, 2019). Thus, both approaches are considered to yield reliable results for the targeted exothermal gas-phase reactions.

3.5 Modeling Turbulence

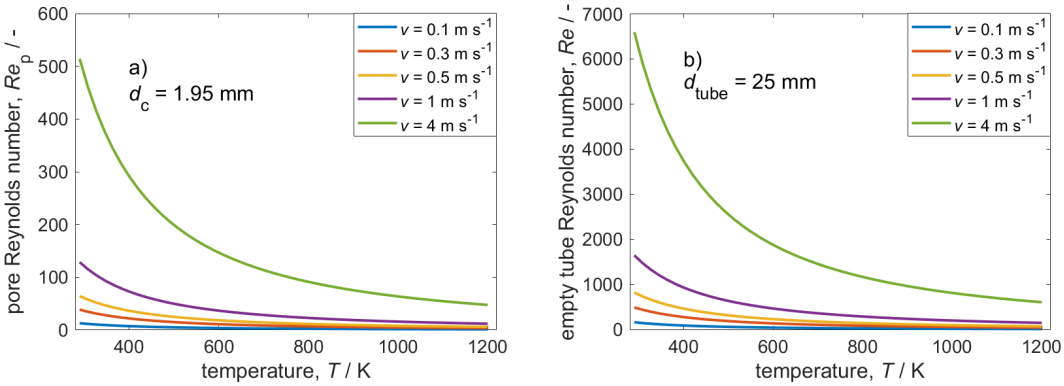

FIGURE 3.3: Calculated Reynolds numbers plotted against temperature levels for investigated superficial velocity range. a) Pore Reynolds number. b) Empty tube Reynolds number.

The occurrence of turbulence has a significant impact on lateral mixing of all transport properties due to strong fluctuations in all spatial directions (Jurtz, Kraume, and Wehinger, 2019). Usually, the Reynolds number (Re) is used for an estimation of flow regimes. In case of open-cell foams, one can also use the pore Reynolds number (Re) with the cell diameter as characteristic diameter. Although exact limits of flow regimes in open-cell foams are still under discussion, flow regimes can be approximately distinguished from the literature (Hutter et al., 2011; Pedras and De Lemos, 2001):

- Darcy regime (or creeping flow) for $Re_\mathrm{p} < 1$.
- Forchheimer regime for $1 < Re_\mathrm{p} < 150$.
- post-Forchheimer regime (unsteady) for $150 < Re_\mathrm{p} < 300$.
- fully-turbulent regime (highly unsteady and chaotic) for $Re_\mathrm{p} > 300$.

In Figure 3.3, both, the pore Reynolds number as well as the empty tube Reynolds number are plotted for different temperatures and superficial velocities that correspond to the conditions investigated in this thesis. As in most simulated cases, the temperature level is $T_\mathrm{wall} > 500\,\mathrm{K}$, it can be seen that (except for the highest superficial velocity $v > 4\,\mathrm{m\,s^{-1}}$), the flow is in the Forchheimer regime (see Re_p in panel a)). Further, the empty tube sections in front and behind the foam (see Figure 3.1), only require a turbulence model for the highest investigated superficial velocities (as $Re_\mathrm{emptytube} < 2200$). In their study, Della Torre and colleagues showed that in open-cell foams, even in the fully turbulent regime, laminar models are sufficient to resolve the pressure drop (Della Torre et al., 2014). However, at elevated superficial

velocities ($v = 0.5\,\mathrm{m\,s^{-1}}$) convergence problems were encountered. This was also mentioned by Wehinger, Heitmann, and Kraume, 2016. Therefore in this work, all simulations with $v > 0.5\,\mathrm{m\,s^{-1}}$ contain a turbulence model.
Turbulence models can roughly be categorized in direct numerical simulations (DNS), large eddy simulations (LES) and Reynolds-Averaged Navier-Stokes models (RANS). The approaches differ significantly in their required mesh resolution (Jurtz, Kraume, and Wehinger, 2019). DNS do not require for subgrid turbulence models as this technique resolves vortexes on all length scales. This technique is considered to be the most accurate one, but it also requires a lot of computational resources. It is thus considered as non practical for the simulation of fixed or packed-bed simulations (Jurtz, Kraume, and Wehinger, 2019). LES ignore the smallest length scale (that is resolved in DNS) by applying filters that serve as time and spatial averaging on that scale. Still, the solution time as well as requirements for grids are not yet practical (Shams et al., 2015)). Widely used in academia and industry are RANS models, that do not resolve single eddys but use subgrid models instead. Here, a property ϕ consists of an averaged value $\bar{\phi}$ and a fluctuating one ϕ'

$$\phi = \bar{\phi} + \phi'. \tag{3.26}$$

When applied to the conservation equations, a turbulent stress tensor τ_t results. For closing the equations with the additional properties from turbulence modeling, one approach is the class of eddy viscosity models. For pore-scale CFD reactions (or particle-resolved in case of fixed beds), the so-called two-equation models $k\omega$ and $k\epsilon$ are frequently used (Deutschmann, 2015; Dixon and Partopour, 2020). Turbulence might not only affect the stress tensor in reactor models, but also the energy and mass conservation equation (turbulent diffusion). Additionally, kinetic models might be inaccurate when partial pressure of the species differ due to turbulence (Deutschmann, 2015).
In this work, turbulence effects are considered using the *realizable* $k\epsilon$ RANS model with *All y+ wall-treatment*. This model is an extension of the standard $k\epsilon$ model and shows improved behavior in many applications (Wehinger, 2016; PLM, 2021). In the literature, the model showed good results and has been applied to validated reactive foam simulations as well as pellet-related simulations (Wehinger, Heitmann, and Kraume, 2016; Wehinger, 2019; Wehinger et al., 2019). Currently, there is no clear recommendation on what turbulence model should be used in pore-scale CFD simulations (Dixon and Partopour, 2020). Like in radiation modeling, there is still a lot of research needed (Dixon and Partopour, 2020).

Chapter 4

Heat Sources — Concept and Thermal Behavior

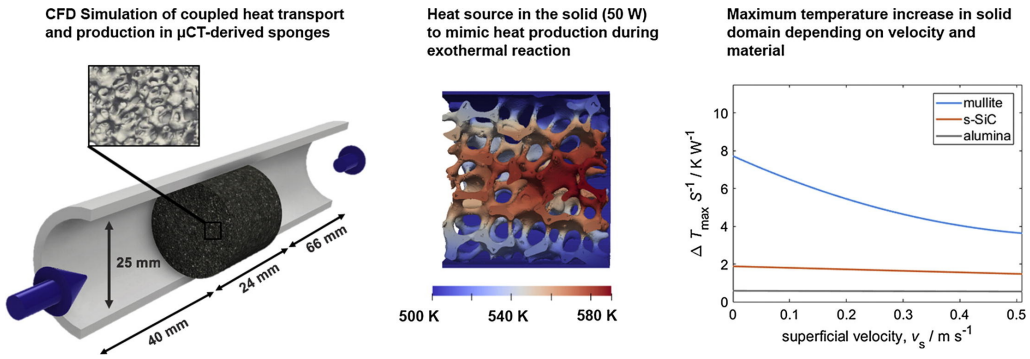

FIGURE 4.1: Graphical abstract of the manuscript Sinn et al., 2019.

The content of the first result chapter is published under the name *Coupled conjugate heat transfer and heat production in open-cell ceramic foams investigated using CFD* (Sinn et al., 2019)[1].
This chapter of the results basically contains first investigations on the thermal effect of homogeneously and volumetrically distributed heat sources (Figure 4.1). In this context, integral conductive and convective heat flows are analyzed to asses which mechanism dominantly determines the heat removal. This is relevant, as foams can only be advantageous over pellets when heat is mainly removed radially via thermal conduction (instead of axially via convection). In this study, a 10 ppi ceramic irregular foam scan (alumina, Al_2O_3, cylindrical, diameter = 25 x 24 mm) serves as geometrical input for the conjugate heat transfer simulations using air as fluid. The model is validated and verified against pressure drop and heat transfer coefficients from the literature (Inayat et al., 2016; Dietrich et al., 2009; Dietrich, 2013; Gancarczyk et al., 2018; Meinicke, Wetzel, and Dietrich, 2017.) From CO_2 methanation experiments (Kiewidt and Thöming, 2019a), the heat production in the reactor for such a foam can be approximated to 50 W. To account for other reactions or reacting conditions, the total heat source intensity is varied from 5 to 150 W. Furthermore, the thermal behavior of different ceramic materials (mullite, alumina or s-Sic) and superficial velocities is investigated. The aim of this chapter is thus, to analyze heat flows and temperature fields as a result from heat sources implemented in the solid.

[1]The Supporting Documents can be found in Appendix B.

International Journal of Heat and Mass Transfer 139 (2019) 600–612

Contents lists available at ScienceDirect

International Journal of Heat and Mass Transfer

journal homepage: www.elsevier.com/locate/ijhmt

Coupled conjugate heat transfer and heat production in open-cell ceramic foams investigated using CFD

Christoph Sinn [a], Georg R. Pesch [a], Jorg Thöming [a], Lars Kiewidt [b,*]

[a] University of Bremen, Chemical Process Engineering, Leobener Strasse 6, 28359 Bremen, Germany
[b] Wageningen University & Research, Biobased Chemistry and Technology, P.O. Box 17, 6700 AA Wageningen, the Netherlands

ARTICLE INFO

Article history:
Received 28 March 2019
Received in revised form 10 May 2019
Accepted 15 May 2019

Keywords:
Open-cell foam
Solid sponge
Computational fluid dynamics (CFD)
Conjugate heat transfer
Volumetric heat source
Pseudo-homogeneous model

ABSTRACT

Combining low pressure drop and remarkable heat transport properties, open-cell foams offer a combination that makes them a highly attractive option as monolithic catalyst support. The coupled thermal behavior of foams and fluids during heat production, e.g., exothermic chemical reactions, is still not thoroughly described despite their potential to optimize temperature control in fixed-bed reactors. Hence, the aim of this study is to get deeper insight into coupled conjugate heat transfer and heat production in open-cell foams used in a tubular reactor with constant wall temperature. Therefore, we conducted μCT-based CFD simulations of open-cell foams with artificial heat sources that mimic the heat of reaction during an exothermal chemical reaction and allow to study the effect of heat production on heat transfer while requiring lower computational cost than simulating actual chemical reactions. We implemented a range of heat source intensities, that covers typical exothermic reactions, to study their effect on heat flows as well as temperature fields and used CO_2 methanation as a case study. We further quantified the influence of superficial velocity, heat source intensity, and material on the temperature fields inside the foam and found conduction being the dominant heat transport mechanism. We further evaluated the feasible range of even more simplified pseudo-homogeneous models and found high thermal conductivities and low superficial velocities to be appropriate. In conclusion, the presented approach offers the possibility to study thermal effects regarding catalytic supports and give valuable insight in heat transport mechanisms under relevant process conditions in heterogeneous catalysis (heat sources: 5–150 W for a reaction volume of 1.2×10^{-5} m^3, superficial velocities 0–0.51 m s^{-1}, thermal conductivities 5–50 W m^{-1} K^{-1}).

1. Introduction

Open-cell ceramic foams, often referred to as solid sponges, are interconnected cellular materials. They have been subject of great interest for over a decade in the field of thermal and chemical engineering due to their combination of low pressure loss, large specific surface area, and good heat transfer properties [1]. Applications for solid sponges in terms of process intensification are, among others, heat exchangers [2], filters for molten metals [3], solar receivers [4,5] and especially support material in heterogeneous catalysis [6–8]. When used as catalyst supports, e.g., in exothermic gas phase reactions, open-cell foams can help to maintain or customize certain temperature profiles in order to maximize yields, minimize hot spots and prevent thermal runaways [9–11]. Those hot spots might decrease selectivity or even lead to catalyst deactivation due to sintering of active sites [12]. Hence, the prediction and analysis of hot spots is vital for the development of long lasting catalysts. Knowing the temperature fields during reactions is thus crucial for better understanding the thermal behavior of open-cell foams. Despite their advantages, the usage of open-cell foams as monolithic catalyst support in large production scale is not common yet. However, Ref. [13] recently demonstrated the applicability of open-cell foams in a pilot-scale reactor for the autothermal reformation of methane (biogas). Other porous structures such as pellets are already commonly used in the industry. A major reason, besides higher acquisition costs and the more complex mounting of monolithic sponges, is the lack of knowledge in terms of heat and mass transfer as well as fluid dynamics which makes a scale-up more challenging [1,14].

For a better understanding of the thermal behavior of foams in chemical reactors, not only the solid part is of interest but also the thermal interaction of solid and fluid domains. Hence, investigat-

* Corresponding author.
E-mail addresses: gpesch@uni-bremen.de (G.R. Pesch), lars.kiewidt@wur.nl (L. Kiewidt).

https://doi.org/10.1016/j.ijheatmasstransfer.2019.05.042
0017-9310/

Nomenclature

Roman

A	area, m^2
d_w	window diameter, m
d_c	cell diameter, m
d_s	strut diameter, m
F	heat flow, W
h	specific enthalpy, kJ kg^{-1}
ΔH_R^0	standard reaction enthalpy, kJ mol^{-1}
p	pressure, Pa
R	universal gas constant for air (8.314), JK^{-1} mol^{-1}
S	energy source term, W m^{-3}
S_V	specific surface area, m^{-1}
T	temperature, K
T_{dev}	normalized temperature deviation, –
T_{av}	average temperature, K
T_i	temperature of cell i, K
ΔT_{log}	logarithmic mean temperature, K
ΔT_{max}	maximum temperature increase, K
ΔT_{mean}	mean temperature increase, K
U	velocity, m s^{-1}
V	volume, m^3
$\dot{V}$	volume flow, m^3 s^{-1}
v_s	superficial velocity, m s^{-1}
Y	yield, –

Greek

α	heat transfer coefficient, W m^{-2} K^{-1}
ϵ_0	open porosity, –
ρ_s	solid sponge's density, kg m^{-3}
ρ_f	fluid's density, kg m^{-3}
τ	shear stress, Pa
λ_s	solid sponge's thermal conductivity, W m^{-1} K^{-1}
λ_f	fluid's thermal conductivity, W m^{-1} K^{-1}
μ_f	fluid's dynamic viscosity, Pa s
σ	standard deviation, –

Dimensionless groups

Re_p	pore Reynolds number, –

ing coupled conjugate heat transfer is key to improve the overall reaction system. To asses heat transfer properties of open-cell foams, the temperature inside them has been studied through experiments and simulations. Non-invasive measurement techniques such as infrared thermography (IRT; [15]) or magnetic resonance imaging (MRI; [16–18]) can provide the opportunity to measure temperature fields. However, these methods are limited to low flow rates, low temperatures, and are often complex and expensive to perform. Offering high precision and an easy change of parameters, computational fluid dynamic (CFD) simulations allow full field mapping of solid and fluid temperatures and already proved to be a valuable tool for better understanding coupled conjugate heat transport in solid sponges [19–21]. With the aid of CFD simulations, researchers investigated heat transfer [22,23], thermal effects of wall coupling [24,25] and the influence of strut designs on the heat transport properties of the foam [26]. Due to the complex modeling, CFD studies dealing with chemical reactions on open-cell foams are scarce [27,28]. Recently, Dong *et al.* [29] were the first to simulate CO oxidation on a real foam geometry, that was obtained through X-ray microtomography (μCT). They reported good agreements with experiments.

In order to significantly decrease computational cost, researchers also developed homogeneous models for describing the thermal behavior of open-cell foams and simulate chemical reactions. The homogenization of the porous foam media can be achieved either through general porous media approaches [30,31] or sponge-tailored models [32–34]. In contrast to fully heterogeneous models, homogeneous models neither consider the morphology nor distinguish between the fluid and the solid phase. Consequently, they are only valid for a certain range of parameters and materials. Clearly, homogeneous models often have lower precision than fully-heterogeneous CFD models, but yield reasonable results. Generally, detailed CFD modeling and simulation of chemical reactions in open-cell foams takes a lot of effort and requires high computational costs because of the complex (real) geometry and thus the complex flow field [27].

To bridge the gap between the CFD simulation of chemical reactions (i.e., heat production or heat consumption) and heat transport, we simulated uniformly distributed heat sources in a μCT-based ceramic open-cell foam, which approximate heat of reaction. With the aid of fully-heterogeneous steady-state CFD simulations, we evaluated the proportion of the heat flow that is transported radially via conduction in the open-cell foam and the heat flow that is transferred from open-cell foam to fluid (convection). For this purpose we conducted a parameter study for relevant materials and process conditions in heterogeneous catalysis. Furthermore, we analyzed the resulting temperature distributions in that very parameter range. In the literature, to investigate heat transport, open-cell foams were either heated (or cooled) through the fluid or trough the wall but not through heat production within the solid.

Artificial heat sources, which have not been described in literature yet, should be able to mimic the heat of reaction, to offer the opportunity to investigate conjugate heat transfer isolated from chemical reactions and to save computational cost. Studying heat flows as a result of uniformly distributed heat sources in industrially relevant order of magnitude allows us to identify the dominant mechanism in the investigated parameter range. The simulated temperature distributions further yield the minimum temperature increases that will occur in ceramic open-cell foams during exothermal chemical reactions. Hence, the simplification made offers the potential to deduce design guidelines. Furthermore, we compared the temperature distributions of the fluid and solid phases delivered by the CFD simulations. We evaluated to what extend it is possible to use simplified (pseudo-homogeneous) models to describe heat production in open-cell foams.

2. Models and methods

2.1. Geometry and meshing

To obtain a digital representation of the real open-cell foam morphology, we performed X-ray absorption tomography of a foam sample. Within this method, 2D voxelized grey-scale images were stacked to obtain an image of the original open-cell foam (X-ray source: XS160NFOF, GE Sensing & Inspection Technologies, USA; acceleration voltage: 90k V; detector: Shad-o-Box 4K EV, Rad-icon Imaging Corporation, USA; angular resolution 0.25°). A Gaussian filter (radius 2 px) was applied on the grey-scale images in order to reduce noise. For distinguishing between solid and fluid phase a threshold gray value was specified (minimum between open-cell foam and gas peak in the grey-scale histogram). After binning (2×2), the final isotropic voxel-size was 32 µm. Additionally, the digital model was used for obtaining the geometric properties of the investigated commercial 10 ppi alumina sample (see Table 1, manufactured by Hofman Ceramics GmbH, Breitscheid,

Germany). Diameter and height of the sample were determined using a standard caliper. To represent a tubular fixed-bed reactor, the foam's digital representation was then positioned inside a 25 mm diameter tube with an inlet zone of 40 mm in front of the foam and an outlet zone of 66 mm after the foam using CAD software (FreeCAD, https://www.freecadweb.org/; see Fig. 1). The investigation of the conjugate heat transfer required the meshing of the fluid and solid regions, i.e., a multi-region mesh was needed. For this purpose, the widely used cartesian mesh generator snappyHexMesh (SHM) was used. SHM is included in the open source CFD toolbox OpenFOAM ([35], Version 5.0). SHM generates a computational mesh from geometry files (e.g., STL) created by segmentation (thresholding). The generated mesh is shown in Fig. 1. All simulations in this work were performed with the same foam geometry. This includes the investigated change of material. The advantage is that the geometry itself was preserved and therefore the influence of morphology on conjugate heat transfer was isolated in this study. The investigated solid materials were alumina (Al_2O_3), sintered silicon carbide (s-SiC) and mullite (Al_2O_3-SiO_2) with their most distinctive property being the thermal conductivity λ_s. For the fluid phase, we considered air.

2.2. Governing equations and numerical procedure

OpenFOAM is based on the finite volume method (FVM) and was used for the CFD simulations of this work (FVM; [36]). We used the solver chtMultiRegionSimpleFoam which aims to solve steady-state, compressible, conjugate heat transfer problems between solid and fluid phases. All investigated cases consider superficial velocities equal or below 0.51 m s^{-1} and temperatures above 500 K. Hence, the pore Reynolds number $Re_p = \rho_f v_s d_c / \epsilon_o \mu_f$ stays below 150 in all cases, which indicates a Forchheimer flow regime [37]. Thus, laminar flow is assumed and turbulence effects are neglected; albeit, the exact boundaries of the flow regimes are still under discussion [38]. The steady-state assumption was tested for an isothermal transient case and found to be appropriate (see Appendix A). Additionally, thermal radiation is not considered. Neglecting thermal radiation might not always be an appropriate assumption and the impact of this simplification is depicted in the Supplementary Material. We used the pseudo-homogeneous model depicted in Ref. [34] for evaluating contributions of heat transport mechanisms to the total effective thermal conductivity. Here, the ratio of heat transported via radiation to the total transported heat in an alumina foam remains below 10 % for temperatures lower than 600 K in the investigated velocity range.

Generally, the FVM is based on the discretization of the domain and the conservation equations. As we investigated conjugate heat transfer, there are two regions (fluid and open-cell foam) with different conservation equations. The mandatory set of equations for a Newtonian fluid domain (here air) with neglected gravitational acceleration consists of the following equations [36]. The conservation of mass can be characterized with

$$\nabla \cdot (\rho_f \mathbf{U}) = 0, \tag{1}$$

where ρ_f describes the fluid's density and $\mathbf{U}$ the velocity field. The conservation of momentum is expressed as

$$\nabla \cdot (\rho_f \mathbf{U} \otimes \mathbf{U}) + \nabla \cdot \boldsymbol{\tau} - \nabla p = 0, \tag{2}$$

with p denoting the pressure and $\boldsymbol{\tau}$ describing shear stress. Since air is a Newtonian fluid, the shear stress can be expressed as

$$\boldsymbol{\tau} = \mu[\nabla \otimes \mathbf{U} + (\nabla \otimes \mathbf{U})^T] - \frac{2}{3}\mu(\nabla \cdot \mathbf{U})\mathbf{I}, \tag{3}$$

where μ is the fluid's viscosity. The conservation of energy can be described as

$$-\nabla \cdot (\rho_f \mathbf{U} h) - \nabla \cdot (\lambda_f \nabla T_f) = 0, \tag{4}$$

where h denotes enthalpy, λ_f the fluid's thermal conductivity and T_f the fluid's temperature. The compilation of equations for the fluid phase is completed by the ideal gas law:

$$pV = nRT_f. \tag{5}$$

Furthermore, the temperature dependency of the dynamic viscosity was expressed through the Sutherland equation (see Supplementary Material), whereas the temperature dependency of the fluid's thermal conductivity was taken into account via the Eucken approximation [39]. In contrast, the solid phase (i.e., the solid open-cell foam) is soley described by the conservation of energy which diminishes the set of equations to:

$$\lambda_s(\nabla^2 T_s) + S = 0, \tag{6}$$

with λ_s denoting the solid's thermal conductivity, S denoting an artificial heat source (specified in W m^{-3}, see next section) and T_s denoting the solid's temperature. All terms, except for the divergence terms, were discretized using second order central differencing schemes. The divergence terms were discretized using second order upwind differencing schemes. Moreover, a fixed temperature and a fixed velocity were applied as inlet boundary condition, whereas at the outlet, a fixed pressure was set. At the pipe walls as well as at the foam's surface the velocity is set to zero (no slip). Furthermore, the temperature at the tube walls (T_{wall}) is set to be constant. The open-cell foam, the fluid and the tube are linked since the outer points of the regions collapse at their interfaces. This way energy can be passed from one region to another. At the interface, the regions are coupled through the continuous heat flux from both sides ([40])

$$\lambda_{region1} \frac{\partial T_{region1}}{\partial n} = \lambda_{region2} \frac{\partial T_{region2}}{\partial n} \tag{7}$$

and equal temperatures

$$T_{region1} = T_{region2}. \tag{8}$$

Furthermore, all simulations were performed on 8 cores (Intel® Xeon®, 2.1 GHz) with 96 GB RAM and each simulation took a computational time of approx. 24 h, with final relative residuals of 10^{-7}.

Table 1
Properties used for the simulations. The geometric properties of the investigated alumina foam sample were measured with μCT. The sample is identical to the sample used in Ref. [10].

Parameter		Value
Pore count		10 ppi
Open porosity	ϵ_o	0.77
Specific surface area	S_V	521.3 m^{-1}
Cell diameter	d_c	5.76 ± 1.9mm
Window diameter	d_w	3.3 ± 0.9mm
Strut diameter	d_s	1.5 ± 0.5mm
Thermal conductivity	λ_s	alumina: 15 W m^{-1} K^{-1} s-SiC: 50 W m^{-1} K^{-1} mullite: 3 W m^{-1} K^{-1}

2.3. Implementation of heat sources

Artificial heat sources are introduced mathematically by adding a source term to the energy equation of the solid region (see Eq. (6)). In reality, heat sources can be inserted electrically using the Joule effect [14], by laser beams or by an occurring exothermal reaction. In order to simulate an industrially relevant heat source, the evolving heat of reaction of a model catalytic reaction was esti-

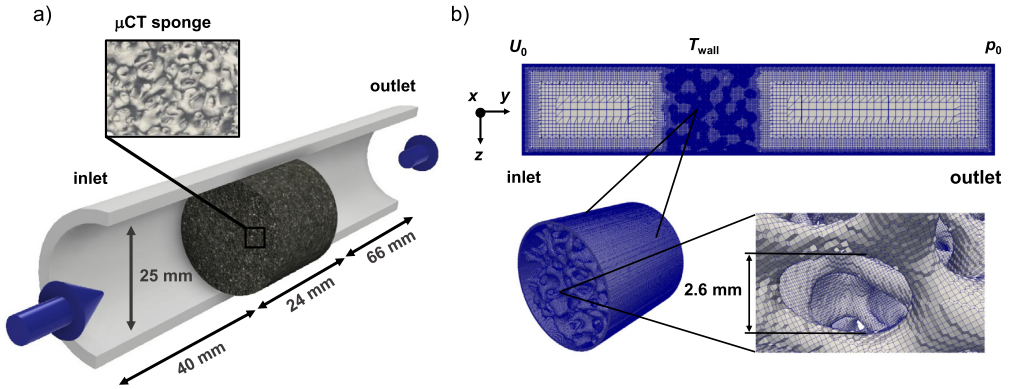

Fig. 1. Problem setup and mesh used for CFD simulations. (a) Illustration of the tube and open-cell foam with dimensions. The blue arrows indicate the direction of gas flow. The geometrical information of the open-cell foam were obtained by μCT. (b) Multi-region mesh generated by SHM for the simulations with a total cell count of 3.7 million cells. (For interpretation of the references to colour in this figure legend, the reader is referred to the web version of this article.)

mated. For this work, the exothermal CO_2 methanation is chosen as model reaction. The CO_2 methanation is commonly described as [12]:

$$CO_2 + 4H_2 \leftrightarrows CH_4 + 2H_2O, \quad \Delta H_R^0 = -165 \text{ kJ mol}^{-1}. \tag{9}$$

Typically, temperatures inside the reactor rise significantly when undiluted molar feed ratios of $CO_2 : H_2 = 1 : 4$ are used and no proper cooling is applied [41]. The overall evolving heat $\dot{Q}$ inside the tube can be estimated by the product of the volume flow $\dot{V}$, the molar concentration of carbon dioxide C_{CO_2}, the yield Y, and the standard heat of reaction ΔH_R^0,

$$\dot{Q} = \dot{V} C_{CO_2} Y (-\Delta H_R^0). \tag{10}$$

By applying the ideal gas law, the molar concentration C_{CO_2} can be calculated assuming $T_f = 500$ K. A yield of 30% was assumed, which is consistent with experiments [10]. Note that the experiments were conducted for four foams which resulted in a higher overall conversion. We further assumed that no side reactions take place and thus, CO_2 only reacts to CH_4 (selectivity equals one). With the assumption of a constant pressure, the reaction enthalpy at $T = 500$ K can be corrected to $\Delta H_{R,500}^0 = -174.6$ kJ mol^{-1}. The detailed calculation can be found in the Supporting Material. Inserting the parameters as well as a flow rate of 1.5 L min^{-1} (considering a single reactor tube) for carbon dioxide into Eq. (10) leads to 44.1 W. In conclusion, a $S = 50$ W heat source seems to be a good estimation for the order of magnitude of a chemical reaction and was implemented into the energy model of the solid. Furthermore, the energy source was distributed equally over the entire volume of the open-cell foam. This differs to actual chemical reactions where the heat evolves at the interface between fluid and solid (i.e., in the active washcoat, [12]). Consequently, the heat source only has model character and does not simulate actual chemical reactions.

2.4. Radial averaging of CFD results

The 3D CFD temperature distributions of solid and fluid phases were averaged for a comparison with each other. For this purpose, 11 slices along the open-cell foam as well as the fluid part inside the foam were cut. Within these slices, 10 equal-area annuli further subdivided each of the axial slices (see Fig. 2). The temperature of both phases was then averaged by area-weight for their corresponding area. This procedure was done inside each of the annuli in order to get the radial 2D profile for the two phases.

3. Results and discussion

3.1. Verification of the CFD simulations

For ensuring a sufficiently high quality of the used mesh, grid independence studies were performed. For a multi-region mesh, both fluid and solid region need to be analyzed for independence separately. The maximum foam temperature was tested for grid independence since it is an investigated target value in this study. In order to address the fluid domain as well, the transferred heat flow between the fluid and solid domain is studied. For the gird independence study we chose the very same boundary conditions as applied in the latter Sections 3.2–3.4. Here, all fixed-temperature boundary conditions were set to 500 K. Hence, only the energy from the volumetric heat sources enters the system. Both tested parameters, maximum foam temperature and transferred heat flow, appear to be grid independent at a total cell number of 1.7 million cells (see Fig. 3a). To allow for a safety margin, we chose that all meshes consist of 3.7 million cells. .

In contrast to the grid-independence studies as well as the following cases (Sections 3.2–3.4), the verification was done for heating of the foam through the wall as no correlations for cases including heat sources are available. A verification of the used models was conducted using well established correlations for pressure drop and heat transfer coefficients as well as available literature data. For verifying the fluid zone, we conducted a comparison between simulated pressure drop per length obtained in this work, plotted against the superficial velocity, and the correlations of Refs. [42,43] (see Fig. 4a). The CFD results show good agreement with both correlations. For this results, isothermal conditions were assumed (i.e, ambient temperatures) which means no energy equation was solved. Using isothermal conditions is consistent with other CFD studies from the literature [44,47]. In order to verify the energy transfer of the model, conjugate heat transfer simulations were conducted. We recreated the setup used in Ref. [44] with our CFD model to compare our simulated heat transfer coefficients against their published results. Their simulative work investigates an open-cell foam (SiSiC; 20 ppi; $\epsilon_0 = 0.84$; $S_V = 1050$ m^2 m^{-3}) with geometrical properties in a comparable order of magnitude to the 10 ppi foam used in this study. They assumed a hypothetical relatively high solid thermal conductivity of $\lambda_s = 10,000$ W m^{-1} K^{-1} in order to reach a uniform temperature within their open-cell foam. We used the same thermal conductivity (instead of $\lambda_S = 15$ W m^{-1} K^{-1}) and boundary conditions for our verification. The integral heat transfer coefficient α was calculated from the simulated data by

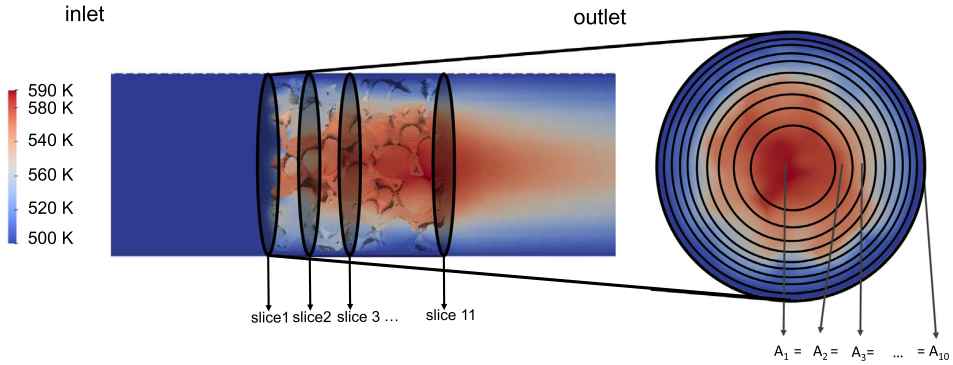

Fig. 2. Illustration of temperature averaging method. Axial slices at 11 equidistant positions (slice1, slice2, …) were further subdivided into 10 annuli along the open-cell foam. The areas of all annuli are equal. The temperature of each annulus was averaged in order to get a 2D profile for the corresponding phase.

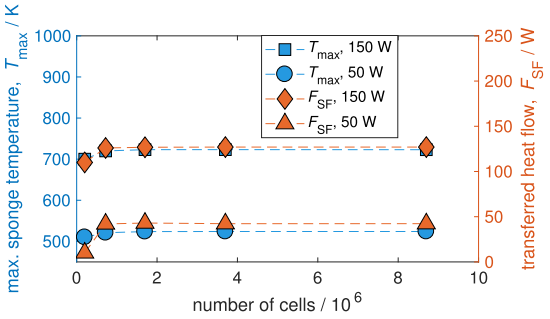

Fig. 3. Mesh-independence studies. Simulated maximum open-cell foam temperatures (T_{max}) and transferred heat flow between solid and fluid phases (F_{SF}) against number of computational cells for a superficial velocity of 0.51 m s^{-1} and for heat source intensities of 50 W and 150 W, respectively. Here, the dashed lines only serve as guidance.

$$\alpha = \frac{F_{SF}}{A \cdot \Delta T_{log}}, \quad \Delta T_{log} = \frac{T_{air,in} - T_{air,out}}{\ln \frac{T_{air,in} - T_s}{T_{air,out} - T_s}}, \tag{11}$$

with F_{SF} being the transferred heat flow between open-cell foam and fluid, A the surface area of the foam and ΔT_{log} the logarithmic temperature difference between foam and fluid. In Fig. 4b, CFD results of the present work (10 ppi) are plotted against correlations from Refs. [46,14,45] applied for the same open-cell foam (10 ppi, i.e., same open porosity and window diameter). Additionally, the CFD simulations of Ref. [44] for their 20 ppi SiSiC sample as well as the correlation for different foam types of Ref. [46], as it was presented in Ref. [44], are also plotted. The obtained CFD data from this work and the one from Ref. [44] follow the same trend and also show good agreement. This does confirm our data. However, due to the higher specific surface area and higher open porosity one would expect higher heat transfer coefficients for the 20 ppi foam [47]. For this range of porosities, the surface area is dominated by the window diameter. The windows of Ref. [44] should thus have been smaller. The higher open porosity and the lower window diameter might thus compensate the changes in the transfer coefficient and lead to the good match with between the CFD results. Furthermore, the correlation of Ref. [45] and the obtained simulated results match well. Assuming a homogeneous temperature distribution in the solid domain, this correlation was originally designed for highly conductive metal foams (Cu). In contrast, the correlations based on ceramic samples [46,14] deviate from the CFD results since they consider less conductive samples. Due to the scarce literature data available, heat transfer coefficients of open-cell foams still need more thorough research. In conclusion, the model could reproduce literature data of heat transfer coefficients and pressure drop and hence is expected to provide realistic results.

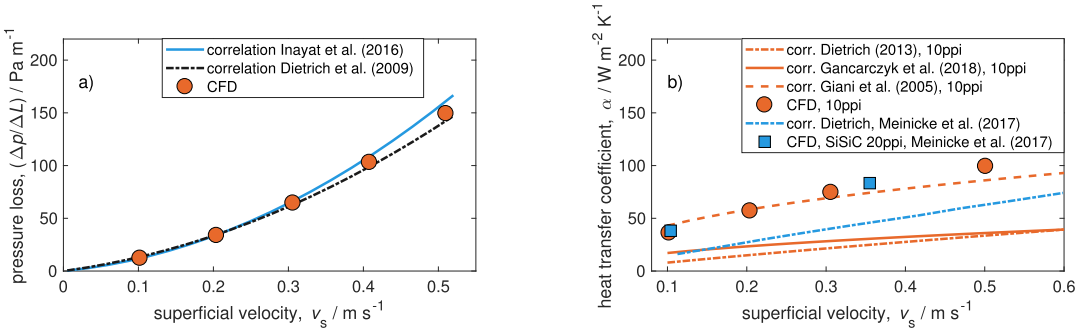

Fig. 4. Verification of the simulation results. (a) Pressure loss per unit length against superficial velocity v_s calculated with CFD (isothermal; symbols) and correlations of Ref. [42] (solid line) and [43] (dashed line). (b) Determination of heat transfer coefficient α against superficial velocity. Orange lines and symbols indicate results for this work's 10 ppi foam, whereas the blue line and symbols display literature data and correlations taken from Ref. [44]. Here the symbols represent CFD results and the lines show values that were calculated using the 10 ppi alumina foam with correlations of Ref. [45] (orange dashed line), [46] (orange dashdot line) and [14] (orange solid line). The data from [44] show good agreement in the order of magnitude with the results of this study. Their 20 ppi has a porosity of $\epsilon = 0.84$ and a specifiv surface area of $S_V = 1050$ m^2 m^{-3} (compared to $\epsilon = 0.77$ and $S_V = 521.3$ m^2 m^{-3} in this study). For comparison, the same boundary conditions were applied as in Ref. [44]. (For interpretation of the references to colour in this figure legend, the reader is referred to the web version of this article.)

3.2. Investigation of the heat flows

In this section, all fixed temperature boundaries, i.e., inlet gas temperature as well as tube walls (T_{wall}), were set to 500 K. Moreover, the foam has an initial temperature of 500 K as well. The only heat entering the system is thus caused by volumetric heat sources which represent a chemical reaction or heat production. Hence, the tube wall can be seen as actively cooled in comparison with the rest of the system. Using uniform temperature boundary conditions allows us to analyze the influence of the heat sources separately compared to settings where other thermal energy enters the tube. In order to quantify the heat flows and temperature increases, we applied five heat sources with intensities spanning from 5 W to 150 W. This covers a range of realistically occurring thermal power during chemical reactions. Generally, the foam heats up due to the induced thermal energy. The air that flows through the voids of the foam with an initial temperature of 500 K cools down the foam, eventually.

In steady-state conditions, the applied heat source power can either be transported via conduction or be transferred to the fluid via convection. This behavior can be expressed by

$$S = F_{SW} + F_{SF} \rightarrow 1 = \frac{F_{SW}}{S} + \frac{F_{SF}}{S}, \tag{12}$$

where S denotes the heat source intensity, F_{SW} denotes the heat flow that is transported from the open-cell foam to the wall and F_{SF} denotes the heat flow that is transferred between open-cell foam and fluid. In order to investigate which cooling mechanism (conduction in the solid or convective heat transfer to the fluid) is dominant in the parameter range of this study, Fig. 5a shows the ratio of conductive transported heat flow to heat source intensity (F_{SW}/S) plotted against the superficial velocity. A ratio above 0.5 shows the dominant mechanism is conduction, whereas a ratio below 0.5 indicates convective transfer being dominant (see red dashed line: transition line). The data points for the five investigated heat sources (5 W, 25 W, 50 W, 75 W and 150 W) collapse for the corresponding superficial velocities (0 m s^{-1}, 0.102 m s^{-1}, 0.204 m s^{-1}, 0.306 m s^{-1}, 0.408 m s^{-1} and 0.51 m s^{-1}) and follow a linear trend ($\frac{F_{SF}}{S} = -0.224 \cdot v_s + 0.954$, for alumina). The decrease of the conductive heat flow with increasing superficial velocities is consistent with literature [47]. All data points for alumina are above the transition line, hence conduction seems to be the dominant mechanism. The results for different materials (from alumina to mullite and s-Sic, respectively) also indicate that conduction is the dominant mechanism (Fig. 5b). Moreover, it can be deduced that higher superficial velocities are needed to actually reach a convective dominant case for all investigated materials. It is further questionable that the linear relation will be valid for higher superficial velocities since a convergence of the trend is expected (values must be between 1 and 0). According to the results in Fig. 5a and b, there is almost no effect of increasing heat source intensities on the ratio between conductive heat flow and convective heat flow for alumina and s-Sic. Only the results for the poor conducting mullite point to minor influence for low superficial velocities. In contrast, decreasing thermal conductivities lead to a shift towards convective dominance (compare blue symbols with grey symbols and orange line). This influence grows for increasing superficial velocities. An explanation for the shift towards convective dominance for lower thermal conductivities could be the shift of heat transport resistances. The ratio of heat transfer (convection) and heat transport resistances (conduction) decreases for lower thermal conductivities since the conductive resistance increases relatively.

3.3. Evaluation of the solid temperature distribution

In addition to the heat flows, the knowledge of the temperature distribution inside open-cell foams rounds up the description of thermal behavior which enables the better understanding of open-cell foams used as catalyst supports. Hence, this section examines temperature distributions as a result of applied uniform heat sources. At first glance, the alumina foam's temperature field reveals significant inhomogeneities covering a range of almost 90 K for an applied 50 W heat source (see Fig. 6). For the current boundary conditions, a higher velocity results in a better cooling of the open-cell foam, since heat transfer from the solid to the fluid is increased (i.e., convection). The temperature increase is then lower. The heat transfer between solid and fluid phases is directly coupled with the fluid's velocity field. Hence, a closer look at the fluid's velocity field can be advantageous for the understanding of the energy transport. The velocity fields of two superficial velocities (0.51 m S^{-1} and 0.102 m S^{-1}) are shown in Fig. 7a. Naturally, the magnitude of the velocity varies throughout the foam as the diameter for the passing fluid changes as well as the fluid's temperature. However, the flow around the hot-spot is stronger compared to the fluid flow on the right rear part of the foam (see Fig. 7a and b). This leads to a less effective cooling of the foam struts in the hot-spot area through the fluid and might result in an even more enhanced hot-spot temperature. As the geometry remains unchanged for all simulations, this weak current behind the hot-spot area occurs in all cases. If we assume the foam's material to be s-Sic instead of alumina, the maximum temperatures inside the foam decrease, whereas assuming mullite enhances them. This was expectable, since the results for the different materials correlate with their ability to transport heat via conduction, i.e., their thermal conductivity. The volume fraction of the open-cell foam with a certain temperature increase for different heat sources is

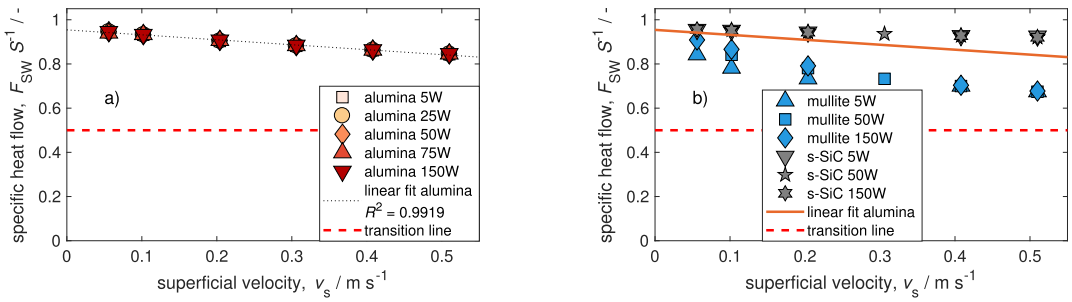

Fig. 5. Ratio of heat flow, which is transported via conduction, and applied heat source intensity. (a) Specific heat flow between the alumina open-cell foam and wall F_{SW} plotted against superficial velocity. The drawn transition line (dashed red line) represents the transition from dominant (radial) heat transport via conduction (> 0.5) to dominant heat transfer to the fluid (< 0.5). (b) Specific heat flow between open-cell foam for different materials and wall F_{SW} plotted against superficial velocity. Thermal conduction in the solid is the dominant mechanism for all investigated materials and parameters.

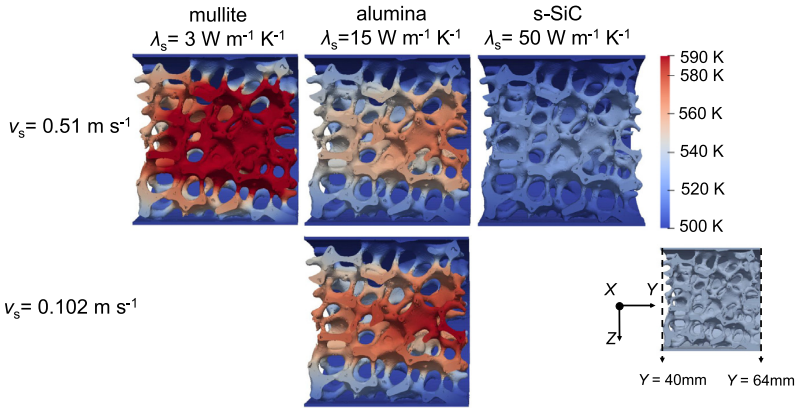

Fig. 6. Temperature distributions inside an open-cell foam for a $S = 50$ W volumetric heat source at different superficial velocities and for three different materials. The three different materials are reflected by different thermal conductivities, while the geometry is always that of a μCT-scanned alumina foam. For all cases, the temperature distribution is not uniform. Higher superficial velocities lead to increased heat transfer and thus, at given boundary conditions, lower foam temperatures.

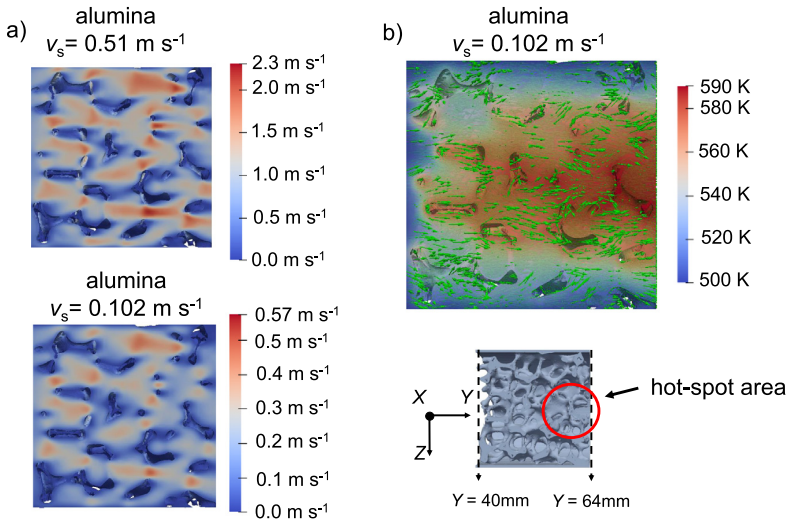

Fig. 7. Velocity field of an open-cell alumina foam for a $S = 50$ W volumetric heat source. (a) Magnitude of velocity for superficial velocities of 0.102 m s^{-1} and 0.51 m s^{-1}. (b) Velocity vectors (green arrows) for a superficial velocity of 0.102 m s^{-1} and depiction of temperature. Both figures indicate a relatively weak current behind the temperature hot-spot in the rear part of the foam. (For interpretation of the references to colour in this figure legend, the reader is referred to the web version of this article.)

shown in Fig. 8. Here, at least 15% of the volume stays cooler than $\Delta T \leqslant 10$ K for all cases. These volume parts are close to the wall and thus are efficiently cooled. With increasing velocity, heat transfer is enhanced and the open-cell foam's temperature distribution shifts to lower temperatures (compare a) vs. b)). In contrast, increasing the heat source power leads to a shift towards higher temperatures (blue bars vs. orange bars in all panels). Hence, the qualitative impact of the superficial velocity, of the thermal conductivity (material), and of the applied heat source power becomes obvious.

In order to quantify the change of the temperature distribution, Fig. 9a shows the results for the mean temperature increase (from the initial temperature 500 K) per applied thermal power ($\Delta T_{mean}/S$) plotted against the superficial velocity for alumina. It can be seen that for certain velocities (0m s, 0.102 m s^{-1}, 0.204 m S^{-1}0.306 m S^{-1}0.408 m S^{-1}0.51 m s^{-1}) the data points for the five investigated heat sources (5 W, 25 W, 50 W, 75 W and 150 W) collapse and follow a linear trend (Eq. (13)). The same trend can be observed for the maximum temperature increase per applied heat source ($\Delta T_{max}/S$) with the difference of a higher offset as well as a higher slope (Fig. 9 b) and Eq. (14). A possible explanation for the difference between mean and maximum value is the moderating influence of the prior described cool close-to-wall parts on the mean temperature distribution. In contrast to the absolute maximum temperature, the cool areas lower the mean value.

$$\frac{\Delta T_{mean}}{S} = -0.297 \cdot v_s + 0.629 \text{ (for alumina)}. \tag{13}$$

$$\frac{\Delta T_{max}}{S} = -0.796 \cdot v_s + 1.879 \text{ (for alumina)}, \tag{14}$$

Since mean and maximum temperature increases per heat source show a linear relation, it can be deduced that the entire temperature distribution obeys the same trend. Furthermore, it is expected that for higher velocities, the slope embraces asymptotic behavior since temperatures decreases would not have a physical explanation. Hence, linear behavior would not be an appropriate

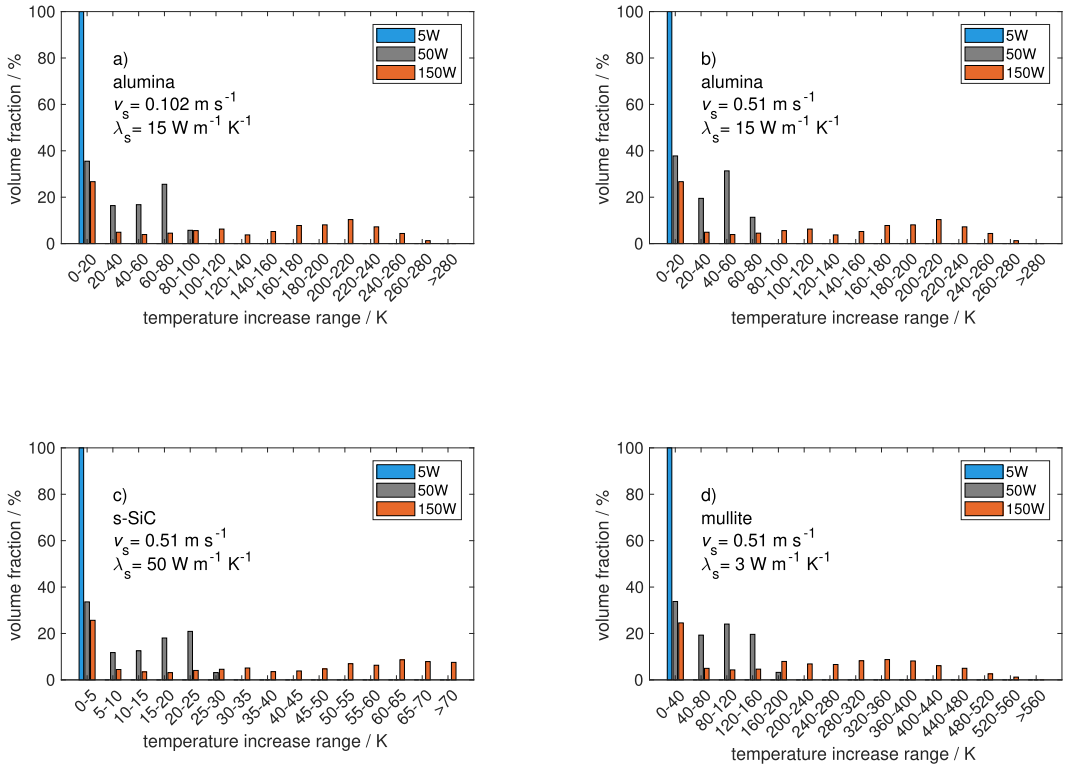

Fig. 8. Volume fraction of open-cell foams with a specific temperature increase (from initial temperature 500 K) for different implemented heat sources. (a) Alumina; superficial velocity $v_s = 0.102$ m s^{-1}, (b) alumina; superficial velocity $v_s = 0.51$ m s^{-1}, (c) s-SiC; superficial velocity $v_s = 0.51$ m s^{-1}, (d) mullite; superficial velocity $v_s = 0.51$ m s^{-1}.

assumption anymore. Nevertheless, the linear nature of the relation offers the opportunity to easily predict maximum and mean temperature increase with known thermal power and velocity for open-cell foams. Moreover, the overall temperature distribution inside the foam might be estimated. Still, this is only valid in the investigated range of parameters and assumptions made and ought to be kept in mind. When assuming s-SiC as material, the investigation again leads to a linear relation where data points of different heat sources collapse (see Fig. 9c and d). The corresponding regression equations are depicted in Appendix B. In contrast, the change to the poorly conducting mullite indicates slight non linear behavior. A possible reason might be the occurring of transport limitations, since the thermal energy cannot be transported radially sufficiently. Hence, the mullite foam heats up and a higher ratio of thermal energy is transferred to the fluid (Fig. 5b). Moreover, the expected influence becomes evident that higher thermal conductivities correlate with lower temperature increases when heat sources are implemented.

The above presented results indicate significant changes inside the open-cell foam's temperature field. Therefore, we introduce the normalized standard deviation of the temperature, T_{dev},

$$T_{dev} = \frac{\sigma}{T_{av}} = \frac{\sqrt{\sum_0^i (T_i - T_{av})^2}}{\sum_0^i i \cdot T_{av}}, \tag{15}$$

where, σ denotes standard deviation, T_{av} denotes the volume-weighted average temperature of the solid or fluid phase (inside the foam voids) and T_i denotes the temperature of a cell of the corresponding region. This number indicates the sum of the deviation of each cell's temperature from the average temperature and can be determined for both phases. A very low T_{dev} shows that the temperature field approximately is uniform. In contrast, a large T_{dev} reveals major temperature changes within the temperature field of the corresponding phase. The values for the solid phase as well as for the fluid phase are shown in Fig. 10. It can be seen, that for the same case (same material, heat source and superficial velocity), the normalized deviation of the average solid temperature $T_{dev,s}$ is generally higher than the average fluid temperature $T_{dev,f}$. This makes sense, since thermal energy is only inserted in the solid phase. Moreover, the foam has perfect wall contact which results in cool areas of the foam due to good heat transport via conduction. In contrast, the fluid can only transfer energy to the cool wall areas which have poor gas/solid heat transfer properties due to higher heat transport resistances. Generally, T_{dev} increases with higher intensity of the heat source, lower superficial velocity, and lower thermal conductivity.

Considering the often inhomogeneous heat generation of several reactions due to their characteristic kinetics, the temperature field most certainly varies even more compared to the uniformly distributed heat sources of this study. Therefore, the quantification serves as a minimum discrepancy that is to be expected when heat sources are applied. Other materials, such as metallic foams (Cu or Al) have the ability to radially conduct more thermal energy out of the system in comparison to ceramic foams and might even show no temperature increase for the investigated range of parameters in this study. Still, this needs to be investigated in the context of heat sources. It is also expected that the fluid's thermal conductiv-

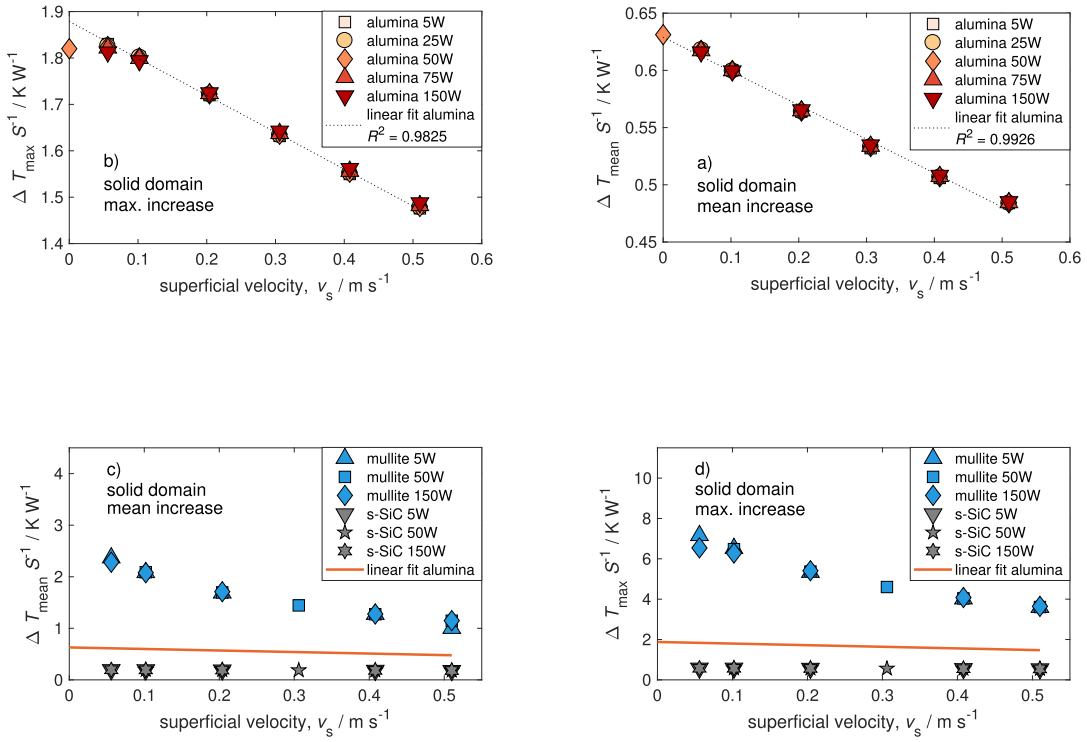

Fig. 9. Temperature increase (from initial temperature 500 K) per applied heat source intensity plotted against superficial velocity. (a) Mean temperature increase per applied heat source for alumina. (b) Maximum temperature increase per applied heat source for alumina. (c) Mean temperature increase per applied heat source for alumina (orange), s-SiC (grey) and mullite (blue). (d) Maximum temperature increase per applied heat source for alumina (orange), s-SiC (grey) and mullite (blue). (For interpretation of the references to colour in this figure legend, the reader is referred to the web version of this article.)

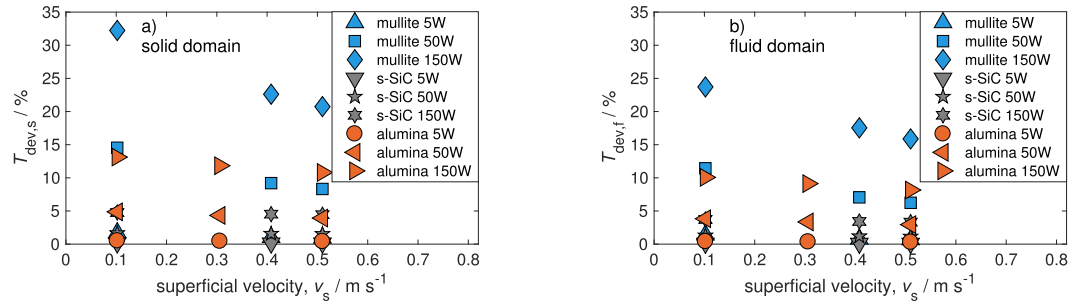

Fig. 10. Normalized deviation of temperature, T_{dev}. (a) Normalized deviation of temperature for open-cell foam, ($T_{dev,s}$), plotted against superficial velocity. (b) Normalized deviation of temperature for voids (fluid region) inside the foam, ($T_{dev,f}$), plotted against superficial velocity. The discrepancy of temperatures is generally higher for the open-cell foam in comparison to the fluid in the voids. Moreover, the lower the thermal conductivity and the lower the velocity the higher is the T_{dev}. Additionally, an increased intensity of the heat source raises T_{dev} as well.

ity λ_f [25] as well as geometrical properties [47] most certainly have an influence on the temperature distribution.

3.4. Feasibility of homogeneous models

So far, we analyzed possible outcomes of the modeling of heat production in open-cell foams and discussed whether this simplification gives new insight into the modeling and design of open-cell foams. In this section, we test whether the simplified CFD model can be reduced even more in its complexity and still yield comparable results. Therefore, we deployed radial temperature profiles of fluid and solid phases. Theoretically, the profiles of the phases could be merged in order to have a homogeneous profile. Whether this would be a valid method is discussed in the following. The 2D radial averaged temperature profiles for a 50 W heat source intensity of both, fluid and solid phases, are depicted in Fig. 11. The radial profiles at two axial positions (Position 1: $y_1 = 48$ mm, front part of foam; Position 2: $y_2 = 62$ mm, rear part of the foam) were evaluated.

For an alumina foam with a superficial velocity of 0.102 m s^{-1}, the temperature difference between the two phases stays below 10 K (compare left panel) at both positions. A higher discrepancy between the temperatures occurs in the center of the foam (low value of r/R). With increasing normalized radius the lines collapse. Furthermore, the second position indicates a general lower offset between the fluid and solid temperatures. The temperature gradi-

ents between solid and fluid are higher at the beginning of the foam compared to the rear of the foam. With increasing superficial velocity (compare left panel with left center panel) the discrepancies between the two phases grow. This makes sense as a higher superficial velocity correlates with a higher mass flow of the fluid which results in a cooler fluid. The foam's temperature is not affected by the velocity increase as much as the fluid is. One could also expect that higher velocities induce higher heat transfer, which would bring the solid and fluid temperatures closer together (as shown in Fig. 10, temperature deviation decreases). For lower velocities, the residence time for the fluid is also higher, which provides more time for developing a homogeneous temperature profile (bringing solid and fluid closer to each other). In contrast, higher velocities lead to a general cooler fluid temperature and might only cool outer parts of the struts. As the heat is produced over the entire foam volume, this would lead to hot solid cores inside the struts and higher differences between solid and fluid temperatures (i.e., a more heterogeneous temperature field). Hence, this explanation would mean that at even higher velocities (beyond investigated range of this study) the fluid and solid temperatures might even diverge further. We note that packed-bed reactors (pellets) show different behavior. The radial heat transport via conduction is significantly lower for pellets than for monolithic foams. Hence, the pellets and the fluid usually show a homogeneous temperature for high superficial velocities.

For alumina and a superficial velocity of 0.51 m s^{-1}, the absolute discrepancy between solid and fluid temperature thus increases up to 20 K. An increase of the thermal conductivity from 15 to 50 W m^{-1} K^{-1} reduces the maximum temperature discrepancies between the phases to 7 K ($v_s = 0.51$ m s^{-1}, compare right panel). In contrast, a decrease of the thermal conductivity from 15 to 5 W m^{-1} K^{-1} enhances the temperature differences up to 48 K (compare center right panel). The overall trend of higher discrepancies at the beginning of the foam as well as at a lower normalized radius can be confirmed for s-SiC and mullite.

At all axial positions as well as for all cases, discrepancies between solid and fluid temperature become apparent. The biggest differences between the phases occur in central regions of the foam (up to 48 K). Moreover, lower thermal conductivities and higher superficial velocities result in bigger discrepancies. Obviously, with bigger temperature discrepancies, the propagated error for an homogenization would increase. It can therefore be deduced that a homogenization of the CFD cases of this study would have caused tremendous errors. Nevertheless, when homogeneous models coupled with heat production are used one should limit the application to high thermal conductivities and low superficial velocities, respectively. Assuming CFD simulations deliver more precise results compared to the pseudo-homogeneous concept, the propagated error for the utilization of pseudo-homogeneous models would then decrease.

4. Conclusion

This study investigated heat flows as well as temperature distributions in open-cell ceramic foams as a result of heat production and simplified heat of reaction, respectively. We demonstrated that this approach gives new insight into the modeling and design

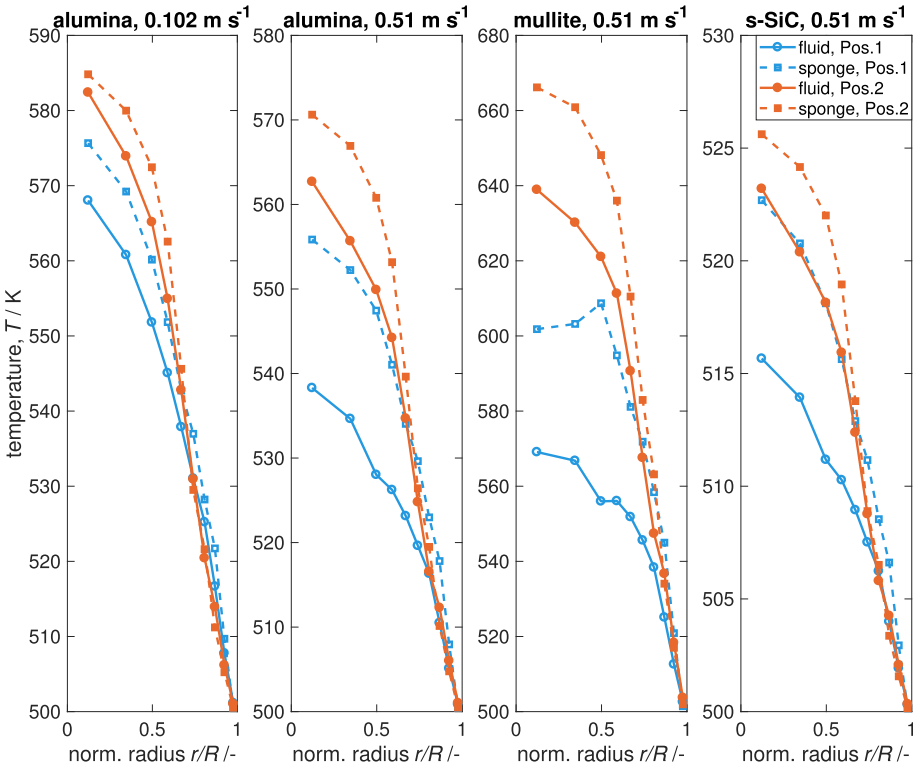

Fig. 11. Comparison of simulated radial temperature profiles for fluid and solid phases with a 50 W heat source intensity. Modeled 2D radial temperature profiles are plotted against normalized radius for 2 axial positions (Position 1: $y_1 = 48$ mm; Position 2: $y_2 = 62$ mm). Blue lines indicate axial position 1 and orange lines position 2. The solid lines depict the results for the averaged fluid's temperature, whereas the dashed lines represent the averaged solid's results. Please note the different scale of the y-axis. For all cases (except alumina at 0.102 m s^{-1}), the temperatures of both phases show considerable discrepancies. Here, the utilization of a homogeneous model would have resulted in significant deviations of the local temperature fields. (For interpretation of the references to colour in this figure legend, the reader is referred to the web version of this article.)

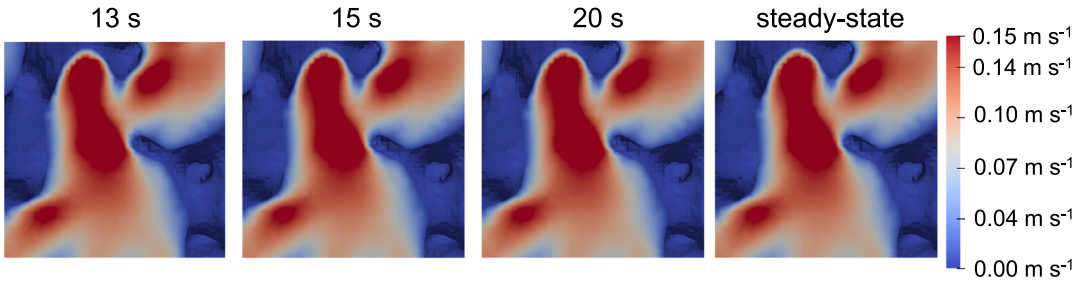

Fig. 12. Visual inspection of struts for isothermal transient (after 13, 15 and 20 s) and steady-state cases for an superficial velocity of 0.05 m s^{-1}.

of open-cell foams. The results clearly indicate that coupling conjugate heat transfer and heat production offers possibilities for better understanding heat transport and heat transfer in monolithic sponges and consequently might lead to improved foam design.

With the demonstrated estimation of occurring heat flows, the dominant mechanism can easily be determined and can be utilized for counteractions. Designers of open-cell foams can then decide whether they have to increase conduction (e.g., improve wall contact) or convection (e.g., change the foam's morphology). Furthermore, the outcome of this work helps to contribute the designing of catalyst supports of exothermal reactions in discarding unfavorable support materials or reaction setups since thermal stress can be estimated. High discrepancies in the temperature distribution of a material indicates that selecting a material with higher thermal conductivity is appropriate. For our case study (CO_2 methanation), maximum temperature increases of about 80 K (for alumina), 30 K (for s-SiC), and 300 K (for mullite) at least need to be expected in an actual reaction. Moreover, it is clearly shown that the temperature field in ceramic open-cell foams can generally not be assumed as uniform and homogeneous when heat is generated inside the solid open-cell foam in the order of magnitude of industrially relevant chemical reactions. The presented approach emphasizes the legitimate ranges of even more simplified models such as homogeneous models since temperature fields of fluid and solid phase show significant deviations. Therefore, heat sources can not only lead to improved open-cell foams but also to the development of more precise models to describe chemical reactions in open-cell foams.

Furthermore, the knowledge gained in this work underpinned the value of CFD since high resolution of temperature fields are difficult to obtain experimentally, especially for non-transparent foams (IRT) and gaseous flows (MRI, weak signals). Obviously, the applicability to actual occurring chemical reactions needs to be proven.

Declaration of Competing Interest

None.

Acknowledgments

Christoph Sinn and Jorg Thöming thank the German Research Foundation (DFG) for funding through the priority program SPP 2080 (Katalysatoren und Reaktoren unter dynamischen Betriebsbedingungen für die Energiespeicherung und -wandlung) under grant TH 893/23-1. We would like to thank Gerd Mikolajczyk from the Chair of Magnetofluiddynamics, Measurement and Automation Technology at Technical University Dresden for conducting X-ray computer tomography and analysis of the resulting data. Moreover, Christoph Sinn wants to thank Harm Ridder and Jasper Giesler for discussion and Mehrdad Sadeghi for his assistance with OpenFOAM (all Chemical Process Engineering group, Bremen). Furthermore, Christoph Sinn gives many thanks to Tobias Holzmann from Holzmann-CFD (https://holzmann-cfd.de) for his comprehensive meshing and OpenFOAM tutorials.

Appendix A. Transient isothermal simulations

In order to check the steady-state assumption, transient isothermal simulations were conducted using the default OpenFOAM pisoFOAM solver. This was done as transient vortex shredding might occur in this study's investigated parameter range. Therefore, we visually inspected the fluid areas for both, transient and steady state cases and could not find any evidence of transient behavior (see Fig. 12). To fully check the steady-state assumption for flow in open-cell foams, however, more studies with a high space and time resolution are needed in the future. .

Appendix B. Regression equations

This section shows the regression equations for the s-SiC temperature increase (from initial temperature 500 K) per applied heat source intensity. The mean temperature increase can be expressed as

$$\frac{\Delta T_{\text{mean}}}{S} = -0.032 \cdot v_s + 0.197 \ (R^2 = 0.9993), \tag{16}$$

whereas the maximum temperature increase follows

$$\frac{\Delta T_{\text{max}}}{S} = -0.077 \cdot v_s + 0.583 \ (R^2 = 0.9977). \tag{17}$$

Appendix C. Supplementary material

The provided Supplementary Material contains information about the influence of radiation on the overall heat transport, properties of the Sutherland equation, temperature corrected reaction enthalpy as well as the calculation of the evolving heat of reaction during methanation. Supplementary data associated with this article can be found, in the online version, at https://doi.org/10.1016/j.ijheatmasstransfer.2019.05.042.

References

[1] A. Reitzmann, F.C. Patcas, B. Kraushaar-Czarnetzki, Keramische schwämme - Anwendungspotenzial monolithischer netzstrukturen als katalytische packungen, 2006. https://doi.org/10.1002/cite.200600029.
[2] A. Sommers, Q. Wang, X. Han, C. T'Joen, Y. Park, A. Jacobi, Ceramics and ceramic matrix composites for heat exchangers in advanced thermal systems-A review, 2010. https://doi.org/10.1016/j.applthermaleng.2010.02.018.
[3] Z. Taslicukur, C. Balaban, N. Kuskonmaz, Production of ceramic foam filters for molten metal filtration using expanded polystyrene, J. Eur. Ceram. Soc. 27 (2–3) (2007) 637–640, https://doi.org/10.1016/j.jeurceramsoc.2006.04.129, URL http://www.sciencedirect.com/science/article/pii/S0955221906002809.

[4] X. Chen, X.L. Xia, X.L. Meng, X.H. Dong, Thermal performance analysis on a volumetric solar receiver with double-layer ceramic foam, Energy Convers. Manage. 97 (2015) 282–289, https://doi.org/10.1016/j.enconman.2015.03.066, URL http://www.sciencedirect.com/science/article/pii/S0196890415002848.

[5] S. Mey-Cloutier, C. Caliot, A. Kribus, Y. Gray, G. Flamant, Experimental study of ceramic foams used as high temperature volumetric solar absorber, Sol. Energy 136 (2016) 226–235, https://doi.org/10.1016/j.solener.2016.06.066, URL http://www.sciencedirect.com/science/article/pii/S0038092X1630247X.

[6] M.V. Twigg, J.T. Richardson, Fundamentals and applications of structured ceramic foam catalysts, Ind. Eng. Chem. Res. 46 (12) (2007) 4166–4177, https://doi.org/10.1021/ie061122o, URL http://pubs.acs.org/doi/abs/10.1021/ie061122o.

[7] I. Gräf, G. Ladenburger, B. Kraushaar-Czarnetzki, Heat transport in catalytic sponge packings in the presence of an exothermal reaction: Characterization by 2D modeling of experiments, Chem. Eng. J. 287 (2016) 425–435, https://doi.org/10.1016/j.cej.2015.11.042, URL https://www.sciencedirect.com/science/article/pii/S1385894715015855.

[8] M. Frey, A. Bengaouer, G. Geffraye, D. Edouard, A.C. Roger, Aluminum open cell foams as efficient supports for carbon dioxide methanation catalysts: pilot-scale reaction results, Energy Technol. 5 (11) (2017) 2078–2085, https://doi.org/10.1002/ente.201700188.

[9] I. Gräf, A.K. Rühl, B. Kraushaar-Czarnetzki, Experimental study of heat transport in catalytic sponge packings by monitoring spatial temperature profiles in a cooled-wall reactor, Chem. Eng. J. 244 (2014) 234–242, https://doi.org/10.1016/j.cej.2014.01.060, URL https://www.sciencedirect.com/science/article/pii/S1385894714000850?via%3Dihub.

[10] L. Kiewidt, J. Thöming, Multiscale modelling of monolithic sponges as catalyst carrier for the methanation of carbon dioxide, Chem. Eng. Sci.: X 2 (2019), https://doi.org/10.1016/j.cesx.2019.100016, 100016. URL https://www.sciencedirect.com/science/article/pii/S2590140019300231.

[11] L. Kiewidt, J. Thöming, Pareto-optimal design and assessment of monolithic sponges as catalyst carriers for exothermic reactions, Chem. Eng. J. 359 (2019) 496–504, https://doi.org/10.1016/j.cej.2018.11.109, URL https://www.sciencedirect.com/science/article/pii/S138589471832343X.

[12] S. Rönsch, J. Schneider, S. Matthischke, M. Schlüter, M. Götz, J. Lefebvre, P. Prabhakaran, S. Bajohr, Review on methanation - From fundamentals to current projects, 2016. arXiv:NIHMS150003, https://doi.org/10.1016/j.fuel.2015.10.111.

[13] Y.S. Montenegro Camacho, S. Bensaid, S. Lorentzou, N. Vlachos, G. Pantoleontos, A. Konstandopoulos, M. Luneau, F.C. Meunier, N. Guilhaume, Y. Schuurman, E. Werzner, A. Herrmann, F. Rau, H. Krause, E. Rezaei, A. Ortona, S. Gianella, A. Khinsky, M. Antonini, L. Marchisio, F. Vilardo, D. Trimis, D. Fino, Development of a robust and efficient biogas processor for hydrogen production. Part 2: Experimental campaign, Int. J. Hydrogen Energy 43 (1) (2018) 161–177, https://doi.org/10.1016/j.ijhydene.2017.10.177, URL https://www.sciencedirect.com/science/article/pii/S0360319917342854.

[14] A. Gancarczyk, M. Iwaniszyn, M. Pitek, K. Sindera, M. Korpyś, P.J. Jodłowski, J. Łojewska, A. Kołodziej, Interfacial heat and momentum transfer relation for porous media, Int. J. Therm. Sci. 132 (2018) 42–51, https://doi.org/10.1016/j.ijthermalsci.2018.04.028, URL https://www.sciencedirect.com/science/article/pii/S1290072918301091.

[15] J. Kopyscinski, T.J. Schildhauer, F. Vogel, S.M. Biollaz, A. Wokaun, Applying spatially resolved concentration and temperature measurements in a catalytic plate reactor for the kinetic study of CO methanation, J. Catal. 271 (2) (2010) 262–279, https://doi.org/10.1016/j.jcat.2010.02.008, URL https://www.sciencedirect.com/science/article/pii/S0021951710000412.

[16] J. Ulpts, W. Dreher, M. Klink, J. Thöming, NMR imaging of gas phase hydrogenation in a packed bed flow reactor, Appl. Catal. A: General 502 (2015) 340–349, https://doi.org/10.1016/j.apcata.2015.06.011, URL https://www.sciencedirect.com/science/article/pii/S0926860X15300272?via%3Dihub.

[17] J. Ulpts, W. Dreher, L. Kiewidt, M. Schubert, J. Thöming, In situ analysis of gas phase reaction processes within monolithic catalyst supports by applying NMR imaging methods, Catal. Today 273 (2016) 91–98, https://doi.org/10.1016/j.cattod.2016.02.062, URL https://www.sciencedirect.com/science/article/pii/S0920586116301729?via%3Dihub.

[18] J. Ulpts, L. Kiewidt, W. Dreher, J. Thöming, 3D characterization of gas phase reactors with regularly and irregularly structured monolithic catalysts by NMR imaging and modeling, Catal. Today 310 (2018) 176–186, https://doi.org/10.1016/j.cattod.2017.05.009, URL https://www.sciencedirect.com/science/article/pii/S0920586117303176?via%3Dihub.

[19] E. Bianchi, G. Groppi, W. Schwieger, E. Tronconi, H. Freund, Numerical simulation of heat transfer in the near-wall region of tubular reactors packed with metal open-cell foams, Chem. Eng. J. 264 (2015) 268–279, https://doi.org/10.1016/j.cej.2014.11.055, URL http://www.sciencedirect.com/science/article/pii/S1385894714015149.

[20] P. Ranut, E. Nobile, L. Mancini, High resolution X-ray microtomography-based CFD simulation for the characterization of flow permeability and effective thermal conductivity of aluminum metal foams, Exp. Thermal Fluid Sci. 67 (2015) 30–36, https://doi.org/10.1016/j.expthermflusci.2014.10.018, URL https://www.sciencedirect.com/science/article/pii/S089417771400260X.

[21] Z. Wu, C. Caliot, G. Flamant, Z. Wang, Numerical simulation of convective heat transfer between air flow and ceramic foams to optimise volumetric solar air receiver performances, Int. J. Heat Mass Transf. 54 (7–8) (2011) 1527–1537, https://doi.org/10.1016/j.ijheatmasstransfer.2010.11.037, URL https://www.sciencedirect.com/science/article/pii/S0017931010006514.

[22] A. Diani, K.K. Bodla, L. Rossetto, S.V. Garimella, Numerical investigation of pressure drop and heat transfer through reconstructed metal foams and comparison against experiments, Int. J. Heat Mass Transf. 88 (2015) 508–515, https://doi.org/10.1016/j.ijheatmasstransfer.2015.04.038, URL https://www.sciencedirect.com/science/article/pii/S0017931015003981.

[23] Z. Nie, Y. Lin, Q. Tong, Modeling structures of open cell foams, Comput. Mater. Sci. 131 (2017) 160–169, https://doi.org/10.1016/j.commatsci.2017.01.029, URL https://www.sciencedirect.com/science/article/pii/S0927025617300435.

[24] E. Bianchi, T. Heidig, C.G. Visconti, G. Groppi, H. Freund, E. Tronconi, Heat transfer properties of metal foam supports for structured catalysts: Wall heat transfer coefficient, Catalysis Today, vol. 216, Elsevier, 2013, pp. 121–134, https://doi.org/10.1016/j.cattod.2013.06.019.

[25] S. Razza, T. Heidig, E. Bianchi, G. Groppi, W. Schwieger, E. Tronconi, H. Freund, Heat transfer performance of structured catalytic reactors packed with metal foam supports: Influence of wall coupling, Catal. Today 273 (2016) 187–195, https://doi.org/10.1016/j.cattod.2016.02.058, URL https://www.sciencedirect.com/science/article/pii/S0920586116301687.

[26] M. Bracconi, M. Ambrosetti, M. Maestri, G. Groppi, E. Tronconi, A fundamental analysis of the influence of the geometrical properties on the effective thermal conductivity of open-cell foams, Chem. Eng. Process.- Process Intensificat. 129 (2018) 181–189, https://doi.org/10.1016/j.cep.2018.04.018, URL https://www.sciencedirect.com/science/article/pii/S0255270118303088.

[27] A. Della Torre, F. Lucci, G. Montenegro, A. Onorati, P. Dimopoulos Eggenschwiler, E. Tronconi, G. Groppi, CFD modeling of catalytic reactions in open-cell foam substrates, Comput. Chem. Eng. 92 (2016) 55–63, https://doi.org/10.1016/j.compchemeng.2016.04.031, URL https://linkinghub.elsevier.com/retrieve/pii/S0098135416301272.

[28] G.D. Wehinger, H. Heitmann, M. Kraume, An artificial structure modeler for 3D CFD simulations of catalytic foams, Chem. Eng. J. 284 (2016) 543–556, https://doi.org/10.1016/j.cej.2015.09.014, URL http://www.sciencedirect.com/science/article/pii/S138589471501270X.

[29] Y. Dong, O. Korup, J. Gerdts, B. Roldán Cuenya, R. Horn, Microtomography-based CFD modeling of a fixed-bed reactor with an open-cell foam monolith and experimental verification by reactor profile measurements, Chem. Eng. J. 353 (2018) 176–188, https://doi.org/10.1016/j.cej.2018.07.075, URL https://www.sciencedirect.com/science/article/pii/S1385894718313196.

[30] F. Arpino, N. Massarotti, A. Mauro, Efficient three-dimensional FEM based algorithm for the solution of convection in partly porous domains, Int. J. Heat Mass Transf. 54 (21–22) (2011) 4495–4506, https://doi.org/10.1016/j.ijheatmasstransfer.2011.06.030, URL https://www.sciencedirect.com/science/article/pii/S0017931011003528.

[31] F. Arpino, A. Carotenuto, N. Massarotti, A. Mauro, New solutions for axial flow convection in porous and partly porous cylindrical domains, Int. J. Heat Mass Transf. 57 (1) (2013) 155–170, https://doi.org/10.1016/j.ijheatmasstransfer.2012.10.030, URL https://www.sciencedirect.com/science/article/pii/S001793101200796X.

[32] M. Wallenstein, M. Kind, B. Dietrich, Radial two-phase thermal conductivity and wall heat transfer coefficient of ceramic sponges - Experimental results and correlation, Int. J. Heat Mass Transf. 79 (2014) 486–495, https://doi.org/10.1016/j.ijheatmasstransfer.2014.08.003, URL http://www.sciencedirect.com/science/article/pii/S0017931014006905.

[33] P. Ranut, On the effective thermal conductivity of aluminum metal foams: Review and improvement of the available empirical and analytical models, Appl. Therm. Eng. 101 (2016) 496–524, https://doi.org/10.1016/j.applthermaleng.2015.09.094, URL https://www.sciencedirect.com/science/article/pii/S1359431115010194?via%3Dihub.

[34] T. Fischedick, M. Kind, B. Dietrich, Radial two-phase thermal conductivity of ceramic sponges up to high temperatures experimental results and correlation, Int. J. Therm. Sci. 114 (2017) 98–113, https://doi.org/10.1016/j.ijthermalsci.2016.11.020, URL https://linkinghub.elsevier.com/retrieve/pii/S1290072916307141.

[35] H.G. Weller, G. Tabor, H. Jasak, C. Fureby, A tensorial approach to computational continuum mechanics using object-oriented techniques, Comput. Phys. 12 (6) (1998) 620, https://doi.org/10.1063/1.168744, URL http://scitation.aip.org/content/aip/journal/cip/12/6/10.1063/1.168744.

[36] H.K. Versteeg, W. Malasekera, An Introduction to Computational Fluid Dynamics: The Finite Volume Method, Pearson Education Ltd, 1995.

[37] A. Della Torre, G. Montenegro, G.R. Tabor, M.L. Wears, CFD characterization of flow regimes inside open cell foam substrates, Int. J. Heat Fluid Flow 50 (2014) 72–82, https://doi.org/10.1016/j.ijheatfluidflow.2014.05.005, URL https://www.sciencedirect.com/science/article/pii/S0142727X14000642.

[38] C. Hutter, A. Zenklusen, S. Kuhn, P.H. Rudolf von Rohr, Large eddy simulation of flow through a streamwise-periodic structure, Chem. Eng. Sci. 66 (3) (2011) 519–529, https://doi.org/10.1016/j.ces.2010.11.015.

[39] B.E. Poling, J.M. Prausnitz, J.P. O'Connell, The Properties of Gases and Liquids, fifth ed., McGraw-Hill International Editions, Chemical Engineering Series, New York, NY, 2001.

[40] A. Kopanidis, A. Theodorakakos, E. Gavaises, D. Bouris, 3D numerical simulation of flow and conjugate heat transfer through a pore scale model of high porosity open cell metal foam, Int. J. Heat Mass Transf. 53 (11–12) (2010) 2539–2550, https://doi.org/10.1016/j.ijheatmasstransfer.2009.12.067, URL https://www.sciencedirect.com/science/article/pii/S0017931009007388.

[41] L. Kiewidt, J. Thöming, Predicting optimal temperature profiles in single-stage fixed-bed reactors for CO2-methanation, Chem. Eng. Sci. 132 (2015) 59–71, https://doi.org/10.1016/j.ces.2015.03.068, URL https://www.sciencedirect.com/science/article/pii/S0009250915002523?via%3Dihub.

[42] A. Inayat, M. Klumpp, M. Lämmermann, H. Freund, W. Schwieger, Development of a new pressure drop correlation for open-cell foams based completely on theoretical grounds: Taking into account strut shape and geometric tortuosity, Chem. Eng. J. 287 (2016) 704–719, https://doi.org/10.1016/j.cej.2015.11.050, URL https://ac.els-cdn.com/S1385894715015934/1-s2.0-S1385894715015934-main.pdf?_tid=e8beb7d8-f85e-11e7-ac38-00000aacb35e&acdnat=1515847398_b31edb2fb3ef18c19680fc69fc773143.

[43] B. Dietrich, W. Schabel, M. Kind, H. Martin, Pressure drop measurements of ceramic sponges-Determining the hydraulic diameter, Chem. Eng. Sci. 64 (16) (2009) 3633–3640, https://doi.org/10.1016/j.ces.2009.05.005, URL http://www.sciencedirect.com/science/article/pii/S0009250909003133.

[44] S. Meinicke, T. Wetzel, B. Dietrich, Scale-resolved CFD modelling of single-phase hydrodynamics and conjugate heat transfer in solid sponges, Int. J. Heat Mass Transf. 108 (2017) 1207–1219, https://doi.org/10.1016/j.ijheatmasstransfer.2016.12.052, URL http://www.sciencedirect.com/science/article/pii/S0017931016323201.

[45] L. Giani, G. Groppi, E. Tronconi, Heat transfer characterization of metallic foams, Ind. Eng. Chem. Res. 44 (24) (2005) 9078–9085, https://doi.org/10.1021/ie050598p, URL http://pubs.acs.org/doi/abs/10.1021/ie050598p.

[46] B. Dietrich, Heat transfer coefficients for solid ceramic sponges Experimental results and correlation, Int. J. Heat Mass Transf. 61 (2013) 627–637, https://doi.org/10.1016/j.ijheatmasstransfer.2013.02.019, URL http://www.sciencedirect.com/science/article/pii/S0017931013001348. http://linkinghub.elsevier.com/retrieve/pii/S0017931013001348.

[47] M. Zafari, M. Panjepour, M.D. Emami, M. Meratian, Microtomography-based numerical simulation of fluid flow and heat transfer in open cell metal foams, Appl. Therm. Eng. 80 (2015) 347–354, https://doi.org/10.1016/j.applthermaleng.2015.01.045, URL http://www.sciencedirect.com/science/article/pii/S1359431115000599.

Chapter 5

Validity of Heat Sources

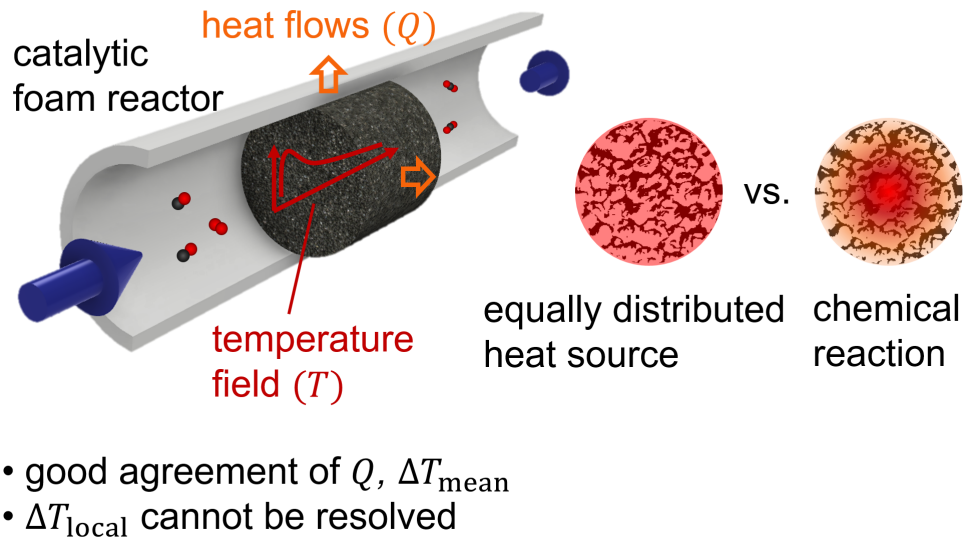

FIGURE 5.1: Graphical abstract of the manuscript dealing with the comparison of heat sources against fully-resolved reactions.

This chapter consists of the manuscript *Heat Transport in Open-Cell Foams: CFD Analysis of Artificial Heat Sources vs Fully Resolved Exothermal Reactions* (Sinn et al., 2021a)[1].

An open question from the previous chapters certainly is how the thermal fields and heat flows from the heat source simplification compare to an actual exothermal catalytic reaction. This chapter aims to close this knowledge gap. To understand similarities and differences of the two approaches, the strongly exothermal CO oxidation is implemented as model reaction and compared to a literature experiment and simulation for plausibility (Dong et al., 2018). The comparison of the fully resolved reaction with the heat source simplification reveals what information can and cannot be gathered from the heat source simplification (Figure 5.1).

[1]The Supporting Documents can be found in Appendix B.

I&EC research
Industrial & Engineering Chemistry Research
pubs.acs.org/IECR
Article

Heat Transport in Open-Cell Foams: CFD Analysis of Artificial Heat Sources vs Fully Resolved Exothermal Reactions

Christoph Sinn,[§] Jonas Wentrup,[§] Georg R. Pesch,* and Jorg Thöming

Cite This: *Ind. Eng. Chem. Res.* 2021, 60, 4542−4551
Read Online

ABSTRACT: Catalytic structured foam reactors show promising characteristics for process intensification such as low pressure drop, high specific surface area, and remarkable heat transport. Especially for the design of small-scale dynamically operated reactors, the understanding of heat transport is crucial. With computational fluid dynamics (CFD), we can thoroughly investigate the thermal field of the coupled gas/solid under reaction conditions and understand heat transport in structured reactors. In the past, we mimicked the heat production during exothermal reactions with uniformly distributed volumetric heat sources in the solid. Here, we compare thermal fields of such simplifications with full-model calculations using the strongly exothermal CO oxidation as a model reaction. We find that heat flows of the reaction and of artificial heat source calculations match well, and reliable mean temperature increases can be computed. While it cannot compute exact hot-spot magnitude and location, this method helps to determine heat removal mechanisms and estimate thermal stress.

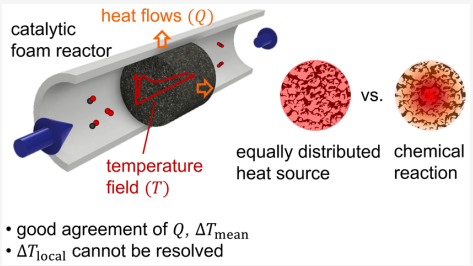

1. INTRODUCTION

Open-cell foams are interconnected cellular materials that combine desirable characteristics for catalyst carriers such as low pressure drop, high surface areas, and excellent radial heat transport.[1,2] When used as catalyst carriers, they allow us to decouple and thus optimize catalyst coatings and the foam individually.[3] Their ability to efficiently remove (or supply) heat from strongly exothermal (or endothermal) reactions makes them especially interesting to control temperatures and reaction progress.[4] This way, temperature hot spots (or cold spots) in catalytic structured beds can be reduced. Hot spots are undesired during exothermal reactions as they might harm the catalysts through sintering or cause thermal runaway (e.g., during Fischer−Tropsch synthesis).[5] The outstanding potential of open-cell foams for process intensification has been shown for the CO_2 methanation, Fischer−Tropsch synthesis, CH_4 combustion, and other processes.[6−8] A recent study, however, showed that open-cell foams embedded in reactors (i.e., structured reactors) are only advantageous over conventional pellet-bed reactors when heat is mainly removed radially via conduction (i.e., to the wall) and not axially via convection (i.e., through the fluid).[9] For the design of efficient and robust structured reactors, it is therefore important to understand the fundamental heat transport mechanisms, namely, conduction, convection, and radiation. Further, the thermal behavior, and thus, the performance of catalytic foams during exothermal (and endothermal) reactions needs more extensive research to design foams perfectly tailored for their usage.[10,11]

The thermal behavior of open-cell foams can be studied using three-dimensional (3D) computational fluid dynamics (CFD) simulations. They allow us to predict local temperatures and heat flows undisturbed (from e.g., experimental probes) and give valuable insight into transport phenomena that are not yet fully understood. The required geometrical representation of the foams for CFD simulations can be obtained through images (e.g., μCT scans[12,13]), idealized geometries (e.g., periodic open-cell foams (POCS)[14,15]), or computer algorithms (e.g., tessellations[16,17]). Several researchers used CFD to investigate the thermal performance of open-cell foams. For instance, the effect of foam-wall coupling on temperatures and heat transfer was analyzed.[18,19] Furthermore, different foam morphologies and materials were studied with respect to heat transport mechanisms.[20−23] In different studies, the strut diameter and the strut-to-node ratio were found to be especially influential on the foam's ability to transport and remove heat radially via conduction.[15,24] Additionally, the amount of solid content (i.e., porosity) is a key driver for radial heat transport.[25,26] Distributing the solid material preferentially in a radial direction further increases the radial heat exchange.[23]

So far, CFD studies on catalytic reactions in foams have rarely been published and often dealt with the CO oxidation

Received: December 9, 2020
Revised: March 2, 2021
Accepted: March 3, 2021
Published: March 16, 2021

https://dx.doi.org/10.1021/acs.iecr.0c05982
Ind. Eng. Chem. Res. 2021, 60, 4542−4551

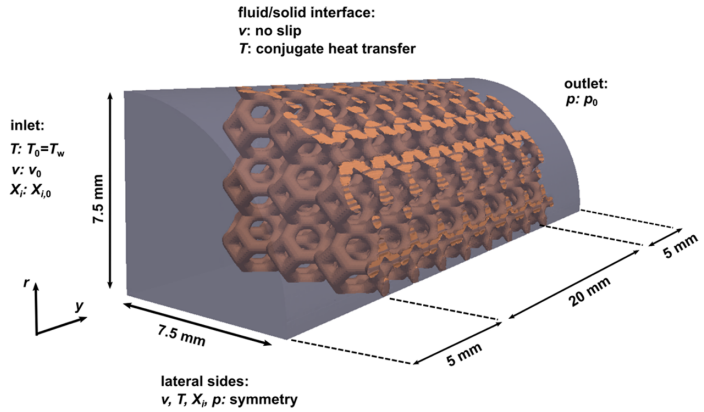

Figure 1. Geometry and boundary conditions of the CFD model.

reaction,[27−29] as this reaction is a popular model reaction.[30] It has fast kinetics (e.g., for Pt[31]), so that short catalytic beds are sufficient for high conversion rates. The kinetics of the reaction can be implemented by three general approaches: (1) infinitely fast reaction,[27,32,33] (2) rate-determining step,[28] or (3) microkinetics.[16,29] Both accuracy and computational cost increase from the first to the third due to an increase in the number and complexity of equations that are solved. Simulating full-field catalytic reactors usually requires a high modeling effort and a lot of knowledge about the catalyst activity as well as the reaction routes of all participating species.[34,35] Additionally, postprocessing and evaluation of the results might be challenging due to complex interactions of reaction kinetics and transport phenomena.

To study heat flows and temperature fields of open-cell foam catalyst carriers decoupled from actual reactions, we proposed to mimic the exothermicity (or endothermicity) of the reaction through uniform volumetric heat sources (or sinks) in the solid foam.[36] Heat sources are easy to implement and simplify the reaction model to a pure conjugate heat transfer problem. We previously investigated steady-state heat transfer in a 10 ppi μCT foam using air as fluid.[36] The resulting heat flows for several heat source intensities (5−150 W), for a range of superficial velocities (0−0.51 m s^{-1}), and thermal conductivities (1−50 W m^{-1} K^{-1}) revealed that conduction was the dominant heat removal mechanism for these conditions. Furthermore, temperature fields of both fluid and solid phases for the same parameter range showed significant temperature inhomogeneities and, thus, thermal stress for the catalytic foam. The same approach was also used to quantify the impact of thermal radiation on the heat transport for different temperature levels, thermal conductivities, and superficial velocities,[37] for an increased velocity (0.5−4 m s^{-1}) and pressure range (1−10 bar)[38] as well as to conduct a structure-heat transport analysis.[25]

The heat source approach assumes homogeneously and volumetrically distributed heat production. This contrasts actual catalytic reactions in which the evolving heat in the reactor usually varies locally due to spatially varying kinetics. Obviously, such approaches yield differences in computed temperature fields. To quantify the difference between both approaches, in this study, we compare the resulting heat flows and 3D temperature fields of exothermal reactions with the ones resulting from uniformly distributed heat sources in the solid foam. For this purpose, we use CFD to model CO oxidation (as a model reaction) and compare the temperatures and species concentrations against literature studies. Simpler approaches such as pseudo-homogeneous models do not deliver reliable temperatures in the parameter range of this study.[36,37] The evolving heat of reaction is further used as an input parameter for the simplified heat source approach. We then analyze the suitability of the approach for a variety of superficial velocities (i.e., volume flows) and thermal conductivities. We focus the investigation on the computed heat flows (to evaluate the heat removal mechanism) as well as the mean and maximum temperature increases (to estimate the thermal stress and hot spot formation). With this study, we highlight and quantify the suitability, potential, and limitations of the heat source approach for the thermal assessment of catalytic foams.

2. METHODS

2.1. Geometrical Model and Meshing. We generated a CFD setup similar to the recent study by Dong et al.[29] (see Figure 1). They simulated CO oxidation over Pt in a fixed-bed reactor filled with a μCT-reconstructed 45 ppi foam and validated their model by their own experiments. We rebuilt their CFD setup but simplified the reticulated foam geometry with a Kelvin cell lattice (i.e., tetrakaidekahedral unit cell lattice; see Figure 1). Such a model foam is very popular and common for investigating open-cell foam geometries without recreating the exact strut network.[28,39−41] This morphological simplification saves a lot of computational costs and allows for an extensive parameter variation (e.g., the effect of fluid or solid properties, boundary conditions, etc.). Recently, unit cell structures attracted additional interest as POCS catalyst supports.[42,43] Recent advances in 3D-printing capability allow for tailored and well-defined monoliths that are individually manufactured for their application.[15] The Kelvin cell lattice was generated using the CAD software Autodesk Fusion 360 (Autodesk, Inc., San Rafael, CA),[44] and its properties are shown in Table 1.

The computational effort of this study was further reduced using only a quarter clip of the monolith (see Figure 1). In contrast to reticulated open-cell foams, the Kelvin cell lattice is isotropic. Thus, a quarter clipping combined with symmetry boundary conditions does not cause any loss of information. All principal boundary conditions are included in Figure 1 for

https://dx.doi.org/10.1021/acs.iecr.0c05982
Ind. Eng. Chem. Res. 2021, 60, 4542−4551

Table 1. Kelvin Cell Properties

cell diameter, d_c (mm)	1.924
strut diameter, d_s (mm)	0.591
open porosity, ε_o (dimensionless)	0.724
specific surface area, S_V (1/m)	1467.8

illustration. At the inlet, the temperature $T = T_0$, fluid velocity $v = v_0$, and molar fractions $X_i = X_{i0}$ are defined for each species i. The inlet boundary conditions are set to T_0 = 1000 K and X_{i0} ($CO/O_2/Ar$) = 0.133/0.066/0.801 in all cases. Constant pressure p is implemented at the outlet. At the fluid/solid interface, a no-slip condition is applied for the velocity, and the conjugate heat transfer is solved for the temperature. At the wall, the temperature is set to a constant value (T_w = 1000 K), equivalent to previous heat source investigations,[36,37] and a no-slip condition is applied for the velocity. Equivalent to the study from Dong et al.,[29] the model was meshed using polyhedral cells and solved using the CFD software STAR-CCM+ (Siemens PLM, Plano, TX).[45] The grid independent study and a depiction of the used mesh can be found in the Supporting Information (Figures S3 and S4). All relevant simulation assumptions are listed in Table 2. Furthermore, the washcoat factor $F_{cat/geo}$ was set to be 0.03 in all simulations as suggested by Dong et al.[29]

Table 2. Model Properties and Assumptions

reaction conditions		
outlet pressure	p	100 kPa
inlet temperature	T_0	1000 K
wall temperature	T_w	1000 K
superficial velocity	v_0	0.1−0.5 m s^{-1}
inlet molar fractions	X_i (CO/O_2/Ar)	0.133/0.066/0.801
washcoat factor	$F_{cat/geo}$	0.03
fluid properties		
dynamic viscosity	μ	Mathur−Saxena averaging
isobaric heat capacity	$c_{p,f}$	mass-weighted mixture
thermal conductivity	λ_f	Mathur−Saxena averaging
density	ρ_f	ideal gas law
species' diffusion coefficients	$D_{i,m}$	mass-weighted diffusion model
foam properties		
thermal conductivity	λ_s	2, 10, 50 W m^{-1} K^{-1}
heat capacity	$c_{p,s}$	1000 J kg^{-1} K^{-1}
density	ρ_s	2500 kg m^{-3}
solid emissivity	ε	0.9
additional models		
gravitational forces		neglected
radiation		surface-to-surface (S2S) model
turbulence		neglected
gas-phase reactions		neglected

2.2. Numerical Modeling and CFD Procedure. In this study, the numerical calculation of the reactive-flow simulation follows the general conservation of mass, momentum, species, and energy within the commercial STAR-CCM+ software package. As stated in Table 2, the steady-state model neglects gravitational forces, turbulent effects, and homogenous gas-phase reactions. The conservation of mass is expressed as

$$\nabla\cdot(\rho_f\vec{v}) = 0 \tag{1}$$

where ρ_f is the fluid's density and $\vec{v}$ is the three-dimensional velocity field. Momentum conservation is solved via

$$\nabla\cdot(\rho_f\vec{v}\otimes\vec{v}) + \nabla p + \nabla\cdot\boldsymbol{\tau} = 0 \tag{2}$$

where p is the pressure and τ is the stress tensor for Newtonian fluids

$$\boldsymbol{\tau} = \mu_f[\nabla\otimes\vec{v} + (\nabla\otimes\vec{v})^T] - \frac{2}{3}\mu_f(\nabla\cdot\vec{v})\mathbf{I} \tag{3}$$

with μ_f being the dynamic viscosity and $\mathbf{I}$ the unit matrix. The conservation of each species i is defined as

$$\nabla\cdot(\rho_f Y_i\vec{v}) + \nabla\cdot\vec{j}_i = R_i^{het} \tag{4}$$

where Y_i is the species' mass fraction, $\vec{j}_i$ is the diffusion mass flux, and R_i^{het} is the net rate of species production at the catalytic surface. The diffusion mass flux is calculated as

$$j_i = -\rho_f\frac{Y_i}{X_i}D_{i,m}\nabla X_i \tag{5}$$

where X_i is the mass fraction of species i. $D_{i,m}$ is the mass-averaged diffusion coefficient

$$D_{i,m} = \frac{1 - Y_i}{\sum_{j\neq i}^{N_s}(X_j/D_{j,i})} \tag{6}$$

using the binary diffusion coefficients $D_{j,i}$ of species j and i in the mixture of N_s species. Energy conservation is expressed as

$$\nabla\cdot(\rho_f\vec{v}h_f) + \nabla\cdot\vec{j}_q - \vec{v}\nabla p + \sum_i(h_i^0\cdot R_i^{het}) = 0 \tag{7}$$

where h_f is the fluid mixture's enthalpy, $\vec{j}_q$ is the diffusive heat flow, and $\sum_i(h_i^0\cdot R_i^{het})$ is the heat production caused by chemical reactions, with h_i^0 being the standard enthalpy of formation of the species. Obviously, heat production due to heterogeneous catalytic reactions occurs only in the fluid cells that bound on the solid domain.

The diffusion heat flow is defined as

$$j_q = -\lambda_f\nabla T + \sum_{i=1}^{N_s}(h_i j_i) \tag{8}$$

where λ_f is the thermal heat conductivity of the fluid. The species' enthalpies h_i and the mixture's enthalpy h_f are connected via

$$h_f = \sum_{i=1}^{N_s} Y_i h_i(T) \tag{9}$$

As usual, for gas-phase reactions, the set of the fluid's governing equations is completed by the ideal gas law

$$p = \frac{\rho_f RT}{\sum_{i=1}^{N_s}(X_i M_i)} \tag{10}$$

where R is the universal gas constant and M_i is the molar mass of species i. The solid phase is described only by the conservation of energy

$$\nabla\cdot(-\lambda_s\nabla T) = 0 \tag{11}$$

where λ_s is the solid thermal conductivity. In the case of the heat source approximation, the set of equations reduces and simplifies. The conservation equation of species (eq 4) and the reaction term in the fluid energy balance (eq 7) are omitted.

https://dx.doi.org/10.1021/acs.iecr.0c05982
Ind. Eng. Chem. Res. 2021, 60, 4542−4551

Table 3. Surface Mechanisms for CO Oxidation on Pt Catalyst Used in This Study[b]

k	reaction	A_k (cm mol^{-1} s^{-1})	β_k (dimensionless)	E_{a_k} (kJ mol^{-1})
1	CO + Pt(s) → CO(s)	1.618×10^{20}	0.5	0
2	O_2 + 2 Pt(s) → 2O(s)	0.023[a]		
3	CO_2 + Pt(s) → CO_2(s)	0.005[a]		
4	CO(s) + O(s) → CO_2(s) + Pt(s)	3.7×10^{21}	0	105.0
5	CO(s) + Pt(s) → C(s) + O(s)	1.0×10^{18}	0	184.0
6	C(s) + O(s) → CO(s) + Pt(s)	3.7×10^{21}	0	62.8
7	CO(s) → CO + Pt(s)	1.0×10^{13}	0	125.5
8	2O(s) → O_2 + 2Pt(s)	3.7×10^{21}	0	213−60 $\theta_{O(s)}$
9	CO_2(s) → CO_2 + Pt(s)	1.0×10^{13}	0	20.5

[a]Sticking coefficient (dimensionless). [b]Values from Deutschmann et al.[31]

The fluid phase is described as single species with one set of fluid properties. In contrast to the actual reaction, the heat production is added as heat source term (S_{rel}) in the solid energy balance (eq 11)

$$\nabla\cdot(-\lambda_s\nabla T) + S_{rel} = 0 \tag{12}$$

Due to high temperatures, the heat transport by thermal radiation was modeled in addition to the energy balance equations for conductive and convective heat transport. Dong et al.[29] showed a significant error in the resulting temperature field when neglecting radiation effects. We additionally examined the influence of radiation for our test case (see Figure S5). Equivalent to the study by Dong et al.,[29] the surface-to-surface model within STAR-CCM+ was used. It calculates a matrix of view factors for all solid surface cells via ray tracing prior to the actual simulation. These view factors are later used to compute the thermal energy exchange between the surfaces. The fluid phase is treated as a nonparticipating medium, which was shown to be valid for applications of gas-phase reactions.[46,47]

On the catalytic surface, species' production or consumption via chemical reaction is calculated by balancing the diffusive mass flux normal to the surface and the net rate of heterogeneous surface reactions

$$\vec{n}\cdot\vec{j}_i = \eta F_{cat/geo} M_i \dot{s}_i \tag{13}$$

where $\vec{n}$ is the unit vector normal to the surface, η is the effectiveness factor, $F_{cat/geo}$ is the ratio of catalytically active surface and geometrical surface, and $\dot{s}_i$ is the molar surface reaction rate of the species.

The reaction rates for a set of R_s reactions are solved via the elementary mass-action kinetics

$$\dot{s}_i = \sum_{k=1}^{R_s} \upsilon_{i,k} k_k \prod_{j=1}^{N_s} c_j^{\upsilon'_{i,k}} \tag{14}$$

where $\upsilon_{i,k}$ are the stoichiometric coefficients, k_k are the rate constants, and c_j are the species' molar concentrations. All rate constants are determined in terms of the Arrhenius expression

$$k_k = A_k T^{\beta_k} \exp\left(-\frac{E_{a_k}}{RT}\right) \prod_{i=1}^{N_s} \theta_i^{\mu_{i_k}} \exp\left(\frac{\varepsilon_{i_k}\theta_i}{RT}\right) \tag{15}$$

where A_k is the pre-exponential factor, β_k is the temperature exponent, and E_{a_k} is the activation energy. The reaction order and activation energy are influenced by the number of occupied surface sites and corrected via the surface coverage of species i, θ_i, in combination with two correction terms μ_{i_k} and ε_{i_k}. The adsorption processes of O_2 and CO_2 are modeled via a sticking coefficient S_i

$$\dot{s}_i = \frac{S_i}{1 - 0.5S_i}\sqrt{\frac{RT}{2\pi M_i}}\, c_i \tag{16}$$

The elementary surface reaction mechanism for the CO oxidation over Pt from Deutschmann et al.[31] is implemented as a kinetic model, equivalent to the study by Dong et al.[29] The k values of all reactions are listed in Table 3.

3. RESULTS AND DISCUSSION

3.1. Literature Comparison and Mesh Independence. To check the plausibility of the implemented reactive CFD model, we re-created the conditions of the experimental and numerical study from Dong et al.[29] The reference study analyzed the CO oxidation reaction on a reticulated 45 ppi foam. The Kelvin cell geometry in this work was used to construct a geometry with similar properties. Therefore, we do not aim for an exact model validation but rather ensure reliable and plausible results. The assessment can be found in the Supporting Information (Section 1) and shows the general plausibility of the reactive model for the investigated parameter range. Furthermore, a grid independence study was conducted confirming mesh-independent behavior or the results (see the Supporting Information, Figure S3). A comparison of the pressure drop along the reactor against common correlations is also provided in the Supporting Information (Figure S2).

3.2. Heat Production of CO Oxidation. This study investigates heat transport in foams as a result of heat production due to exothermal reactions. Previous studies identified the superficial velocity v and the solid thermal conductivity λ_s as two major parameters influencing heat transport phenomena inside a catalytic reactor.[25,36] Before analyzing the effect of both values on the applicability of artificial heat sources, we investigate their impact on the catalytic reaction itself. Four different superficial velocities (v = 0.1, 0.2, 0.34, 0.5 m s^{-1}) and three different solid thermal conductivities (λ_s = 2, 10, 50 W m^{-1} K^{-1}) representing common ceramic materials[48] were implemented. The analysis is conducted for the constant temperature boundary condition $T_0 = T_w$ = 1000 K. The resulting CO conversion and released reaction heat Q_{prod} are listed in Table 4 for all cases. Note that the Q_{prod} values in Table 4 account only for the simulated quarter reactor. Consequently, to calculate the total heat production of the complete reactor it is multiplied by 4. The resulting Q_{prod} per parameter combination is then used as input for the heat source intensity for comparison (Section 3.3). In general, for the given boundary conditions, the CO conversion

https://dx.doi.org/10.1021/acs.iecr.0c05982
Ind. Eng. Chem. Res. 2021, 60, 4542−4551

Table 4. CO Conversion and Released Reaction Heat Q_{prod} for Different Inlet Superficial Velocities v and Solid Thermal Conductivities λ_s

v [m s^{-1}]	λ_s [W m^{-1} K^{-1}]	conversion [dimensionless]	Q_{prod} [W]
0.5	2	0.97	10.4
0.5	10	0.85	9.26
0.5	50	0.69	7.48
0.34	2	0.99	7.21
0.34	10	0.97	7.08
0.34	50	0.91	6.59
0.2	2	0.99	4.24
0.2	10	0.99	4.24
0.2	50	0.99	4.24
0.1	2	0.99	2.15
0.1	10	0.99	2.14
0.1	50	0.99	2.14

decreases with superficial velocity and solid thermal conductivity. The velocity dependence is due to a decreasing residence time with increasing velocity. The dependence on solid thermal conductivity comes from the improved heat transport causing overall lower temperatures and thus kinetic limitations. For the superficial velocities v = 0.1 and 0.2 m s^{-1}, nearly full conversion is reached for all cases independent of solid thermal conductivity. For v = 0.34 m s^{-1} and, especially, v = 0.5 m s^{-1}, the conversion clearly decreases with increasing conductive heat transport. Moreover, despite lower conversions, the evolving reaction heat increases with the flow rate. The reason is simply a higher mass flow entering the system, which leads to a higher heat release. Obviously, at constant v, the reaction heat decreases in concert with CO conversion.

3.3. Comparison of Heat Sources with the CO Oxidation Reaction. To compare evolving reaction heat with homogeneously distributed heat sources, the same intensities of heat releases (as listed in Table 4) were implemented in the solid foam for the corresponding heat source cases. A general comparison of the temperature distributions within the solid region between a reaction case and a heat source case is shown in Figure 2, depicting the case for v = 0.5 m s^{-1} and λ_s = 2 W m^{-1} K^{-1}. The fluid flow direction is from the left to the right (the wall is at the top). The main difference between the two approaches is obvious from this picture: The reaction generates a temperature hot spot in the first part of the foam structure, which is absent in the heat source approach. The kinetics are temperature-dependent and more heat is produced at increased temperatures. This leads to self-amplifying reaction rates and local hot spots.

The exact location and magnitude of the hot spot depend on the reaction conditions and the resulting local CO conversion. As shown in Table 4, the overall CO conversion is close to 100% in many cases, especially at low solid thermal conductivities. However, some differences in the axial CO concentration profiles can be observed at different velocities. Figure 3 shows the axial CO mole fractions in the center (Figure 3a) and the corresponding temperature profiles (Figure 3b) for λ_s = 2 W m^{-1} K^{-1} at all four investigated superficial velocities. The stronger heat release at higher velocities is evident from the resulting temperatures (Figure 3b). Further, the slope of the CO concentration profile influences the hot spot location. At low velocities, the

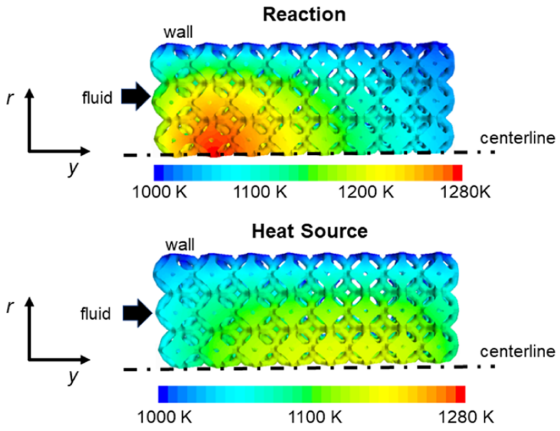

Figure 2. Comparison of the temperature distribution within the solid region in case of an exothermal reaction (CO oxidation; top) and a nonreactive conjugate heat transfer simulation including a volumetric uniformly distributed heat source (bottom). The heat production is the same in both cases. Conditions: v = 0.5 m s^{-1} and λ_s = 2 W m^{-1} K^{-1}.

residence time is high, which leads to steep concentration profiles and a concentrated heat release close to the front of the reactor. In contrast, at high flow rates (as the example case of Figure 2), the heat release is less localized. In combination with the convective heat transport, the temperature hot spot location is pushed closer toward the rear of the foam. Still, in all shown cases, almost full conversion is achieved in the first half of the foam (y < 10 mm), leading to maximum temperatures in the front half.

In contrast, the maximum temperatures in the heat source cases always occur in the rear of the foam (see Figure 2) and cover a broader area (i.e., less local). The shifted hot spot location is caused by the uniformly implemented heat production coupled with the convective cooling in the front part of the foam. This was also reported in a previous study[36] and demonstrates the inaccuracy of homogeneously implemented heat sources in contrast to actual locally distributed heat production. In the homogeneous heat source approach, the fluid flow cools the solid foam most effectively at the beginning of the structure (because the fluid is coolest at the inlet), resulting in higher temperatures at the end. In typical exothermal gas-phase reactions, however, while the fluid still cools best in the front, the reaction rates are usually the highest in front, resulting in a temperature hot spot in or near the catalyst entrance (e.g., CO_2 methanation reaction[49]). Additionally, the concentrated heat release leads to a higher maximum temperature in case of a chemical reaction, which is here as high as 1300 K in contrast to about 1200 K in the case of the heat source (Figures 2 and 4).

This opposing axial tendency of the temperature profiles in the heat source cases is present at all investigated flow rates (see Figure 4). The resulting maximum temperatures increase with superficial velocities in the heat source case, which is caused by an increasing heat source intensity. The value of the heat source is tied to the value resulting from the equivalent reaction case (see Table 4). The largest absolute deviation in the maximum temperature is at v = 0.5 m s^{-1} (see Figure 4d). Generally, the absolute deviation in temperatures between the two approaches increases with the heat of reaction. In our

https://dx.doi.org/10.1021/acs.iecr.0c05982
Ind. Eng. Chem. Res. 2021, 60, 4542−4551

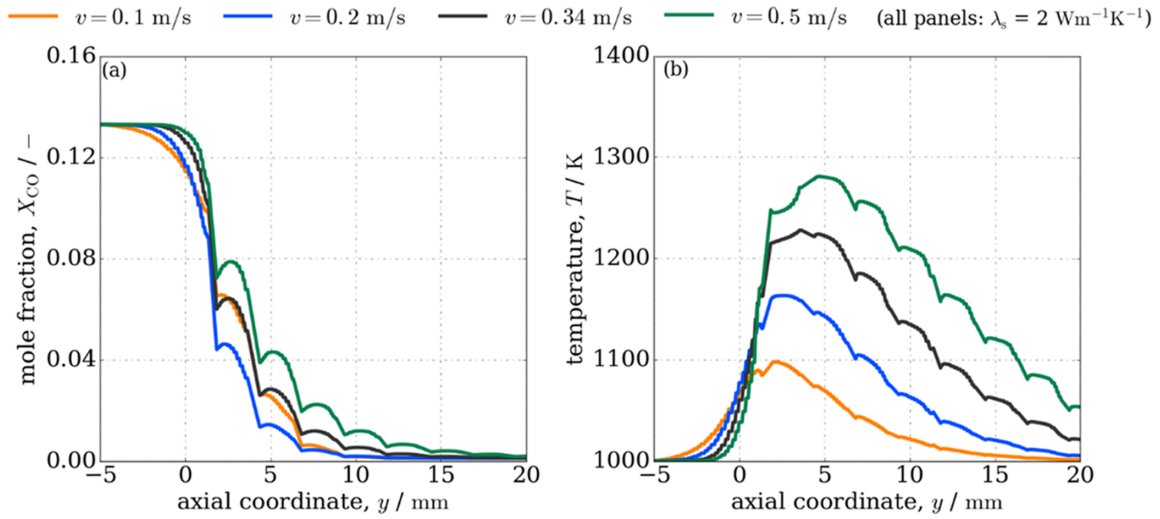

Figure 3. Axial concentration (a) and temperature (b) profiles for CO oxidation at varying superficial velocities; λ_s = 2 W m^{-1} K^{-1}.

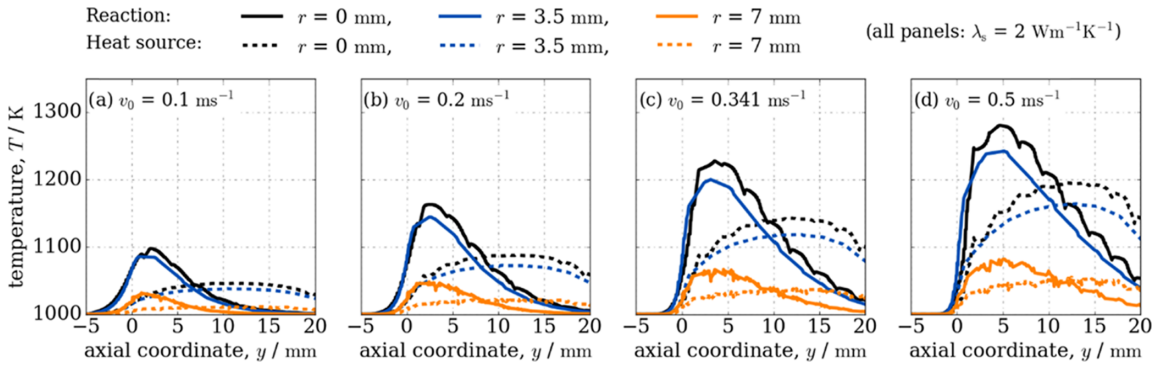

Figure 4. Comparison of axial fluid temperature profiles of reaction and heat source simulations at different radii r with a solid thermal conductivity λ_s = 2 W m^{-1} K^{-1} and varying superficial velocities: (a) v = 0.1 m s^{-1}, (b) v = 0.2 m s^{-1}, (c) v = 0.34 m s^{-1}, and (d) v = 0.5 m s^{-1}. The highest temperatures are located in the front part of the foam for reaction cases, while at the back for the heat source cases. Additionally, the hot spot is of higher magnitude and more localized in the case of exothermal chemical reactions. An increased flow rate pushes the profiles forward and upward in both approaches (due to increased heat of reaction).

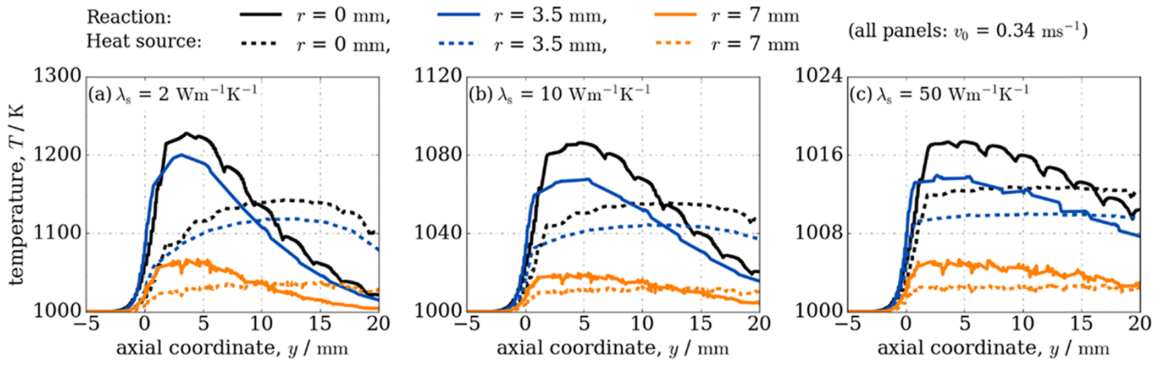

Figure 5. Comparison of axial fluid temperature profiles of reaction and heat source simulations at different radii with a superficial velocity v = 0.34 m s^{-1} and varying solid thermal conductivities: (a) λ_s = 2 W m^{-1} K^{-1}, (b) λ_s = 10 W m^{-1} K^{-1}, and (c) λ_s = 50 W m^{-1} K^{-1}. Conductive heat transport increases with solid thermal conductivity, resulting in significantly lower temperature profiles. Additionally, the profiles agree better, indicating improved applicability of the heat source approximation.

https://dx.doi.org/10.1021/acs.iecr.0c05982
Ind. Eng. Chem. Res. 2021, 60, 4542−4551

setup, an increasing superficial velocity causes such an increase of heat of reaction. The temperature curves are generally flatter at radii closer to the wall, as the wall temperature is kept constant for all cases. The temperature difference between the inner radius (r = 0 mm) and the medium radius (r = 3.5 mm) is lower than between the medium and outer radius (r = 7 mm) as the heat can obviously be removed more efficiently close to the wall. At all three investigated radii, the temperature profiles from the heat source approach and the actual reaction case do not match in the range of investigated superficial velocities.

So far, the solid thermal conductivity was set to 2 W m^{-1} K^{-1}. We will now address the influence of the solid thermal conductivity on the computed temperature fields (see Figure 5). With increasing thermal conductivity, the temperature profiles of both approaches shift toward lower temperatures (note the different temperature scales). The agreement between temperature profiles from the reaction and heat source approach increases with solid thermal conductivity. Near-wall temperatures (i.e., r = 7 mm) are almost identical between the two approaches at λ_s = 10 and 50 W m^{-1} K^{-1}. Hence, increasing the solid thermal conductivities increases the resemblances of the temperature fields in the axial and radial directions.

To determine the dominant heat removal mechanisms, we analyze global heat flows. All temperature boundaries (fluid inlet and tube walls) are fixed at 1000 K. Therefore, thermal energy can only enter the system via heat production. For this case, a simple global energy balance for the solid domain (i.e., foam) can be expressed as

$$Q_{prod} = Q_{SF} + Q_{SW} \tag{17}$$

where Q_{prod} is the heat production in the solid (either through reaction or through heat source), Q_{SF} is the convective heat flow transferred from solid to fluid, and Q_{SW} is the conductive heat flow transported from the solid foam to the wall. If the specific conductive heat flow $Q_{SW}\,Q_{prod}^{-1}$ is above 0.5, conduction is the dominant heat removal mechanism. In contrast, if $Q_{SW}\,Q_{prod}^{-1}$ is below 0.5, heat is dominantly removed through axial convection.

The specific conductive heat flow is plotted against the superficial velocity in Figure 6. In general, all $Q_{SW}\,Q_{prod}^{-1}$ are above 0.5, indicating a conduction-dominant heat removal. As expected, higher values for the solid thermal conductivity enhance $Q_{SW}\,Q_{prod}^{-1}$ (i.e., more heat removed through conduction) and reduce the influence of velocity. This was also reported in our previous study.[36] The dependence of $Q_{SW}\,Q_{prod}^{-1}$ on v is decreasing with λ_s. There is almost no dependency observable at λ_s = 50 W m^{-1} K^{-1}. In heat source cases, $Q_{SW}\,Q_{prod}^{-1}$ decreases linearly with v (i.e., more heat is removed through convection at higher superficial velocities), agreeing with ref 36. $Q_{SW}\,Q_{prod}^{-1}$ in reaction cases behaves slightly different and depends nonlinearly on v. Additionally, and differently from heat source cases, $Q_{SW}\,Q_{prod}^{-1}$ increases with v. This means the influence of convection on the overall heat transport decreases with v. This dependency is more pronounced at low solid thermal conductivity. With increasing velocity, $Q_{SW}\,Q_{prod}^{-1}$ approaches asymptotically the value of the corresponding heat source case. We attribute this behavior to the locally varying heat production. At low flow rates and solid thermal conductivities, the reaction heat evolves concentrated in a small part of the foam (i.e., in the central front part at r close to 0). When heat is mainly produced in the central front part, there is a relatively long axial pathway through the strut network for conductive heat removal. Therefore, convection becomes more likely for heat removal and more emphasized as a transport mechanism at these low velocities and low thermal conductivities. In contrast, heat production is always homogeneously distributed for the heat source cases, resulting in a higher fraction of generated heat close to the wall. Thus, conduction tends to be more important compared to the actual reaction (for low velocity and low thermal conductivity).

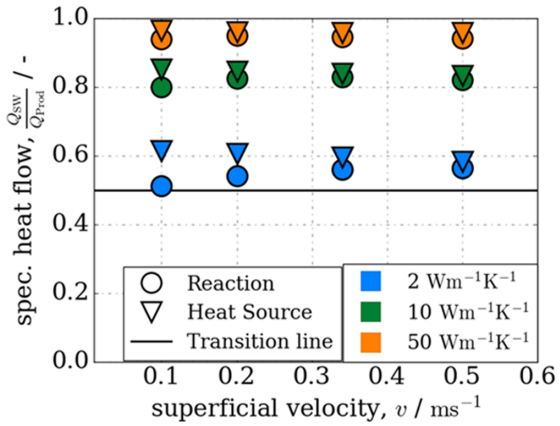

Figure 6. Specific conductive heat flow $Q_{SW}\,Q_{prod}^{-1}$ plotted against the superficial velocity v. The conductive heat flow is normalized by the heat production either through reaction or through the heat source. The transition line describes the change from dominant conduction ($Q_{SW}\,Q_{prod}^{-1}$ > 0.5) to dominant convection ($Q_{SW}\,Q_{prod}^{-1}$ < 0.5). For all investigated parameters, thermal conduction is the dominant heat transport mechanism.

For hot spot prediction, the maximum temperature increase within the catalyst carrier is of major interest. As assumed in the previous study,[36] homogeneous, uniformly distributed heat sources generate the minimal value of the expected maximum temperature increase during a chemical reaction of the same heat release. The axial profiles from Figures 4 and 5 underline this assumption, showing that $T_{max,heat\ source} \leq T_{max,reaction}$.

To further investigate this, we plotted the maximum temperature increase per evolving heat release, $T_{max,s}/Q_{prod}$, against the superficial velocity in Figure 7a. Here, the heat release Q_{prod} is multiplied by 4 to account for the whole reactor. Again, the linearly falling trend of $T_{max,s}/Q_{prod}$ is visible for the heat source cases, confirming the results from the previous studies.[36] However, the influence of the flow rate in the reaction cases is significantly higher and not linear. At high superficial velocities (at least at high thermal conductivities), the results from the reaction and heat source cases are similar. With decreasing flow rates, $T_{max,s}/Q_{prod}$ increases exponentially in the reaction cases, leading to increasing deviations compared to the heat source results. As described before, a low superficial velocity concentrates the whole amount of released heat in a smaller area of the catalyst. Therefore, the approximation of a homogeneously distributed heat source becomes more inappropriate, resulting in major deviations between the two approaches up to about 6 K W^{-1} (equal to 100%) for v = 0.1 m s^{-1} and λ_s = 2 W m K^{-1}. The differences decrease with increasing solid thermal conductivity, showing once again the increasing accuracy of the heat source approach.

https://dx.doi.org/10.1021/acs.iecr.0c05982
Ind. Eng. Chem. Res. 2021, 60, 4542−4551

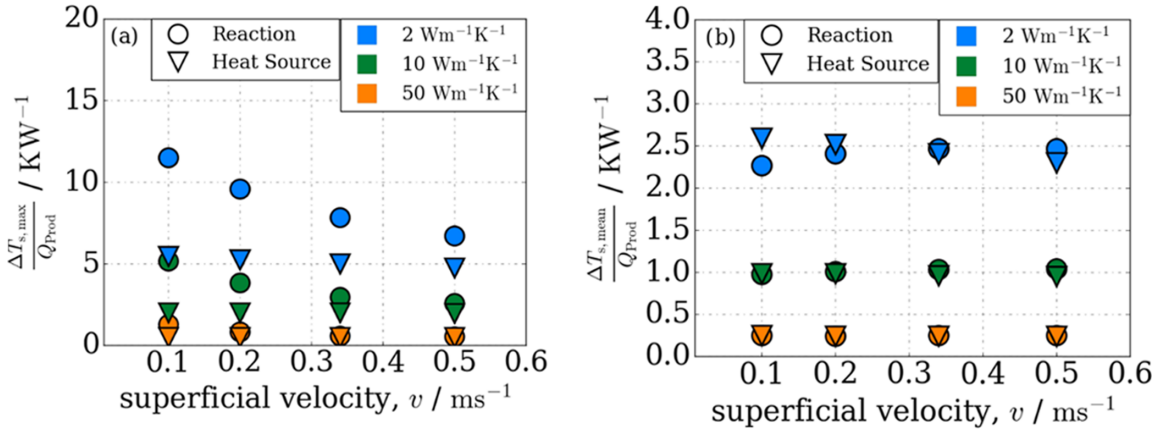

Figure 7. Specific temperature increase in the solid region per evolving heat for reaction and heat source cases. (a) Specific maximum temperature increase of the solid foam and (b) specific mean temperature increase of the solid foam.

In addition to the maximum temperature increase, the mean temperature increase per heat release is shown in Figure 7b. The mean temperature values are calculated by weighting over their individual cell volume. The values of reaction and heat source cases resemble better compared to the maximum temperature increase and are of significantly lower magnitude. This is probably caused by the near-wall regions where the two approaches reach similar values due to the equal wall boundary condition. Especially at the highest solid thermal conductivity, almost no average temperature increase is observed at all.

4. DISCUSSION AND CONCLUSIONS

The heat source approximation can predict global heat flows quite accurately. This allows for rapid prototyping of the catalyst carriers with efficient heat removal as multiple simulations can be carried out fast. Such a simplification is especially beneficial when detailed knowledge about catalyst characteristics (e.g., effectiveness factor or kinetic mechanism) is missing. Moreover, since the evolving heat is decoupled from complex chemistry, isolated parameter studies can be conducted. Still, differences between modeling a chemical reaction and mimicking the reaction heat with homogeneously distributed heat sources are evident. The evolving hot spot at the beginning of the catalyst as well as the magnitude of local temperature gradients cannot be depicted with the simplified approach. The maximum temperatures occur at the rear part of the solid instead and are of lower magnitude than in the case of a chemical reaction. However, valuable information about the temperature field can be extracted. As the simulated mean temperature increases of heat sources and actual reactions resemble well, the expected thermal stress under operating conditions can be estimated. Furthermore, the computed temperature hot spots should at least be considered when designing both the foam catalyst carrier and the reactive washcoat in order to prevent catalyst deactivation or thermal runaways. Generally, with increasing superficial velocity v and solid thermal conductivity λ_s, the applicability of the heat source simplification increases. The normalization by heat source intensities suggests validity of this approach also for other gas-phase reactions (e.g., CO_2 methanation) with different reaction enthalpies. Still, especially for endothermic reactions, this issue should be subject to further investigations. Additionally, it needs to be examined whether the application of heat sources can contribute to the process intensification of packed beds or honeycomb structures similarly.

We note in passing that the presented comparison of heat sources and chemical reactions would also have been possible using simpler kinetics, for example, by expressing the rate through a rate-determining step. In that case, the computational cost savings from using the heat source model are less significant as they are in this study. We do not want to highlight computational savings but rather emphasize the reduced modeling effort when using the heat source approach. Regardless of the chemical reaction, this method allows for an estimated temperature field without any knowledge about participating species, their kinetic parameters, and their reaction paths, requiring only an educated guess of the evolving heat. In general, we expect that this study helps to understand heat transport in foam structures and further facilitates the design of catalyst carriers and chemical reactors.

■ ASSOCIATED CONTENT

Supporting Information

The Supporting Information is available free of charge at https://pubs.acs.org/doi/10.1021/acs.iecr.0c05982.

Plausibility study (comparison of the CO oxidation case with the literature data); grid independence study; correlations and results for Kelvin cells; and influence of radiation modeling on CO oxidation (PDF)

■ AUTHOR INFORMATION

Corresponding Author

Georg R. Pesch − *Chemical Process Engineering and MAPEX Center for Materials and Processes, University of Bremen, 28359 Bremen, Germany;* orcid.org/0000-0003-4676-1908; Email: gpesch@uni-bremen.de

Authors

Christoph Sinn − *Chemical Process Engineering, University of Bremen, 28359 Bremen, Germany*

Jonas Wentrup − *Chemical Process Engineering, University of Bremen, 28359 Bremen, Germany*

Jorg Thöming − *Chemical Process Engineering and MAPEX Center for Materials and Processes, University of Bremen,*

https://dx.doi.org/10.1021/acs.iecr.0c05982
Ind. Eng. Chem. Res. 2021, 60, 4542−4551

28359 Bremen, Germany; orcid.org/0000-0002-5374-114X

Complete contact information is available at: https://pubs.acs.org/10.1021/acs.iecr.0c05982

Author Contributions

[§]C.S. and J.W. contributed equally.

Notes

The authors declare no competing financial interest.

■ ACKNOWLEDGMENTS

C.S. and J.T. appreciate the funding by the German Research Foundation (DFG) through the priority program SPP 2080 (Katalysatoren und Reaktoren unter dynamischen Betriebsbedingungen für die Energiespeicherung und -wandlung) under Grant TH 893/23-1. Furthermore, J.W. and J.T. thank the BMWi and BMBF for funding through the research project "QUARREE100—Quartiersentwicklung mit 100% Regenerativer Energie" under Grant 03SBE113B, part of promotional program "Solares Bauen/Energieeffiziente Stadt". The authors thank Augusto Della Torre and Gianluca Montenegro from Politecnico di Milano (Department of Energy, Milan, Italy) for valuable discussion. The authors also wish to thank Olaf Deutschmann and Matthias Hettel from the KIT (Karlsruhe Institute of Technology, Karlsruhe, Germany) and Eric Daymo from Tonkomo LLC (Gilbert, Arizona, United States) for extensive support regarding numerical methods.

■ LIST OF SYMBOLS

Roman

A_k	pre-exponential factor of reaction k, m mol^{-1} s^{-1}
c_i	concentration of species i, mol m^{-3}
$c_{p,f}$	fluid isobaric heat capacity, J kg^{-1} K^{-1}
$c_{p,s}$	solid isobaric heat capacity, J kg^{-1} K^{-1}
d_c	cell diameter, m
d_s	strut diameter, m
$D_{j,i}$	binary diffusion coefficient of species j and i, m^{-2} s^{-1}
$D_{i,m}$	mixture-averaged diffusion coefficient of species i, m^{-2} s^{-1}
$E_{A,k}$	activation energy of reaction k, J mol^{-1}
$F_{cat/geo}$	ratio of catalytic surface to geometrical surface, dimensionless
h_f	fluid specific enthalpy, J kg^{-1}
h_i	specific enthalpy of species i, J kg^{-1}
h_i^0	standard enthalpy of formation of species i, J kg^{-1}
$\vec{j}_i$	diffusion mass flux vector, kg m^{-2} s^{-1}
j_q	diffusive energy flux vector, J m^{-2} s^{-1}
k_k	rate constant of reaction k, s^{-1}
M_i	molar mass of species i, kg mol^{-1}
$\vec{n}$	normal vector, dimensionless
N_s	number of species, dimensionless
p	pressure, Pa
p_0	outlet pressure, Pa
Q_{prod}	produced heat flow (heat source or reaction), W
Q_{SW}	heat flow from solid to wall, W
Q_{SF}	heat flow from solid to fluid, W
R	universal gas constant, 8.314 J kg^{-1}
R_i^{het}	net reaction rate due to het. reactions of species i, kg m^{-2} s^{-1}
R_s	number of reactions, dimensionless
S	total heat source, W
S_{rel}	relative heat source, W m^{-3}
S_V	specific surface area, m^{-1}
$\dot{s}_i$	surface reaction rate of species i, mol m^{-2} s^{-1}
S_i	sticking coefficient, dimensionless
T	temperature, K
T_0	inlet fluid temperature, K
T_W	wall temperature, K
v	superficial velocity, m s^{-1}
v_0	inlet velocity, m s^{-1}
X_i	mole fraction, dimensionless
Y_i	mass fraction, dimensionless

■ GREEK

β_k	temperature exponent in reaction k, dimensionless
Γ	surface site density, mol m^{-2}
ε_o	open porosity, dimensionless
ε	surface emissivity, dimensionless
$\varepsilon_{i,k}$	activation energy adjustment of species i in reaction k, J mol^{-1}
η	effectiveness factor, dimensionless
θ_i	surface coverage of species i, dimensionless
μ_f	dynamic viscosity, Pa s
$\mu_{i,k}$	reaction order adjustment of species i in reaction k, dimensionless
λ_f	fluid thermal conductivity, W m^{-1} K^{-1}
λ_s	solid thermal conductivity, W m^{-1} K^{-1}
ρ_f	fluid density, kg m^{-3}
ρ_s	solid density, kg m^{-3}
ν_i'	stoichiometric coefficient of reactant i, dimensionless
$\nu_{i,k}$	stoichiometric coefficient of species i in reaction k, dimensionless
τ	stress tensor, Pa

■ REFERENCES

(1) Richardson, J. T.; Remue, D.; Hung, J. K. Properties of ceramic foam catalyst supports: Mass and heat transfer. *Appl. Catal., A* **2003**, *250*, 319−329.

(2) Gräf, I.; Rühl, A. K.; Kraushaar-Czarnetzki, B. Experimental study of heat transport in catalytic sponge packings by monitoring spatial temperature profiles in a cooled-wall reactor. *Chem. Eng. J.* **2014**, *244*, 234−242.

(3) Kiewidt, L.; Thöming, J. Multiscale modelling of monolithic sponges as catalyst carrier for the methanation of carbon dioxide. *Chem. Eng. Sci. X* **2019**, *2*, No. 100016.

(4) Fratalocchi, L.; Visconti, C. G.; Groppi, G.; Lietti, L.; Tronconi, E. Intensifying heat transfer in Fischer-Tropsch tubular reactors through the adoption of conductive packed foams. *Chem. Eng. J.* **2018**, *349*, 829−837.

(5) Merino, D.; Sanz, O.; Montes, M. Effect of the thermal conductivity and catalyst layer thickness on the Fischer-Tropsch synthesis selectivity using structured catalysts. *Chem. Eng. J.* **2017**, *327*, 1033−1042.

(6) Frey, M.; Bengaouer, A.; Geffraye, G.; Edouard, D.; Roger, A. C. Aluminum Open Cell Foams as Efficient Supports for Carbon Dioxide Methanation Catalysts: Pilot-Scale Reaction Results. *Energy Technol.* **2017**, *5*, 2078−2085.

(7) Fratalocchi, L.; Groppi, G.; Visconti, C. G.; Lietti, L.; Tronconi, E. Adoption of 3D printed highly conductive periodic open cellular structures as an effective solution to enhance the heat transfer performances of compact Fischer-Tropsch fixed-bed reactors. *Chem. Eng. J.* **2020**, *386*, No. 123988.

(8) Ercolino, G.; Stelmachowski, P.; Specchia, S. Catalytic Performance of Pd/Co_3O_4 on SiC and ZrO_2 Open Cell Foams for Process Intensification of Methane Combustion in Lean Conditions. *Ind. Eng. Chem. Res.* **2017**, *56*, 6625−6636.

(9) Kiewidt, L.; Thöming, J. Pareto-optimal design and assessment of monolithic sponges as catalyst carriers for exothermic reactions. *Chem. Eng. J.* **2019**, *359*, 496−504.
(10) Kapteijn, F.; Moulijn, J. A. Structured Catalysts and Reactors − Perspectives for demanding applications. *Catal. Today* **2020**, DOI: 10.1016/j.cattod.2020.09.026.
(11) Tronconi, E.; Groppi, G.; Visconti, C. G. Structured catalysts for non-adiabatic applications. *Curr. Opin. Chem. Eng.* **2014**, *5*, 55−67.
(12) Diani, A.; Bodla, K. K.; Rossetto, L.; Garimella, S. V. Numerical analysis of air flow through metal foams. *Energy Procedia* **2014**, *45*, 645−652.
(13) Meinicke, S.; Wetzel, T.; Dietrich, B. Scale-resolved CFD modelling of single-phase hydrodynamics and conjugate heat transfer in solid sponges. *Int. J. Heat Mass Transfer* **2017**, *108*, 1207−1219.
(14) Iasiello, M.; et al. Numerical analysis of heat transfer and pressure drop in metal foams for different morphological models. *J. Heat Transfer* **2014**, *136*, No. 112601.
(15) Bianchi, E.; Schwieger, W.; Freund, H. Assessment of Periodic Open Cellular Structures for Enhanced Heat Conduction in Catalytic Fixed-Bed Reactors. *Adv. Eng. Mater.* **2016**, *18*, 608−614.
(16) Wehinger, G. D.; Heitmann, H.; Kraume, M. An artificial structure modeler for 3D CFD simulations of catalytic foams. *Chem. Eng. J.* **2016**, *284*, 543−556.
(17) Bracconi, M.; Ambrosetti, M.; Maestri, M.; Groppi, G.; Tronconi, E. A systematic procedure for the virtual reconstruction of open-cell foams. *Chem. Eng. J.* **2017**, *315*, 608−620.
(18) Razza, S.; et al. Heat transfer performance of structured catalytic reactors packed with metal foam supports: Influence of wall coupling. *Catal. Today* **2016**, *273*, 187−195.
(19) Bianchi, E.; Groppi, G.; Schwieger, W.; Tronconi, E.; Freund, H. Numerical simulation of heat transfer in the near-wall region of tubular reactors packed with metal open-cell foams. *Chem. Eng. J.* **2015**, *264*, 268−279.
(20) Meinicke, S.; Dubil, K.; Wetzel, T.; Dietrich, B. Characterization of heat transfer in consolidated, highly porous media using a hybrid-scale CFD approach. *Int. J. Heat Mass Transfer* **2020**, *149*, No. 119201.
(21) Zafari, M.; Panjepour, M.; Emami, M. D.; Meratian, M. Microtomography-based numerical simulation of fluid flow and heat transfer in open cell metal foams. *Appl. Therm. Eng.* **2015**, *80*, 347−354.
(22) Della Torre, A.; Montenegro, G.; Onorati, A.; Tabor, G. CFD characterization of pressure drop and heat transfer inside porous substrates. *Energy Procedia* **2015**, *81*, 836−845.
(23) Bracconi, M.; Ambrosetti, M.; Maestri, M.; Groppi, G.; Tronconi, E. Analysis of the effective thermal conductivity of isotropic and anisotropic Periodic Open Cellular Structures for the intensification of catalytic processes. *Chem. Eng. Process. Process Intensif.* **2020**, *158*, No. 108169.
(24) Bracconi, M.; Ambrosetti, M.; Maestri, M.; Groppi, G.; Tronconi, E. A fundamental analysis of the influence of the geometrical properties on the effective thermal conductivity of open-cell foams. *Chem. Eng. Process. Process Intensif.* **2018**, *129*, 181−189.
(25) Sinn, C.; Wentrup, J.; Pesch, G. R.; Thöming, J.; Kiewidt, L. Chemical Engineering Research and Design Structure-heat transport analysis of periodic open-cell foams to be used as catalyst carriers. *Chem. Eng. Res. Des.* **2021**, *166*, 209−219.
(26) Ranut, P. On the effective thermal conductivity of aluminum metal foams: Review and improvement of the available empirical and analytical models. *Appl. Therm. Eng.* **2016**, *101*, 496−524.
(27) Lucci, F.; Della Torre, A.; Montenegro, G.; Kaufmann, R.; Eggenschwiler, P. D. Comparison of geometrical, momentum and mass transfer characteristics of real foams to Kelvin cell lattices for catalyst applications. *Int. J. Heat Mass Transfer* **2017**, *108*, 341−350.
(28) Della Torre, A.; et al. CFD modeling of catalytic reactions in open-cell foam substrates. *Comput. Chem. Eng.* **2016**, *92*, 55−63.
(29) Dong, Y.; Korup, O.; Gerdts, J.; Cuenya, B. R.; Horn, R. Microtomography-based CFD modeling of a fixed-bed reactor with an open-cell foam monolith and experimental verification by reactor profile measurements. *Chem. Eng. J.* **2018**, *353*, 176−188.
(30) von Rickenbach, J.; Lucci, F.; Narayanan, C.; Eggenschwiler, P. D.; Poulikakos, D. Effect of washcoat diffusion resistance in foam based catalytic reactors. *Chem. Eng. J.* **2015**, *276*, 388−397.
(31) Deutschmann, O.; Schmidt, R.; Behrendt, F.; Warnat, J. Numerical modeling of catalytic ignition. *Symp. Combust.* **1996**, *26*, 1747.
(32) Bracconi, M.; Ambrosetti, M.; Maestri, M.; Groppi, G.; Tronconi, E. A fundamental investigation of gas/solid mass transfer in open-cell foams using a combined experimental and CFD approach. *Chem. Eng. J.* **2018**, *352*, 558−571.
(33) Aguirre, A.; Chandra, V.; Peters, E. A. J. F.; Kuipers, J. A. M.; D'Angelo, M. F. N. Open-cell foams as catalysts support: A systematic analysis of the mass transfer limitations. *Chem. Eng. J.* **2020**, *393*, No. 124656.
(34) Jurtz, N.; Kraume, M.; Wehinger, G. D. Advances in fixed-bed reactor modeling using particle-resolved computational fluid dynamics (CFD). *Rev. Chem. Eng.* **2019**, *35*, 139−190.
(35) Dixon, A. G.; Partopour, B. Computational Fluid Dynamics for Fixed Bed Reactor Design. *Annu. Rev. Chem. Biomol. Eng.* **2020**, *11*, 109−130.
(36) Sinn, C.; Pesch, G. R.; Thöming, J.; Kiewidt, L. Coupled conjugate heat transfer and heat production in open-cell ceramic foams investigated using CFD. *Int. J. Heat Mass Transfer* **2019**, *139*, 600−612.
(37) Sinn, C.; et al. CFD Simulations of Radiative Heat Transport in Open-Cell Foam Catalytic Reactors. *Catalysts* **2020**, *10*, No. 716.
(38) Sinn, C.; Wentrup, J.; Thöming, J.; Pesch, G. R. Influence of Pressure, Velocity and Fluid Material on Heat Transport in Structured Open-Cell Foam Reactors Investigated Using CFD Simulations. *ChemEngineering* **2020**, *4*, No. 61.
(39) Inayat, A.; Freund, H.; Zeiser, T.; Schwieger, W. Determining the specific surface area of ceramic foams: The tetrakaidecahedra model revisited. *Chem. Eng. Sci.* **2011**, *66*, 1179−1188.
(40) Lucci, F.; et al. Performance of randomized Kelvin cell structures as catalytic substrates: Mass-transfer based analysis. *Chem. Eng. Sci.* **2014**, *112*, 143−151.
(41) Ambrosetti, M.; Bracconi, M.; Groppi, G.; Tronconi, E. Analytical Geometrical Model of Open Cell Foams with Detailed Description of Strut-Node Intersection. *Chem. Ing. Tech.* **2017**, *89*, 915−925.
(42) Stiegler, T.; et al. Development of a Structured Reactor System for CO_2 Methanation under Dynamic Operating Conditions. *Energy Technol.* **2019**, *7*, No. 1900047.
(43) Busse, C.; Freund, H.; Schwieger, W. Intensification of heat transfer in catalytic reactors by additively manufactured periodic open cellular structures (POCS). *Chem. Eng. Process. Process Intensif.* **2018**, *124*, 199−214.
(44) *3D Design, Engineering & Construction Software*; Autodesk, Inc., 2020. https://www.autodesk.com/.
(45) Siemens, P. L. M. STAR-CCM+, 2021. https://www.plm.automation.siemens.com/global/en/products/simcenter/STAR-CCM.html.
(46) Wehinger, G. D.; Flaischlen, S. Computational Fluid Dynamics Modeling of Radiation in a Steam Methane Reforming Fixed-Bed Reactor. *Ind. Eng. Chem. Res.* **2019**, *58*, 14410−14423.
(47) Hettel, M.; Daymo, E.; Deutschmann, O. 3D modeling of a CPOX-reformer including detailed chemistry and radiation effects with DUO. *Comput. Chem. Eng.* **2018**, *109*, 166−178.
(48) Gräf, I.; Ladenburger, G.; Kraushaar-Czarnetzki, B. Heat transport in catalytic sponge packings in the presence of an exothermal reaction: Characterization by 2D modeling of experiments. *Chem. Eng. J.* **2016**, *287*, 425−435.
(49) Kiewidt, L.; Thöming, J. Predicting optimal temperature profiles in single-stage fixed-bed reactors for CO_2-methanation. *Chem. Eng. Sci.* **2015**, *132*, 59−71.

https://dx.doi.org/10.1021/acs.iecr.0c05982
Ind. Eng. Chem. Res. 2021, 60, 4542−4551

Chapter 6

Heat Sources — Influence of the Fluid Properties

The content of this results chapter is published under the name *Influence of Pressure, Velocity and Fluid Material on Heat Transport in Structured Open-Cell Foam Reactors Investigated Using CFD Simulations* (Sinn et al., 2020b).
In the previous chapters, the general thermal behavior of structured foam reactors (i.e., temperature fields and heat flows) resulting from heat sources were addressed in certain parameter field. So far, the thermal analysis using heat sources showed for air, at 1 bar, neglected gravitational acceleration, and velocities lower than 0.5 ms^{-1} that conduction is the dominant heat removal mechanism under these conditions. However, industrially relevant reactions (such as the CO_2 methanation) often require higher pressure ranges, contain fluid mixtures (e.g., hydrogen and carbon dioxide) and are operated vertically or horizontally (i.e., gravitational acceleration affects heat transport differently). This might be especially relevant when reactors are operated under changing fluid conditions as it might be the case in dynamically operated PtX plants. In the literature, the fluid side is often neglected in heat transport studies on reactive foams. Therefore, this chapter extends the heat source approach on the fluid side and analyses the heat transport behavior under more realistic conditions.

chemengineering

MDPI

Article

Influence of Pressure, Velocity and Fluid Material on Heat Transport in Structured Open-Cell Foam Reactors Investigated Using CFD Simulations

Christoph Sinn [1], Jonas Wentrup [1], Jorg Thöming [1,2] and Georg R. Pesch [1,2,*]

[1] Faculty of Production Engineering, Chemical Process Engineering Group, University of Bremen, Leobener Strasse 6, 28359 Bremen, Germany; sinn@uni-bremen.de (C.S.); jwentrup@uni-bremen.de (J.W.); thoeming@uni-bremen.de (J.T.)

[2] MAPEX Center for Materials and Processes, University of Bremen, Postbox 330 440, 28334 Bremen, Germany

* Correspondence: gpesch@uni-bremen.de

Received: 4 September 2020; Accepted: 2 November 2020; Published: 14 November 2020

Abstract: Structured open-cell foam reactors are promising for managing highly exothermic reactions such as CO_2 methanation due to their excellent heat transport properties. Especially at low flow rates and under dynamic operation, foam-based reactors can be advantageous over classic fixed-bed reactors. To efficiently design the catalyst carriers, a thorough understanding of heat transport mechanisms is needed. So far, studies on heat transport in foams have mostly focused on the solid phase and used air at atmospheric pressure as fluid phase. With the aid of pore-scale 3d CFD simulations, we analyze the effect of the fluid properties on heat transport under conditions close to the CO_2 methanation reaction for two different foam structures. The exothermicity is mimicked via volumetric uniformly distributed heat sources. We found for foams that are designed to be used as catalyst carriers that the working pressure range and the superficial velocity influence the dominant heat removal mechanism significantly. In contrast, the influence of fluid type and gravity on heat removal is small in the range relevant for heterogeneous catalysis. The findings might help to facilitate the design-process of open-cell foam reactors and to better understand heat transport mechanisms in foams.

Keywords: computational fluid dynamics (CFD); conjugate heat transfer; open-cell foams; structured reactors; volumetric heat sources; fluid properties; STAR-CCM+; dynamic operation

1. Introduction

Open-cell foams are promising monolithic catalyst support structures for exo- and endothermal heterogeneous gas-phase reactions such as the CO_2 methanation, due favorable characteristics such as good heat transport, low pressure drop and high porosities [1–3]. The CO_2 methanation currently attracts much attention in the chemical engineering community as it can be a cornerstone the future transition to a sustainable energy supply within the Power-to-X (PtX) concept [4]. Here, excess energy from wind turbines or solar panels is converted via electrolysis into hydrogen, and usually reacted catalytically with carbon dioxide to methane. As the power grids might not be resilient enough to withstand the high energy load during wind or sun peak hours, dynamically operated small-scale plants for storage of excess energy are needed in the future [5]. Small-scale plants are operated at low flow rates making heat removal traditionally difficult. The dynamic operation can cause tremendous jumps of pressure, velocity and even change the fluid composition resulting in undesired or uncontrollable temperature increases. Thus, the heat transport (and heat removal) inside these reactors needs to be addressed to protect the catalyst's activity and ensure safe as well as robust operation [6]. Generally,

for the methanation reaction, low temperatures are thermodynamically favorable [7]. Therefore, an effective heat removal ensures efficient conversion and protects the catalyst particles from sintering.

Recently it was shown that, at low flowrates, foam-structured reactors can be advantageous over conventional pellets for CO_2 methanation [8]. The reason is that heat is dominantly removed via radial conduction in foam reactors, whereas pellets in fixed-bed reactors remove heat axially via convection [9]. However, only when heat conduction dominates over convection, foams can be advantageous over pellets as pellets generally have a higher axial convective heat transport [8].

To study heat flows and heat transport mechanisms in structured reactors, computational fluid dynamics (CFD) simulations have been well established [10]. With the aid of CFD simulations, the three heat transport mechanisms, conduction [11,12], convection [13,14] and radiation [15], have been addressed in open-cell foams. Among others, the influences of superficial velocity [16,17], wall coupling [18], solid thermal conductivity [19], geometrical influences (i.e., strut shape [20,21] and porosity [22,23]) on heat transport were studied simulatively. Most of the studies targeted solely heat transport in the solid or conjugate heat transport between a fluid and a foam with no superimposed catalytic reaction. Simulations of detailed catalytic reactions on foams are costly and only a few studies have been published so far that mainly dealt with the CO oxidation reaction [24–28].

In order to reduce complexity of the reaction system and to speed up simulations, we recently proposed to mimic exothermal reactions via uniformly distributed heat sources in the solid foam [19]. Heat sources (or heat sinks) mimic the exothermicity (or endothermicity) and can be used to study heat flows and temperature increases in open-cell foams decoupled from reaction mechanisms. This approach has been utilized to study the influence of heat sources intensities (from 5–150 W), laminar superficial velocities (0–0.5 m s^{-1}), solid thermal conductivities (1–200 W m^{-1} K^{-1}), and thermal radiation (temperature levels 500–1200 K, solid emissivities 0–1) [15,19]. It was found that the solid thermal conductivity and the superficial velocity are key parameters for designing efficient heat-removing foams for the usage as catalyst carriers [19]. Moreover, for reactor tube diameters below 25 mm and superficial velocities lower than 0.5 m s^{-1}, the investigated structure (irregular foam) showed conduction being the dominant heat removal mechanism (this parameter range is in relevant order of magnitude for decentralized small scale methanation plants [29,30]). Furthermore, thermal radiation can contribute significantly to the heat transport at conditions relevant for methanation [15].

Our previous studies focused mainly on the properties of the solid foam, whereas the fluid has only been addressed by ramping the superficial velocity in the laminar regime for air at 1 bar pressure [15,19]. Other CFD studies dealing with heat transport in foams also mainly considered air as fluid with often constant fluid properties such as density, thermal conductivity and specific heat [16,22,31,32]. The study of Razza et al. investigated the influence of wall coupling between foam and tubular wall utilizing He as well as N_2 as fluids [18]. They found significant changes in computed fluid temperatures and justified the deviation through the six times higher thermal conductivity of He (they also assumed constant fluid properties). Additionally, Bianchi et al. [31] found a significant difference for computed heat transfer of either air or water (liquid).

The methanation reaction (CO_2 + $4H_2$ $\rightleftarrows$ CH_4 + $2H_2O$), however, involves gas mixtures (CO_2, H_2 and CH_4), higher velocity ranges (i.e., ≥0.5 m s^{-1}) and elevated pressure ranges (4–10 bar) [6]. Furthermore, the effect of gravitational acceleration has not been addressed so far in CFD studies of heat transport in open-cell foams. This might be relevant, because reactors can be operated vertically or horizontally leading to a different effective direction of gravity (i.e., natural convection).

In this study, we thus investigate the influence of the fluid properties on the overall heat transport, heat flows, and solid temperatures; a topic which has largely been neglected in the past. In detail, we analyze the influence of pressure, velocity, fluid composition and gravitational acceleration on the dominant heat transport (i.e., heat removal) mechanisms. We further determine under what circumstances the fluid properties need to be explicitly accounted for to study catalyst carriers for, e.g., the CO_2 methanation reaction.

2. Materials and Methods

The CFD model investigated in this study consists of a foam embedded in a tube (i.e., a tubular structured reactor) and is similar to our previous study [19]. The problem is the steady-state conjugate heat transfer between the flowing fluid and the foam. The simulations were carried out with the commercial CFD software STAR-CCM+ from Siemens PLM (Plano, TX, USA) [33]. Heat production through exothermal reactions is represented by volumetric homogeneously distributed heat sources in the solid (S = 12.5 W in all cases) [19]. The heat source intensity of 12.5 W was chosen as it corresponds to the heat released during the CO_2 methanation for a foam in this order of magnitude (50 W for a full sponge equals 12.5 W for one quarter of the sponge) [19].

Two foams (radius 7.5 mm; length 20 mm) are investigated in this study, modeled through Kelvin cell lattices (KC1 and KC2) that differ strongly in their strut diameter (see Figure 1 and Table 1). Only a quarter of the foams as well as the pipe are simulated due to the regularity of the structure and to further reduce computational cost. Polyhedral meshes were created using the integrated STAR-CCM+ meshing utilities (see Figure A1 in Appendix A). The utilized meshes were tested and results were found to be grid independent (see Figure A2 in Appendix B).

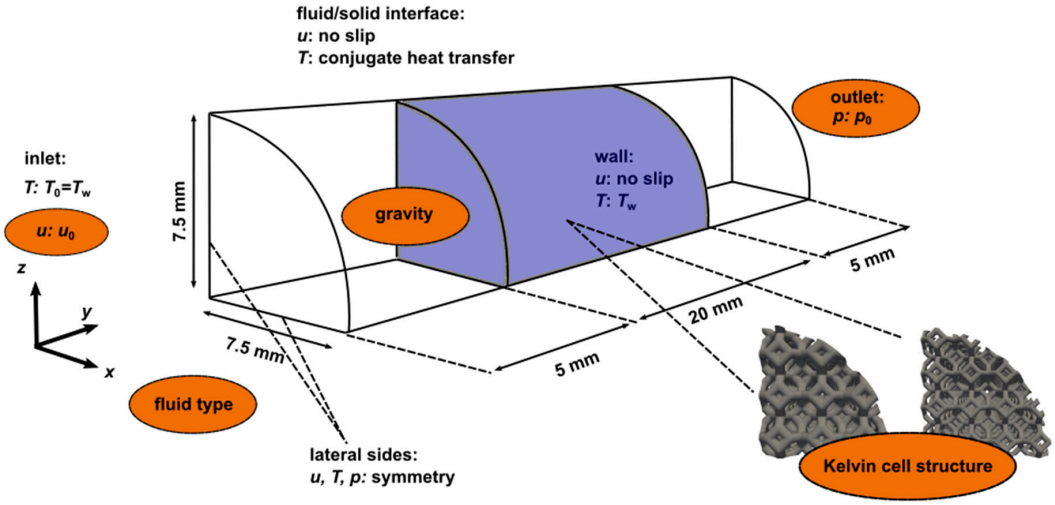

Figure 1. Illustration of model with boundary conditions. The orange highlighted fluid properties are investigated in this study.

Table 1. Properties of the investigated Kell cell lattices.

Parameter, Symbol.	Kelvin Cell 1 (KC1)	Kelvin Cell 2 (KC2)
open porosity, ε_O	0.724	0.845
specific surface area, S_V	1467.8 m^{-1}	1518.9 m^{-1}
cell diameter, d_c	1.924 mm	1.733 mm
strut diameter, d_s	0.591 mm	0.35 mm

The basic equations that are solved for a Newtonian fluid domain are the conservation of mass, momentum and energy:

$$\nabla \cdot (\rho_f \mathbf{U}) = 0, \tag{1}$$

$$\nabla \cdot (\rho_f \mathbf{U} \otimes \mathbf{U}) + \nabla \cdot \left(\mu \left(\nabla \otimes \mathbf{U} + (\nabla \otimes \mathbf{U})^T \right) - \frac{2}{3\mu} (\nabla \cdot \mathbf{U}) \mathbf{I} \right) - \nabla p + \rho_f \mathbf{g} = 0, \tag{2}$$

$$-\nabla \cdot (\rho_f \mathbf{U} h) - \nabla \cdot (\lambda_f \nabla T_f) = 0, \tag{3}$$

with ρ_f denoting the fluid's density, **U** the velocity field, h the enthalpy, μ the fluid's dynamic viscosity, T_f the fluid's temperature and λ_f the fluid's thermal conductivity. The solid phase is solely described by the conservation of energy

$$\lambda_s \left(\nabla^2 T_s\right) + S = 0, \tag{4}$$

with λ_s donating the solid thermal conductivity, T_s the solid temperature and S the specific artificial heat source. Furthermore, the fluid density is expressed via the ideal gas law.

The solid properties are kept constant, whereas the fluid properties such as dynamic viscosity, specific heat and thermal conductivity depend on the temperature (see Table 2). The model properties and assumptions are also listed in Table 2 and the basic boundary conditions can be found in Figure 1. In this study, fluid and wall temperatures are kept constant as a fixed temperature boundary at 500 K. This way, the only energy that enters the system is due to the volumetric heat source. Thermal radiation is not explicitly considered in the simulation as the temperatures are moderate and this study wants to investigate heat transport of fluid properties independently. Moreover, the influence of radiation has already been quantified in a comparable setup [15]. Furthermore, turbulence effects were taken into account through a *realizable k-ε* RANS turbulence model with *All* y^+ *wall-treatment* [34].

Table 2. Properties of this study's model.

Property		Assumption
Fluid dynamic viscosity	μ	Sutherland equation
Fluid heat capacity	$c_{p,f}$	polynomial
Fluid thermal conductivity	λ_f	Sutherland equation
Fluid density	δ_f	ideal gas law
Superficial velocity	v	const. (0.1–4 m s^{-1})
Pore Reynolds number (air)	$Re_p = \frac{v \cdot d_s \cdot \rho}{\mu}$	const. (0.3–76)
Wall/inlet temperature	$T_w = T_{in}$	const. (500 K)
Outlet pressure	p	const. (1–10 bar)
Solid heat capacity	$c_{p,s}$	const. (1000 J kg^{-1} K^{-1}).
Solid thermal conductivity	λ_s	const. (5 W m^{-1} K^{-1})
Solid density	δ_s	const. (3950 kg m^{-3})
Solid heat source	S	const. (total: 12.5 W)
Gravitational acceleration		considered
Turbulence		Realizable *k-ε* RANS (All y^+ wall-treatment)
Radiation		neglected [15]

For studying the influence of gravitational acceleration in different directions, gravity is considered in y direction (in flow direction, representing a vertical reactor) as well as in z direction (perpendicular to flow, representing a horizontal reactor). Additionally, the varied and investigated properties are highlighted in orange in Figure 1.

In our previous studies, similar models were validated against pressure drop correlations, heat transfer correlations and verified against CFD data [15,19]. Here, the principial changed model property is the CAD-created geometry. We therefore omit the validation as the models are virtually identical.

3. Results and Discussion

All simulated cases have a total heat source of S = 12.5 W, which would correspond to a 50 W total heat source in a full foam setup (i.e., four quarters). As already described, the only thermal energy entering the system is due to the volumetric heat source (i.e., heat production in the solid foam). The global energy balance thus reads

$$S = 12.5\,\text{W} = Q_{SF} + Q_{SW}, \tag{5}$$

with Q_{SF} being the transferred heat flow from fluid to solid and Q_{SW} being the conducted heat flow from solid to the wall. Which heat removal mechanism dominates (i.e., convection or conduction), can be expressed through the specific heat flow from solid to wall Q_{SW} S^{-1} through non-dimensionalization of Equation (4). For values above 0.5, thermal conduction is the dominant mechanism and for values below 0.5 convection is the dominant one. We note that due to the normalization by the heat source intensity, the actual implemented heat source value becomes less crucial. In our previous study it was shown that in the heat source intensity range between 5 W and 150 W temperature increases (in solid and fluid phases) and heat flows show the almost identical values.

The impact of the several investigated fluid properties on the heat flows is shown in Figure 2. Panel a shows the specific heat flow for a superficial velocity of the two investigated foams up to 4 m s^{-1}. Previous studies only investigated heat flows with coupled heat production in the solid has only up to 0.51 m s^{-1} [15,19]. Obviously, both foam structures switch from being dominated by conduction to being dominated by convection at a certain velocity. KC2 switches at a superficial velocity of approximately v = 1.2 m s^{-1} whereas KC1 switches not until a superficial velocity of approximately v = 3 m s^{-1}. This is most certainly based on the different strut diameters of the foams (KC1: d_s = 0.591 mm compared to KC1: d_s = 0.35 mm), which ensures a better radial heat removal for KC1 through thermal conduction. This is line with the findings from the studies of Bracconi et al. [11] and Bianchi et al. [21], that investigated the role of the strut diameter in conductive heat transport.

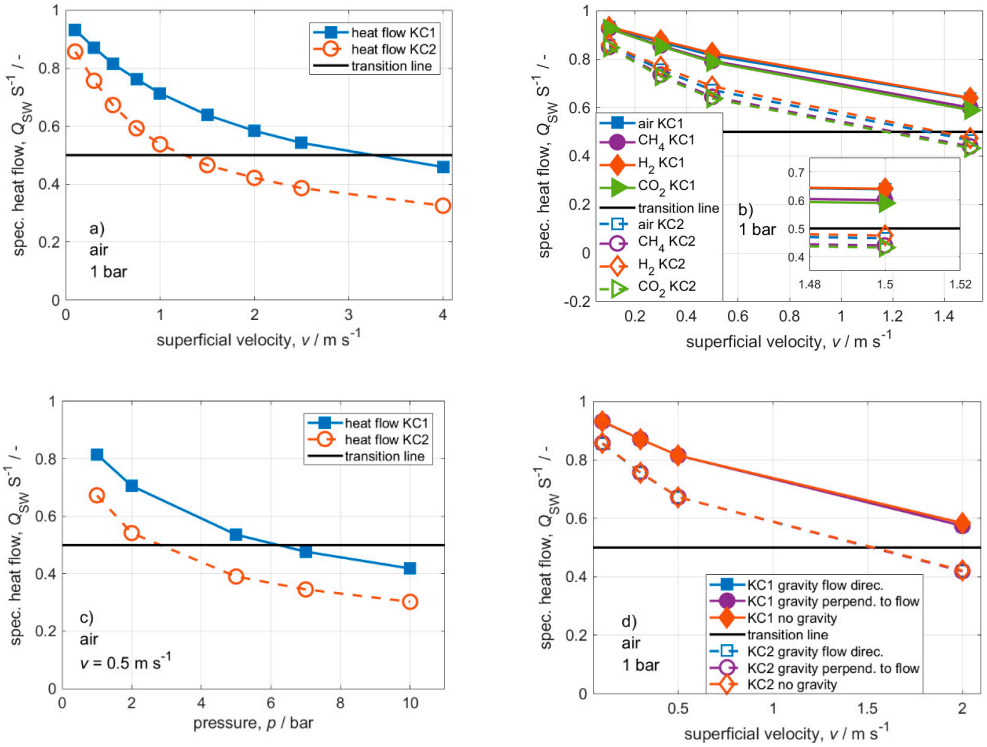

Figure 2. Heat flows for fluid property variation (**a**) Increase in inlet velocity incl. turbulence modelling; (**b**) Influence of fluid type; (**c**) Influence of pressure; (**d**) Influence of gravitational acceleration. Conditions: S = 12.5 W; λ_s = 5 W m^{-1} K^{-1}.

Figure 2a shows results using air as fluid as usually done in literature. Panel b shows the impact of the gas type, which is related to the CO_2 methanation, on heat removal. For both KC's, the difference in computed heat flows does not change distinctively, although a small difference between air and hydrogen on the one side and methane and carbon dioxide on the other side becomes

apparent. The small differences between the gas types can be explained through the interplay of gas viscosity, density, heat capacity and thermal conductivity which change over temperature for each gas individually. The order of thermal conductivities for the gases at 1 bar from highest to lowest is air, carbon dioxide, methane and hydrogen which is not the same order as in Panel b.

The influence of the pressure on the simulated heat flows at $v = 0.5$ m s^{-1} is shown in Figure 2c. Again, most of the literature investigated heat transport phenomena in foams only at 1 bar absolute pressure [14,35]. With increasing pressure, the heat transport switches from conduction dominated to convection dominated for both foams. At a pressure of 6 bar, both foams dominantly remove heat over convection and hence lose their advantage over standard pellets. The consideration of the actual working pressure thus influences the performance of the catalyst carriers tremendously. Structures that are designed to work efficiently, i.e., conduction dominated, at 1 bar, might already lose their efficiency at 2.5 bar (compare KC2 in panel c). The general effect is obvious, as both gas density and thus the ability of the fluid to cool down the foam via convection increase with pressure.

Often, CFD models omit gravitational acceleration [14,18,19]. Depending on the reactor setup (vertical pipe or horizontal pipe), gravitational acceleration affects the fluid in flow direction (vertical setup) or perpendicular to the flow direction (horizontal setup). Figure 2d shows the specific heat flow as a function of superficial velocity for both foams with gravity in flow direction, perpendicular to the flow as well as neglected gravity. In the investigated superficial velocity range (0.1–2 m s^{-1}), no significant influence of the consideration of gravity could be found. The reason probably lies in forced convection (i.e., pronounced velocity) being a lot more substantial for the overall convection than natural convection (i.e., effect of gravity). To our knowledge, correlations for the Grashof and Rayleigh numbers for this temperature distribution together with the velocity and pressure do not exist. Thus, this result could not have been anticipated by observing dimensionless numbers alone.

The analyzed heat flows for elevated velocities, changing fluid type, influence of pressure and gravity show the influence of the fluid properties on the overall heat transport in open-cell foam carriers. Additionally, Figure 3 shows the corresponding solid temperature rises of the cases shown in Figure 2. For brevity, we only show maximum temperature rises of the solid (instead of additional solid mean and fluid max/mean temperature rises) as they represent the entire solid temperature distribution in foams satisfactory [19]. In Figure 3, it can be seen that the curves of temperature rises of the two structures converge in the convection dominant regime. This behavior happens regardless of the applied pressure or superficial velocity (see panels a and c). Hence, at certain velocities (>3 m s^{-1}) and pressure (>7 bar), the temperature increase seems to be become independent of the foam geometry.

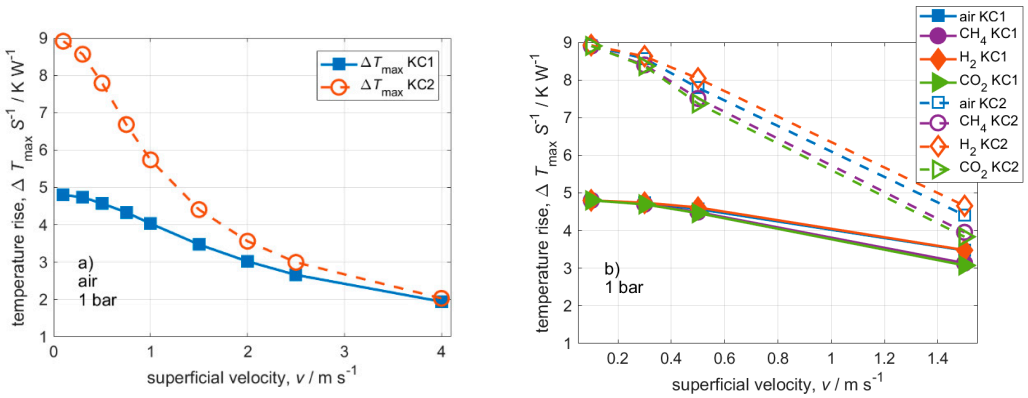

Figure 3. *Cont.*

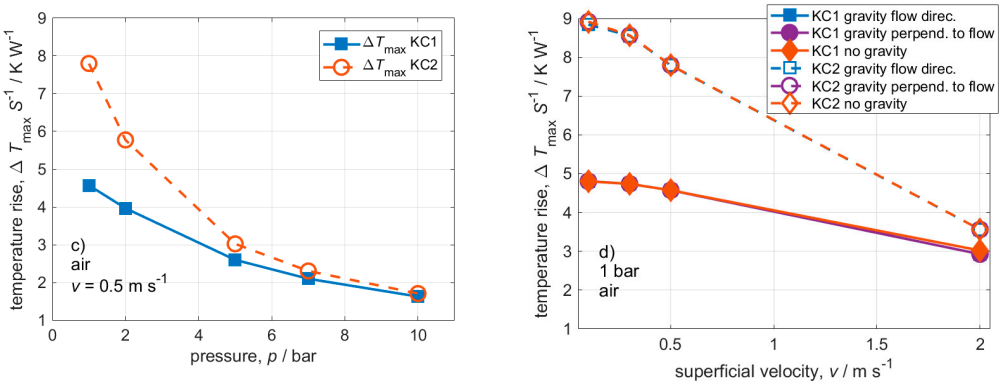

Figure 3. Solid temperature rises per applied heat source intensity for fluid property variation (**a**) Increase in inlet velocity incl. turbulence modelling; (**b**) Influence of fluid type; (**c**) Influence of pressure; (**d**) Influence of gravitational acceleration. Conditions: S = 12.5 W; λ_s = 5 W m^{-1} K^{-1}.

For superficial velocities lower or equal than 1.5 m s^{-1}, the influence of the fluid type on the temperature rise varies for the two structures (see Figure 3b). The effect of the fluid type on the temperature rise increases with convective heat transport. Therefore, KC2 has a more pronounced difference (starting from 0.3 m s^{-1}) than KC1 (difference obvious starting from 1.5 m s^{-1}). This behavior could be expected as the fluid type influences the convective heat transport and becomes more important when the overall contribution of convection increases. To conclude, the fluid type seems to be less influential in the dominant conduction area where a structured foam reactor should be operated. Equivalently to the heat flows, no significant effect of gravity on the temperature rise could be found (Figure 3d).

4. Conclusions

This study analyzed the often-neglected influence of fluid properties on heat transport in open-cell foam reactors. As pointed out, usually heat transport in open-cell foams is investigated using air at 1 bar pressure absolute.

When foams are designed as catalyst carriers (for, e.g., dynamic CO_2 methanation), they should at best remove all heat radially via conduction (here: for working pressure between 4 and 10 bar, the velocity should be lower 0.5 m s^{-1}). At elevated velocities even structures with relatively thick struts can shift into the convection dominated regime. Not only for elevated velocities, but especially for pressure higher than 1 bar (usual operation conditions of CO_2 methanation 4–10 bar) the shift towards convection being dominant might proceed rapidly. In contrast, the choice of fluid mixture seems not as significant as pressure and velocity ranges. Obviously, this has to be checked for other gases of other reactions or inert gases. Nevertheless, air seems a reasonable fluid to study the general heat transport behavior of new foam designs, as the deviations of thermal fields to other gases are not that severe. This way, fluid mixture equations can be omitted and computational effort can be reduced. Additionally, the reactor orientation (represented through gravity) does not seem to have an impact on the heat transport in foams which is relevant for heterogeneous catalysis.

In conclusion, for the design of structured reactors for highly exothermic gas phase reactions, it is crucial to consider the exact velocity and pressure ranges of the investigated reaction. This is especially important, when the catalyst carriers are designed for dynamic or changing load operation. This type of operation might cause tremendous jumps in superficial velocity, pressure or fluid composition which further might influence the overall heat transport and might cause a thermal runaway or serious harm to the catalyst.

Author Contributions: Conceptualization, C.S., J.W., G.R.P. and J.T.; methodology, C.S.; software, C.S.; writing—original draft preparation, C.S.; writing—review and editing, G.R.P. and J.T.; visualization, C.S. and J.W.; supervision, G.R.P. and J.T.; All authors have read and agreed to the published version of the manuscript.

Funding: Christoph Sinn and Jorg Thöming thank the German Research Foundation (DFG) for funding by the priority program SPP 2080 (Katalysatoren und Reaktoren unter dynamischen Betriebsbedingungen für die Energiespeicherung und -wandlung) under grant TH 893/23-1.

Acknowledgments: CS also thanks Harm Ridder for his kind support with the simulation computers that were essential for this study and Kevin Kuhlmann for fruitful discussion about meshing.

Conflicts of Interest: The authors declare no conflict of interest.

Nomenclature

Latin

c_p	isobaric heat capacity, J kg^{-1} K^{-1}
d_c	cell diameter, m
d_s	strut diameter, m
g	gravitational acceleration, 9.81 m s^{-2}
Q	heat flow, W
Q_{SF}	heat flow solid to fluid, W
Q_{SW}	heat flow solid to wall, W
h	specific enthalpy, J kg^{-1}
p	pressure, Pa
S	total heat source intensity, W
S_v	specific surface area, m^{-1}
T	temperature, K
T_w	wall temperature, K
T_{max}	maximum temperature, K
U	velocity, m s^{-1}
v	superficial velocity, m s^{-1}

Greek

ε_O	open porosity, -
μ	dynamic viscosity, Pa s
λ	thermal conductivity, W m^{-1} K^{-1}
ρ	density, kg m^{-3}

Appendix A. Depiction of Volume Meshes

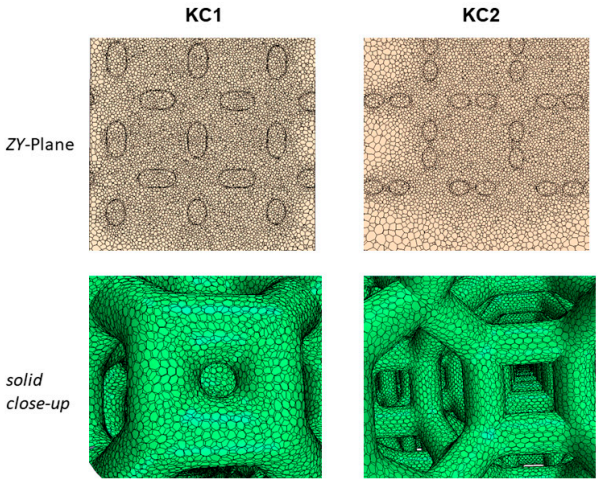

Figure A1. Depiction of volume meshes that were used in this study.

Appendix B. Grid Independence Study

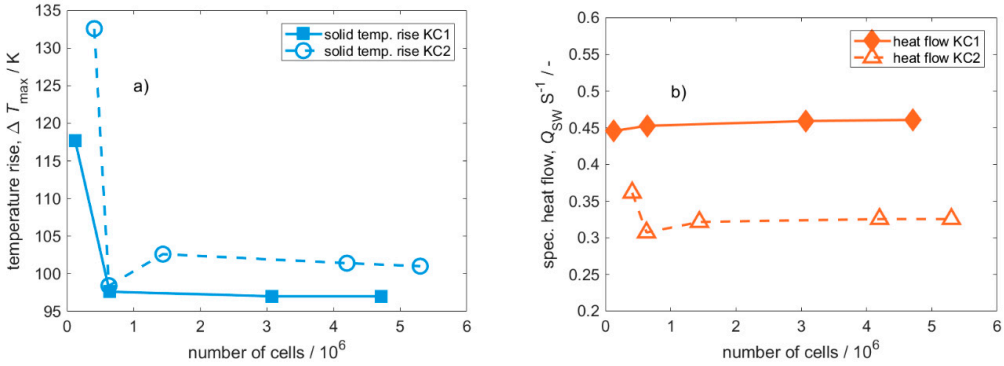

Figure A2. Grid independence study. (**a**) Solid temperature rise from initial 500 K plotted against number of cells; (**b**) specific heat flow from solid to wall plotted against number of cells. For both used geometries, the second-largest meshes (KC1: 3.1 mio. Cells; KC2 4.1 mio cells) were found to give reasonable results. Conditions: air; p = 1 bar, v = 4 m s^{-1}.

References

1. Kiewidt, L.; Thöming, J. Multiscale modelling of monolithic sponges as catalyst carrier for the methanation of carbon dioxide. *Chem. Eng. Sci. X* **2019**, *2*, 100016. [CrossRef]
2. Stiegler, T.; Meltzer, K.; Tremel, A.; Baldauf, M.; Wasserscheid, P.; Albert, J. Development of a Structured Reactor System for CO_2 Methanation under Dynamic Operating Conditions. *Energy Technol.* **2019**, *7*, 1900047. [CrossRef]
3. Gräf, I.; Ladenburger, G.; Kraushaar-Czarnetzki, B. Heat transport in catalytic sponge packings in the presence of an exothermal reaction: Characterization by 2D modeling of experiments. *Chem. Eng. J.* **2016**, *287*, 425–435. [CrossRef]
4. Vogt, C.; Monai, M.; Kramer, G.J.; Weckhuysen, B.M. The renaissance of the Sabatier reaction and its applications on Earth and in space. *Nat. Catal.* **2019**, *2*, 188–197. [CrossRef]
5. Kalz, K.F.; Kraehnert, R.; Dvoyashkin, M.; Dittmeyer, R.; Gläser, R.; Krewer, U.; Reuter, K.; Grunwaldt, J.D. Future Challenges in Heterogeneous Catalysis: Understanding Catalysts under Dynamic Reaction Conditions. *ChemCatChem* **2017**, *9*, 17–29. [CrossRef]
6. Rönsch, S.; Schneider, J.; Matthischke, S.; Schlüter, M.; Götz, M.; Lefebvre, J.; Prabhakaran, P.; Bajohr, S. Review on methanation—From fundamentals to current projects. *Fuel* **2016**, *166*, 276–296. [CrossRef]
7. Kiewidt, L.; Thöming, J. Predicting optimal temperature profiles in single-stage fixed-bed reactors for CO2-methanation. *Chem. Eng. Sci.* **2015**, *132*, 59–71. [CrossRef]
8. Kiewidt, L.; Thöming, J. Pareto-optimal design and assessment of monolithic sponges as catalyst carriers for exothermic reactions. *Chem. Eng. J.* **2019**, *359*, 496–504. [CrossRef]
9. Gräf, I.; Rühl, A.K.; Kraushaar-Czarnetzki, B. Experimental study of heat transport in catalytic sponge packings by monitoring spatial temperature profiles in a cooled-wall reactor. *Chem. Eng. J.* **2014**, *244*, 234–242. [CrossRef]
10. Dixon, A.G.; Partopour, B. Computational Fluid Dynamics for Fixed Bed Reactor Design. *Annu. Rev. Chem. Biomol. Eng.* **2020**, *11*, 109–130. [CrossRef] [PubMed]
11. Bracconi, M.; Ambrosetti, M.; Maestri, M.; Groppi, G.; Tronconi, E. A fundamental analysis of the influence of the geometrical properties on the effective thermal conductivity of open-cell foams. *Chem. Eng. Process. Process Intensif.* **2018**, *129*, 181–189. [CrossRef]
12. Ranut, P.; Nobile, E.; Mancini, L. High resolution X-ray microtomography-based CFD simulation for the characterization of flow permeability and effective thermal conductivity of aluminum metal foams. *Exp. Therm. Fluid Sci.* **2015**, *67*, 30–36. [CrossRef]
13. Iasiello, M.; Bianco, N.; Chiu, W.K.S.; Naso, V. Anisotropic convective heat transfer in open-cell metal foams: Assessment and correlations. *Int. J. Heat Mass Transf.* **2020**, *154*, 119682. [CrossRef]

14. Della Torre, A.; Montenegro, G.; Onorati, A.; Tabor, G. CFD characterization of pressure drop and heat transfer inside porous substrates. *Energy Procedia* **2015**, *81*, 836–845. [CrossRef]
15. Sinn, C.; Kranz, F.; Wentrup, J.; Thöming, J.; Wehinger, G.D.; Pesch, G.R. CFD Simulations of Radiative Heat Transport in Open-Cell Foam Catalytic Reactors. *Catalysts* **2020**, *10*, 716. [CrossRef]
16. Zafari, M.; Panjepour, M.; Emami, M.D.; Meratian, M. Microtomography-based numerical simulation of fluid flow and heat transfer in open cell metal foams. *Appl. Therm. Eng.* **2015**, *80*, 347–354. [CrossRef]
17. Wu, Z.; Caliot, C.; Flamant, G.; Wang, Z. Numerical simulation of convective heat transfer between air flow and ceramic foams to optimise volumetric solar air receiver performances. *Int. J. Heat Mass Transf.* **2011**, *54*, 1527–1537. [CrossRef]
18. Razza, S.; Heidig, T.; Bianchi, E.; Groppi, G.; Schwieger, W.; Tronconi, E.; Freund, H. Heat transfer performance of structured catalytic reactors packed with metal foam supports: Influence of wall coupling. *Catal. Today* **2016**, *273*, 187–195. [CrossRef]
19. Sinn, C.; Pesch, G.R.; Thöming, J.; Kiewidt, L. Coupled conjugate heat transfer and heat production in open-cell ceramic foams investigated using CFD. *Int. J. Heat Mass Transf.* **2019**, *139*, 600–612. [CrossRef]
20. Ambrosio, G.; Bianco, N.; Chiu, W.K.S.; Iasiello, M.; Naso, V.; Oliviero, M. The effect of open-cell metal foams strut shape on convection heat transfer and pressure drop. *Appl. Therm. Eng.* **2016**, *103*, 333–343. [CrossRef]
21. Bianchi, E.; Schwieger, W.; Freund, H. Assessment of Periodic Open Cellular Structures for Enhanced Heat Conduction in Catalytic Fixed-Bed Reactors. *Adv. Eng. Mater.* **2016**, *18*, 608–614. [CrossRef]
22. Diani, A.; Bodla, K.K.; Rossetto, L.; Garimella, S.V. Numerical investigation of pressure drop and heat transfer through reconstructed metal foams and comparison against experiments. *Int. J. Heat Mass Transf.* **2015**, *88*, 508–515. [CrossRef]
23. Du, S.; Tong, Z.X.; Zhang, H.H.; He, Y.L. Tomography-based determination of Nusselt number correlation for the porous volumetric solar receiver with different geometrical parameters. *Renew. Energy* **2019**, *135*, 711–718. [CrossRef]
24. Aguirre, A.; Chandra, V.; Peters, E.A.J.F.; Kuipers, J.A.M.; Neira D'Angelo, M.F. Open-cell foams as catalysts support: A systematic analysis of the mass transfer limitations. *Chem. Eng. J.* **2020**, *393*, 124656. [CrossRef]
25. Dong, Y.; Korup, O.; Gerdts, J.; Roldán Cuenya, B.; Horn, R. Microtomography-based CFD modeling of a fixed-bed reactor with an open-cell foam monolith and experimental verification by reactor profile measurements. *Chem. Eng. J.* **2018**, *353*, 176–188. [CrossRef]
26. Della Torre, A.; Lucci, F.; Montenegro, G.; Onorati, A.; Dimopoulos Eggenschwiler, P.; Tronconi, E.; Groppi, G. CFD modeling of catalytic reactions in open-cell foam substrates. *Comput. Chem. Eng.* **2016**, *92*, 55–63. [CrossRef]
27. Wehinger, G.D.; Heitmann, H.; Kraume, M. An artificial structure modeler for 3D CFD simulations of catalytic foams. *Chem. Eng. J.* **2016**, *284*, 543–556. [CrossRef]
28. Bracconi, M.; Ambrosetti, M.; Maestri, M.; Groppi, G.; Tronconi, E. A fundamental investigation of gas/solid mass transfer in open-cell foams using a combined experimental and CFD approach. *Chem. Eng. J.* **2018**, *352*, 558–571. [CrossRef]
29. Frey, M.; Bengaouer, A.; Geffraye, G.; Edouard, D.; Roger, A.C. Aluminum Open Cell Foams as Efficient Supports for Carbon Dioxide Methanation Catalysts: Pilot-Scale Reaction Results. *Energy Technol.* **2017**, *5*, 2078–2085. [CrossRef]
30. Montenegro Camacho, Y.S.; Bensaid, S.; Lorentzou, S.; Vlachos, N.; Pantoleontos, G.; Konstandopoulos, A.; Luneau, M.; Meunier, F.C.; Guilhaume, N.; Schuurman, Y.; et al. Development of a robust and efficient biogas processor for hydrogen production. Part 2: Experimental campaign. *Int. J. Hydrogen Energy* **2018**, *43*, 161–177. [CrossRef]
31. Bianchi, E.; Groppi, G.; Schwieger, W.; Tronconi, E.; Freund, H. Numerical simulation of heat transfer in the near-wall region of tubular reactors packed with metal open-cell foams. *Chem. Eng. J.* **2015**, *264*, 268–279. [CrossRef]
32. Nie, Z.; Lin, Y.; Tong, Q. Modeling structures of open cell foams. *Comput. Mater. Sci.* **2017**, *131*, 160–169. [CrossRef]
33. STAR-CCM+. Available online: https://www.plm.automation.siemens.com/global/en/products/simcenter/STAR-CCM.html (accessed on 6 October 2020).

34. Wehinger, G.D. Radiation Matters in Fixed-Bed CFD Simulations. *Chemie-Ingenieur-Technik* **2019**, *91*, 583–591. [CrossRef]
35. Iasiello, M.; Cunsolo, S.; Bianco, N.; Chiu, W.K.S.; Naso, V. Developing thermal flow in open-cell foams. *Int. J. Therm. Sci.* **2017**, *111*, 129–137. [CrossRef]

Chapter 7

Application of Heat Sources I — Thermal Radiation

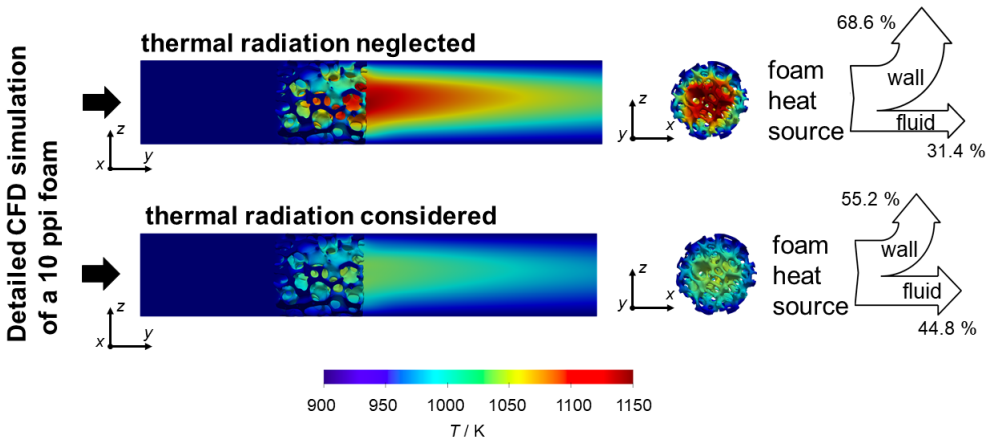

FIGURE 7.1: Graphical abstract of the manuscript on radiative heat transport.

The content of the first application chapter is published under the name *CFD Simulations of Radiative Heat Transport in Open-Cell Foam Catalytic Reactors* (Sinn et al., 2020a).

In the literature, CFD models often neglect modeling of thermal radiation. This chapter applies the heat source approach on studying the impact of thermal radiation on the overall heat transport in foam reactors. In this regard, a quantification of resulting heat flows and temperatures is conducted for different temperature levels (corresponding to different reactions), velocities, and foam properties (Figure 7.1). Thus, this chapter shows under which conditions thermal radiation needs to be considered and demonstrates the deviation when neglecting thermal radiation.

catalysts

MDPI

Article

CFD Simulations of Radiative Heat Transport in Open-Cell Foam Catalytic Reactors

Christoph Sinn [1], Felix Kranz [1], Jonas Wentrup [1], Jorg Thöming [1,2], Gregor D. Wehinger [3] and Georg R. Pesch [1,2,*]

1 Chemical Process Engineering, University of Bremen, Leobener Strasse 6, 28359 Bremen, Germany; sinn@uni-bremen.de (C.S.); fkranz@uni-bremen.de (F.K.); jwentrup@uni-bremen.de (J.W.); thoeming@uni-bremen.de (J.T.)
2 MAPEX Center for Materials and Processes, University of Bremen, Postbox 330 440, 28334 Bremen, Germany
3 Institute of Chemical and Electrochemical Process Engineering, Clausthal University of Technology, Leibnizstr. 17, 38676 Clausthal-Zellerfeld, Germany; wehinger@icvt.tu-clausthal.de
* Correspondence: gpesch@uni-bremen.de; Tel.: +49-421-218-63386

Received: 3 June 2020; Accepted: 23 June 2020; Published: 26 June 2020

Abstract: The heat transport management in catalytic reactors is crucial for the overall reactor performance. For small-scale dynamically-operated reactors, open-cell foams have shown advantageous heat transport characteristics over conventional pellet catalyst carriers. To design efficient and safe foam reactors as well as to deploy reliable engineering models, a thorough understanding of the three heat transport mechanisms, i.e., conduction, convection, and thermal radiation, is needed. Whereas conduction and convection have been studied extensively, the contribution of thermal radiation to the overall heat transport in open-cell foam reactors requires further investigation. In this study, we simulated a conjugate heat transfer case of a μCT based foam reactor using OpenFOAM and verified the model against a commercial computational fluid dynamics (CFD) code (STAR-CCM+). We further explicitly quantified the deviation made when radiation is not considered. We studied the effect of the solid thermal conductivity, the superficial velocity and surface emissivities in ranges that are relevant for heterogeneous catalysis applications (solid thermal conductivities 1–200 W m^{-1} K^{-1}; superficial velocities 0.1–0.5 m s^{-1}; surface emissivities 0.1–1). Moreover, the temperature levels correspond to a range of exo- and endothermal reactions, such as CO_2 methanation, dry reforming of methane, and methane steam reforming. We found a significant influence of radiation on heat flows (deviations up to 24%) and temperature increases (deviations up to 400 K) for elevated temperature levels, low superficial velocities, low solid thermal conductivities and high surface emissivities.

Keywords: open-cell foams; conjugate heat transfer; CFD; radiation; OpenFOAM; STAR-CCM+

1. Introduction

The management of heat transport in catalytic reactors is known to be key for optimizing yield and ensuring safe and robust operation [1]. Especially in exothermic reactions (e.g., CO_2 methanation), ignoring proper heat transport design of the reactor can lead to uncontrollable hot-spot formation or even thermal runaways. Moreover, catalysts can be harmed due to sintering effects or unwanted byproducts that might be formed, which then lead to catalyst poisoning [2]. The highly exothermic CO_2 methanation reaction is part of the power-to-gas (PtG) concept where renewable excess energy (e.g., from wind turbines) is stored (electro-)chemically by converting hydrogen and carbon dioxide to methane. This process, among others, has the potential to drastically reduce the dependence on fossil fuels and reduce carbon dioxide emissions. The supply of renewable energy is fluctuating, which leads

to a demand of dynamic operable reactors [3]. Additionally, the power grids might not be able to withstand and transport all renewable energy during peak wind or sun hours, which makes small scale dynamic operated plants a current research topic [4]. Usually, catalytic fixed-bed reactors that contain pellets are used for steady conversion of hydrogen to methane. Recent studies have shown, that, for small-scale reactors and low flow rates, structured catalyst carriers (such as open-cell foams) have advantageous heat transport properties over conventional packed bed reactors [5–7]. Open-cell foams are characterized by an interconnected solid matrix, allowing for unhindered radial heat transport as well as high porosities and relatively high specific surface areas, yielding low pressure drop and proper catalyst inventory, respectively [8].

The three heat transport mechanisms, i.e., conduction, convection, and thermal radiation, in the bed need to be understood to properly design catalyst carriers. For the investigation of heat transport mechanisms in catalyst carriers, computational fluid dynamics (CFD) simulations have proven to deliver valuable insight [9–13]. Using CFD techniques, pure thermal conduction and conjugate heat transfer were studied in irregular foams [14–16] as well as idealized foams [17–19]. In contrast, studies on radiative heat transport in open-cell foams and structured reactors are rare. The Stefan–Boltzmann law describes the maximum heat flow emitted by a surface of a black body depending on the body temperature:

$$q = \sigma \, T_s^4, \tag{1}$$

with q being the specific heat flow, σ the Stefan–Boltzmann constant and T_s the solid body temperature. This relationship underlines that the contribution of radiation to the overall heat transport is low for reactions at low to medium temperature and explains why radiation is often neglected in modeling. Studies dealing with thermal radiation in open-cell foams mainly focused on deriving optical parameters and deploying analytical or pseudo-homogeneous models that are based on the so-called Rosseland approximation [20–25]. The pseudo-homogeneous approaches do not distinguish between solid and fluid phase and utilize effective transport properties (e.g., effective or two-phase thermal conductivity) which can be used to estimate general contributions of radiation to the overall heat transport. For instance, the general influence of temperature levels, window diameter, or thermal conductivity on the total heat flows can be evaluated. However, homogeneous models are only suitable for a certain parameter range (i.e., velocity, foam properties, and temperature range) and, compared to experiments, can deviate in the order magnitude of about 30–40% [26,27]. Furthermore, homogeneous models are not always suitable for prediction of temperatures when heat is produced in the solid (i.e., exothermic reaction) [28]. An overview of currently available pseudo-homogenous models for open-cell foams as well as their range is for example given in [6]. Furthermore, experimental techniques and pseudo-homogeneous models generally cannot resolve occurring heat flows between the solid foam, fluid, and reactor wall parts that might give valuable insight in the foam's heat transport ability. In contrast, three-dimensional CFD simulations of an open-cell foam embedded in a tube can supply information about the different heat flows that are mandatory to fully understand structured reactors and, hence, improve the general design [28]. Some researchers considered radiation in their CFD models, e.g., for solar receivers [29] and for catalytic exothermic reactions (catalytic partial oxidation of methane [30]; dry reforming of methane [31]; CO oxidation [32]; methane steam reforming [33]). The explicit consideration of radiation in catalytic gas-phase reactors has a significant influence on the computed concentration and temperature fields which was shown in a honeycomb reactor for the partial oxidation of methane [34] and in a pellet reactor for the methane steam reforming reaction [35]. Hettel et al. [34] found temperature increases of up to 56 K and Wehinger and Flaischlen [35] found a maximum yield increase of up to 70% with temperature differences below 40 K. The influence of radiation modeling on simulated temperature and yields decreased for a higher Reynolds number (i.e., superficial velocity) as the relative contribution of dispersion increases [35]. In a different study, a pure conjugate heat transfer case in a fixed-bed pellet reactor also indicated the importance of radiation modeling for the design of catalytic reactors since neglecting radiation led to a 6% temperature increase

for a wall temperature of 800 K [36]. To sum up, radiation in CFD simulations of catalytic reactors should generally be considered for elevated temperatures and low superficial velocities [37].

The real geometry of open-cell foams are complex, thus modeling and simulation of catalytic reactions in such reactors are highly demanding in terms of mesh quality and computational time [38]. In order to mimic exothermic (or endothermic) reactions and study heat flows and temperature fields by means of CFD simulations, we proposed to implement uniformly distributed heat sources (or sinks) in the solid [28]. For the CO_2 methanation reaction in a 25 × 24 mm foam, we estimated a heat source intensity of 50 W (i.e., 1.9×10^7 W m^{-3}). Generally, this approach supplies the desired heat flows and allows to study thermal effects decoupled from chemistry. However, radiation was not considered in the study. As the explicit simulation of thermal radiation is computationally expensive, it is therefore important to quantify under which conditions radiation can be neglected.

In this study, we quantify the effect of thermal radiation on heat flows and temperature distributions in a 10 ppi open-cell foam structured reactor with heat production in the solid, i.e., homogeneously distributed heat sources. The steady-state conjugate heat transfer simulations are carried out with and without radiation for several input parameters, such as solid thermal conductivity (1–200 W m^{-1} K^{-1}), superficial velocity (0.1–0.5 m s^{-1}), surface emissivity (0–1) and temperature level that are relevant for heterogeneous catalysis and industrial process conditions. For this close-to-reactor setup, the temperature levels and the analyzed range correspond roughly with prominent reactions like the Fischer–Tropsch synthesis (500 K, [39]), CO_2 methanation (700 K, [2]), dry reforming of methane (900 K, [40]), and steam reforming of methane (1200 K, [41]). The geometry information of the open-cell foam is based on a µCT scan, and the simulation is carried out in the open source CFD framework OpenFOAM. Further, the model is verified against a commercial CFD code (STAR-CCM+). In particular, we analyze the influence of radiation modeling on occurring heat flows as well as solid temperature distributions. We expect this study to guide through the conditions under which the modeling of thermal radiation in a foam reactor is necessary.

2. Results and Discussion

2.1. Model Verification

In our previous study [28], the conjugate heat transfer model of the 10 ppi foam was validated against correlations and verified against other CFD data for heat transfer coefficients and pressure drop. To ensure reliable results, a grid independence study was conducted (Figure 1), where the mesh with approximately 4 million cells indicated sufficient results for the model with and without radiation.

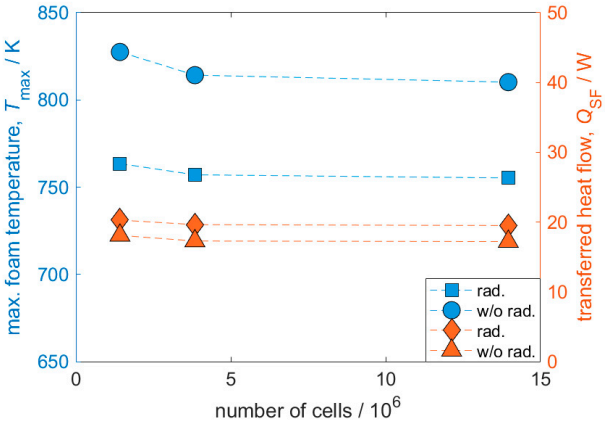

Figure 1. Grid independence study for the OpenFOAM mesh. The mesh with approx. 4 million cells was found to be sufficient for this study. Conditions: T_w = 600 K; v = 0.5 m s^{-1}; S = 50 W; ε = 0.9; λ_s = 5 W m^{-1} K^{-1}.

In a second step, the open source OpenFOAM model was verified against the commercial STAR-CCM+ model (see Figure 2). All fluid parameters, except for the emissivity κ, are temperature-dependent and corrected in both models. In contrast, the solid properties are fixed. Resulting heat flows for both models are depicted in Figure 2a,b. All fixed temperature boundary conditions have the same value, which means the only energy entering the system is caused by the volumetric homogeneously distributed heat source in the solid (see Figure 3).

Therefore, the simple global energy balance for the system reads:

$$S = 50\ \text{W} = Q_{\text{SF}} + Q_{\text{SW}}, \tag{2}$$

where Q_{SF} denotes the heat flow transferred from the solid to the fluid and Q_{SW} denotes the conductive heat flow from the solid to the wall. The bar graphs in Figure 2a,b, thus all individually sum up to 50 W. For a wall temperature of T_{w} = 900 K (a) and without considering radiation, the convective part of the stacked bar (blue: solid/fluid) is less than 20% of the overall heat flow for both, the OpenFOAM as well as the STAR-CCM+ model. When radiation is accounted for, this ratio becomes larger than 20%. The consideration of radiation in the conjugate heat transfer model enables another heat transport path for the thermal energy. Hence, the solid temperature distribution becomes more homogeneous (see Figure 3). Here, the heat flow from solid to wall is purely conductive whereas computed heat flow from solid to fluid combines convective as well as radiative heat transfer. Consequently, the computed heat flow from solid to fluid increases. This is because the more homogeneous solid temperature causes a larger (i.e., distributed over a larger foam part) temperature gradient between solid and fluid at the parts of the foam that were cooler when radiation was neglected. For a wall temperature of T_{w} = 1200 K (b), the same behavior can be observed. In general, the calculated heat flows from OpenFOAM and STAR-CCM+ are comparable for both temperature levels and with or without radiation, indicating the applicability of either software.

The extra heat transport pathway due to radiation significantly influences the temperature distribution. A flattening of maximum and mean solid temperatures can be observed upon consideration of radiation for both temperatures (see Figure 2c,d). Comparing the maximum and median temperature with and without radiation between OpenFOAM and STAR-CCM+, the differences between both software packages are more pronounced compared to the heat flows, especially when looking at the maximum solid temperature calculated from both software packages. This deviation is, however, still insignificant, with a maximum discrepancy of less than 15 K at most. The temperature histograms (Figure 4a,b) show a qualitatively comparable distribution of the temperature increases per volume fraction regardless if radiation is considered or not. However, deviations between both software packages are identifiable especially for the last bins of Figure 4a,b. It can therefore be concluded that the alternating applied discretization methods (e.g., cell morphology) could be the reason for the slight deviations. The negligible deviations between both software packages indicates the applicability of either tool. The detailed solid and fluid temperature distribution of all cases are not shown in the following, since for the very same foam we already analyzed temperature fields of both phases for several applied heat source intensities, superficial velocities, and thermal conductivities systematically [28]. We concluded that the entire solid and fluid temperature fields shift similarly and hence show same trends. In the following, we also omit showing both heat flows, i.e., solid/fluid and solid/wall, since the missing can easily be calculated using Equation (2).

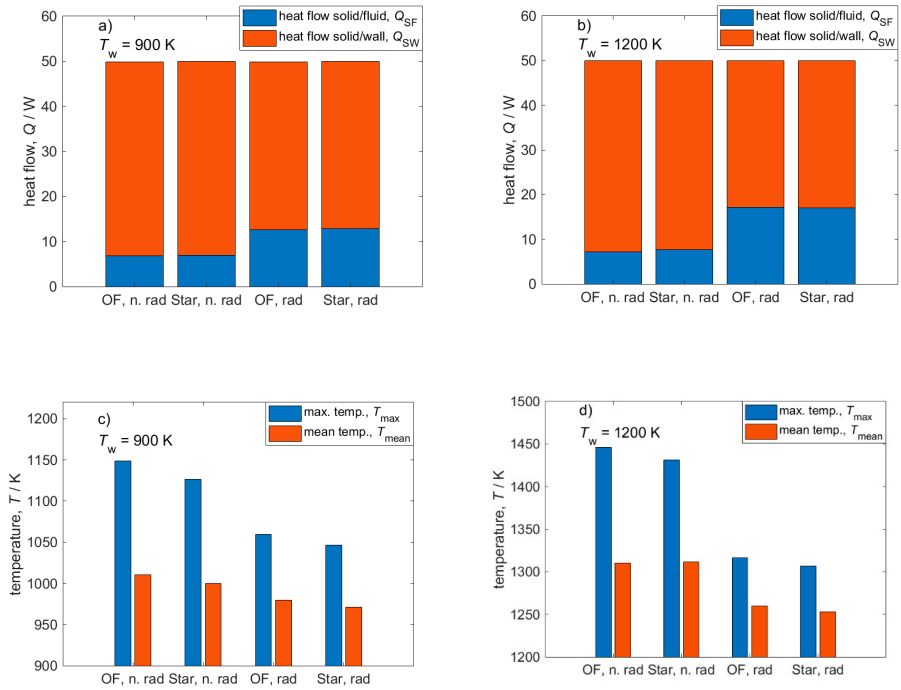

Figure 2. Verification of OpenFOAM results w/and w/o radiation against commercial software STAR-CCM+. Conditions: λ_s = 5 W m^{-1} K^{-1}; v = 0.5 m s^{-1}; ε = 0.9. (**a**) Heat flows at T_W = 900 K; (**b**) heat flows at T_W = 1200 K; (**c**) temperatures at T_W = 900 K; (**d**) temperatures at T_W = 1200 K.

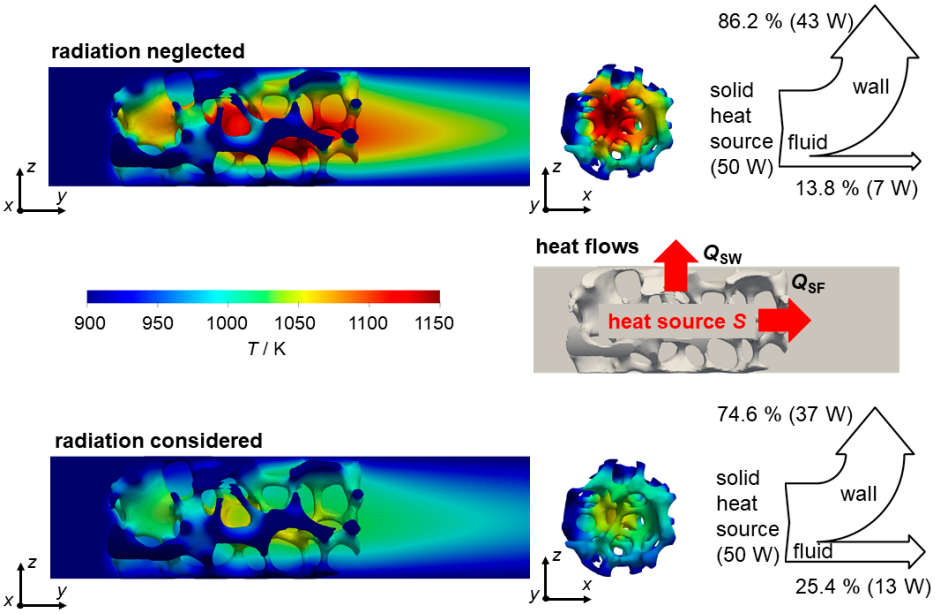

Figure 3. Depiction of temperature fields and heat flows with and without radiation for the verification case simulated in OpenFOAM. The applied heat source S causes a conductive heat flow to the wall (Q_{SW}) and a convective heat flow to the fluid (Q_{SF}). Conditions: T_w = 900; λ_s = 5 W m^{-1} K^{-1}; v = 0.5 m s^{-1}; ε = 0.9.

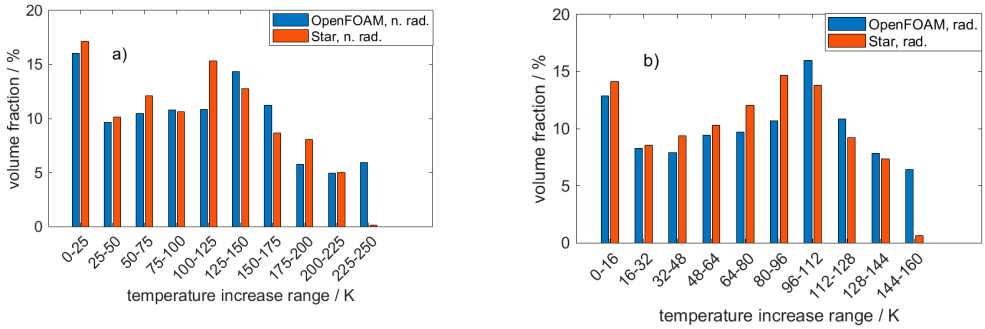

Figure 4. Histogram of temperature increases for the verification case. Conditions: T_w = 900; λ_s = 5 W m^{-1} K^{-1}; v = 0.5 m s^{-1}; ε = 0.9. (**a**) No radiation considered; (**b**) radiation considered.

2.2. Quantification of Heat Flows and Temperature Distributions

2.2.1. Influence of the Wall Temperature and Solid Thermal Conductivity

Figure 5 shows fluid temperature in the center plane for a case with and without radiation (T_w = 900; λ_s =5 W m^{-1} K^{-1}). Here, the fluid temperature drastically increases when radiation in the model is neglected. Furthermore, the overall increased fluid temperature also enhances the development of the temperature wake behind the foam. Consequently, the solid foam temperature increases when radiation is neglected (Figure 5). Keep in mind that a constant heat source (50 W) is set in the solid volume. A perfect wall contact between foam and wall ensures unhindered heat transport [42], which results in a relatively cool outer zone of the foam. In contrast, inside the solid, hot spots develop which strongly depend on the thermal conductivity [28]. The drastic changes in both fluid and solid temperatures, due to radiation effects, can cause dramatically different results when an actual catalytic chemical reaction is simulated. This is especially true when the overall conversion is mainly influenced by the temperature (i.e., kinetically controlled regime). The homogeneously distributed heat source approach cannot determine the actual maximum temperature of a chemical reaction, because the heat production varies locally due to temperature-dependent kinetics. Nevertheless, the maximum temperature increase, calculated by the heat source approach, can at least be expected in an actual exothermal reaction when the same amount of heat is released.

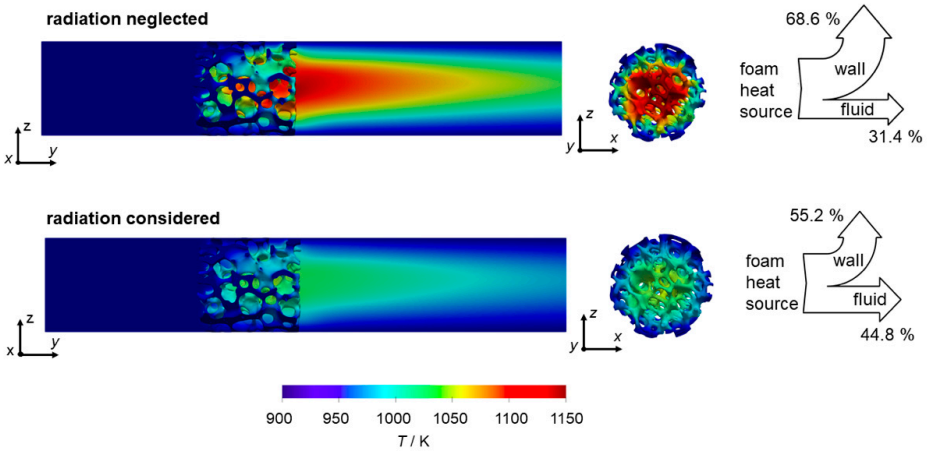

Figure 5. Depiction of temperature fields w/and w/o radiation. Conditions: T_w = 900; λ_s = 5 W m^{-1} K^{-1}; v = 0.5 m s^{-1}; ε = 0.9.

The fact that neglecting thermal radiation effects in fixed-bed reactors can cause significantly different simulated temperature distributions was already reported [35,36]. These results were obtained for a specific reaction and pellets used as catalyst carriers. With the aid of heat sources, as shown here, the thermal effects can be described decoupled from specific chemistry or reaction and are thus more universal. To assess the deviation caused by neglecting radiation in heterogeneous catalysis, we conduct a systematic parameter variation and quantify the influence of radiation modeling on temperature profiles and heat flows. Firstly, we investigate the influence of the applied temperature level on the heat flows (Figure 6). Since the absolute temperature level affects the radiative heat flow by the power of 4 (see Equation (8)), the absolute deviation between cases with and without considered radiation increases distinctively with temperature (as we will see). For the cases depicted in Figure 5 (T_w = 900 K and λ_s = 5 W m^{-1} K^{-1}), the absolute deviation amounts to almost 7 W (14%). Furthermore, we observe that, from a threshold on (λ_s = 5 W m^{-1} K^{-1}), the absolute deviations in radiative heat flow decrease with increasing solid thermal conductivities. This is due to the less pronounced heat transport limitations in the foam center for high conducting materials. Here, heat is more likely transported via conduction through the continuous solid strut network and thus, the two models yield more comparable results. Even for quite high solid thermal conductivities the absolute deviations in radiative heat flow can be substantial. For instance, for λ_s = 50 W m^{-1} K^{-1} at T_w = 1200 K the absolute deviation amounts to 8 W (16%) and for λ_s =200 W m^{-1} K^{-1} still to approx. 4 W (8%), respectively. That means even for highly conducting materials (e.g., metals) radiation in open-cell foams cannot generally be neglected at low flowrates.

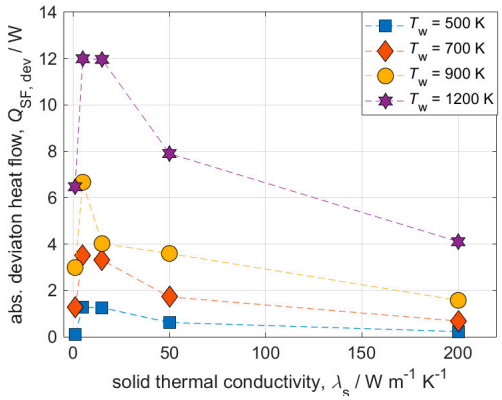

Figure 6. Influence of thermal conductivity on absolute deviations in heat flows for different temperature levels. Conditions: v = 0.5 m s^{-1}; ε = 0.9.

Interestingly, the absolute deviation in heat flows is not monotonically decreasing with λ_s, but the values for very low thermal conductivities, i.e., λ_s = 1 W m^{-1} K^{-1}, are all lower than for intermediate values. Here, the absolute deviation caused in radiative heat flow can be almost 50% lower than at λ_s = 5 W m^{-1} K^{-1} (which is the second data point, compare for instance purple line in Figure 6). The reason for that diverging behavior certainly lies in the drastic temperature increase of both phases (fluid and solid) at very low solid thermal conductivity. The corresponding maximum and mean deviations in temperature increases support this hypothesis (Figure 7). Between the two smallest investigated solid thermal conductivities, i.e., when λ_s is increased from 1 W m^{-1} K^{-1} to 5 W m^{-1} K^{-1}, the deviations in maximum and mean temperatures decrease tremendously. As a consequence, for the given boundary conditions, the impact of radiation modeling on heat flows is negligible at very low λ_s as the entire system itself (fluid and solid temperatures) forms a temperature hot spot. Here, the relative difference between the phase temperatures decrease and hence the absolute deviation of the heat flows.

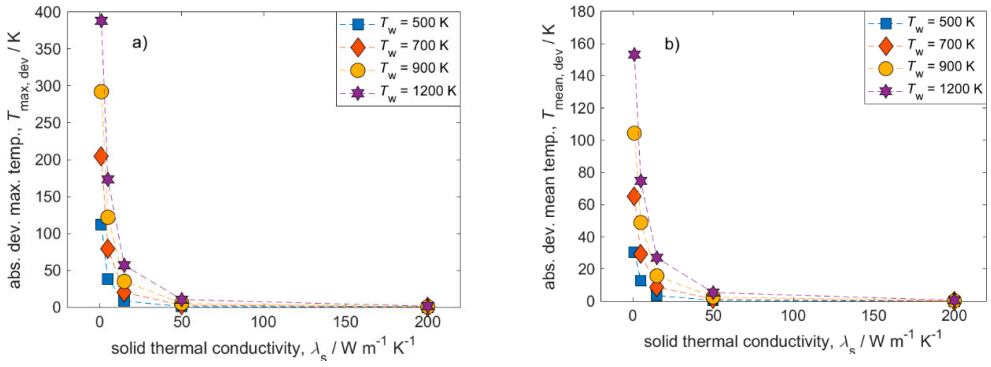

Figure 7. Influence of thermal conductivity on absolute deviations in solid temperatures for different temperature levels. Conditions: $v = 0.5$ m s^{-1}; $\varepsilon = 0.9$. (**a**) Maximum temperature; (**b**) mean temperature.

The absolute deviations in radiative heat flows and in maximum and mean temperature increase show a similar general trend. Hence, increasing thermal conductivities generally decreases the deviation caused when radiation is not considered. However, the absolute deviations of radiative heat flows might significantly differ from the temperature deviation when compared at the same certain condition. As an example, for a solid thermal conductivity of $\lambda_s = 50$ W m^{-1} K^{-1}, the absolute deviation for both maximum and mean temperature increase are negligible regardless of the applied temperature level (Figure 7a,b). In contrast, the absolute deviations in heat flows can still be as high as 8 W (of 50 W total heat flow). Even at $\lambda_s = 200$ W m^{-1} K^{-1}, there is a 4 W (i.e., almost 10%) deviation in radiative heat flow at 1200 K wall temperature while deviations in mean and maximum temperature increase are virtually non-existent. This indicates that the ability of the foam to transport heat via conduction (i.e., the thermal conductivity) is not limiting and can balance the missing contribution of the radiation. Concluding, even though no temperature changes can be identified between models with and without radiation, the absolute and relative deviation in computing the heat flows can still be significant. Hence, one should consider these findings before omitting radiation modeling in open-cell foams at elevated temperatures. Once again, we want to stress that, for actual chemical reactions, the absolute deviations for maximum temperatures between models with and without radiation should be even more severe (when equal amounts of heat production are compared).

2.2.2. Influence of the Superficial Velocity

Catalytic foam reactors can outperform conventional pellet fixed-bed reactors at low velocities [5]. Therefore, the influence of radiation modeling on heat flows as well as temperature increases at different superficial velocities was also quantified. For a wall temperature of $T_w = 900$ K and a solid thermal conductivity of $\lambda_s = 5$ W m^{-1} K^{-1}, the corresponding absolute deviations in heat flow as well as deviations in maximum and mean temperature are plotted against the superficial velocity in Figure 8a. Both the absolute deviation for heat flows and temperatures decrease with increasing superficial velocity. In the investigated range of superficial velocities, the absolute error for heat flows increases from about 7 W (14%, for 0.5 m s^{-1}) to about 12 W (24%, for $v = 0.1$ m s^{-1}). Due to increasing convective heat transfer between the fluid and solid at higher superficial velocities, the foam is cooled more efficiently. Therefore, the contribution of radiation as heat transport mechanism obviously decreases with increasing superficial velocity, as convection becomes more dominant. This is underlined by the specific heat flow from solid to wall plotted against the superficial velocity (Figure 8b). The transition line indicates the dominant heat removal mechanism. A value greater than 0.5 means conduction is dominant whereas a value lower than 0.5 mean convection is dominant. Here, all simulations are conduction dominated, although the case with highest investigated velocity (0.5 m s^{-1}) and considered radiation becomes close to convection dominated. Concluding, for foam reactors with conditions where convection is dominant, the consideration of radiation is definitely less important. Here, it can

only be assumed that the absolute error, which can reach values up to 24% (Figure 6), would have an asymptotic behavior for even higher superficial velocities. This should be addressed in further studies. We would like to note that the results from Figures 6 and 7 would have shown even larger absolute deviations at smaller superficial velocities. Hence, the magnitude of superficial velocities plays a major role in the consideration of radiation.

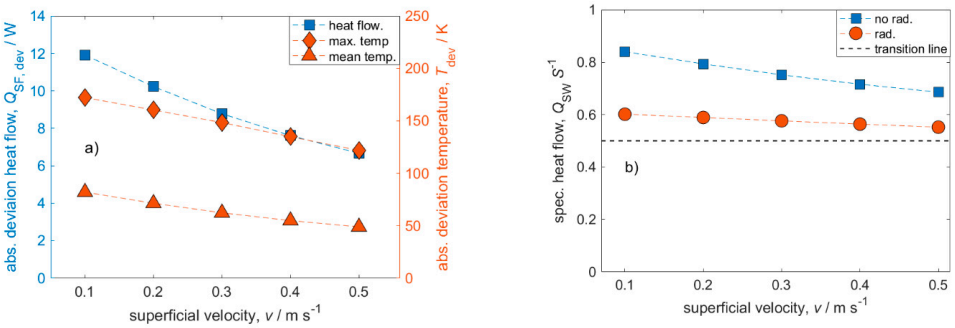

Figure 8. Influence of the superficial velocity on transferred heat flows and maximum and mean solid temperatures. (**a**) Absolute deviations between models w/and w/o considered radiation. (**b**) Specific heat flow solid to wall. The transition line indicates the dominant heat removal mechanism (value > 0.5 = conduction; value < 0.5 = convection). Conditions: T_w = 900 W; ε = 0.9; λ_s = 5 W m^{-1} K^{-1}.

2.2.3. Comparison with a Homogeneous Model

This work's CFD simulations already highlighted and quantified the importance of radiation modeling under certain process conditions (e.g., temperature level and solid thermal conductivity). To assess if the modeling and simulation effort of CFD simulations for the presented cases is justified, a comparison between CFD simulation results and analytical results calculated using a simple pseudo-homogeneous model is conducted in the following. Pseudo-homogeneous models consider only one effective phase and, thus, have an average temperature and an effective (or two-phase) thermal conductivity. For homogeneous models this effective thermal conductivity is the key transport property, which can be obtained through experiments or heterogeneous models. Since homogeneous models only consider one phase, there is technically no heat transfer, only effective heat transport. Currently, there are only two pseudo-homogeneous models available that consider thermal radiation and forced convection [21,26]. The parameter range from Fischedick et al. [26] is more suitable for this study and is consequently used in this study. The radial contribution to the effective thermal conductivity resembles approximately with the heat flow from solid to wall and further consists of a stagnant part (conduction + radiation) and a dispersive part (convection):

$$\lambda_r^{(eff)} = \left(\lambda_{cond}^{(eff)} + \lambda_{rad}^{(eff)}\right) + \lambda_{disp}^{(eff)}. \quad (3)$$

The ratio of conductive effective thermal conductivity to total effective thermal conductivity should give the same trend as the specific heat flow solid to wall (Q_{SW} S^{-1}). This approximation should be valid as long as temperature differences remain low between the cases (i.e., high thermal solid conductivities). The heat flow ratios and ratios of the effective thermal conductivities, respectively, are plotted against the full range of thermal conductivities at different temperature levels in Figure 9. Both approaches show the same qualitative trend regardless of the consideration of radiation or the applied temperature level. The homogeneous model reflects the trends of decreasing importance of radiation modeling for increasing thermal conductivities as well as decreasing temperature levels. It can also be seen that the simulation results as well as the analytical model agree better at high thermal conductivity and low temperature level. With increasing temperature levels, the contribution

of radiation in the analytical model seems to be more pronounced than in the CFD simulations. When compared to experimental data, the homogeneous model was able to match approximately 80% of the data points with less than 30% deviation [26]. Hence, the homogeneous model can give a convenient fast glance on the general contribution of radiation on the total heat transport. However, for a more thorough quantification, CFD simulations or experiments are needed. Further, the need for even more accurate (engineering) models that can be used for the estimation of heat transport contributions becomes obvious.

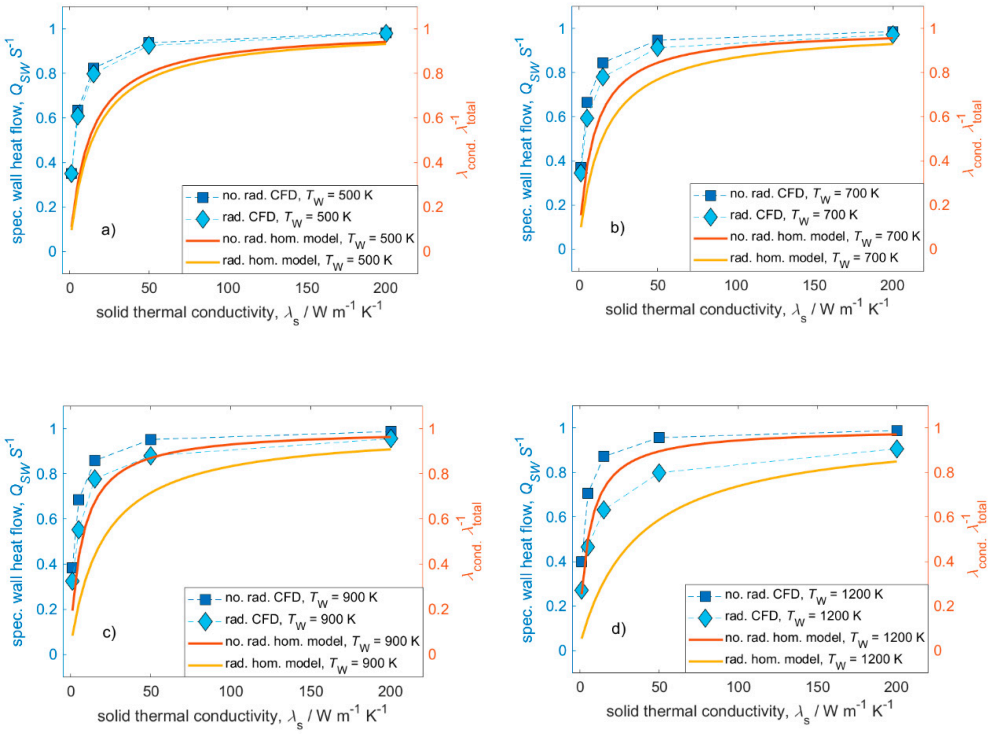

Figure 9. Comparison between heat flow ratios of CFD simulations and homogeneous model [26] for different solid thermal conductivities and temperature levels. Conditions: v = 0.5 m s^{-1}; ε = 0.9. (**a**) T_W = 500; (**b**) T_W = 700; (**c**) T_W = 900; (**d**) T_W = 1200.

2.2.4. Influence of the Surface Emissivity

So far, the surface (or solid) emissivity has been set to a fixed value of ε = 0.9 in all simulations. This value depends on surface texture, material, wavelengths, absorbed molecules, and other parameters [43]. In practice, the exact determination of the surface emissivity might be challenging. For catalytic reactions, the foams are generally coated with active catalytic material (i.e., washcoat). The washcoats might change and differ in their surface emissivity. On top of that, the surface emissivity might change during chemical reactions due to soot or coke deposition. Therefore, it is often only practical to estimate a range of surface emissivities.

Generally, the surface emissivity describes the participation of the solid phase in radiative heat transport. Hence, with decreasing surface emissivity, the radiative heat flow drops while the solid temperature rises (Figure 10). A low surface emissivity thus indicates little solid contribution to the radiation. However, when ε larger than 0.5 and at wall temperatures of T_W = 900 K and T_W = 700 K, heat flows and solid temperature (mean and maximum) are almost independent of ε. For the elevated wall temperature, T_W = 1200 K, changes in heat flows and solid temperatures are more pronounced and heat flows and temperatures become independent of ε only for ε almost 1. Concluding, increased

wall temperatures also increase the influence of ε on heat flows and temperature fields. In the surface emissivity range $0 < \varepsilon < 0.5$, the changes in heat flows and temperatures are more severe. Hence, inaccurately determined emissivity values influence simulation results more significantly for materials with general lower emissivity.

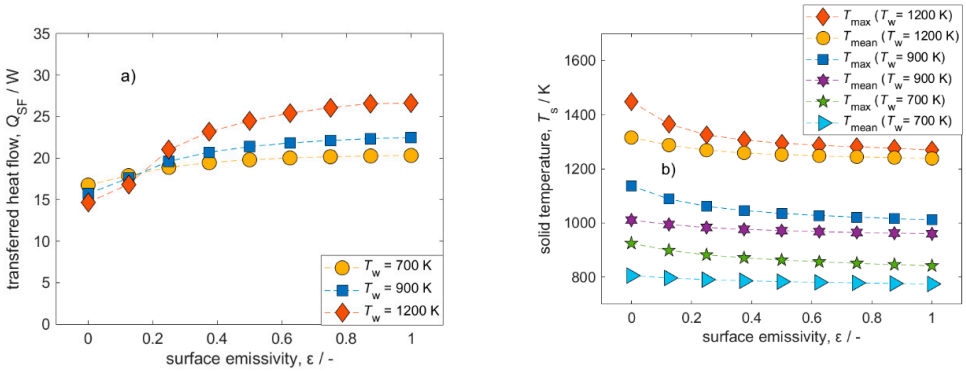

Figure 10. Influence of surface emissivity on transferred heat flows and maximum as well as mean solid temperatures. (**a**) Transferred heat flow. (**b**) Solid temperatures. Conditions: v = 0.5 m s^{-1}; λ_s = 5 W m^{-1} K^{-1}.

3. Materials and Methods

3.1. General Model and Meshing

The investigated geometry represents a structured reactor, consisting of a 10 ppi alumina µCT-based foam embedded in a tube (see Figure 11). In front and behind the embedded foam are a 40 mm inlet and a 64 mm outlet section, respectively. The overall processing (from scanning to actual CAD model) of the 10 ppi µCT foam is described in more detail in [28]. Furthermore, the geometrical properties of the foam can be found in Appendix A (Table A1). The model of this study addresses the laminar steady-state conjugate heat transfer between air and foam with the explicit consideration of radiation. The same fixed temperature boundary conditions are prescribed at the wall as well as the fluid inlet. The solid phase contains a homogeneously distributed heat source which is the only energy that enters the system. The fixed value of S = 50 W was determined in a previous study to be the representative thermal power that evolves during the CO_2 methanation reaction in a foam [6,28], which was adopted for this study. We note that, the effect of heat source can be easily extrapolated to other heat source intensities as it was shown in [28] for the range of $5 \leq S \leq 150$ W.

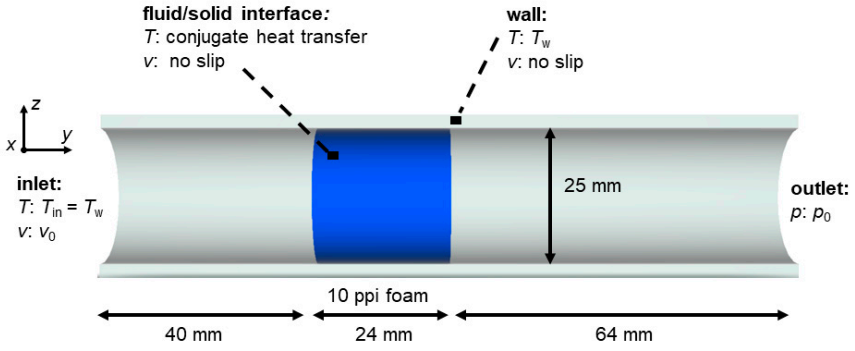

Figure 11. Geometrical model and main boundary conditions investigated in this study. The 10 ppi foam is similar to the one from [28].

Most of the results of this work were gained using the open source finite-volume-based toolbox OpenFOAM (version 7, [44]) and the solver chtMultiRegionFoam. For the OpenFOAM multi-region meshes, the cartesian mesh creator snappyHexMesh was utilized. For the verification against the commercial CFD software STAR-CCM+ from Siemens PLM (Plano, TX, USA) [45], a polyhedral mesh was created with the integrated STAR-CCM+ meshing utility. To speed up meshing and simulations, only a representative part of the foam (Ø12 × 24 mm, see Appendix B, Figure A1) was used for comparison and verification.

3.2. Governing Equations and Thermal Radiation Modeling

Aside from the radiation modeling, the major parts of this work's model are similar to our previous study [28]. The essential model properties are listed in Table 1. For additional information regarding the model, the reader is thus referred to [28].

Table 1. Model properties investigated in this study.

Property		Assumption
Fluid dynamic viscosity	μ	Sutherland equation
Fluid heat capacity	$c_{p,f}$	Janaf model (OpenFOAM); polynomial (STAR-CCM+)
Fluid thermal conductivity	λ_f	Eucken approximation (OpenFOAM); polynomial (STAR-CCM+)
Fluid density	δ_f	ideal gas law
Superficial velocity	v	const. (0.1–0.5 m s^{-1})
Pore Reynolds number	$Re_p = \frac{v \cdot d_s \cdot \rho}{\mu}$	const. (1–20)
Fluid absorption coefficient	κ	const. (10^{-9})
Solid heat capacity	$c_{p,s}$	const. (1000 J kg^{-1} K^{-1})
Solid thermal conductivity	λ_s	const. (1–200 W m^{-1} K^{-1} [46])
Solid density	δ_s	const. (3950 kg m^{-3})
Solid heat source	S	const. (total: 50 W; specific: 1.9×10^7 W m^{-3})
Solid surface emissivity	ε	const. (0.1–1)
Wall surface emissivity	ε_w	const. (0.65)
Gravitational acceleration	-	neglected
Radiation	-	fvDOM model (OpenFOAM); DOM model (STAR-CCM+)
Turbulence	-	neglected

For the Newtonian fluid (air) with neglected gravitation, the conservation equations for mass reads:

$$\nabla \cdot (\rho_f \mathbf{U}) = 0, \tag{4}$$

with ρ_f denoting the fluid's density and $\mathbf{U}$ denoting the velocity field. The conservation of momentum can be described by:

$$\nabla \cdot (\rho_f \mathbf{U} \otimes \mathbf{U}) + \nabla \cdot (\mu (\nabla \otimes \mathbf{U} + (\nabla \otimes \mathbf{U})\mathrm{T}) - 2/3\mu (\nabla \cdot \mathbf{U})\mathbf{I}) - \nabla p = 0, \tag{5}$$

where h denotes the enthalpy, which is followed by the conservation of energy:

$$-\nabla \cdot (\rho_f \mathbf{U} h) - \nabla \cdot (\lambda_f \nabla T_f) = 0, \tag{6}$$

with λ_f being the fluid's thermal conductivity. The solid phase, in contrast, is described only by the conservation of energy:

$$\lambda_s \left(\nabla^2 T_s\right) + S = 0, \tag{7}$$

with λ_s being the solid's thermal conductivity, T_s the solid's temperature, and S the specific artificial heat source. The set of equations is completed by the ideal gas law.

At high temperatures the effect of thermal radiation on the overall heat transport might be severe. In contrast to conduction and convection, radiation does not need media to transport heat since electromagnetic waves can spread in vacuum. Further, heat transport by radiation does not only depend on the value of the temperature gradient, but also on the absolute temperature level. The maximum specific heat flow (W m^{-2}), that a real solid body emits, can be expressed by the Stefan–Boltzman law (Equation (1)) extended by the surface emissivity ε:

$$\dot{q} = \sigma \, \varepsilon \, T_s^4, \tag{8}$$

with σ being the Stefan-Boltzmann constant (5.67×10^{-8} W m^{-2} K^{-4}); the surface emissivity is generally between 0 and 1 (colored or real body: $\varepsilon = f(T)$; grey body: ε = const.; black body: $\varepsilon = 1$). When radiation hits a material, the energy can be reflected, absorbed or transmitted (depending on e.g., wavelength or material):

$$\dot{q} = \gamma \, \dot{q} + \alpha \, \dot{q} + \tau \, \dot{q}, \tag{9}$$

with γ denoting the degree of reflection, α the degree of absorption and τ the degree of transmission.

Furthermore, the radiant intensity I is the specific radiant heat flux per unit solid angle (W m^{-2} sr^{-1}):

$$I = \sigma \, \varepsilon \, T_s^4 \frac{1}{\pi}. \tag{10}$$

Generally, radiation modeling in CFD codes can be distinguished in approaches with and without fluid participation. OpenFOAM contains the three radiation models viewFactor (no fluid participation), fvDOM (finite volume discrete ordinate model), and the P1 model. In a preliminary study we found that an inappropriate model can severely overestimate the contribution of radiation to the overall heat transport (relative error E_{rel} = 50%; Appendix C). In this study, only fluid participating approaches are used as they have been successfully applied in literature for high temperature heat transfer and are also suitable for symmetry boundary conditions [34,35,47]. We also note that the fluid participation should not play a significant role in this study for the model fluid (air) as well as the model conditions (i.e., atmospheric pressure, temperatures and geometrical dimensions) [34,35]. Both models basically solve the radiative transfer equation (RTE) that describes the change of the radiant intensity at any point along a path through a participating medium (fluid) depending on scattering, emission and adsorption effects [43]. For further explanation and discussion the reader is referred to [43] and [48]. The RTE reads [34,48]:

$$\frac{dI\,(r,s)}{d\,s} = \kappa I_b\,(r) - \kappa\, I\,(r,\,s) - \sigma_s I\,(r,s) + \frac{\sigma_s}{4\pi} \int_{4\pi} I_{incident}\,(s_i)\Phi(s_i,\,s)d\Omega_i, \tag{11}$$

where r denotes the position vector, s the direction vector, κ the fluid's absorption coefficient and I_b denotes the black body intensity, σ_s the scattering coefficient, $I_{incident}$ the incident intensity, $\Phi(s_i,s)$ the scattering phase function and Ω_i the solid angle.

The calculated radiative heat flows are eventually included in the energy conservation source term. In this study, only the fvDOM (OpenFOAM) and DOM (STAR-CCM+ for verification) models are used. The choice of the fvDOM model over the P1 model is justified in Appendix C. The P1 radiation model (or P-1 model) is the simplest approximation of P-N models. It is based on the expansion of the RTE into an orthogonal series of spherical harmonics [49]. The P1 model is particularly useful for accounting for the radiative exchange between gas and particles [49]. In contrast, the fvDOM as well as the DOM model solve the RTE for a finite number of solid angles Ω with an associated vector direction s [43]. The full solid angle of 4π is divided into discrete angular parts of the sphere. The number of divisions is a trade-off between accuracy and computational cost as it determines the number of rays and hence the size of the equation system that need to be solved. For all OpenFOAM simulations we found

the azimuthal angle $\Phi = 3$ and the polar angle $\Theta = 4$ to be sufficient, whereas for all STAR-CCM+ simulations we found the number of ordinates equal 4 (S4) as satisfactory.

Due to the lack of (soot) particles as well as relatively low distances, no scattering model is needed for this study [34]. For a non-scattering medium, the RTE reads:

$$\frac{dI\,(r,s)}{d\,s} = \kappa I_{\mathrm{b}}\,(r) - \kappa\, I\,(r,\,s). \tag{12}$$

Moreover, a radiation boundary condition that applies for all solid walls needs to be set up. For an opaque, grey and diffusely emitting wall with the position vector r_{w}, the initial intensity from all possible directions s_{i} reads [48]:

$$\frac{dI\,(r_{\mathrm{wall}},\,s)}{ds} = \varepsilon I_{\mathrm{b}}\,(r_{\mathrm{w}}) + \frac{(1-\varepsilon)}{2\,\pi}\int_{2\,\pi} I\,(r_{\mathrm{w}},\,s_{\mathrm{i}})|\,n s_{\mathrm{i}}\,|\,d\Omega_{\mathrm{i}} \tag{13}$$

with n being the unit normal vector. All other main boundary conditions are depicted in Figure 11.

4. Conclusions

In this study, the contribution of thermal radiation modeling of a foam reactor was quantified with respect to several key parameters in heterogeneous catalysis. Firstly, the choice of a suitable radiation model is very important when investigating the heat transport behavior of open-cell foams. An inappropriate model can severely overestimate the contribution of radiation to the overall heat transport (relative error $E_{\mathrm{rel}} = 50\%$). Secondly, an influence of radiation on the simulated heat flows and temperature increases was found for the following parameters in decreasing order: 1. overall temperature level (here, wall temperature T_{w} and inlet temperature T_{in}), 2. solid thermal conductivity, 3. superficial velocity, and 4. surface emissivity. At four temperature levels corresponding with a range of industrially-relevant chemical reactions in heterogeneous catalysis (500 K: Fischer–Tropsch synthesis; 700 K: CO_2 methanation; 900 K: dry reforming of methane; 1200 K: methane steam reforming), the influence of radiation modeling was quantified. At most, we found maximum temperature deviations of up to 400 K and a discrepancy in heat flows of about 12 W (24%).

Even though highly conductive materials (e.g., metals) do not show significant deviations in temperature increases when radiation is neglected, their heat flow ratio (transferred from solid to fluid or transport from solid to wall) still might change distinctively. Hence, temperature increases cannot be the only measure to justify the neglect of radiation. Furthermore, during actual reactions, ignoring radiation can lead to a wrong interpretation as thermal effects might be attributed to reaction kinetics. Once again, we want to highlight that temperature deviations for negligence of radiation in actual chemical reactions might be more significant due to locally varying, temperature-dependent heat production. Prospectively, the influence of geometry also needs to be further addressed as this study only focused on an individual foam sample. Such study should target a range of irregular foams as well as regular structures (e.g., Kelvin cells), in order to more accurately quantify the influence of radiation in reactor modeling. Equivalently, the current parameter range could be extended to quantify radiation at higher velocities and coupled turbulence modeling as well as quantify the effect of different participating fluids (e.g., CO_2) with potential scattering. The heat source approach further underlined its suitability to effectively study thermal effects of catalyst carriers decoupled from chemistry. A deeper understanding of heat transport processes in foams in particular and structured reactors in general can lead to more accurate foam reactor models and consequently to intensified processes. This knowledge might help to facilitate the launch of structured reactors into industrial application.

Author Contributions: Conceptualization: C.S., F.K., J.W., G.R.P., and J.T.; methodology: C.S., F.K., J.W., and G.D.W.; software: F.K. and C.S.; writing—original draft preparation: C.S.; writing—review and editing: G.R.P., G.D.W., and J.T.; visualization: C.S.; supervision: G.R.P. All authors have read and agreed to the published version of the manuscript.

Funding: Christoph Sinn and Jorg Thöming thank the German Research Foundation (DFG) for funding by the priority program SPP 2080 (Katalysatoren und Reaktoren unter dynamischen Betriebsbedingungen für die Energiespeicherung und -wandlung) under grant TH 893/23-1.

Conflicts of Interest: The authors declare no conflict of interest.

Appendix A Geometrical Foam Properties

Table A1. Properties of the 10 ppi alumina foam used in this study.

Parameter	Symbol	Value
pore count		10 ppi
open porosity	ε_0	0.77
specific surface area	S_V	521.3 m^{-1}
cell diameter	d_c	5.76 ± 1.9 mm
window diameter	d_w	3.3 ± 0.9 mm
strut diameter	d_s	1.5 ± 0.5 mm

Appendix B Geometry for Verification

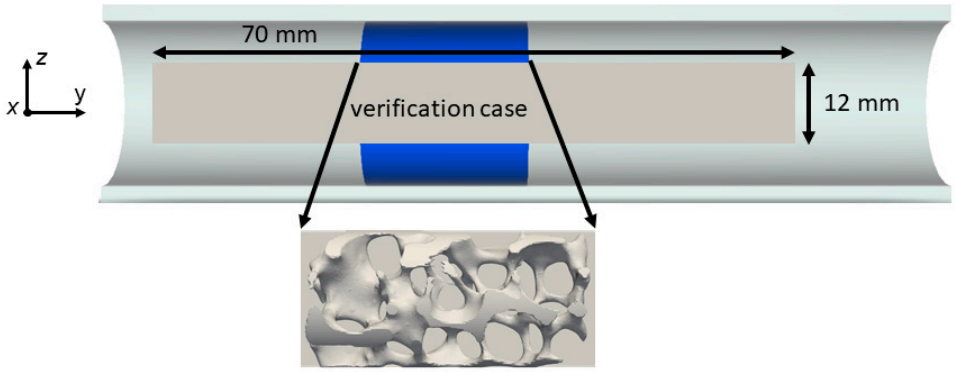

Figure A1. Illustration of foam clip used for the verification study.

Appendix C Analysis of P1 and fvDOM Radiation Models for Suitability in Open-Cell Foams

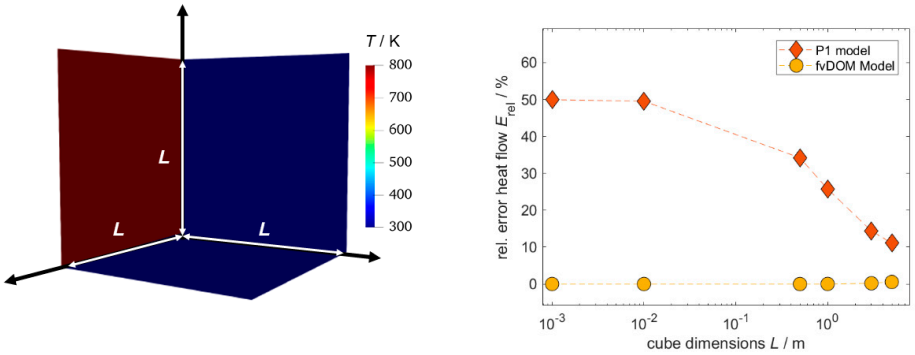

Figure A2. Test for suitability of P1 and fvDOM models used for radiation modeling in open-cell foams. Left: illustration of case (geometry = cube) and temperature boundary condition. Right: relative error of radiative heat flow between numerical solution and analytical solution plotted against cube dimensions.

In order to check which fluid participating radiation model in OpenFOAM is suitable for utilizing in heat transport simulations in open-cell foams, a simple test case was set up (Figure A2). The test case is a cube with flexible dimensions and fixed temperature boundary conditions of 300 K at five sides and one side with 800 K. Vacuum is assumed inside the cubes, which makes radiation the principal heat transport mechanism. The resulting steady-state specific radiative heat flux can easily be calculated analytically (for a $\varepsilon = 1$) as:

$$\dot{q} = \sigma \left({T_1}^4 - {T_2}^4 \right) = 5.67 \times 10^{-8} \text{ W m}^{-2} \text{ K}^{-4} \left(800^4 - 300^4 \right) \text{K}^4 \approx 22765 \text{ W m}^2 . \quad (14)$$

We also set up simulation cases that solved for the very same specific heat flux with both, fvDOM and P1 model, for various cube dimensions (solver buoyantSimpleFoam). We note that all meshes (single region) were created with the blockMesh utility of OpenFOAM and tested for grid independence. The relative error between analytical and numerical solution plotted against the cube dimensions for both models is also shown in Figure A2. A significant deviation between P1 model and analytical solution (>20%) can be observed for small cube dimensions, while for increasing cube dimensions the error shrinks. In contrast, the fvDOM model shows almost no deviation to the analytical model for all cube dimensions. For the fixed number of solid angles, the error slightly increases for dimensions larger than 3 m. This behavior might change when more solid angles and thus more equations are solved. At the small distances relevant for this study, the error due to the P1 model is almost 50% which is not acceptable for appropriate results. Thus, only the fvDOM model is used for quantification in this work.

List of Symbols

Latin	
c_p	Isobaric heat capacity, J Kg^{-1} K^{-1}
d_c	Cell diameter, m
d_s	Strut diameter, m
d_w	Window diameter, m
E_rel	Relative error of heat flow, -
I	Intensity, W m^{-2} sr^{-1}
L	Cube dimensions, m
Q	Heat flow, W
Q_SF	Heat flow solid to fluid, W
Q_SW	Heat flow solid to wall, W
h	Specific enthalpy, J
p	Pressure, Pa
r	Position vector, -
s	Direction vector, -
S	Total heat source intensity, W
S_v	Specific surface area, m^{-1}
T	Temperature, K
T_w	Wall temperature, K
T_max	Maximum temperature, K
T_mean	Mean temperature, K
U	Velocity, m s^{-1}
v	Superficial velocity, m s^{-1}

Greek	
α	Degree of absorption, -
γ	Degree of reflection, -
τ	Degree of transmission, -
Ω	Solid angle, sr
κ	Absorption coefficient, m^{-1}
σ_s	Scattering coefficient, m^{-1}
ε_0	Open porosity, -
ε	Surface emissivity, -
μ	Dynamic viscosity, Pa s
λ	Thermal conductivity, W m^{-1} K^{-1}

References

1. Kiewidt, L.; Thöming, J. Predicting optimal temperature profiles in single-stage fixed-bed reactors for CO_2-methanation. *Chem. Eng. Sci.* **2015**, *132*, 59–71. [CrossRef]
2. Rönsch, S.; Schneider, J.; Matthischke, S.; Schluter, M.; Götz, M.; Lefebvre, J.; Prabhakaran, P.; Bajohr, S. Review on methanation—From fundamentals to current projects. *Fuel* **2016**, *166*, 276–296. [CrossRef]
3. Kalz, K.F.; Kraehnert, R.; Dvoyashkin, M.; Dittmeyer, R.; Gläser, R.; Krewer, U.; Reuter, K.; Grunwaldt, J.-D. Future Challenges in Heterogeneous Catalysis: Understanding Catalysts under Dynamic Reaction Conditions. *ChemCatChem* **2016**, *9*, 17–29. [CrossRef]
4. Solomon, A.; Kammen, D.M.; Callaway, D. The role of large-scale energy storage design and dispatch in the power grid: A study of very high grid penetration of variable renewable resources. *Appl. Energy* **2014**, *134*, 75–89. [CrossRef]
5. Kiewidt, L.; Thöming, J. Pareto-optimal design and assessment of monolithic sponges as catalyst carriers for exothermic reactions. *Chem. Eng. J.* **2019**, *359*, 496–504. [CrossRef]
6. Kiewidt, L.; Thöming, J. Multiscale modeling of monolithic sponges as catalyst carrier for the methanation of carbon dioxide. *Chem. Eng. Sci. X* **2019**, *2*, 100016. [CrossRef]
7. Graf, I.; Rühl, A.-K.; Kraushaar-Czarnetzki, B. Experimental study of heat transport in catalytic sponge packings by monitoring spatial temperature profiles in a cooled-wall reactor. *Chem. Eng. J.* **2014**, *244*, 234–242. [CrossRef]
8. Reitzmann, A.; Patcas, F.C.; Kraushaar-Czarnetzki, B. Keramische Schwämme—Anwendungspotenzial monolithischer Netzstrukturen als katalytische Packungen. *Chem. Ing. Tech.* **2006**, *78*, 885–898. [CrossRef]
9. Meinicke, S.; Dubil, K.; Wetzel, T.; Dietrich, B. Characterization of heat transfer in consolidated, highly porous media using a hybrid-scale CFD approach. *Int. J. Heat Mass Transf.* **2020**, *149*, 119201. [CrossRef]
10. Bianchi, E.; Heidig, T.; Visconti, C.G.; Groppi, G.; Freund, H.; Tronconi, E. Heat transfer properties of metal foam supports for structured catalysts: Wall heat transfer coefficient. *Catal. Today* **2013**, *216*, 121–134. [CrossRef]
11. Razza, S.; Heidig, T.; Bianchi, E.; Groppi, G.; Schwieger, W.; Tronconi, E.; Freund, H. Heat transfer performance of structured catalytic reactors packed with metal foam supports: Influence of wall coupling. *Catal. Today* **2016**, *273*, 187–195. [CrossRef]
12. Della Torre, A.; Montenegro, G.; Tabor, G.R.; Wears, M. CFD characterization of flow regimes inside open cell foam substrates. *Int. J. Heat Fluid Flow* **2014**, *50*, 72–82. [CrossRef]
13. Regulski, W.; Szumbarski, J.; Łaniewski-Wołłk, Ł.; Gumowski, K.; Skibinski, J.; Wichrowski, M.; Wejrzanowski, T. Pressure drop in flow across ceramic foams—A numerical and experimental study. *Chem. Eng. Sci.* **2015**, *137*, 320–337. [CrossRef]
14. Bracconi, M.; Ambrosetti, M.; Maestri, M.; Groppi, G.; Tronconi, E. A fundamental analysis of the influence of the geometrical properties on the effective thermal conductivity of open-cell foams. *Chem. Eng. Process. Process. Intensif.* **2018**, *129*, 181–189. [CrossRef]
15. Diani, A.; Bodla, K.K.; Rossetto, L.; Garimella, S.V. Numerical investigation of pressure drop and heat transfer through reconstructed metal foams and comparison against experiments. *Int. J. Heat Mass Transf.* **2015**, *88*, 508–515. [CrossRef]

16. Zafari, M.; Panjepour, M.; Emami, M.D.; Meratian, M. Microtomography-based numerical simulation of fluid flow and heat transfer in open cell metal foams. *Appl. Therm. Eng.* **2015**, *80*, 347–354. [CrossRef]
17. Bianchi, E.; Schwieger, W.; Freund, H. Assessment of Periodic Open Cellular Structures for Enhanced Heat Conduction in Catalytic Fixed-Bed Reactors. *Adv. Eng. Mater.* **2015**, *18*, 608–614. [CrossRef]
18. Iasiello, M.; Cunsolo, S.; Bianco, N.; Chiu, W.; Naso, V. Developing thermal flow in open-cell foams. *Int. J. Therm. Sci.* **2017**, *111*, 129–137. [CrossRef]
19. Nie, Z.; Lin, Y.; Tong, Q. Numerical investigation of pressure drop and heat transfer through open cell foams with 3D Laguerre-Voronoi model. *Int. J. Heat Mass Transf.* **2017**, *113*, 819–839. [CrossRef]
20. Mendes, M.; Skibina, V.; Talukdar, P.; Wulf, R.; Gross, U.; Trimis, D.; Ray, S. Experimental validation of simplified conduction–radiation models for evaluation of Effective Thermal Conductivity of open-cell metal foams at high temperatures. *Int. J. Heat Mass Transf.* **2014**, *78*, 112–120. [CrossRef]
21. Bianchi, E.; Heidig, T.; Visconti, C.G.; Groppi, G.; Freund, H.; Tronconi, E. An appraisal of the heat transfer properties of metallic open-cell foams for strongly exo-/endo-thermic catalytic processes in tubular reactors. *Chem. Eng. J.* **2012**, *198*, 512–528. [CrossRef]
22. Fischedick, T.; Kind, M.; Dietrich, B. High temperature two-phase thermal conductivity of ceramic sponges with stagnant fluid—Experimental results and correlation including thermal radiation. *Int. J. Therm. Sci.* **2015**, *96*, 1–11. [CrossRef]
23. Dietrich, B.; Fischedick, T.; Heissler, S.; Weidler, P.; Wöll, C.; Kind, M. Optical parameters for characterization of thermal radiation in ceramic sponges—Experimental results and correlation. *Int. J. Heat Mass Transf.* **2014**, *79*, 655–665. [CrossRef]
24. Zhao, C.; Tassou, S.A.; Lu, T. Analytical considerations of thermal radiation in cellular metal foams with open cells. *Int. J. Heat Mass Transf.* **2008**, *51*, 929–940. [CrossRef]
25. Patel, V.M.; Talukdar, P. Evaluation of radiative properties of a representative foam structure using blocked-off region approach integrated with finite volume method. *Int. J. Therm. Sci.* **2016**, *108*, 89–99. [CrossRef]
26. Fischedick, T.; Kind, M.; Dietrich, B. Radial two-phase thermal conductivity of ceramic sponges up to high temperatures—Experimental results and correlation. *Int. J. Therm. Sci.* **2017**, *114*, 98–113. [CrossRef]
27. Dietrich, B.; Schell, K.G.; Bucharsky, E.C.; Oberacker, R.; Hoffmann, M.; Schabel, W.; Kind, M.; Martin, H. Determination of the thermal properties of ceramic sponges. *Int. J. Heat Mass Transf.* **2010**, *53*, 198–205. [CrossRef]
28. Sinn, C.; Pesch, G.R.; Thöming, J.; Kiewidt, L. Coupled conjugate heat transfer and heat production in open-cell ceramic foams investigated using CFD. *Int. J. Heat Mass Transf.* **2019**, *139*, 600–612. [CrossRef]
29. Wu, Z.; Caliot, C.; Flamant, G.; Wang, Z. Numerical simulation of convective heat transfer between air flow and ceramic foams to optimise volumetric solar air receiver performances. *Int. J. Heat Mass Transf.* **2011**, *54*, 1527–1537. [CrossRef]
30. Wehinger, G.D.; Heitmann, H.; Kraume, M. An artificial structure modeler for 3D CFD simulations of catalytic foams. *Chem. Eng. J.* **2016**, *284*, 543–556. [CrossRef]
31. Wehinger, G.D.; Kraume, M.; Berg, V.; Korup, O.; Mette, K.; Schlögl, R.; Behrens, M.; Horn, R. Investigating dry reforming of methane with spatial reactor profiles and particle-resolved CFD simulations. *AIChE J.* **2016**, *62*, 4436–4452. [CrossRef]
32. Dong, Y.; Korup, O.; Gerdts, J.; Cuenya, B.R.; Horn, R. Microtomography-based CFD modeling of a fixed-bed reactor with an open-cell foam monolith and experimental verification by reactor profile measurements. *Chem. Eng. J.* **2018**, *353*, 176–188. [CrossRef]
33. Behnam, M.; Dixon, A.G.; Wright, P.M.; Nijemeisland, M.; Stitt, E.H. Comparison of CFD simulations to experiment under methane steam reforming reacting conditions. *Chem. Eng. J.* **2012**, *207*, 690–700. [CrossRef]
34. Hettel, M.; Daymo, E.; Deutschmann, O. 3D modeling of a CPOX-reformer including detailed chemistry and radiation effects with DUO. *Comput. Chem. Eng.* **2018**, *109*, 166–178. [CrossRef]
35. Wehinger, G.D.; Flaischlen, S. Computational Fluid Dynamics Modeling of Radiation in a Steam Methane Reforming Fixed-Bed Reactor. *Ind. Eng. Chem. Res.* **2019**, *58*, 14410–14423. [CrossRef]
36. Wehinger, G.D. Radiation Matters in Fixed-Bed CFD Simulations. *Chem. Ing. Tech.* **2019**, *91*, 583–591. [CrossRef]
37. Dixon, A.G.; Partopour, B. Computational Fluid Dynamics for Fixed Bed Reactor Design. *Annu. Rev. Chem. Biomol. Eng.* **2020**, *11*, 109–130. [CrossRef]

38. Della Torre, A.; Lucci, F.; Montenegro, G.; Onorati, A.; Eggenschwiler, P.D.; Tronconi, E.; Groppi, G. CFD modeling of catalytic reactions in open-cell foam substrates. *Comput. Chem. Eng.* **2016**, *92*, 55–63. [CrossRef]
39. Güttel, R.; Turek, T. Improvement of Fischer-Tropsch Synthesis through Structuring on Different Scales. *Energy Technol.* **2015**, *4*, 44–54. [CrossRef]
40. Jang, W.-J.; Shim, J.-O.; Kim, H.-M.; Yoo, S.-Y.; Roh, H.-S. A review on dry reforming of methane in aspect of catalytic properties. *Catal. Today* **2019**, *324*, 15–26. [CrossRef]
41. Meloni, E.; Martino, M.; Palma, V. A Short Review on Ni Based Catalysts and Related Engineering Issues for Methane Steam Reforming. *Catalysts* **2020**, *10*, 352. [CrossRef]
42. Bianchi, E.; Groppi, G.; Schwieger, W.; Tronconi, E.; Freund, H. Numerical simulation of heat transfer in the near-wall region of tubular reactors packed with metal open-cell foams. *Chem. Eng. J.* **2015**, *264*, 268–279. [CrossRef]
43. Modest, M.F. *Radiative Heat Transfer*, 3rd ed.; Academic Press: New York, NY, USA, 2013. Available online: https://doi.org/10.1016/C2010-0-65874-3 (accessed on 6 April 2020).
44. Weller, H.G.; Tabor, G.; Jasak, H.; Fureby, C. A tensorial approach to computational continuum mechanics using object-oriented techniques. *Comput. Phys.* **1998**, *12*, 620. [CrossRef]
45. STAR-CCM+ (n.d.). Available online: https://www.plm.automation.siemens.com/global/en/products/simcenter/STAR-CCM.html (accessed on 6 April 2020).
46. Gräf, I.; Ladenburger, G.; Kraushaar-Czarnetzki, B. Heat transport in catalytic sponge packings in the presence of an exothermal reaction: Characterization by 2D modeling of experiments. *Chem. Eng. J.* **2016**, *287*, 425–435. [CrossRef]
47. Habibi, A.; Merci, B.; Heynderickx, G. Impact of radiation models in CFD simulations of steam cracking furnaces. *Comput. Chem. Eng.* **2007**, *31*, 1389–1406. [CrossRef]
48. Versteeg, H.K.; Malasekera, W. *An Introduction to Computational Fluid Dynamics: The Finite Volume Method*, 2nd ed.; Pearson Education Ltd.: Harlow, UK, 2007.
49. Sazhin, S.; Sazhina, E.; Faltsi-Saravelou, O.; Wild, P. The P-1 model for thermal radiation transfer: Advantages and limitations. *Fuel* **1996**, *75*, 289–294. [CrossRef]

Chapter 8

Application of Heat Sources II — Structure-Heat Transport Analysis

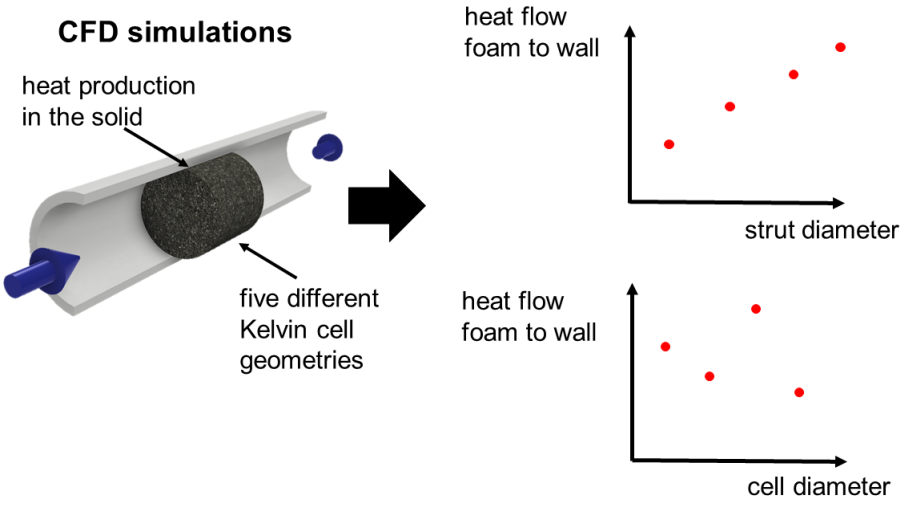

FIGURE 8.1: Graphical abstract of the manuscript on the structure-heat transport relations.

The content of the second application chapter is published under the name *Structure-heat transport analysis of periodic open-cell foams to be used as catalyst carriers* (Sinn et al., 2021b).
This chapter applies the heat source approach on investigating the geometrical influence of the geometrical structure of the foam on the overall heat transport. Here, five different periodic foams (Kelvin cells) are utilized to conduct a structure-heat transport analysis. With the aid of the well-defined periodic structure, the influence of, for instance, strut diameter and cell diameter on the heat transport is quantified (Figure 8.1). Moreover, it is tested if the general thermal behavior of foams caused by heat sources is also valid for arbitrary foam structures. Hence, this chapter serves as a confirmation of the findings from Chapter 4.

Chemical Engineering Research and Design 166 (2021) 209–219

Contents lists available at ScienceDirect

Chemical Engineering Research and Design

journal homepage: www.elsevier.com/locate/cherd

Structure-heat transport analysis of periodic open-cell foams to be used as catalyst carriers

Christoph Sinn[a], *Jonas Wentrup*[a], *Georg R. Pesch*[a,*], *Jorg Thöming*[a], *Lars Kiewidt*[b,*]

[a] *University of Bremen, Chemical Process Engineering, Leobener Strasse 6, 28359 Bremen, Germany*
[b] *Wageningen University & Research, Biobased Chemistry and Technology, P.O. Box 17, 6700 AA Wageningen, The Netherlands*

ARTICLE INFO

Article history:
Received 12 June 2020
Received in revised form 18 November 2020
Accepted 9 December 2020
Available online 17 December 2020

Keywords:
Open-cell foams
Kelvin cells
Conjugate heat transfer
CFD
Temperature distribution
Tailored design

ABSTRACT

Open-cell foams are promising catalyst supports as they provide a low pressure drop, radial mixing, and exceptional heat transport properties. Even though their large potential for the design of small-scale, dynamically operated reactors with strongly exothermic reactions is known, their application is not yet common. To design efficient and safe structured reactors in the future, the understanding of structure-heat transport relations is key. Fully resolved CFD simulations of non-isothermal structured reactors including chemical surface reactions require a high modeling effort and are computationally expensive. In a previous study we therefore implemented volumetrically distributed heat sources in the solid to mimic the heat production during an exothermal reaction, and evaluated the resulting heat flows and temperature distributions via CFD. The previous analysis, however, was limited to one specific open-cell foam geometry. In this study, we extend the conjugate heat transfer problem including heat production in the solid to five periodic open-cell foams (Kelvin cell-lattices) with defined but different structural parameters to establish structure-heat transport relations. We confirmed conduction being the dominant heat removal mechanism and found the strut diameter and the solid thermal conductivity being the key parameters to improve heat transport and reduce hot spots.

1. Introduction

Cellular and interconnected open-cell foam structures provide a remarkable potential for process intensification in, among others, solar receivers, pore burners, and catalytic reactors (Wu and Wang, 2013; Gao et al., 2014; Kiewidt and Thöming, 2019a). Their potential for intensification of exo- and endothermic catalytic reactions is based on their outstanding radial heat transport, high radial mixing, and low pressure loss (Bianchi et al., 2012; Gräf et al., 2014).

The thermal management during catalytic reactions is crucial in reactor design to obtain optimal temperature profiles (Kiewidt and Thöming, 2015) and to avoid hot-spot formation (Gräf et al., 2016). Although the use of open-cell foams in highly exothermic reactions, such as the CO_2-methanation in Power-to-Gas (PtG) applications, has been reported several times, they are not yet widely used in commercial applications (Montenegro Camacho et al., 2018; Kiewidt and Thöming, 2019b). A main reason is the difficult mounting with proper wall coupling, especially for large multi-tubular fixed-bed reactors (e.g., Haber-Bosch process, methane reforming) (Reitzmann et al., 2006). For small-scale dynamic reactors, which are needed in the future for Power-to-X (PtX) processes, however, open-cell foams provide resilient heat transport over

* *Corresponding authors.*
E-mail addresses: gpesch@uni-bremen.de (G.R. Pesch), lars.kiewidt@wur.nl (L. Kiewidt).
https://doi.org/10.1016/j.cherd.2020.12.007

Nomenclature

Roman

A_s	strut surface area, m^2
A_W	wall contact area of the solid, m^2
$c_{p,f}$	fluid isobaric heat capacity, J Kg^{-1} K^{-1}
$c_{p,s}$	solid isobaric heat capacity, J Kg^{-1} K^{-1}
C	coefficients for surrogate model
d_c	cell diameter, m
d_s	strut diameter, m
F	heat flow, W
F_{SW}	heat flow from solid to wall, W
F_{SF}	heat flow from solid to fluid, W
h	specific enthalpy, kJ
p	pressure, p
S	total heat source, W
S_{spec}	specific heat source, W m^{-3}
S_V	specific surface area, m^{-1}
T	temperature, K
T_s	solid temperature, K
T_f	fluid temperature, K
T_W	wall temperature, K
T_{max}	maximum solid temperature, K
u, U	velocity, m s^{-1}
V_s	solid volume, m^3
v	superficial velocity, m s^{-1}

Greek

α	heat transfer coefficient, W m^{-2} K^{-1}
ε_o	open porosity, -
μ	dynamic viscosity, Pa s
λ_f	fluid thermal conductivity, W m^{-1} K^{-1}
λ_s	solid thermal conductivity, W m^{-1} K^{-1}
ρ_f	fluid density, Kg m^{-3}
ρ_s	solid density, Kg m^{-3}
β	parameter of surrogate model, m^{-1}

Dimensionless groups

Re_p	pore Reynolds number, -

a wide range of flow rates due to dominant heat removal by thermal conduction in the solid phase (Kalz et al., 2017; Kiewidt and Thöming, 2019b).

Foam structured reactors, however, are only able to outperform conventional pellet fixed-bed reactors if conduction is the dominant heat removal mechanism (Kiewidt and Thöming, 2019b). The fractions of heat removal by thermal conduction, convective transport, and thermal radiation depend largely on the structure (strut diameter, cell and window diameter) of the open-cell foam (Bianchi et al., 2012; Wallenstein et al., 2014; Fischedick et al., 2017; Xu et al., 2019). To design small-scale structured reactors with robust heat transport and parametric stability, fundamental understanding and quantification of the relations between the structure of open-cell foams and the dominant mechanisms of heat removal is key. Although several studies already related a high effective two-phase thermal conductivity of open-cell foams to low porosities (high solid content) and high intrinsic material thermal conductivities (Fourie and Du Plessis, 2004; Edouard, 2011; Bianchi et al., 2012; Kumar and Topin, 2014; Wallenstein et al., 2014; Ranut, 2016; Fischedick et al., 2017), the contributions of different mechanisms to actual heat removal in open-cell foams with internal heat production have not been quantified yet.

In the past, full-field three-dimensional CFD simulations of open-cell foams proved to be valuable to get insight into different heat transport mechanisms in open-cell foams as they allow the computation of undisturbed (e.g. from experimental probes) temperature fields and heat flows of solid and fluid phases. CFD was successfully applied to study the influence of geometry, material, velocity, and wall coupling (Zafari et al., 2015; Torre et al., 2015; Bianchi et al., 2015; Razza et al., 2016). Despite their advantages, CFD simulations of full-field catalytic surface reactions in open-cell foams are challenging due to the high computational cost and modeling effort (Torre et al., 2016; Wehinger et al., 2016; Dong et al., 2018). Furthermore, CFD simulations usually provide results for only one specific foam structure and thus require the creation and meshing of several geometries to establish structure-transport relations. The geometries can be obtained through tomography (image-based Ranut et al., 2015; Sadeghi et al., 2020), through idealization (e.g., Kelvin cells and periodic open-cell foams (POCS), Torre et al., 2016; Iasiello et al., 2017; Lucci et al., 2017) or computer algorithms (i.e., Voronoi-tessellations, Bracconi et al., 2018; Wehinger et al., 2016). Generally, image-based CFD models preserve the original open-cell foam geometry accurately but are time consuming if several foam geometries need to be compared. Furthermore, geometrical properties of these reticulated foams are distributed and thus more difficult to characterize in comparison to regular structures. Hence, methods for the creation of artificial, regular open-cell foam geometries were mostly used to investigate structure-transport relations (Bracconi et al., 2018; Bianchi et al., 2016). These studies investigated the effect of the strut-to-node ratio on the effective thermal conductivity and found that the solid distribution along the strut and between strut and nodes is key for the overall foam's conduction properties. In another recent study, Bracconi et al. varied the solid content (i.e., the porosity) radially and axially along the foam lattice and found an increased effective solid thermal conductivity if more solid material (i.e., thicker struts) is aligned radially (Bracconi et al., 2020). Nevertheless, the influence of the strut and cell design of foams on temperature distributions and heat flows under coupled conductive and convective heat transport as well as heat production within the solid (for example through chemical reactions) has not been analyzed yet. These close-to-realistic conditions with gas flow and heat production within the solid (instead of heating through the wall or the fluid inlet) contribute to the better understanding and quantification of heat removal mechanisms, and thus enable the improved design of structured chemical reactors.

In a previous study, we analyzed conjugate heat transfer simulations including heat production within the solid to mimic an exothermic chemical reaction (Sinn et al., 2019). The procedure allows to investigate the effect of heat production on solid and fluid temperature fields as well as on heat flows while saving the modeling and solution effort of species transport and chemical surface reactions. In the previous study, we found inhomogeneous temperature fields in a solid ceramic foam due to the heat production in the solid. We concluded that solid temperature distributions in foams during exothermal reactions cannot generally be assumed as homogeneous for relevant process conditions in heterogeneous catalysis (heat sources from 5 to 150 W, e.g., for CO_2 methanation reaction, solid thermal conductivities from 5 to 50 W m^{-1} K^{-1}, i.e., ceramic foams, and superficial velocities from 0 to 0.5 m s^{-1}).

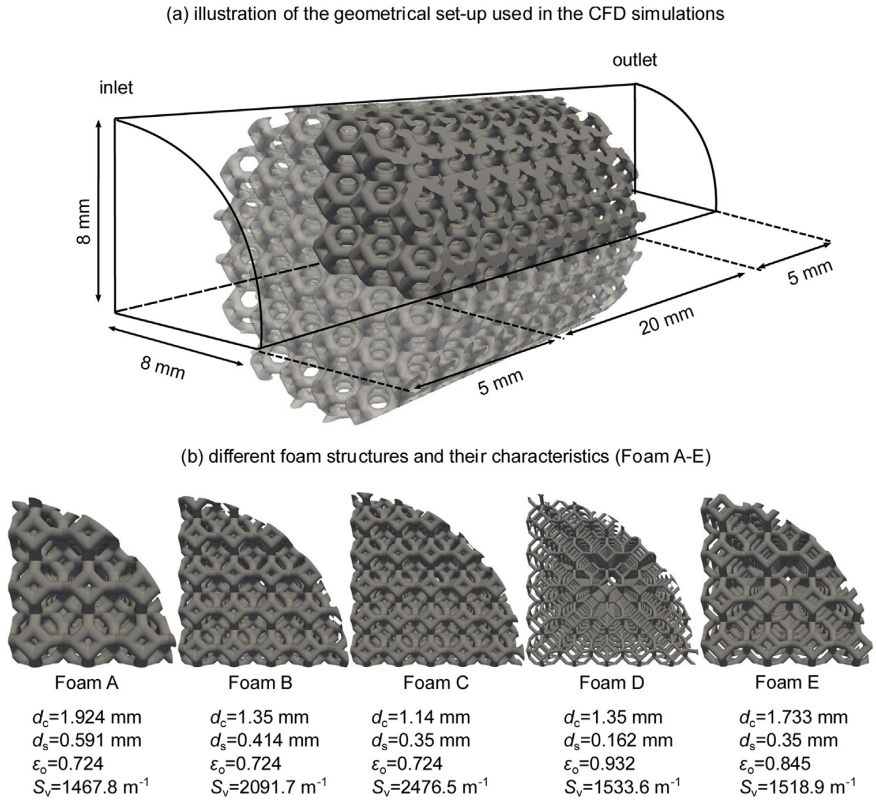

Fig. 1 – Geometries of the five periodic open-cell foams (Kelvin lattices) investigated in this study.

We also showed that homogeneous models cannot resolve the temperature inhomogeneities sufficiently so that detailed 3D simulations are necessary (Sinn et al., 2019; 2020). Further, we showed that the ratio between convective and conductive heat flows from the solid shifts from conduction-dominated to convection-dominated with increasing superficial velocities and decreasing solid thermal conductivities. The study thus demonstrated the potential of the approach to mimic exothermic chemical reactions by a distributed heat source in the solid domain. The present study expands the heat source approach to other open-cell foam geometries and conducts a structure-heat transport analysis for geometries, solid thermal conductivities, and fluid velocities relevant in heterogeneous catalysis.

Here, we investigate five different periodic open-cell foam geometries (POCS, Kelvin cell lattices) via CFD and correlate heat flows and temperature increases for heat production within the solid with the geometrical descriptors strut and cell diameter via a semi-empirical model. The novel contribution of this work is thus the quantification and modelling of the contributions of conductive and convective heat removal from open-cell foam structures with heat production in the solid, as it occurs in open-cell foams in structured catalytic fixed-bed reactors.

2. Methods

2.1. *Creation of foam geometries and setup of CFD model*

To establish structure-transport relations of the periodic open-cell foams, we adopted the same CFD model as described in our previous work (Sinn et al., 2019). The model describes a laminar steady-state conjugate heat transfer problem between flowing air and an open-cell foam (see Appendix A and Sinn et al., 2019). The model was established in the OpenFOAM® simulation framework (Version 5.0, Weller et al., 1998). The solid foam contained a uniformly distributed volumetric heat source that mimics the heat of reaction (called S). The model was verified against other CFD data from literature as well as against heat transfer and pressure drop correlations in a previous study (Sinn et al., 2019).

For this study, we chose five different Kelvin cell lattices (see Fig. 1). Due to their well-defined morphology, the Kelvin cell properties could be easily varied and examined according to their impact on fluid flow and thermal phenomena (Torre et al., 2014). Although, Kelvin cell lattices (or POCS) underperformed reticulated foams in terms of heat and mass transfer due to lower radial mixing (Horneber et al., 2012), recent studies showed the potential of idealized structures for process intensification (Bracconi et al., 2018). Especially the rise of additive manufacturing techniques facilitates using POCS to tailor catalyst supports (Zhou and Liu, 2017).

Kelvin cells are characterized by the four foam properties: cell diameter d_c, strut diameter d_s, open porosity ε_o and specific surface area S_v. Due to explicit dependencies, two of them are sufficient to define the overall structure (Inayat et al., 2011). The lattices were created using the CAD tool Autodesk Fusion 360, using the cell diameter d_c and the strut diameter d_s as input parameters. The open porosity ε_o and the specific surface area S_v were extracted from the final lattice geometries using the CAD software. The selected Kelvin

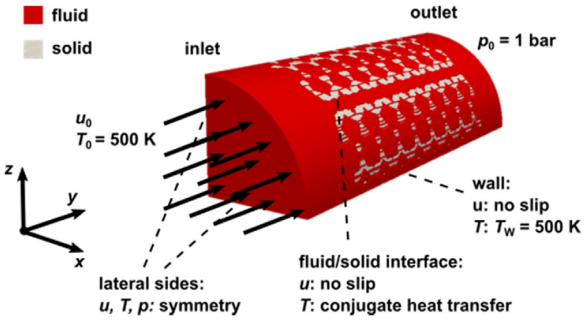

Fig. 2 – Illustration of the applied boundary conditions.

cell lattices have geometric properties that are relevant in heterogeneous catalysis and therefore are suitable for the investigation of heat production in different foam geometries. Additionally, the periodic Kelvin cell lattice allowed for accelerated computation by only simulating a quarter of the geometry. Grid independence studies were conducted to ensure mesh-independent results (see Appendix B).

2.2. Boundary conditions

This study extends the parameter range of the previous study (Sinn et al., 2019) by varying the geometry. Hence, the same process and boundary conditions as in our previous study were applied (Sinn et al., 2019). The only difference is caused by the choice of the quarter pipe system, which has two symmetry boundary conditions to account for the whole geometry (see Fig. 2). The initial temperature of the air flow was identical to the fixed wall temperature (500 K). Heat energy could thus only enter the system through the applied heat sources.

2.3. Selection of structure descriptors

The geometric foam properties (cell diameter d_c, strut diameter d_s, open porosity ε_o and specific surface area S_v) might not all be necessary to properly conduct a structure heat transport analysis. Therefore, the scatter plots shown in Fig. 3 indicate trends between the geometrical properties of the structures. Note that specific surface area and open porosity were determined from the created geometry and not from model equations. The trendlines and correlation coefficients were computed using conventional univariate linear regression. The specific surface area correlates negatively with the cell diameters (R^2 = 0.628, panel d), while the strut diameter correlates negatively with the open porosity (R^2 = 0.637, panel a). In contrast, neither cell diameter and open porosity (R^2 = 0.002, panel b) nor strut diameter and specific surface area (R^2 = 0.001, panel c) indicate any correlation for the investigated structures. The results thus suggest to choose the strut and cell diameter as principal geometric descriptors for the structure-transport analysis. Note that the data in Fig. 3 is not intended to derive general quantitative correlations of the structural parameters but highlights principal qualitative trends in the dependencies between the structural parameters, which are in line with existing semi-empirical correlations for the open porosity ε_o and the specific surface area S_v (Inayat et al., 2011; Lucci et al., 2014). For reticulated foams one would probably use the specific surface area and the open porosity as descriptors as these two parameters are easily determined experimentally.

3. Results and discussion

3.1. Influence of heat sources on heat flows and temperature distributions

The only thermal energy entering the system is caused by the volumetric heat source within the solid, the energy balance at steady state thus reads (Sinn et al., 2019):

$$S = F_{SW} + F_{SF} \rightarrow 1 = \frac{F_{SW}}{S} + \frac{F_{SF}}{S} \quad (1)$$

where S denotes heat source intensity, F_{SW} denotes the heat flow from solid to the wall (conducted heat flow) and F_{SF} denotes the heat flow from solid to the fluid phase (convective heat flow). The influence of the heat source intensity on the specific heat flow from the solid foam to the wall for Foam A is plotted against the superficial velocity v in Fig. 4a. A value lower than 0.5 (see dashed read line in Fig. 4a) indicates that convection is the dominant heat transport mechanism whereas a value above 0.5 indicates thermal conduction being dominant. By normalizing the conducted heat flow F_{SW} with the applied heat source intensity S, the data for the three investigated heat sources (5 W, 50 W and 150 W) collapsed for alumina (15 W m^{-1} K^{-1}) at every superficial velocity. The same behavior was observed for the 10 ppi foam in (Sinn et al., 2019) as well as for the structures B–E (not plotted here). The normalization indicates that the fraction of heat removed through thermal conduction or convection is independent of the intensity of the heat source. Furthermore, the general trend of a decreasing conductive heat transport (hence, increasing convective heat transport) for increasing superficial velocities was seen for all five geometries. Generally, the material with the highest thermal conductivity (sSiC, 50 W m^{-1} K^{-1}) showed the highest ratio of conducted heat flow to heat source intensity.

Next to the influence of heat sources on the heat flows, the influence on the temperature distribution in a foam has also been addressed. The approach revealed significant temperature inhomogeneities within the solid domain. Fig. 5 shows temperature fields for the investigated geometries with an applied 50 W heat source for a superficial velocity of 0.104 m s^{-1}. Here again, all foams and setups exhibited strong radial differences in the temperature field, which indicates that solid temperature fields in catalyst carriers based on ceramic foams can generally not be assumed as homogeneous. The position of the simulated hot-spots was in the rear part of the foam even though the axial temperature differences were comparably small. The axial temperature difference occured due to the cooling effect of the fluid when the flow entered the porous structure, while it is heated up already when reaching the rear part of the foam. Moreover, it became obvious that the temperature deviations from 500 K depend significantly on the structure (see Fig. 5). A severe maximum temperature increase was clearly seen for foams A–E. Moreover, for the given boundary conditions we observed a decreasing solid maximum temperature with increasing velocity (see Fig. 4b). This behavior was more pronounced for mullite than for alumina and sSiC. For the latter two materials, the decrease was only slight.

Similar to the specific heat flows, when the maximum temperature increase was normalized by the heat source intensities, ΔT_{max} S^{-1}, and plotted against superficial velocity, the points collapsed for identical solid thermal conductiv-

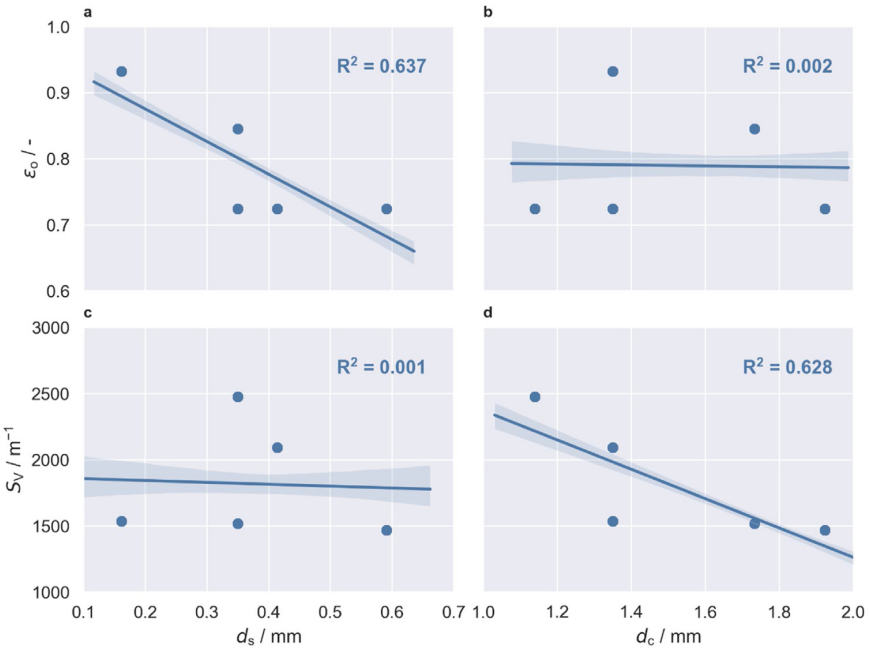

Fig. 3 – Analysis of the created foam geometries. Trends between strut diameter d_s and open porosity ε_o (a) as well as between cell diameter d_c and specific surface area S_V (d) can be observed. The shaded areas indicate 95% confidence intervals of the estimated slope. The strut diameter and cell diameters are thus used as structure descriptors. Note that both S_V and ε_o are determined from the created geometry and not from model equations.

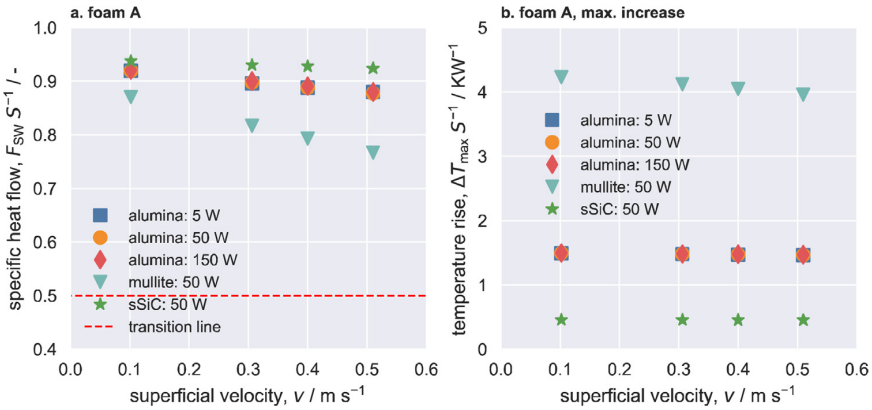

Fig. 4 – Thermal effects of heat sources on Foam A for different materials (i.e., thermal conductivities). a) Specific conductive heat flow F_{SW} S^{-1} plotted against the velocity v for different materials and heat sources; the transition line indicates the crossing from dominant convection (F_{SW} S^{-1} < 0.5) to dominant conduction (F_{SW} S^{-1} > 0.5). b) Specific temperature increase ΔT_{max} S^{-1} (from initial 500 K) against the superficial velocity v.

ity (Fig. 4b). That means, that regardless of the heat source intensity between 5 W and 150 W, the maximum temperature increase can be estimated. Furthermore, the trends of maximum and mean temperature increases behave similarly and indicate that the entire temperature distribution shifts consistently (see Fig. 5). This behavior was also reported in the previous study (Sinn et al., 2019). When comparing the materials, all relations between temperature increase and superficial velocity show linear behavior regardless of the structure or material. For the μCT foam sample from the previous publication, mullite had an asymptotic trend, indicating heat transport limitations of the material and corresponding setup.

3.2. *Influence of structure parameters on heat flows and temperature distributions*

So far, the results for the 10 ppi foam found in Sinn et al. (2019) were also observed for the different periodic open-cell foams in this study. Severe differences in the temperature fields caused by the different geometries became apparent (see Fig. 5). To understand the relation between the foams' structure and their heat transport properties, we analyzed results from 100 simulations with unique combinations of strut and cell diameter, solid thermal conductivity, and fluid velocity. The specific conductive heat flows and maximum temperature increases, both normalized by the heat source

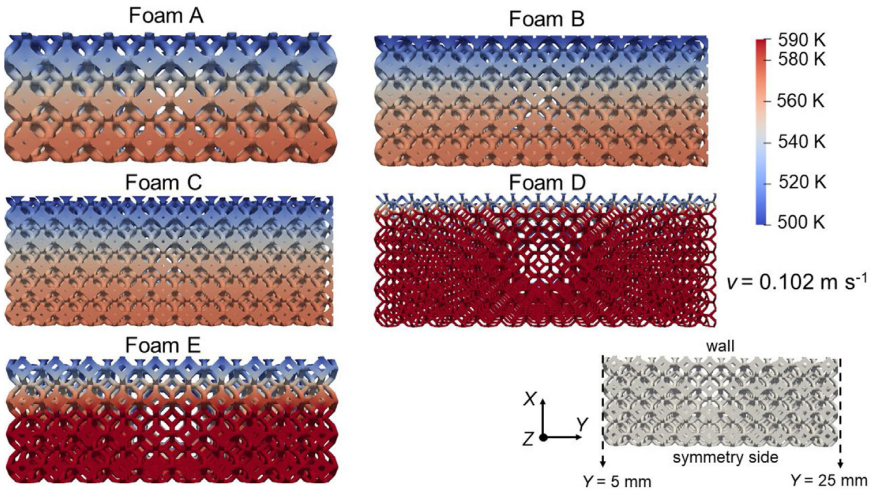

Fig. 5 – Temperature fields in the center plane for a 50 W heat source, a thermal conductivity of 15 W m^{-1} K^{-1} (i.e., alumina) and superficial velocity of 0.102 m s^{-1} for Foams A–E. Note that for clarity the temperature scale is limited to 590 K.

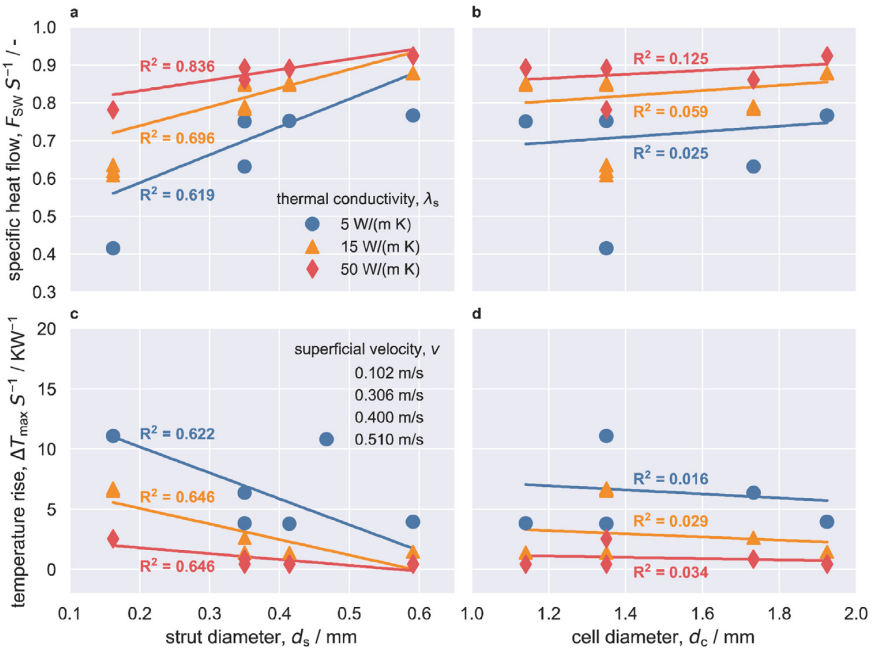

Fig. 6 – Relations between strut and cell diameter and specific heat flows (a and b) as well as specific maximal temperature increase (c and d). In total, results from 100 simulations of unique combinations of the strut and cell diameter, solid thermal conductivity, and fluid velocity were included. Different symbols and colors encode different solid thermal conductivities; different color shades indicate different fluid velocities. The trendlines and coefficients of determination (R^2) were determined using linear regression for the sets of different solid thermal conductivities.

intensity, were plotted against the strut and cell diameter (the chosen geometrical descriptors) in Fig. 6.

The specific conductive heat flows for almost all investigated cell and strut diameters were above 0.5 indicating dominant conduction (panels a and b). Only the smallest strut diameter (0.162 mm, Foam D) alongside with the lowest solid thermal conductivity (5 W m^{-1} K^{-1}) showed specific heat flows below 0.5 and thus dominant heat removal through convection (see Fig. 6a). The reason certainly is the small strut diameter which hinders conductive heat transport through the solid struts. This is in accordance with the findings of Zafari et al. (2015) and Bracconi et al. (2018).

Fig. 6a also clearly shows that an increasing strut diameter shifts the conduction/convection ratio significantly to conduction. The structure with the highest conduction ratio is thus the one with the largest strut diameter (d_s = 0.591 mm). The strong influence of the strut diameter is also reflected in the coefficients of determination (R^2) of the fitted linear trendlines. The coefficients of determination decrease from 0.836 over 0.696 to 0.619 with decreasing solid thermal conductivity indicating a significant relation between the strut diameter and the specific conductive heat flows. The strength of the correlation between the strut diameter and the specific conductive heat flow decreases for lower solid thermal

conductivities due the increasing influence of conductive heat removal. In contrast, the highest coefficient of determination between the cell diameter and the specific heat flow is 0.125 (Fig. 6b). The cell diameter does thus not influence the specific heat flow.

Inversely to the specific heat flow, the specific temperature increase (from the initial 500 K) decreased with increasing strut diameter and thermal conductivity (Fig. 6c). Again, the strut diameter significantly determines the observed temperature rise as indicated by the coefficients of determination around 0.6 for all solid thermal conductivities. In contrast, to the heat flows, the coefficients of determination did not change with the solid thermal conductivity. Again, the obtained coefficients of determination between the cell diameter and the specific temperature increase were below 0.1 (Fig. 6d), confirming the observation that the cell diameter does not determine the heat transport in the investigated parameter space.

3.3. *Quantitative analysis of structure-transport relations*

The previous exploratory analysis showed that the strut diameter d_s, the solid thermal conductivity λ_s, and the fluid velocity v are the principal structure and process parameters that determine heat flows in POCS with heat generation. To quantify the described structure-transport relations, we developed a simple yet physically sound surrogate model that describes the heat flows in the investigated system (see Fig. 7). The model consists of a cylindrical strut representing the periodic open-cellular structure. The strut reaches from the center of the tube at $y = 0$ to the wall at $y = C_L$. C_L is a characteristic length that describes the pathway for thermal conduction within the strut. Along the strut, energy is transferred to the surrounding fluid by convection. As in the CFD model, energy is produced within the strut. At the center of the strut ($y = 0$), a symmetry boundary condition is applied. At the wall ($y = C_L$), a fixed temperature equal to the incoming fluid temperature is assumed as for the CFD model. The steady state energy balance and boundary conditions for the strut thus read

$$\lambda_s \frac{d^2 T_s}{dy^2} = \frac{A_s}{V_S}\alpha (T_s - T_f) - \frac{S}{V_S} \text{ subject to } \left.\frac{dT_s}{dy}\right|_{y=0} = 0 \text{ and } T_s(y = C_L) = T_f \quad (2)$$

The differential Eq. (2) is solved analytically using Matlab's Symbolic Math Toolbox (The MathWorks, 2019). Afterwards, the conductive heat flow is calculated from the temperature gradient at the wall ($y = C_L$). The resulting expression for the normalized conductive heat flow is

$$\frac{F_{SW}}{S} = \frac{C_A}{\sqrt{C_S}\beta}\tanh\left(\sqrt{C_S}\, C_L\, \beta\right) \text{ . with } \beta = \sqrt{\frac{\alpha}{d_s \lambda_s}} \quad (3)$$

As previously explained, the parameter C_L describes the pathway of heat conduction within the solid. The parameter C_s describes the shape of the strut so that

$$\frac{A_s}{V_s} = \frac{C_s}{d_s} \quad (4)$$

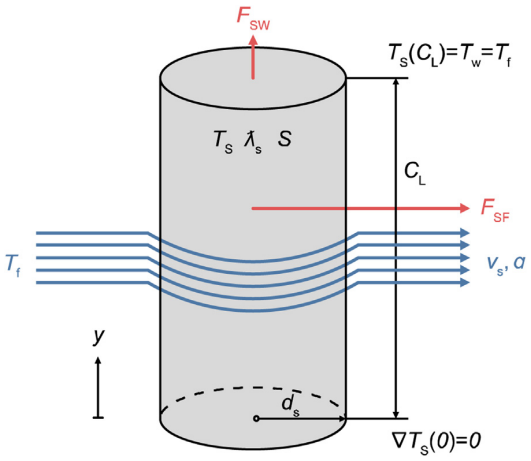

Fig. 7 – Illustration of the surrogate structure-transport model.

Table 1 – Summary of the setup and results of the non-linear least-squares minimization.

Quantity	Initial value	Final value
C_A (in m^{-1})	657.8	486.1 ± 8.7 (1.80%)
C_L (in mm)	21.85	1.91 ± 0.04 (2.19%)
C_s	4 (fixed)	4 (fixed)
correlation coeff. (C_A, C_L)		−0.98
number of data points		100
number of parameters		2
reduced SSE		$7.415\ 10^{-4}$

For the cylindrical struts in this study, C_s was set to 4. The parameter

$$C_A = \frac{A_w}{V_s} \quad (5)$$

describes the ratio of the wall contact area of the solid A_W and the solid volume V_s.

The heat transfer coefficient α depends on the strut diameter d_s and the fluid velocity v. For the present study, the heat transfer coefficient was estimated from Gnielinski's expression for laminar flow over a single cylinder (Martin and Gnielinski, 2000).

The influence of the principal parameters (strut diameter, solid thermal conductivity, and fluid velocity) is thus captured in the single parameter β in Eq. (3). The remaining unknown parameters are C_A and C_L. Both parameters were determined from the CFD data using non-linear least-squares minimization. To avoid local minima, 1000 random combinations from the parameter space $C_A \in 0\,m^{-1}, 1000\,m^{-1}$ and $C_L \in 0\,m, 1\,m$) were sampled, and the combination with the lowest sum of square errors (SSE) was selected.

Table 1 shows the setup and summary of the non-linear least-squares minimization. For both parameters, C_A and C_L, the standard deviation of the estimated values is below 5%, however, both parameters are strongly negatively correlated. The strong correlation is reasonable from a physical perspective as both parameters describe geometric features of the solid structure, and thus depend on the geometric structure parameters. Nevertheless, the developed structure-transport model describes the CFD data with an overall accuracy of ±10% (see Fig. 8). The deviations increase for small strut diameters and high fluid velocities, for which complex flow patterns

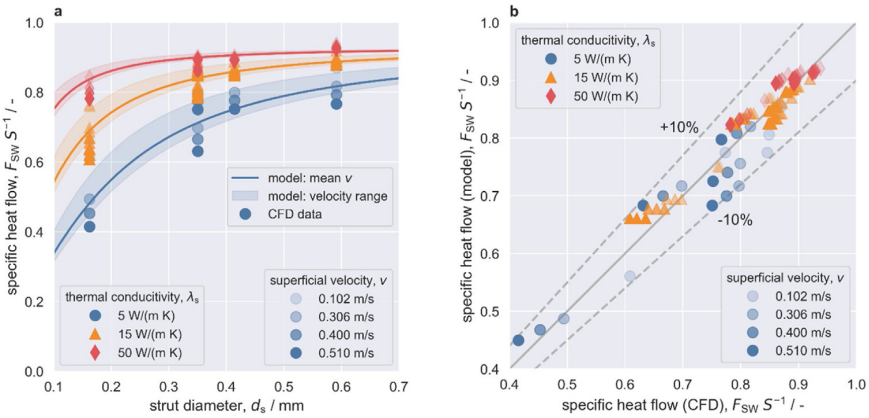

Fig. 8 – Comparison of model predictions with the CFD data (a), and parity plot of specific heat flow calculated with the structure-transport model and the CFD model (b). The structure-transport model predicts the CFD data within ±10% accuracy. The solid lines in (a) were calculated with the mean of the investigated velocity (0.31 m s^{-1}); the shaded areas represent the velocity range in the structure-transport model.[2]

increase the influence of the convective heat transfer. The complexity of the flow patterns is not fully captured in the surrogate structure-transport model.

Overall, the developed structure-transport model provides a valuable tool to quickly estimate the contributions of different heat transport mechanisms in POCS with heat generation in the solid, and will thus facilitate the design of tailored structured catalyst carriers in the future. Furthermore, the physical basis of the structure-transport model allows its extension to other structures such as irregular open-cell foams.

4. Conclusion

The conducted structure-heat transport analysis shows that the strut diameter and the thermal conductivity are the dominant structural parameters to control heat removal in periodic open-cell foams for typical materials and conditions found in gas-phase heterogeneous catalysis. The cell diameter, in contrast, does not influence heat removal. The fluid velocity plays a significant role only for materials with a low solid thermal conductivity. The high influence of the strut diameter and the thermal conductivity underpins the impact of thermal conduction in the solid domain. Due to the close resemblance of the Kelvin unit cell with the cells found in regular open-cell foams, the results obtained in this study for periodic open-cell foams (Kelvin lattices) are likely to translate well to regular open-cell foams. The found structure-heat transport relations thus underline the potential of open-cell foams (periodic and regular) to decouple effective heat removal from the fluid velocity in the design of catalyst carriers. In contrast to packed beds with point contacts between the individual catalyst particles, the decoupling trough structured catalyst carriers allows to use low flow rates in fixed-bed reactors, which leads to lower pressure drops and shorter reactors, while heat removal is guaranteed through the structure. In this case, sufficient mass transfer from the gas to the solid phase is the only constraint on the fluid velocity, which is typically less severe than for heat transfer.

Declaration of Competing Interest

The authors report no declarations of interest.

Acknowledgments

Christoph Sinn and Jorg Thöming appreciate the funding by the German Research Foundation (DFG) through the priority program SPP 2080 (Katalysatoren und Reaktoren unter dynamischen Betriebsbedingungen für die Energiespeicherung und -wandlung) under grant TH 893/23-1.

Appendix A. Governing equations and model assumptions (similar to (Sinn et al., 2019))

For the Newtonian fluid (air) with neglected gravitation, the conservation equations for mass, momentum, and energy as well as the ideal gas law read

$$\nabla \cdot (\rho_f \mathbf{U}) = 0, \quad (6)$$

$$\nabla \cdot (\rho_f \mathbf{U} \otimes \mathbf{U}) + \nabla \cdot (\mu(\nabla \otimes \mathbf{U} + (\nabla \otimes \mathbf{U})^T) - 2/3\mu(\nabla \cdot \mathbf{U})\mathbf{I}) - \nabla p = 0, \quad (7)$$

$$-\nabla \cdot (\rho_f \mathbf{U} h) - \nabla \cdot (\lambda_f \nabla T_f) = 0, \quad (8)$$

with ρ_f denoting fluid's density, $\mathbf{U}$ denoting the velocity field, h denoting the enthalpy and λ_f the fluid's thermal conductivity. In contrast, the solid phase is described by only the conservation of energy

$$\lambda_s(\nabla^2 T_s) + S_{spec} = 0, \quad (9)$$

with λ_s being the solid's thermal conductivity, T_s the solid's temperature and S_{spec} the specific artificial heat source. The simulations were carried out using the OpenFOAM solver chtMultiRegionSimpleFoam.

Table A1.

[2] The dataset from this plot is openly available under Sinn, C. (Christoph); Wentrup, J. (Jonas); Kiewidt, L.W. (Lars) (2020): Structure-heat transport data of periodic open-cell foams. 4TU.ResearchData. Dataset. https://doi.org/10.4121/uuid:58531fa2-067b-4a81-a577-75594df891c3.

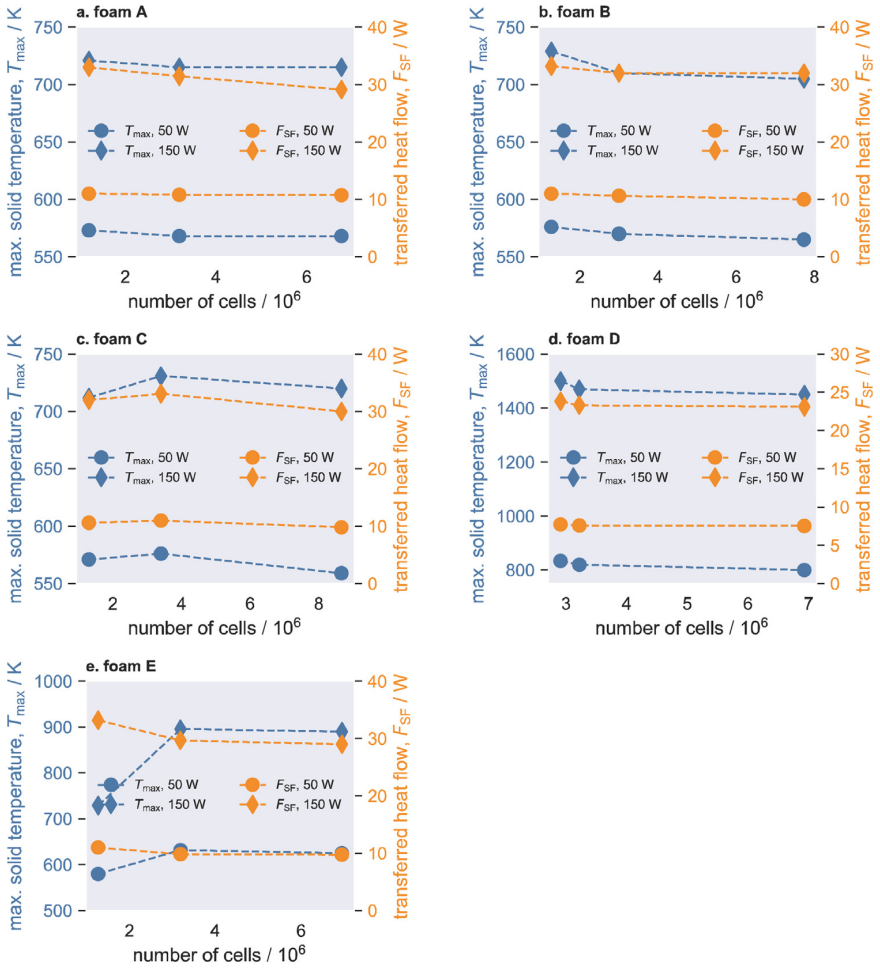

Fig. A1 – Grid independence studies for Foams A–E (λ_s = 15 W m^{-1} K^{-1}, v = 0.51 m s^{-1}). In all cases, the medium sized mesh has been selected.

Table A1 – Model properties investigated in this study.

Property		Assumption
Fluid dynamic viscosity	μ_f	Sutherland equation
Fluid heat capacity	$c_{p,f}$	const. (1030 J kg^{-1} K^{-1})
Fluid thermal conductivity	λ_f	Eucken approximation
Fluid density	ρ_f	ideal gas law (500 K: 0.7 Kg m−3)
Superficial velocity	v	const. (0.1–0.5 m s−1)
Pore Reynolds number	$Re_p = \frac{\rho_f v d_s}{\mu_f}$	const. (0.5–8)
Solid heat capacity	$c_{p,s}$	const. (1000 J kg^{-1} K^{-1}).
Solid thermal conductivity	λ_s	const. (5, 15 and 50 W m^{-1} K^{-1}) (alumina, mullite, sSiC)
Solid density	ρ_s	const. (4000 kg m^{-3})
Gravitational acceleration		neglected
Radiation		neglected
Turbulence		neglected

Appendix B. Grid independence studies

All meshes were created using the meshing utility snappyHexMesh. For further information regarding the meshing procedure the reader is referred to (Sinn et al., 2019).

Fig. A1

References

Bianchi, Enrico, Heidig, Tobias, Visconti, Carlo Giorgio, Groppi, Gianpiero, Freund, Hannsjorg, Tronconi, Enrico, 2012. An appraisal of the heat transfer properties of metallic open-cell foams for strongly exo-/Endo-Thermic catalytic processes in tubular reactors. Chem. Eng. J. 198–199, 512–528, http://dx.doi.org/10.1016/j.cej.2012.05.045.

Bianchi, Enrico, Groppi, Gianpiero, Schwieger, Wilhelm, Tronconi, Enrico, Freund, Hannsjörg, 2015. Numerical simulation of heat transfer in the near-wall region of tubular reactors packed with metal open-cell foams. Chem. Eng. J. 264, 268–279, http://dx.doi.org/10.1016/j.cej.2014.11.055.

Bianchi, Enrico, Schwieger, Wilhelm, Freund, Hannsjörg, 2016. Assessment of periodic open cellular structures for enhanced heat conduction in catalytic fixed-bed reactors. Adv. Eng. Mater. 18 (4), 608–614, http://dx.doi.org/10.1002/adem.201500356.

Bracconi, Mauro, Ambrosetti, Matteo, Maestri, Matteo, Groppi, Gianpiero, Tronconi, Enrico, 2018. A fundamental analysis of the influence of the geometrical properties on the effective thermal conductivity of open-cell foams. Chem. Eng. Process. Process. Intensif. 129 (July), 181–189, http://dx.doi.org/10.1016/j.cep.2018.04.018.

Bracconi, Mauro, Ambrosetti, Matteo, Maestri, Matteo, Groppi, Gianpiero, Tronconi, Enrico, 2020. Analysis of the effective

thermal conductivity of isotropic and anisotropic periodic open cellular structures for the intensification of catalytic processes. Chem. Eng. Process. Process. Intensif., 108169, http://dx.doi.org/10.1016/j.cep.2020.108169.

Dong, Ying, Korup, Oliver, Gerdts, Julian, Cuenya, Beatriz Roldán, Horn, Raimund, 2018. Microtomography-based CFD modeling of a fixed-bed reactor with an open-cell foam monolith and experimental verification by reactor profile measurements. Chem. Eng. J. 353, 176–188, http://dx.doi.org/10.1016/j.cej.2018.07.075.

Edouard, David, 2011. The effective thermal conductivity for 'slim' and 'fat' foams. AIChE J. 57 (6), 1646–1651, http://dx.doi.org/10.1002/aic.12372.

Fischedick, T., Kind, M., Dietrich, B., 2017. Radial two-phase thermal conductivity of ceramic sponges up to high temperatures – experimental results and correlation. Int. J. Therm. Sci. 114, 98–113, http://dx.doi.org/10.1016/j.ijthermalsci.2016.11.020.

Fourie, J.G., Du Plessis, J.P., 2004. Effective and coupled thermal conductivities of isotropic open-cellular foams. AIChE J. 50 (3), 547–556, http://dx.doi.org/10.1002/aic.10049.

Gao, H.B., Qu, Z.G., Feng, X.B., Tao, W.Q., 2014. Methane/air premixed combustion in a two-layer porous burner with different foam materials. Fuel 115, 154–161, http://dx.doi.org/10.1016/j.fuel.2013.06.023.

Gräf, Ingo, Rühl, Anne Kathrin, Kraushaar-Czarnetzki, Bettina, 2014. Experimental study of heat transport in catalytic sponge packings by monitoring spatial temperature profiles in a cooled-wall reactor. Chem. Eng. J. 244, 234–242, http://dx.doi.org/10.1016/j.cej.2014.01.060.

Gräf, Ingo, Ladenburger, Georg, Kraushaar-Czarnetzki, Bettina, 2016. Heat transport in catalytic sponge packings in the presence of an exothermal reaction: characterization by 2D modeling of experiments. Chem. Eng. J. 287, 425–435, http://dx.doi.org/10.1016/j.cej.2015.11.042.

Horneber, T., Rauh, C., Delgado, A., 2012. Fluid dynamic characterisation of porous solids in catalytic fixed-bed reactors. Microporous Mesoporous Mater. 154, 170–174, http://dx.doi.org/10.1016/j.micromeso.2011.12.047.

Iasiello, M., Cunsolo, S., Bianco, N., Chiu, W.K.S., Naso, V., 2017. Developing thermal flow in open-cell foams. Int. J. Therm. Sci. 111, 129–137, http://dx.doi.org/10.1016/j.ijthermalsci.2016.08.013.

Inayat, Amer, Freund, Hannsjörg, Zeiser, Thomas, Schwieger, Wilhelm, 2011. determining the specific surface area of ceramic foams: the tetrakaidecahedra model revisited. Chem. Eng. Sci. 66 (6), 1179–1188, http://dx.doi.org/10.1016/j.ces.2010.12.031.

Kalz, Kai F., Kraehnert, Ralph, Dvoyashkin, Muslim, Dittmeyer, Roland, Gläser, Roger, Krewer, Ulrike, Reuter, Karsten, Grunwaldt, Jan Dierk, 2017. Future challenges in heterogeneous catalysis: understanding catalysts under dynamic reaction conditions. ChemCatChem 9 (1), 17–29, http://dx.doi.org/10.1002/cctc.201600996.

Kiewidt, Lars, Thöming, Jorg, 2015. predicting optimal temperature profiles in single-stage fixed-bed reactors for CO_2-methanation. Chem. Eng. Sci. 132, 59–71, http://dx.doi.org/10.1016/j.ces.2015.03.068.

Kiewidt, Lars, Thöming, Jorg, 2019a. Multiscale modelling of monolithic sponges as catalyst carrier for the methanation of carbon dioxide. Chem. Eng. Sci.: X 2, 100016, http://dx.doi.org/10.1016/j.cesx.2019.100016.

Kiewidt, Lars, Thöming, Jorg, 2019b. Pareto-optimal design and assessment of monolithic sponges as catalyst carriers for exothermic reactions. Chem. Eng. J. 359, 496–504, http://dx.doi.org/10.1016/j.cej.2018.11.109.

Kumar, Prashant, Topin, Frederic, 2014. The geometric and thermohydraulic characterization of ceramic foams: an analytical approach. Acta Mater. 75, 273–286, http://dx.doi.org/10.1016/j.actamat.2014.04.061.

Lucci, Francesco, Torre, Augusto Della, Rickenbach, Janvon, Montenegro, Gianluca, Poulikakos, Dimos, Eggenschwiler, Panayotis Dimopoulos, 2014. Performance of randomized Kelvin cell structures as catalytic substrates: mass-transfer based analysis. Chem. Eng. Sci. 112, 143–151, http://dx.doi.org/10.1016/j.ces.2014.03.023.

Lucci, Francesco, Torre, Augusto Della, Montenegro, Gianluca, Kaufmann, Rolf, Eggenschwiler, Panayotis Dimopoulos, 2017. Comparison of geometrical, momentum and mass transfer characteristics of real foams to Kelvin cell lattices for catalyst applications. Int. J. Heat Mass Transf. 108, 341–350, http://dx.doi.org/10.1016/j.ijheatmasstransfer.2016.11.073.

Martin, Holger, Gnielinski, Volker, 2000. Calculation of heat transfer from pressure drop in tube bundles. The 3rd European Thermal Sciences Conference, 1155–1160.

Montenegro Camacho, Y.S., Bensaid, S., Lorentzou, S., Vlachos, N., Pantoleontos, G., Konstandopoulos, A., Luneau, M., et al., 2018. Development of a robust and efficient biogas processor for hydrogen production. Part 2: experimental campaign. Int. J. Hydrogen Energy 43 (1), 161–177, http://dx.doi.org/10.1016/j.ijhydene.2017.10.177.

Ranut, Paola, 2016. On the effective thermal conductivity of aluminum metal foams: review and improvement of the available empirical and analytical models. Appl. Therm. Eng. 101 (May), 496–524, http://dx.doi.org/10.1016/j.applthermaleng.2015.09.094.

Ranut, Paola, Nobile, Enrico, Mancini, Lucia, 2015. High resolution X-ray microtomography-based CFD simulation for the characterization of flow permeability and effective thermal conductivity of aluminum metal foams. Exp. Therm. Fluid Sci. 67, 30–36, http://dx.doi.org/10.1016/j.expthermflusci.2014.10.018.

Razza, S., Heidig, T., Bianchi, E., Groppi, G., Schwieger, W., Tronconi, E., Freund, H., 2016. heat transfer performance of structured catalytic reactors packed with metal foam supports: influence of wall coupling. Catal. Today 273, 187–195, http://dx.doi.org/10.1016/j.cattod.2016.02.058.

Reitzmann, Andreas, Patcas, Florina Corina, Kraushaar-Czarnetzki, Bettina, 2006. Keramische schwämme - anwendungspotenzial monolithischer netzstrukturen als katalytische packungen. ChemieIngenieurTechnik, http://dx.doi.org/10.1002/cite.200600029, WILEY-VCH Verlag.

Sadeghi, Mehrdad, Mirdrikvand, Mojtaba, Pesch, Georg R., Dreher, Wolfgang, Thöming, Jorg, 2020. Full-field analysis of gas flow within open-cell foams: comparison of micro-computed tomography-based CFD simulations with experimental magnetic resonance flow mapping data. Exp. Fluids 61 (5), 124, http://dx.doi.org/10.1007/s00348-020-02960-4.

Sinn, Christoph, Pesch, Georg R., Thöming, Jorg, Kiewidt, Lars, 2019. Coupled conjugate heat transfer and heat production in open-cell ceramic foams investigated using CFD. Int. J. Heat Mass Transf. 139, 600–612, http://dx.doi.org/10.1016/j.ijheatmasstransfer.2019.05.042.

Sinn, Christoph, Kranz, Felix, Wentrup, Jonas, Thöming, Jorg, Wehinger, Gregor D., Pesch, Georg R., 2020. CFD simulations of radiative heat transport in open-cell foam catalytic reactors. Catalysts 10 (6), 716, http://dx.doi.org/10.3390/catal10060716.

The MathWorks, 2019 2019. Symbolic Math Toolbox. Natick, Massachusetts, United States https://de.mathworks.com/help/symbolic/.

Torre, A., Della, G., Montenegro, G.R. Tabor, Wears, M.L., 2014. CFD characterization of flow regimes inside open cell foam substrates. Int. J. Heat Fluid Flow 50, 72–82, http://dx.doi.org/10.1016/j.ijheatfluidflow.2014.05.005.

Torre, A. Della, Montenegro, G., Onorati, A., Tabor, G., 2015. CFD characterization of pressure drop and heat transfer inside porous substrates. Energy Procedia 81, 836–845, http://dx.doi.org/10.1016/j.egypro.2015.12.093.

Torre, A. Della, Lucci, F., Montenegro, G., Onorati, A., Dimopoulos Eggenschwiler, P., Tronconi, E., Groppi, G., 2016. CFD modeling of catalytic reactions in open-cell foam substrates. Comput. Chem. Eng. 92, 55–63, http://dx.doi.org/10.1016/j.compchemeng.2016.04.031.

Wallenstein, M., Kind, M., Dietrich, B., 2014. Radial two-phase thermal conductivity and wall heat transfer coefficient of ceramic sponges – experimental results and correlation. Int. J.

Heat Mass Transf. 70, 486–495, http://dx.doi.org/10.1016/j.ijheatmasstransfer.2014.08.003.
Wehinger, Gregor D., Heitmann, Helge, Kraume, Matthias, 2016. An artificial structure modeler for 3D CFD simulations of catalytic foams. Chem. Eng. J. 284, 543–556, http://dx.doi.org/10.1016/j.cej.2015.09.014.
Weller, H.G., Tabor, G., Jasak, H., Fureby, C., 1998. A tensorial approach to computational continuum mechanics using object-oriented techniques. Comput. Phys. 12 (6), 620, http://dx.doi.org/10.1063/1.168744.
Wu, Zhiyong, Wang, Zhifeng, 2013. Fully coupled transient modeling of ceramic foam volumetric solar air receiver. Sol. Energy 89, 122–133, http://dx.doi.org/10.1016/j.solener.2012.12.016.
Xu, H.J., Xing, Z.B., Wang, F.Q., Cheng, Z.M., 2019. Review on heat conduction, heat convection, thermal radiation and phase change heat transfer of nanofluids in porous media: fundamentals and applications. Chem. Eng. Sci. 195, 462–483, http://dx.doi.org/10.1016/j.ces.2018.09.045.
Zafari, Mohammad, Panjepour, Masoud, Emami, Mohsen Davazdah, Meratian, Mahmood, 2015. Microtomography-based numerical simulation of fluid flow and heat transfer in open cell metal foams. Appl. Therm. Eng. 80, 347–354, http://dx.doi.org/10.1016/j.applthermaleng.2015.01.045.
Zhou, Xintong, Liu, Chang Jun, 2017. Three-dimensional printing for catalytic applications: current status and perspectives. Adv. Funct. Mater. 27 (30), 1701134, http://dx.doi.org/10.1002/adfm.201701134.

Chapter 9

Conclusion and Outlook

9.1 Conclusion

The knowledge gap in the context of heat transport in open-cell foams can be summarized as the need to overcome the one-size fits all solution for foam structured reactors. To get a deeper understanding of the heat transport processes in foams and to be able to derive engineering correlations, a computational fluid dynamics model was set up that can resolve detailed foam structures, conjugate heat transfer, catalytic reactions, thermal radiation and turbulence. The model was validated, verified and checked for plausibility in terms of pressure drop, heat transfer as well as temperature and concentration profiles. This could be done for pure conjugate heat transfer model as well as two gas-phase reactions serving as model reactions (CO oxidation and CPOX of methane, Appendix A.4). Further, three main objectives could be fulfilled:

1. **Heat transport mechanisms in foams**
   In this work, it could be quantified under what conditions conduction and convection are the dominant heat removal mechanisms. Furthermore, the role of thermal radiation as contributing mechanism was thoroughly quantified as well.
   The main influential parameters for the radial heat removal (at constant pressure) are the solid thermal conductivity and the strut diameter. Interestingly, the magnitude of the superficial velocity is less influential and becomes more relevant regarding heat removal at elevated velocities ($> 1\text{m s}^{-1}$). Combining these three parameters, a correlation was presented in Chapter 8. Additionally, the working pressure was found to increase the convective heat transfer significantly. In contrast, free convection (driven solely by density changes) was found to be irrelevant heat transport mechanism in foams under the studied conditions relevant for heterogeneous catalysis. Thermal radiation can influence the heat transport in the reactor, even though no changes in temperature might be observable. Generally, increasing solid thermal conductivity and decreasing solid surface emissivity reduces the contribution of thermal radiation. Lastly, the simulated "changing load" operation (i.e., steady-state jumps in concentration, pressure and velocity typical for dynamically operated plants) underlined the importance of understanding heat transport mechanisms to be able to improve the overall design ensure a robust and safe reactor operation.

2. **Heat source simplification to be used as tool**
   This thesis established uniformly distributed volumetric heat sources as easy to use tool for studying heat transport in structured catalyst carriers. By mimicking only the exothermicity of the gas-phase reaction, no detailed knowledge of the reaction itself is needed (i.e., no kinetics). Since lots of equations can

be omitted (see Chapter 3) and the demands on mesh quality are lowered as well, the computational time and modeling effort can be reduced significantly (see Appendix A.1, arbitrary example: 6 days reduced to 4 hours). Although the origin of the heat production between the approaches varies (heat sources: uniformly; actual reaction: locally different due to temperature depended kinetics), valuable information about heat transport can be extracted using the simplified approach. Integral heat flows and mean temperatures resemble well and can be used for determining heat removal mechanisms and evaluating expected thermal stress. Further, the computed maximum foam temperatures are at least to be expected in an actual reaction and further benefit a thermal stress analysis. However, hot-spot locations and local temperature gradients cannot be resolved. With the aid of heat sources, correlations regarding dominant heat removal mechanisms could be deployed. Furthermore, heat sources were successfully used to demonstrate under what conditions currently available pseudo-homogeneous models are inaccurate and need to be improved. They can therefore be used to improve existing models and help to deploy new engineering correlations. Lastly, the heat source simplification can be utilized in the open source framework OpenFOAM using standard solvers (i.e., free of charge). In contrast, heterogeneous catalytic reactions can currently only be solved in commercial CFD software packages (e.g., Fluent or STAR-CCM+).

3. **Derived design criteria**
   When evaluating both, the results of this work as well as the herein conducted literature study, a design hierarchy regarding the heat transport and heat removal of foam reactors can be deduced. As foams are only advantageous when heat is dominantly removed (or added) radially via thermal conduction, the hierarchy is as follows:

   (a) The first level is the selection of an appropriate solid thermal conductivity (i.e, material) and to ensure a proper wall coupling. This way, an unhindered radial heat removal can be tuned. For reaction systems that rely on proper heat exchange highly conductive materials such as Al or Cu should be favored. When reaction conditions do not allow for metals (e.g., temperature-dependent weakening of material or corrosion), the highest conductive alternative solid material should be selected. In contrast, when the reactive system benefits from temperature increases, poorly conducting materials should be used (see for instance Appendix A.3).

   (b) The second level that can be used for tuning is the structure level. Here, the strut diameter and the porosity are directly linked with radial heat removal. Structures with cavities in the struts (e.g, manufactured from PU templates) should not be used. According to the literature, there is also no sound evidence of irregular foams being advantageous over struts. Since, strut-to-node ratios were shown to be influential on the radial heat removal (Bracconi et al., 2018a) and a uniform strut diameter distribution in radial direction (Bracconi et al., 2020), it seems as POCS structures are the more promising structures. In contrast to irregular foams, POCS can better be tailored for the desired heat transport properties.

   (c) The third level of the heat transport design in foams is the tuning of single secondary heat transport mechanisms (i.e., radiation). This can for instance mean that the cell diameter is increased at high temperature to

increase radiative heat transport (see for instance Appendix A.2). Moreover, a certain strut shape (circular or triangular) or foam morphology (i.e, surface roughness of washcoat) can be used to influence the convective heat transfer.

9.2 Outlook

The herein developed and tested heat source simplification tool could be used in future investigations regarding reactor design. The normalization by the heat source intensity allows to predict foam heat flows accurately and temperature increases fairly for technically all gas-phase reactions and is thus an universally applicable tool.
As the investigated tube diameters were 15 and 25 mm, the relation between tube diameter and foam parameters in terms of heat transport mechanism could be investigated. This way, engineers could identify the maximum possible tube size that still ensures proper radial heat removal. Furthermore, possible temperature changes of a cooling/heating jacket can be characterized using the tool (as done in Zhang et al., 2020). Another open question regarding heat transport in foams, is the role of axial heat conduction in the foam. This might be relevant when stacks of foams (i.e., with axial discontinuity) are used (see for instance Kiewidt and Thöming, 2019a) and could underline the potential of 3D-printed structures (with intact solid matrix). Additionally, heat sources could be used with simultaneous reaction in order to show reaction control through heat sources (see for instance Dou et al., 2019). This is however, limited to electric conductive materials as Joule heating needs to be ensured.
More insight on dynamic processes can also be gathered especially for foam reactor design during the start-up and shut-down periods in dynamically operated reactors. That would mean, that the current model needs to resolve time as well and the requirements for the mesh would probably increase. Lastly, the heat source approach could be extended to multi-phase reactions (such as Fischer-Tropsch Synthesis) and be tested on other catalyst carriers (such as honeycombs or pellets) to investigate isolated heat transport related questions as well.
Obviously, the heat source approach itself is not capable of designing perfect structured foam reactors. The number of groups working on this topic emphasizes the complexity of finding foam designs perfectly adapted to their usage. The heat source approach and the results from this thesis, however, might contribute to the development of robust, safe and efficient reactors.

Appendix A

Additional Reactive Simulation Results

A.1 Reduction of Computational Time

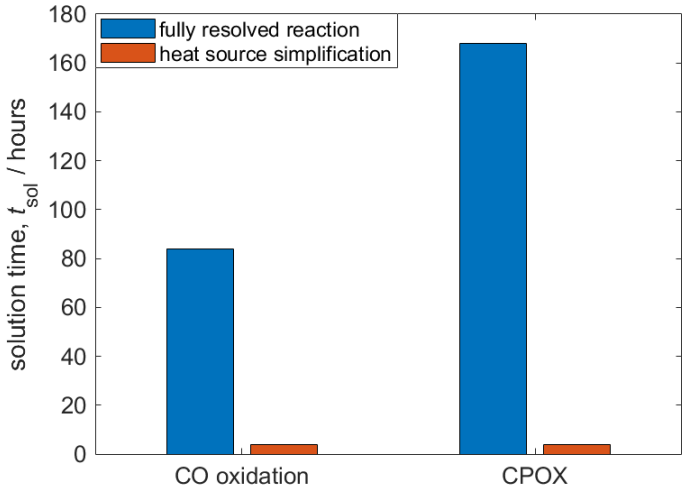

FIGURE A.1: Solution time of fully resolved reactions and heat source simplification shown for a quarter pipe Kelvin cell structure with 2.3 mio. cells computed on 20 cores (Intel Xeon, 2.1 GHz). Note that the exact solution time depend on chosen mesh, resolved model features, and much more. This figure thus, serves only as a rough overview.

At several occasion throughout this thesis, it is mentioned that heat sources are obviously less computational costly than fully resolving exothermal catalytic reactions. To demonstrate the impact on computational cost, Figure A.1 shows solution times for both approaches. Note, that this is an arbitrary example as the solution time depends on many quantities (e.g., mesh size, mesh type, parallelization, amount and complexity of solved sub-models, etc.). However, the figure shows for the very same mesh (approx. 2.3 mio. cells.) calculated on 20 cores (Intel Xeon, 2.1 GHz) with 360 GB RAM that the solution time is reduced significantly. For an arbitrary example of the CO oxidation (from chapter 5), the solution time for reaching final relative residuals of 10^{-5} for the enthalpy is reduced from approximately 80 hours to 4 hours. The kinetic mechanism of the CO oxidation is less complex regarding the number of equations compared to many other reactions such as the catalytic partial oxidation (CPOX) of methane (on Rh, see Schwiedernoch et al., 2003).

Choosing kinetics of CPOX of methane on Rh over the CO oxidation kinetics on Pt, the changes in computational time are reduced from approx. 160 hours to 4 hours. Please note that the CPOX simulation were conducted with the boundary conditions applied in Wehinger, Heitmann, and Kraume, 2016. These arbitrary results underline that extensive structure-heat transport analyses, such as done in Chapter 8, with more than 100 simulations would be very time consuming with the currently available computational power.

A.2 Influence of Radiation during CO Oxidation

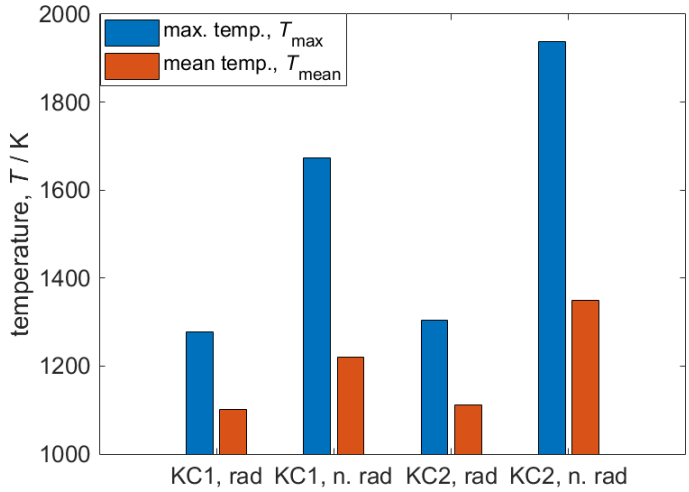

FIGURE A.2: Influence of neglecting radiative heat transport exemplified for the CO oxidation reaction. The model is identical to the one used in Chapter 5 using the S2S radiation model. Conditions: $v = 0.5\,\mathrm{m\,s^{-1}}$; $T_{\mathrm{wall}} = T_{\mathrm{in}} = 1000\,\mathrm{K}$; $\lambda_{\mathrm{s}} = 2\,\mathrm{W\,m^{-1}\,K^{-1}}$.

In Chapter 7 the influence of radiation in a foam reactor is extensively quantified using the heat source simplification. To show the impact during an actual exothermal reaction, Figure A.2 displays the mean and maximum solid temperature increases for two Kelvin cells (same Kelvin cells as used in Chapter 5 and Sinn et al., 2020b, respectively). The results clearly show the immense importance of radiation modeling for the CO oxidation in these foam reactors. Please note, the model conditions are similar to one from Chapter 5. While the computed maximum temperatures differ for KC1 around 400 K, they differ for KC2 around 600 K. Obviously, these deviations are not tolerable and a radiation model clearly is required. Interestingly, the consideration of a radiation model seems to impact the heat transport in KC2 more than in KC1. When radiation is considered, the solid temperature increases only differ by 25 K between KC1 and KC2. The larger strut diameter (increased radial conduction) and cell diameter (increased radiation influence) of KC1 explain the temperature difference. The increase of radiative heat flow by increased cell diameters can be backed up by the pseudo-homogeneous model by Bianchi et al., where the radiative contribution of λ_{eff} increases proportionally with the cell diameter (Bianchi et al., 2012). Obviously, this should be further investigated and included in future structure-heat transport analyses.

A.3 Changing Load Operation

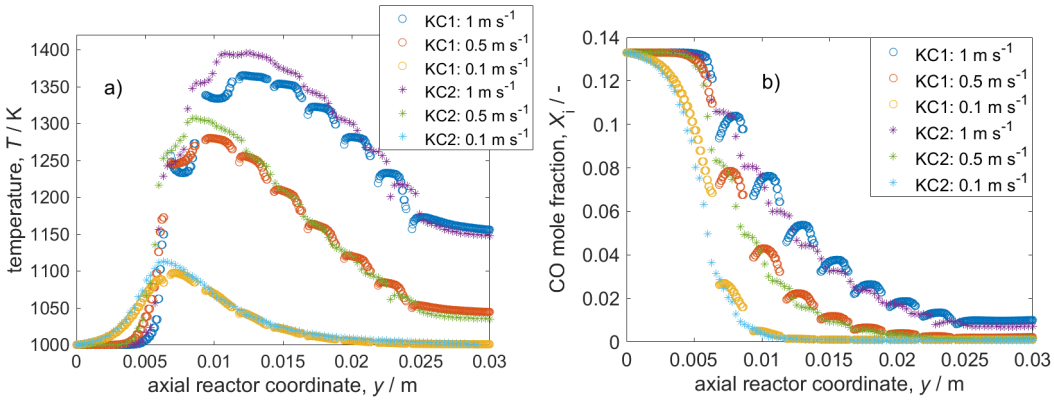

FIGURE A.3: Control of temperature hot spots during changing load operation of CO oxidation for poor conductive solid. KC1 and KC2 have a similar specific surface area, while differing strongly in their diameter. Conditions: $T_{wall} = T_{in} = 1000\,K; \lambda_s = 2\,W\,m^{-1}\,K^{-1}$.

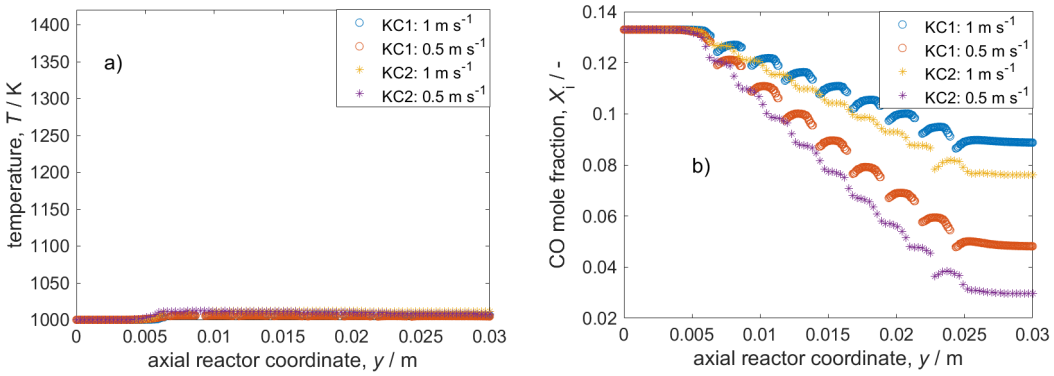

FIGURE A.4: Control of temperature hot spots during changing load operation of CO oxidation with high conductive solid. KC1 and KC2 have a similar specific surface area, while differing strongly in their diameter. Conditions: $T_{wall} = T_{in} = 1000\,K; \lambda_s = 200\,W\,m^{-1}\,K^{-1}$.

As stated earlier in this thesis, open-cell foams are prospectively to be used in flexible small-scale reactors. Flexible might refer to load changes (i.e., superficial velocities or volume flows). Here, it is checked if the findings from the structure-heat transport analysis in Chapter 8 also hold for an actual reaction. The CO oxidation (as done in Chapter 5 is simulated on two Kelvin cells (the same ones from Sinn et al., 2020b) with a solid thermal conductivity of $2\,W\,m^{-1}\,K^{-1}$ (corresponding to a poor conductive ceramic material). The two Kelvin cells have a comparable specific surface area (difference 3 %) and thus a comparable amount of catalytic active material. In contrast, they differ significantly in their strut diameter (difference around 50 %). In Figure A.3, the simulated results for the axial temperature along the reactor as well as the CO concentration are depicted for the two foams. The hot-spot movement to the right can be seen as well as an increase of the hot-spot magnitude. This general behavior can be seen for both foam structures. Increasing the velocity, obviously increase the volume flow and thus the produced heat and the hot-spot magnitude. The hot-spot movement towards the reactor rear is due to the increased

convective cooling resulting from elevated superficial velocities.
The hot-spot temperatures of the foam (KC2) with the smaller diameter are elevated in comparison with KC1. It can therefore be confirmed that the strut diameter can be used to tune radial heat transport in exothermal gas-phase reactions. In this particular reaction, the reaction yield increases for the KC2 with higher hot-spot temperatures due to increased temperature-dependent kinetics. This behavior might be different for other exothermal reactions, such as the CO_2 methanation, with different thermodynamic and kinetic boundaries (Kiewidt and Thöming, 2015).
When the solid thermal conductivity is changed to 200 $W\,m^{-1}\,K$ (i.e., aluminum), the temperature hot spots almost vanish (see Figure A.4). Additionally, the CO conversion is significantly lower than for the poor conductive material ($\lambda_s = 2\,W\,m^{-1}\,K$), resulting from the overall lower temperatures and reduced kinetic conversion. It was also shown in the literature that the CO oxidation can be favored from low conductive foams (Ercolino, Stelmachowski, and Specchia, 2017). The CO oxidation benefits under these reaction conditions from poor radial heat removal which can be realized by small strut diameters and low solid thermal conductivities. It also becomes apparent, that the impact of the solid thermal conductivity on radial heat transport is more severe than the impact of the strut diameter.

A.4 Additional Model Plausibility Study — CPOX of Methane

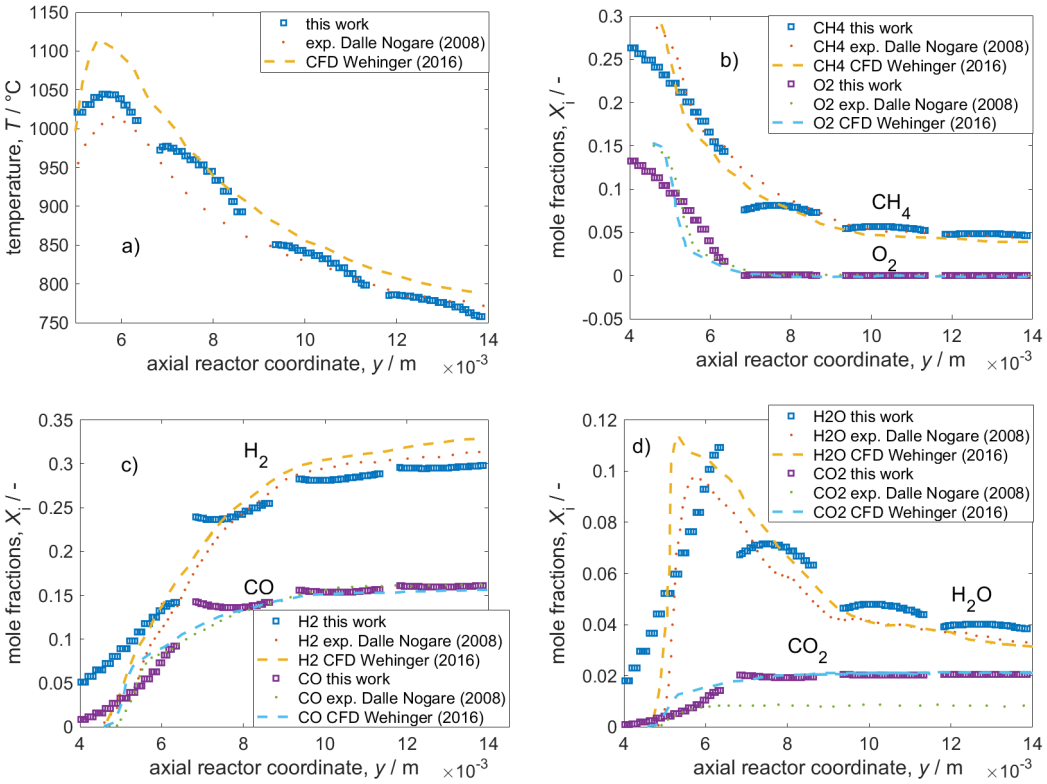

FIGURE A.5: Simulation results for catalytic partial oxidation of methane compared against CFD and experimental literature data (Dalle Nogare et al., 2008; Wehinger, Heitmann, and Kraume, 2016). The data is sampled along the central axial coordinate.

TABLE A.1: Model properties and boundary conditions for the simulation of CPOX of methane.

property	value/assumption
foam: Kelvin cell 1	see values in Chapter 5
λ_s	$2\,W\,m^{-1}\,K^{-1}$
ρ_s	$2000\,kg\,m^{-3}$
$c_{p,s}$	$1100\,J\,kg^{-1}\,K^{-1}$
$F_{cat/geo}$	2
v	$0.471\,m\,s^{-1}$
surface emissivity	0.8
surface reflectivity	0.2
feed $CH_4/O_2/Ar$	0.291/0.153/0.556
inlet gas temperature	1221 K
wall temperature	1023 K

To further check the reactive foam model for plausibility, the principally equivalent reactive model of the CO oxidation is simulated using exchanged micro-kinetics (Schwiedernoch et al., 2003) for the catalytic partial oxidation of methane on Rh for syngas production (see Chapter 2). The results are eventually compared against literature experiments (Dalle Nogare et al., 2008) and CFD simulations (Wehinger, Heitmann, and Kraume, 2016). The experimental description does not contain all required model input. Therefore, properties from Wehinger, Heitmann, and Kraume, 2016 were taken and assumptions regarding the temperature boundary conditions were made (see Table A.1).
The experiment from literature was conducted on a 80 ppi foam with partially blocked pores. The reference CFD study tried to recreate the experimental foam with an artificial structure modeler (Wehinger, Heitmann, and Kraume, 2016). As neither of the structures are identical, this comparison only serves as an additional model plausibility study. The experiments data was gathered by moving a suction capillary through a central drilled channel in the foam (Horn et al., 2006). Additionally in the experiment, a front heat shield was positioned in front of the catalytic foam, which was omitted in this study. The plausibility study was conducted using a Kelvin cell (KC1, Chapter 5).
The results of the CFD simulations as well as literature data are shown in Figure A.5. Here, the values for temperature a), the reactants CH_4 and O_2 b), the products H_2 and CO c) as well as side products H_2O and CO_2 d) are depicted. Even though the foam structural properties differ, this work can reproduce the experiment and the CFD data from literature quite fairly for all properties. Again, this is not about validation as many information are missing. The comparison demonstrates that the principal reactor model works with different kinetics and can thus be used for several exothermic gas-phase reactions.

Appendix B

Supporting Documents of Published Manuscripts

This chapter contains the Supporting Documents of the two published manuscripts Sinn et al., 2019 and Sinn et al., 2021a.

The first one contains the following information (Sinn et al., 2019):

- Influence of radiation on overall heat transport.
- Properties for Sutherland equation.
- Temperature corrected reaction enthalpy.
- Evolving heat of reaction during methanation.

The second document contains the following information (Sinn et al., 2021a):

- Plausibility study with information on the geometrical model and the comparison of pressure drop, temperature and concentration profiles against literature data.
- Correlations and results for Kelvin cells.
- Grid independence study and depiction of utilized mesh.
- Influence of radiation modeling on CO oxidation.

Supplementary Material to: Coupled conjugate heat transfer and heat production in open-cell ceramic foams investigated using CFD

Christoph Sinn[a], Georg R. Pesch[a], Jorg Thöming[a], Lars Kiewidt[b,*]

[a] *University of Bremen, Chemical Process Engineering, Leobener Strasse 6, 28359 Bremen, Germany*
[b] *Wageningen University & Research, Biobased Chemistry and Technology, P.O. box 17, 6700 AA Wageningen, The Netherlands*

Abstract

Combining low pressure drop and remarkable heat transport properties, open-cell foams offer a combination that makes them a highly attractive option as monolithic catalyst support. The coupled thermal behavior of foams and fluids during heat production, e.g., exothermic chemical reactions, is still not thoroughly described despite their potential to optimize temperature control in fixed bed reactors. Hence, the aim of this study is to get deeper insight into coupled conjugate heat transfer and heat production in open-cell foams used in a tube reactor with constant wall temperature. Therefore, we conducted a μCT-based CFD simulation of an alumina foam with artificial heat sources that mimic the heat of reaction during an exothermal chemical reaction and allow to study the effect of heat production on heat transfer while requiring lower computational cost than simulating actual chemical reactions. We implemented a range of heat source intensities, that covers typical exothermic reactions, to study their effect on heat flows as well as temperature fields and used CO_2 methanation as a case study. We further quantified the influence of superficial velocity, heat source intensity and material on the temperature fields inside the foam and found conduction being the dominant heat transport mechanism. We further evaluated the feasible range of even more simplified pseudo-homogeneous models and found high thermal conductivities and low superficial velocities to be appropriate. In conclusion, the presented approach offers the possibility to study thermal effects regarding catalytic supports and give valuable insight in heat transport mechanisms under relevant process conditions in heterogeneous catalysis (heat sources: 5 - 150 W for a reaction volume of 1.2×10^{-5} m^3, superficial velocities 0 - 0.51 m s^{-1}, thermal conductivities 5 - 50 W m^{-1} K^{-1}).

Keywords: open-cell foam, solid sponge, computational fluid dynamics (CFD), conjugate heat transfer, volumetric heat source, pseudo-homogeneous model

*Corresponding author
Email addresses: gpesch@uni-bremen.de (Georg R. Pesch), lars.kiewidt@wur.nl (Lars Kiewidt)

1. Influence of radiation on overall heat transport

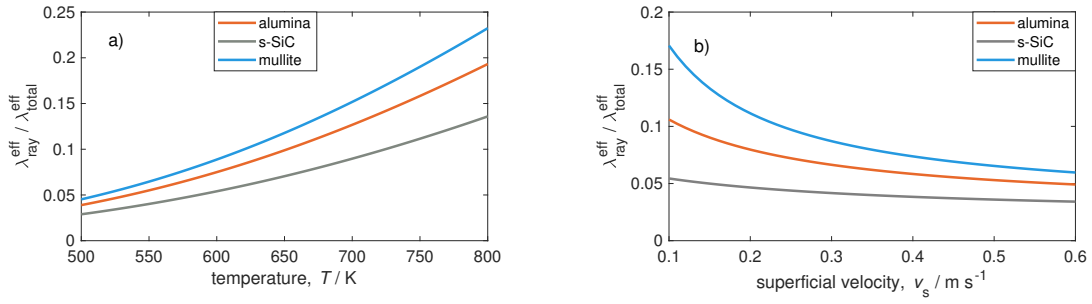

Figure 1: Ratio of effective radiative thermal conductivity to total effective radiative thermal conductivity in order to estimate the effect of radiation on the overall heat transport. The model is taken from Ref. [1]. (a) Ratio plotted against temperature for a superficial velocity of v_s =0.51 m s^{-1}. (b) Ratio plotted against superficial velocity for a uniform temperature of T =500 K. The influence of heat transported via radiation increase significantly with rising temperatures, whereas the effect of velocity is vice versa.

2. Properties for Sutherland equation

In this section the following equations and properties are taken from Ref. [2]. The temperature dependency of the dynamic viscosity $\mu(T)$ can be expressed via Sutherland equation,

$$\mu(T) = \frac{A_{\mathrm{Su}} \cdot T^{\frac{3}{2}}}{T + T_{\mathrm{Su}}}. \tag{1}$$

Within this equation, T is the Temperature and T_{Su} the Sutherland constant. The value A_{Su} can be calculated with

$$A_{\mathrm{Su}} = \frac{\mu_{\mathrm{ref}}(T_{ref} + T_{\mathrm{Su}})}{T_{\mathrm{ref}}^{\frac{2}{3}}}. \tag{2}$$

T_{Su} has a value of 120 for air. μ_0 denotes dynamic viscosity at a reference temperature T_{ref}. With μ_{ref} set to 18.27×10^{-6} Pa s and T_{ref} set to 291.15 K, A_{Su} then becomes

$$A_{\mathrm{Su}} = \frac{18.27 \times 10^{-6}\,\mathrm{Pa\,s} \cdot (291.15 + 120)}{291.15^{\frac{3}{2}}} = 1.51 \times 10^{-6}\,\mathrm{Pa\,s}. \tag{3}$$

The coeffiecients A_{Su} and T_{Su} are specified in OpenFOAM.

3. Temperature corrected reaction enthalpy

In this section the following equations and properties are taken from Ref. [3]. For a constant pressure the temperature dependent reaction enthalpy can be calculated via Kirchoff's Law,

$$\Delta H^0_{\mathrm{R}}(T) = \Delta H^0_{\mathrm{R}}(298.15\,\mathrm{K}) + \Delta c^0_{\mathrm{p,m}}(T - 298.15\,\mathrm{K}). \tag{4}$$

$\Delta c^0_{\mathrm{p,m}}$ describes the integrated heat capacity which is also temperature dependent and can be calculated as follows,

$$\Delta c^0_{\mathrm{p,m}} = R \cdot \Delta A + \Delta B \cdot T_{\mathrm{am}} + \frac{\Delta C}{3}(4T^2_{\mathrm{am}} - T_1 \cdot T_2) + \frac{\Delta D}{T_1 \cdot T_2},\ T_{\mathrm{am}} = \frac{T_1 + T_2}{2}. \tag{5}$$

Within this equation, R is the general gas constant. Either one of the coefficients $\Delta A,\ \Delta B,\ \Delta C$ and ΔD can be calculated as the sum of the product of stoichiometric coefficient ν and equivalent parameter for reaction partner j,

$$\Delta A = \sum_{j=1}^{N} \nu_{\mathrm{j}} \cdot A_{\mathrm{j}},\ \Delta B = \sum_{j=1}^{N} \nu_{\mathrm{j}} \cdot B_{\mathrm{j}},\ \Delta C = \sum_{j=1}^{N} \nu_{\mathrm{j}} \cdot C_{\mathrm{j}},\ \Delta D = \sum_{j=1}^{N} \nu_{\mathrm{j}} \cdot D_{\mathrm{j}}. \tag{6}$$

All needed values for the CO_2 methanation are listed in Table 1.

Table 1: Parameters for determination of temperature dependent reaction enthalpy.

j	ν	A	B $\cdot 10^{-3}$	C $\cdot 10^{-6}$	D $\cdot 10^{5}$
CO_2	-1	5.457	1.045	-	-1.157
4 H_2	-4	3.24	0.422	-	0.083
CH_4	1	1.702	9.081	-2.164	-
$2H_20$	2	3.47	1.45	-	0.121

Inserting these parameters finally leads to

$$\Delta A = -9.775,\ \Delta B = 9.24 \times 10^{-3},\ \Delta C = -2.164 \times 10^{-6},\ \Delta D = 1.067 \times 10^{5}. \tag{7}$$

With $T_1 = 298.15\,\mathrm{K}$, $T_2 = 500\,\mathrm{K}$, $T_{am} = 399\,\mathrm{K}$ and $R = 9.81\,\mathrm{J\,mol^{-1}\,K^{-1}}$, $\Delta c^0_{\mathrm{p,m}}$ then becomes

$$\Delta c^0_{\mathrm{p,m}} = -47.62\,\mathrm{J\,mol^{-1}\,K^{-1}}. \tag{8}$$

Finally, the temperature corrected reaction enthalpy can be determined

$$\Delta H^0_{\mathrm{R},500} = -165\,\mathrm{kJ\,mol^{-1}} + -47.62\,\mathrm{J\,mol^{-1}\,K^{-1}} \cdot (500\,\mathrm{K} - 298.15\,\mathrm{K}) = -174.6\,\mathrm{kJ\,mol^{-1}}. \tag{9}$$

4. Evolving heat of reaction during methanation

The overall evolving heat $\dot{Q}$ inside the tube can be estimated by the product of volume flow $\dot{V}$, molar concentration of carbon dioxide $C_{\mathrm{CO_2}}$, yield Y and heat of reaction ΔH^0_{R},

$$\dot{Q} = \dot{V} \cdot C_{\mathrm{CO_2}} \cdot Y \cdot \Delta H^0_{\mathrm{R}} \tag{10}$$

By applying the ideal gas law, the molar concentration of $C_{\mathrm{CO_2}}$ can be calculated, assuming $T = 500\,\mathrm{K}$ and knowing the partial pressure of CO_2 ($p_{\mathrm{CO_2}}$). The partial pressure results from the molar ratio and a total pressure of $p_{\mathrm{total}} = 6 \times 10^5\,\mathrm{Pa}$,

$$p_{\mathrm{CO_2}} = \frac{n_{\mathrm{CO_2}}}{n_{\mathrm{total}}} \cdot p_{\mathrm{total}}. \tag{11}$$

Any occurring pressure dependence of the system is neglected. With the assumption of a constant pressure, the reaction enthalpy for $T = 500\,\mathrm{K}$ can be corrected to $\Delta H_{\mathrm{R},500} = -174.6\,\mathrm{kJ\,mol^{-1}}$ (as shown above).

Inserting the above listed parameters as well as a fluid rate of $1.5\,\mathrm{L\,min^{-1}}$ for carbon dioxide and a yield of 0.3 into Equation (10) leads to

$$\dot{Q} = 0.025 \times 10^{-3}\,\mathrm{m^3\,s^{-1}} \cdot \frac{0.2 \cdot 7 \times 10^5\,\mathrm{Pa}}{8.314\,\mathrm{J\,mol^{-1}\,K^{-1}} \cdot 500\,\mathrm{K}} \cdot 174.6\,\mathrm{kJ\,mol^{-1}} \cdot 0.3 = 44.1\,\mathrm{W}. \tag{12}$$

Symbols

Symbol :	Description, Unit
Roman	
A_{su} :	constant for Sutherland equation, Pa s
$\Delta c^0_{p,m}$:	integrated heat capacity, J kg^{-1} K^{-1}
A_R, B_R, C_R, D_R :	coefficients for determination of reaction enthalpy, –
C_{CO2} :	molar concentration of CO_2, mol m^{-3}
$\dot{Q}$:	heat, W
ΔH^0_R :	standard reaction enthaply, kJ mol^{-1}
j :	chemical species, –
n_{CO2} :	amount of CO_2, mol
p :	pressure, Pa
p_{CO2} :	partial pressure ofCO_2, Pa
R :	universal gas constant for air (8.314), J K^{-1} mol^{-1}
T :	temperature, K
T_{am} :	mean temperature for determination of reaction enthalpy, K
T_{Su} :	Sutherland constant, K
T_{ref} :	reference temperature, 291.15 K
V :	volume, m^3
$\dot{V}$:	volume flow, m^3 s^{-1}
Y :	yield, –
Greek	
μ_{ref} :	dynamic viscosity at reference temperature, Pa s
λ^{eff}_{total} :	total effective thermal conductivity, W m^{-1} K^{-1}
λ^{eff}_{ray} :	radiative effective thermal conductivity, W m^{-1} K^{-1}

References

[1] T. Fischedick, M. Kind, B. Dietrich, Radial two-phase thermal conductivity of ceramic sponges up to high temperatures experimental results and correlation, International Journal of Thermal Sciences 114 (2017) 98–113. doi:10.1016/j.ijthermalsci.2016.11.020.
URL https://linkinghub.elsevier.com/retrieve/pii/S1290072916307141

[2] F. M. White, Viscous fluid flow, 3rd Edition, McGraw-Hill;, Boston, Mass., 2006.

[3] Thermodynamics Research Center, TRC Thermodynamic Tables Hydrocarbons, 2nd Edition, J.Physical and Chemical Refrence Data, College Station, Texas, 1982.

Supporting Information on

Heat Transport in Open-Cell Foams: CFD Analysis of Artificial Heat Sources vs Fully Resolved Exothermal Reactions

Christoph Sinn[a,1], Jonas Wentrup[a,1], Georg R. Pesch[a,b,*], Jorg Thöming[a,b]

[a] University of Bremen, Chemical Process Engineering,
Leobener Strasse 6, 28359 Bremen Germany

[b] University of Bremen, MAPEX Center for Materials and Processes,
Postbox 330 440, 28334 Bremen, Germany

[*] corresponding author (G.R. Pesch: gpesch@uni-bremen.de)

[1] these authors contributed equally

Keywords: periodic open-cell foam (POCS), conjugate heat transfer, Computational Fluid Dynamics (CFD), CO oxidation, exothermal catalytic reaction

Abstract

Catalytic structured foam reactors show promising characteristics for process intensification such as low pressure drop, high specific surface area, and remarkable heat transport. Especially for the design of small-scale dynamically operated reactors the understanding of heat transport is crucial. With computational fluid dynamics (CFD) we can thoroughly investigate the thermal field of the coupled gas/solid under reaction conditions and understand heat transport in structured reactors. In the past, we mimicked the heat production during exothermal reactions with uniformly distributed volumetric heat sources in the solid. Here, we compare thermal fields of such simplifications with full-model calculations using the strongly exothermal CO oxidation as a model reaction. We find that heat flows of the reaction and of artificial heat source calculations match well and reliable mean temperature increases can be computed. While it cannot compute exact hot-spot magnitude and location, this method helps to determine heat removal mechanisms and estimate thermal stress.

1. Plausibility Study

The CFD setup in the main manuscript was not arbitrarily created but generated in that way that allows for an assessment of plausibility of the reaction model by comparing simulation results against literature data. The reference study was performed by Dong et al. [1] who simulated the CO oxidation over Pt in a fixed-bed reactor filled with a µCT-reconstructed 45 ppi foam and validated their model by own experiments.

1.1 Geometrical Model

The Kelvin cell geometry in this work was used to construct a geometry with similar properties compared to the 45 ppi foam used by Dong et al. [1]. Usually, the open porosity ε_o and the specific surface area S_V of the foam are declared as most crucial geometry characteristics. [2] Several correlations exist in the literature to calculate the corresponding cell and strut diameter d_c and d_s of a Kelvin cell to match ε_o and S_V. In this work, we applied the equations of Inayat et al. [3], Lucci et al. [2] and Ambrosetti et al. [4]. The correlation of Lucci et al. [2] resulted in the most suitable set of parameters (see Section 2), and was therefore chosen for the generation of the Kelvin cell geometry. Whereas the open porosity matches the reference study well, the specific surface area resembles only approximately (see Table S1). Further, the correlation calculated larger cell and strut diameters. The foam radius of the Kelvin cell type slightly differs from the reference foam (this study: 7.5 mm compared to Dong et al. [1]: 8 mm).

Table S1: Kelvin cell properties and μCT foam properties.

	μCT foam from Dong et al.[1]	Kelvin cell (this work)
cell diameter, d_c (mm)	1.35	1.924
strut diameter, d_s (mm)	0.35	0.591
open porosity, ε_o (-)	0.73	0.724
specific surface area, S_V (1/m)	1512	1467.8

We approximated inlet and wall boundary conditions, since no exact values of their simulations were listed in the work of Dong et al. [1]. The boundary conditions of the plausibility case are very similar to the ones used in the main manuscript. From the reference study's experimental description, we could deduce the inlet mole fraction to be X_{i0} (CO/O_2/Ar) = 0.133/0.066/0.801 (A small ratio of helium in the gas mixture was

neglected in our CFD model. We chose argon to be the only inert species; Dong et al. [1]: X_{i0} (Ar/He) = 0.736/0.065), a pressure of 0.1 MPa and an inlet flow rate of 1200 Nml min^{-1}. No detailed information regarding the fluid temperature was presented, since they focused on matching simulative and experimental temperature data. However, they conducted an adiabatic case study. Based on that, we guessed an inlet temperature of T_{in} = 1250 K (see Figure S1 a). An inlet superficial velocity of v_0= 0.48 m s^{-1} results from converting the inlet flow rate of 1200 Nml min^{-1} at standard conditions to a temperature level of 1250 K as well as converting to the slightly smaller foam diameter. From the solid temperature profile, we estimated a fixed wall temperature of T_w = 1000 K. We note, that this comparison serves only as a plausibility study as the detailed experimental and model conditions could not be recreated. We believe, that the assumptions made are suitable for this purpose.

All in all, compared to the simulations presented in the main manuscript, only the fluid inlet temperature and velocity were adjusted to come closer to the assumptions of the reference study. The solid thermal conductivity λ_s was set to a value of 2 W m^{-1} K^{-1}, equivalent to the reference study. The resulting concentration and temperature profiles were analyzed with respect to grid independence (See Section 3 for details).

1.2 Comparison of Pressure Drop, Temperature and Concentration Profiles

The generated profiles for the fluid and solid temperature as well as for the species' mole fractions are plotted in Figure S1 and compared to profiles from Dong et al. [1]. All values are not cross-sectionally averaged but obtained from the center of the pipe, since the experimental data points are based on a capillary suction probe procedure along the centerline.

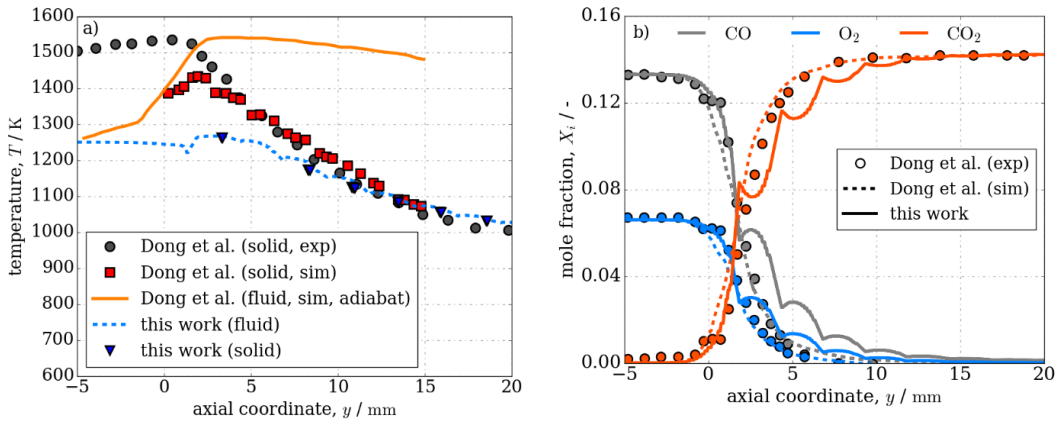

Figure S1: Plausibility of simulation results. a) Fluid and solid temperatures along centerline. b) Temperature along centerline. The origin of the abscissa indicates the beginning of the coated catalyst support. Experimentally, solid temperatures are visible also in front of the catalyst due to an inserted heat shield. In contrast, the simulations of this work and of the reference study neglect the presence of heat shields which results in solid temperature profiles starting at y = 0.

The simulated fluid temperature (Figure S1 a) starts at its initial value of 1250 K (y = -5 mm), cools down slightly before the foam due to the cooler wall temperature (T_w = 1000 K) and rises up to about 1265 K in the hot spot (y = 2 mm). Eventually, it decreases to approx. 1000 K at the catalyst end due to cooling by the wall. The solid temperature matches this profile in the catalyst bed. In contrast, the solid temperature simulated by Dong et al. [1] is higher. It starts at 1400 K (y = 2 mm), increases to ca. 1450 K at the hot spot (y = 2 mm) before dropping to a value of ca. 1000 K. The additionally shown simulated fluid temperature profile of their adiabatic case study begins at a temperature level of 1250 K (y = -5 mm), similar to our assumptions. Eventually, it rises up to about 1550 K and decreases only slightly afterwards (no heat transport through the wall; only radiative heat losses through inlet and outlet). Obviously, an adiabatic assumption is not correct, because temperatures are significantly overpredicted. Therefore, Dong et al. estimated a heat loss through the wall of 20 W, which led to the shown solid temperature profile and almost matches experimental data. Their underestimation of the hot spot at the catalyst front was justified by the missing front heat shield in the simulations. We assumed their simulated fluid temperature profile to be a

combination of their solid's results and their adiabatic fluid temperature output and therefore chose the inlet fluid temperature of 1250 K.

It is evident that the experimentally measured temperature hot spot is even more underpredicted by our Kelvin cell model. In our simulations, we also neglect the heat shield, but two additional aspects probably further decrease the calculated temperatures. First of all, our Kelvin cell is characterized by significantly thicker struts, which enhances radial heat transport via conduction. Their uniform cross-sectional area supports this effect even more [5]. Secondly, the assumption of an ideally cooled wall with a fixed temperature of 1000 K further increases the heat loss through the wall. In our model, a total amount of 10.4 W is transferred through the wall of the quarter pipe. Multiplying this value by four (to account for the whole pipe) this results in 41.6 W, which is more than twice compared to the assumption in the reference study.

Despite these differences regarding the temperature, the concentration profiles match quite well with profiles from Dong et al. [1] (Figure S1b). Along the axial coordinate, CO and O_2 are consumed completely and CO_2 is formed. Up to the axial coordinate of $y \approx 2.5$ mm profiles from this work and the reference match. With increasing y, our results show periodic bulges, which underestimate the mole fraction of CO_2 and simultaneously overestimate the mole fractions of CO and O_2. At the end of the catalyst ($y = 20$ mm), at full CO conversion, the values again agree well. The bulges are very likely to be caused by the regular structure of the Kelvin cell foam. The simple assembly of these ideal cells results in a periodically changing porosity along the reactor length. Therefore, the volumetric CO conversion is periodically changing as well, leading to higher values close to struts (peaks in the plot) and lower values in the middle of a pore (bulges).

As it was already presented in the reference study, temperature variations at this high temperature level play only a minor role for the calculation of the kinetics. Therefore, our simulated differences regarding the temperature hot spot still lead to a good approximation of species' distributions. Only the reported bulge phenomenon shows significant errors compared to the reticulated foam. In summary, very similar results could be achieved with our model despite a simplified geometrical setup and approximated boundary conditions. From this, we deduce that our model generates plausible results.

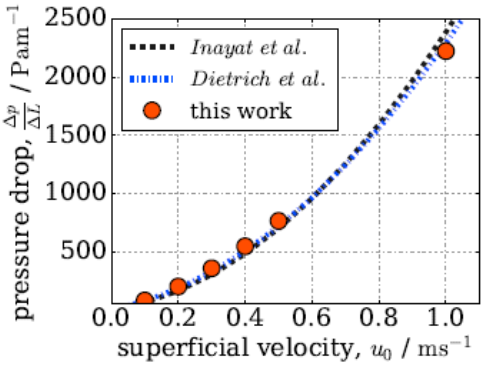

Figure S2: Pressure drop for investigated Kelvin cell foam computed through CFD simulations (this work) and calculated through correlations from literature.

In addition to the detailed comparison to the study from Dong et al. [1], we investigated the pressure drop along the reactor length under isothermal conditions (room temperature) and compared it against state-of-the-art correlations. The simulated pressure drop per length $\Delta p\ \Delta L^{-1}$ agrees well with correlations by Inayat et al. [6] and Dietrich et al. [7] for velocities between 0.1 and 0.5 m s^{-1} as well as 1 m s^{-1} (Figure S2). This further highlights the suitability of the generated Kelvin structure for open-cell foam investigations.

2. Correlations and results for Kelvin cells

The Kelvin cell is usually described by a set of four parameters: d_c, d_s, ε_o , S_V. They are not independent from each other, instead two of them are determined by the other two. Their relation two each other is expressed by geometrical correlations, which can be used to calculate the necessary cell and strut diameter for a matching open porosity and specific surface area. Three literature correlations are examined is this work.

The Kelvin cell correlation by Inayat et al. [3] is given by:

$$d_s = \frac{0.616 d_w (1-\varepsilon_o)^{0.5}}{1-0.971(1-\varepsilon_o)^{0.5}},$$

$$S_V = 4.867 \frac{[1-0.971(1-\varepsilon_o)^{0.5}]}{d_w (1-\varepsilon_o)^{0.5}} (1-\varepsilon_o)$$

The Kelvin cell correlation by Lucci et al. [2] is defined as:

$$\varepsilon_o = 1 - \frac{3\pi}{\sqrt{2}}\left(\frac{d_s}{d_c + d_s}\right)^2 + 7.54\left(\frac{d_s}{d_c + d_s}\right)^3,$$

$$S_V = 10.33\frac{\sqrt{1-\varepsilon_o}}{d_c + d_s} - 5.8\frac{1-\varepsilon_o}{d_c + d_s}$$

The Kelvin cell correlation by Ambrosetti et al. [4] is expressed by:

$$\varepsilon_o = 1 - \frac{-0.3985d_s^3 + 2.8803d_s^2 d_c + 0.2172 d_s d_c^2 + 0.00708 d_c^3}{0.419(d_c + d_s)^3},$$

$$S_V = \frac{-7.377d_s^2 + 10.082 d_s d_c + 0.3548 d_c^2}{0.419(d_c + d_s)^3}$$

The results of each correlation as well as the original parameters from the reference study are shown in Table S2. (Note: The correlation by Inayat et al. [3] uses the window diameter d_w instead of the cell diameter d_c. The given value of d_c was therefore manually calculated afterwards in the CAD file)

Table S2: Kelvin cell parameters due to different correlation results compared to the 45ppi foam from the reference study. The relative errors to the reference foam are the smallest for the correlation of Lucci et al. [2], which was therefore used in this study.

	cell diameter d_c (mm)	strut diameter ds (mm)	open porosity ε_o (-)	specific surface are S_V (m^-1)	relative error $\Delta\varepsilon_o$ (%)	relative error ΔS_V (%)
Dong et al. [1]	1.35	0.35	0.73	1512		
Inayat et al. [3]	1.694	0.536	0.713	1665.7	-2.3	10.17
Lucci et al. [2]	1.924	0.591	0.724	1467.8	-0.88	-2.92
Ambrosetti et al. [4]	1.942	0.459	0.81	1412.8	10.41	-6.56

3. Grid independence study and depiction of utilized mesh

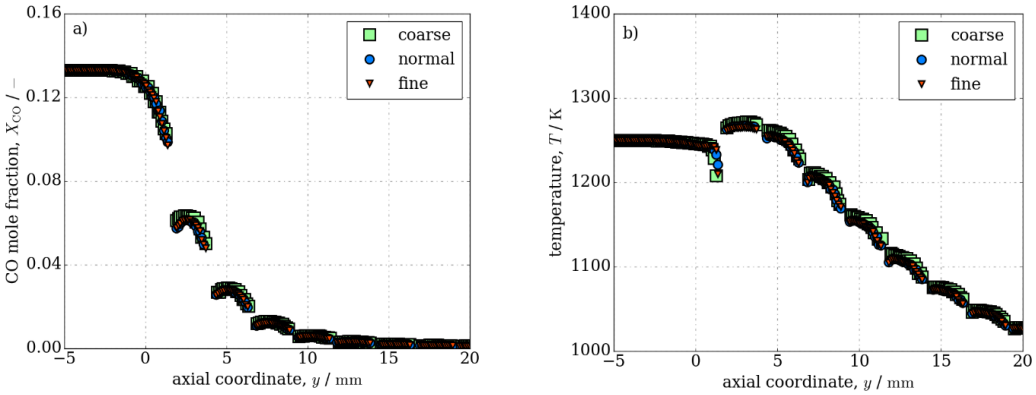

Figure S3: Grid independence study for coarse mesh (0.6 mio. cells), normal mesh (2.3 mio. cells) and fine mesh (4.8 mio. cells). a) CO concentration profile (mole fraction) along centerline. b) Temperature profile along centerline. The mid-size mesh (normal) has been found to be grid-independent and been selected for all investigations in this study.

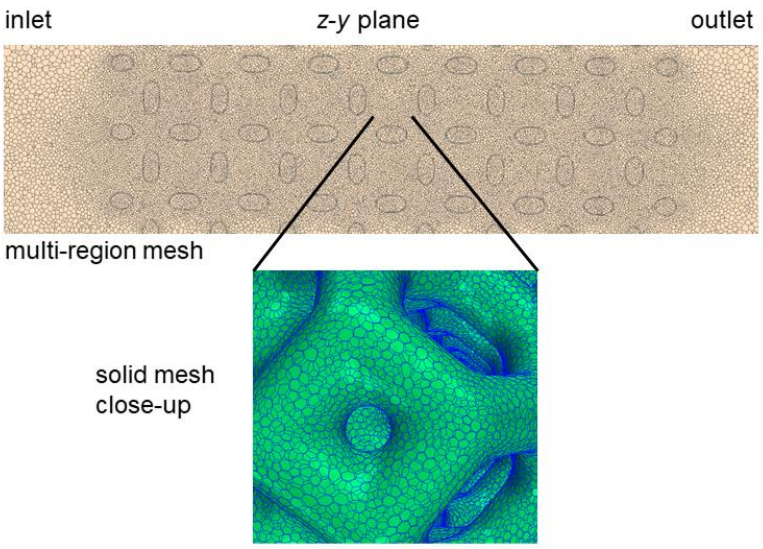

Figure S4: Depiction of the utilized mesh with 2.3 mio. polyhedral cells.

3. Influence of radiation modeling on CO oxidation

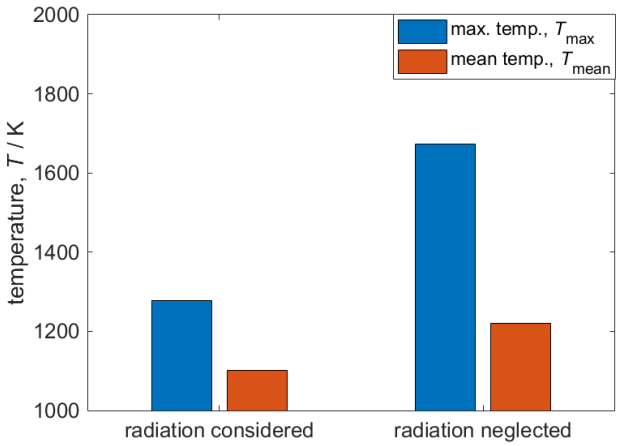

Figure S5: Influence of radiation modeling (surface-to-surface model, STAR-CCM+) on computed solid maximum and mean temperatures. Conditions: λ_s = 2 W m^{-1} K^{-1}; v = 0.5 m s^{-1}. The computed solid temperature increases significantly when radiation is neglected. Therefore, all simulations consider radiative heat transport.

List of symbols

Roman	
p	Pressure, Pa
d_w	window diameter, m
d_s	strut diameter, m
d_c	cell diameter, m
T	temperature, K
S_V	specific surface area, m^{-1}
L	foam length, m
Greek	
X_i	species mole fraction, -
ε_o	open porosity, -

References

1. Dong, Y., Korup, O., Gerdts, J., Roldán Cuenya, B. & Horn, R. Microtomography-based CFD modeling of a fixed-bed reactor with an open-cell foam monolith and experimental verification by reactor profile measurements. *Chem. Eng. J.* **353**, 176–188 (2018).
2. Lucci, F. *et al.* Performance of randomized Kelvin cell structures as catalytic substrates: Mass-transfer based analysis. *Chem. Eng. Sci.* **112**, 143–151 (2014).
3. Inayat, A., Freund, H., Zeiser, T. & Schwieger, W. Determining the specific surface area of ceramic foams: The tetrakaidecahedra model revisited. *Chem. Eng. Sci.* **66**, 1179–1188 (2011).
4. Ambrosetti, M., Bracconi, M., Groppi, G. & Tronconi, E. Analytical Geometrical Model of Open Cell Foams with Detailed Description of Strut-Node Intersection. *Chemie-Ingenieur-Technik* **89**, 915–925 (2017).
5. Bracconi, M., Ambrosetti, M., Maestri, M., Groppi, G. & Tronconi, E. A fundamental analysis of the influence of the geometrical properties on the effective thermal conductivity of open-cell foams. *Chem. Eng. Process. - Process Intensif.* **129**, 181–189 (2018).
6. Inayat, A., Klumpp, M., Lämmermann, M., Freund, H. & Schwieger, W. Development of a new pressure drop correlation for open-cell foams based completely on theoretical grounds: Taking into account strut shape and geometric tortuosity. *Chem. Eng. J.* **287**, 704–719 (2016).
7. Dietrich, B. Pressure drop correlation for ceramic and metal sponges. *Chem. Eng. Sci.* **74**, 192–199 (2012).

Bibliography

Aguirre, A. et al. (2020). "Open-cell foams as catalysts support: A systematic analysis of the mass transfer limitations". In: *Chemical Engineering Journal* 393, p. 124656. DOI: 10.1016/j.cej.2020.124656.

Ambrosetti, Matteo et al. (2020a). "Packed foams for the intensification of catalytic processes: assessment of packing efficiency and pressure drop using a combined experimental and numerical approach". In: *Chemical Engineering Journal* 382, p. 122801. DOI: 10.1016/j.cej.2019.122801.

Ambrosetti, Matteo et al. (2020b). "Packed Periodic Open Cellular Structures – an Option for the Intensification of Non-Adiabatic Catalytic Processes". In: *Chemical Engineering and Processing - Process Intensification* 155. DOI: 10.1016/j.cep.2020.108057.

Ambrosio, Giuseppe et al. (2016). "The effect of open-cell metal foams strut shape on convection heat transfer and pressure drop". In: *Applied Thermal Engineering* 103, pp. 333–343. DOI: 10.1016/j.applthermaleng.2016.04.085.

Bai, Mo and J. N. Chung (2011). "Analytical and numerical prediction of heat transfer and pressure drop in open-cell metal foams". In: *International Journal of Thermal Sciences* 50.6, pp. 869–880. DOI: 10.1016/j.ijthermalsci.2011.01.007.

Balzarotti, Riccardo et al. (2020). "Investigation of packed conductive foams as a novel reactor configuration for methane steam reforming". In: *Chemical Engineering Journal* 391, p. 123494. DOI: 10.1016/j.cej.2019.123494.

Balzarotti, Riccardo et al. (2021). "Periodic open cellular structures (POCS) as enhanced catalyst supports: Optimization of the coating procedure and analysis of mass transport". In: *Applied Catalysis B: Environmental* 283, p. 119651. DOI: 10.1016/j.apcatb.2020.119651.

Bastos Rebelo, Núria F. et al. (2018). "Pressure drop and heat transfer properties of cubic iso-reticular foams". In: *Chemical Engineering and Processing - Process Intensification* 127, pp. 36–42. DOI: 10.1016/j.cep.2018.03.008.

Belimov, Michael, David Metzger, and Peter Pfeifer (2017). "On the temperature control in a microstructured packed bed reactor for methanation of CO/CO2 mixtures". In: *AIChE Journal* 63.1, pp. 120–129. DOI: 10.1002/aic.15461.

Benzinger, Walther et al. (2019). "Reverse water gas shift (RWGS) over Ni – Spatially-resolved measurements and simulations". In: *Chemical Engineering Journal* 362, pp. 430–441. DOI: 10.1016/j.cej.2019.01.038.

Bianchi, Enrico, Wilhelm Schwieger, and Hannsjörg Freund (2016). "Assessment of Periodic Open Cellular Structures for Enhanced Heat Conduction in Catalytic Fixed-Bed Reactors". In: *Advanced Engineering Materials* 18.4, pp. 608–614. DOI: 10.1002/adem.201500356.

Bianchi, Enrico et al. (2012). "An appraisal of the heat transfer properties of metallic open-cell foams for strongly exo-/endo-thermic catalytic processes in tubular reactors". In: *Chemical Engineering Journal* 198-199, pp. 512–528. DOI: 10.1016/j.cej.2012.05.045.

Bianchi, Enrico et al. (2013). "Heat transfer properties of metal foam supports for structured catalysts: Wall heat transfer coefficient". In: *Catalysis Today*. Vol. 216. Elsevier, pp. 121–134. DOI: 10.1016/j.cattod.2013.06.019.

Bianchi, Enrico et al. (2015). "Numerical simulation of heat transfer in the near-wall region of tubular reactors packed with metal open-cell foams". In: *Chemical Engineering Journal* 264, pp. 268–279. DOI: 10.1016/j.cej.2014.11.055.

Boomsma, K., D. Poulikakos, and Y. Ventikos (2003). "Simulations of flow through open cell metal foams using an idealized periodic cell structure". In: *International Journal of Heat and Fluid Flow* 24.6, pp. 825–834. DOI: 10.1016/j.ijheatfluidflow.2003.08.002.

Bracconi, Mauro et al. (2017). "A systematic procedure for the virtual reconstruction of open-cell foams". In: *Chemical Engineering Journal* 315, pp. 608–620. DOI: 10.1016/j.cej.2017.01.069.

— (2018a). "A fundamental analysis of the influence of the geometrical properties on the effective thermal conductivity of open-cell foams". In: *Chemical Engineering and Processing - Process Intensification* 129, pp. 181–189. DOI: 10.1016/j.cep.2018.04.018.

— (2018b). "A fundamental investigation of gas/solid mass transfer in open-cell foams using a combined experimental and CFD approach". In: *Chemical Engineering Journal* 352, pp. 558–571. DOI: 10.1016/j.cej.2018.07.023.

Bracconi, Mauro et al. (2019). "Investigation of pressure drop in 3D replicated open-cell foams: Coupling CFD with experimental data on additively manufactured foams". In: *Chemical Engineering Journal* 377, p. 120123. DOI: 10.1016/j.cej.2018.10.060.

Bracconi, Mauro et al. (2020). "Analysis of the effective thermal conductivity of isotropic and anisotropic Periodic Open Cellular Structures for the intensification of catalytic processes". In: *Chemical Engineering and Processing - Process Intensification*, p. 108169. DOI: 10.1016/j.cep.2020.108169.

Busse, Corinna, Hannsjörg Freund, and Wilhelm Schwieger (2018). "Intensification of heat transfer in catalytic reactors by additively manufactured periodic open cellular structures (POCS)". In: *Chemical Engineering and Processing: Process Intensification* 124, pp. 199–214. DOI: 10.1016/j.cep.2018.01.023.

Chen, Xue et al. (2015). "Thermal performance analysis on a volumetric solar receiver with double-layer ceramic foam". In: *Energy Conversion and Management* 97, pp. 282–289. DOI: 10.1016/j.enconman.2015.03.066.

Clarke, D.A. et al. (2020). "Investigation of flow through triply periodic minimal surface-structured porous media using MRI and CFD". In: *Chemical Engineering Science*, p. 116264. DOI: 10.1016/j.ces.2020.116264.

Dalle Nogare, D. et al. (2008). "Modeling spatially resolved profiles of methane partial oxidation on a Rh foam catalyst with detailed chemistry". In: *Journal of Catalysis* 258.1, pp. 131–142. DOI: 10.1016/j.jcat.2008.06.006.

Danaci, Simge et al. (2016). "Efficient CO2 methanation over Ni/Al2O3 coated structured catalysts". In: *Catalysis Today* 273, pp. 234–243. DOI: 10.1016/j.cattod.2016.04.019.

Danaci, Simge et al. (2018). "Innovative 3D-manufacture of structured copper supports post-coated with catalytic material for CO2 methanation". In: *Chemical Engineering and Processing - Process Intensification* 127, pp. 168–177. DOI: 10.1016/j.cep.2018.03.023.

Danaci, Simge et al. (2019). "Scaling up of 3D printed and Ni/Al2O3 coated reactors for CO2 methanation". In: *Reaction Chemistry and Engineering* 4.7, pp. 1318–1330. DOI: 10.1039/c9re00092e.

Das, Saurish, Niels G. Deen, and J. A.M. Kuipers (2016). "Direct numerical simulation for flow and heat transfer through random open-cell solid foams: Development of an IBM based CFD model". In: *Catalysis Today* 273, pp. 140–150. DOI: 10.1016/j.cattod.2016.03.048.

Daymo, Eric et al. (2019). "Accelerating reactor development with accessible simulation and automated optimization tools". In: *Chemical Engineering and Processing - Process Intensification* 142, p. 107582. DOI: 10.1016/j.cep.2019.107582.

Della Torre, A. et al. (2014). "CFD characterization of flow regimes inside open cell foam substrates". In: *International Journal of Heat and Fluid Flow* 50, pp. 72–82. DOI: 10.1016/j.ijheatfluidflow.2014.05.005.

Della Torre, A. et al. (2015). "CFD characterization of pressure drop and heat transfer inside porous substrates". In: *Energy Procedia*. Vol. 81. Elsevier, pp. 836–845. DOI: 10.1016/j.egypro.2015.12.093.

Della Torre, A. et al. (2016). "CFD modeling of catalytic reactions in open-cell foam substrates". In: *Computers and Chemical Engineering* 92, pp. 55–63. DOI: 10.1016/j.compchemeng.2016.04.031.

Deutschmann, O. et al. (1996). "Numerical modeling of catalytic ignition". In: *Symposium (International) on Combustion* 26.1, pp. 1747–1754. DOI: 10.1016/S0082-0784(96)80400-0.

Deutschmann, Olaf (2015). "Modeling of the Interactions Between Catalytic Surfaces and Gas-Phase". In: *Catalysis Letters* 145.1, pp. 272–289. DOI: 10.1007/s10562-014-1431-1.

Diani, Andrea et al. (2014). "Numerical analysis of air flow through metal foams". In: *Energy Procedia*. Vol. 45. Elsevier, pp. 645–652. DOI: 10.1016/j.egypro.2014.01.069.

Diani, Andrea et al. (2015). "Numerical investigation of pressure drop and heat transfer through reconstructed metal foams and comparison against experiments". In: *International Journal of Heat and Mass Transfer* 88, pp. 508–515. DOI: 10.1016/j.ijheatmasstransfer.2015.04.038.

Dietrich, B. (2013). "Heat transfer coefficients for solid ceramic sponges – Experimental results and correlation". In: *International Journal of Heat and Mass Transfer* 61, pp. 627–637. DOI: 10.1016/j.ijheatmasstransfer.2013.02.019.

Dietrich, Benjamin (2012). "Pressure drop correlation for ceramic and metal sponges". In: *Chemical Engineering Science* 74, pp. 192–199. DOI: 10.1016/j.ces.2012.02.047.

Dietrich, Benjamin et al. (2009). "Pressure drop measurements of ceramic sponges-Determining the hydraulic diameter". In: *Chemical Engineering Science* 64.16, pp. 3633–3640. DOI: 10.1016/j.ces.2009.05.005.

Dixon, Anthony G. and Behnam Partopour (2020). "Computational Fluid Dynamics for Fixed Bed Reactor Design". In: *Annual Review of Chemical and Biomolecular Engineering* 11.1. DOI: 10.1146/annurev-chembioeng-092319-075328.

Dong, Ying et al. (2018). "Microtomography-based CFD modeling of a fixed-bed reactor with an open-cell foam monolith and experimental verification by reactor profile measurements". In: *Chemical Engineering Journal* 353, pp. 176–188. DOI: 10.1016/j.cej.2018.07.075.

Dou, Liguang et al. (2019). "Enhancing CO2 methanation over a metal foam structured catalyst by electric internal heating". In: *Chemical Communications* 56.2, pp. 205–208. DOI: 10.1039/c9cc07525a.

Du, Shen et al. (2019). "Tomography-based determination of Nusselt number correlation for the porous volumetric solar receiver with different geometrical parameters". In: *Renewable Energy* 135, pp. 711–718. DOI: 10.1016/j.renene.2018.12.001.

Edouard, David et al. (2008). "Pressure drop modeling on SOLID foam: State-of-the art correlation". In: *Chemical Engineering Journal* 144.2, pp. 299–311. DOI: 10.1016/j.cej.2008.06.007.

Egana, Ane et al. (2018). "Fischer-Tropsch Synthesis Intensification in Foam Structures". In: *Industrial and Engineering Chemistry Research* 57.31, pp. 10187–10197. DOI: 10.1021/acs.iecr.8b01492.

Ercolino, Giuliana, Paweł Stelmachowski, and Stefania Specchia (2017). "Catalytic Performance of Pd/Co3O4 on SiC and ZrO2 Open Cell Foams for Process Intensification of Methane Combustion in Lean Conditions". In: *Industrial and Engineering Chemistry Research* 56.23, pp. 6625–6636. DOI: 10.1021/acs.iecr.7b01087.

Fan, Xiaolei et al. (2016). "Microtomography-based numerical simulations of heat transfer and fluid flow through β-SiC open-cell foams for catalysis". In: *Catalysis Today* 278, pp. 350–360. DOI: 10.1016/j.cattod.2015.12.012.

Fernengel, Johanna, Leslie Bolton, and Olaf Hinrichsen (2019). "Characterisation and design of single pellet string reactors using numerical simulation". In: *Chemical Engineering Journal* 373, pp. 1397–1408. DOI: 10.1016/j.cej.2019.03.114.

Fischedick, T., M. Kind, and B. Dietrich (2015). "High temperature two-phase thermal conductivity of ceramic sponges with stagnant fluid - Experimental results and correlation including thermal radiation". In: *International Journal of Thermal Sciences* 96, pp. 1–11. DOI: 10.1016/j.ijthermalsci.2015.04.005.

— (2017). "Radial two-phase thermal conductivity of ceramic sponges up to high temperatures – experimental results and correlation". In: *International Journal of Thermal Sciences* 114, pp. 98–113. DOI: 10.1016/j.ijthermalsci.2016.11.020.

Fratalocchi, Laura et al. (2018). "Intensifying heat transfer in Fischer-Tropsch tubular reactors through the adoption of conductive packed foams". In: *Chemical Engineering Journal* 349, pp. 829–837. DOI: 10.1016/j.cej.2018.05.108.

Fratalocchi, Laura et al. (2020). "Adoption of 3D printed highly conductive periodic open cellular structures as an effective solution to enhance the heat transfer performances of compact Fischer-Tropsch fixed-bed reactors". In: *Chemical Engineering Journal* 386. DOI: 10.1016/j.cej.2019.123988.

— (2021). "Packed-POCS with skin: a novel concept for the intensification of non-adiabatic catalytic processes demonstrated in the case of the Fischer-Tropsch synthesis". In: *Catalysis Today*. DOI: 10.1016/j.cattod.2020.12.031.

Frey, Myriam et al. (2017). "Aluminum Open Cell Foams as Efficient Supports for Carbon Dioxide Methanation Catalysts: Pilot-Scale Reaction Results". In: *Energy Technology* 5.11, pp. 2078–2085. DOI: 10.1002/ente.201700188.

Gancarczyk, Anna et al. (2018). "Interfacial heat and momentum transfer relation for porous media". In: *International Journal of Thermal Sciences* 132, pp. 42–51. DOI: 10.1016/j.ijthermalsci.2018.04.028.

Gao, H. B. et al. (2014). "Methane/air premixed combustion in a two-layer porous burner with different foam materials". In: *Fuel* 115, pp. 154–161. DOI: 10.1016/j.fuel.2013.06.023.

Giani, Leonardo, Gianpiero Groppi, and Enrico Tronconi (2005a). "Heat transfer characterization of metallic foams". In: *Industrial and Engineering Chemistry Research* 44.24, pp. 9078–9085. DOI: 10.1021/ie050598p.

— (2005b). "Mass-transfer characterization of metallic foams as supports for structured catalysts". In: *Industrial and Engineering Chemistry Research* 44.14, pp. 4993–5002. DOI: 10.1021/ie0490886.

Gräf, Ingo, Georg Ladenburger, and Bettina Kraushaar-Czarnetzki (2016). "Heat transport in catalytic sponge packings in the presence of an exothermal reaction: Characterization by 2D modeling of experiments". In: *Chemical Engineering Journal* 287, pp. 425–435. DOI: 10.1016/j.cej.2015.11.042.

Gräf, Ingo, Anne Kathrin Rühl, and Bettina Kraushaar-Czarnetzki (2014). "Experimental study of heat transport in catalytic sponge packings by monitoring spatial temperature profiles in a cooled-wall reactor". In: *Chemical Engineering Journal* 244, pp. 234–242. DOI: 10.1016/j.cej.2014.01.060.

Groppi, Gianpiero et al. (2012). "Conductive monolithic catalysts: Development and industrial pilot tests for the oxidation of o-xylene to phthalic anhydride". In: *Industrial and Engineering Chemistry Research* 51.22, pp. 7590–7596. DOI: 10.1021/ie2021653.

Habibi, A., B. Merci, and G. J. Heynderickx (2007). "Impact of radiation models in CFD simulations of steam cracking furnaces". In: *Computers and Chemical Engineering* 31.11, pp. 1389–1406. DOI: 10.1016/j.compchemeng.2006.11.009.

Habisreuther, P., N. Djordjevic, and N. Zarzalis (2009). "Statistical distribution of residence time and tortuosity of flow through open-cell foams". In: *Chemical Engineering Science* 64.23, pp. 4943–4954. DOI: 10.1016/j.ces.2009.07.033.

Hettel, Matthias, Eric Daymo, and Olaf Deutschmann (2018). "3D modeling of a CPOX-reformer including detailed chemistry and radiation effects with DUO". In: *Computers and Chemical Engineering* 109, pp. 166–178. DOI: 10.1016/j.compchemeng.2017.11.005.

Ho, Phuoc Hoang et al. (2020). "Open-cell foams coated by Ni/X/Al hydrotalcite-type derived catalysts (X = Ce, La, Y) for CO2 methanation". In: *Journal of CO2 Utilization* 42, p. 101327. DOI: 10.1016/j.jcou.2020.101327.

Horn, R. et al. (2006). "Syngas by catalytic partial oxidation of methane on rhodium: Mechanistic conclusions from spatially resolved measurements and numerical simulations". In: *Journal of Catalysis* 242.1, pp. 92–102. DOI: 10.1016/j.jcat.2006.05.008.

Horneber, T., C. Rauh, and A. Delgado (2012). "Fluid dynamic characterisation of porous solids in catalytic fixed-bed reactors". In: *Microporous and Mesoporous Materials* 154, pp. 170–174. DOI: 10.1016/j.micromeso.2011.12.047.

— (2014). "Numerical simulations of fluid dynamics in carrier structures for catalysis: Characterization and need for optimization". In: *Chemical Engineering Science* 117, pp. 229–238. DOI: 10.1016/j.ces.2014.06.036.

Hutter, C. et al. (2011). "Large eddy simulation of flow through a streamwise-periodic structure". In: *Chemical Engineering Science* 66.3, pp. 519–529. DOI: 10.1016/j.ces.2010.11.015.

Iasiello, M. et al. (2017). "Developing thermal flow in open-cell foams". In: *International Journal of Thermal Sciences* 111, pp. 129–137. DOI: 10.1016/j.ijthermalsci.2016.08.013.

Iasiello, Marcello et al. (2014). "Numerical analysis of heat transfer and pressure drop in metal foams for different morphological models". In: *Journal of Heat Transfer* 136.11. DOI: 10.1115/1.4028113.

Iasiello, Marcello et al. (2020). "Anisotropic convective heat transfer in open-cell metal foams: Assessment and correlations". In: *International Journal of Heat and Mass Transfer* 154, p. 119682. DOI: 10.1016/j.ijheatmasstransfer.2020.119682.

Inayat, Amer et al. (2011). "Determining the specific surface area of ceramic foams: The tetrakaidecahedra model revisited". In: *Chemical Engineering Science* 66.6, pp. 1179–1188. DOI: 10.1016/j.ces.2010.12.031.

Inayat, Amer et al. (2016). "Development of a new pressure drop correlation for open-cell foams based completely on theoretical grounds: Taking into account strut shape and geometric tortuosity". In: *Chemical Engineering Journal* 287, pp. 704–719. DOI: 10.1016/j.cej.2015.11.050.

Incera Garrido, G. and B. Kraushaar-Czarnetzki (2010). "A general correlation for mass transfer in isotropic and anisotropic solid foams". In: *Chemical Engineering Science* 65.6, pp. 2255–2257. DOI: 10.1016/j.ces.2009.12.016.

Incera Garrido, G et al. (2008). "Mass transfer and pressure drop in ceramic foams: A description for different pore sizes and porosities". In: *Chemical Engineering Science* 63.21, pp. 5202–5217. DOI: 10.1016/j.ces.2008.06.015.

Innocentini, Murilo D.M. et al. (1999). "Prediction of ceramic foams permeability using Ergun's equation". In: *Materials Research* 2.4, pp. 283–289. DOI: 10.1590/S1516-14391999000400008.

Iulianelli, Adolfo et al. (2016). "Advances on methane steam reforming to produce hydrogen through membrane reactors technology: A review". In: *Catalysis Reviews - Science and Engineering* 58.1, pp. 1–35. DOI: 10.1080/01614940.2015.1099882.

Jackson, R. B. et al. (2017). "Warning signs for stabilizing global CO2 emissions". In: *Environmental Research Letters* 12.11, p. 110202. DOI: 10.1088/1748-9326/aa9662.

Jang, Won Jun et al. (2019). "A review on dry reforming of methane in aspect of catalytic properties". In: *Catalysis Today* 324, pp. 15–26. DOI: 10.1016/j.cattod.2018.07.032.

Jurtz, Nico, Matthias Kraume, and Gregor D. Wehinger (2019). "Advances in fixed-bed reactor modeling using particle-resolved computational fluid dynamics (CFD)". In: *Reviews in Chemical Engineering* 35.2, pp. 139–190. DOI: 10.1515/revce-2017-0059.

Kalz, Kai F. et al. (2017). "Future Challenges in Heterogeneous Catalysis: Understanding Catalysts under Dynamic Reaction Conditions". In: *ChemCatChem* 9.1, pp. 17–29. DOI: 10.1002/cctc.201600996.

Kapteijn, Freek and Jacob A. Moulijn (2020). "Structured Catalysts and Reactors – Perspectives for demanding applications". In: *Catalysis Today*. DOI: 10.1016/j.cattod.2020.09.026.

Kiewidt, Lars (2017). "Solid sponges as support for heterogenous catalyst in gas phase reactions". PhD thesis. Universität Bremen.

Kiewidt, Lars and Jorg Thöming (2015). "Predicting optimal temperature profiles in single-stage fixed-bed reactors for CO2-methanation". In: *Chemical Engineering Science* 132, pp. 59–71. DOI: 10.1016/j.ces.2015.03.068.

— (2019a). "Multiscale modelling of monolithic sponges as catalyst carrier for the methanation of carbon dioxide". In: *Chemical Engineering Science: X* 2, p. 100016. DOI: 10.1016/j.cesx.2019.100016.

— (2019b). "Pareto-optimal design and assessment of monolithic sponges as catalyst carriers for exothermic reactions". In: *Chemical Engineering Journal* 359, pp. 496–504. DOI: 10.1016/j.cej.2018.11.109.

Kopanidis, A. et al. (2010). "3D numerical simulation of flow and conjugate heat transfer through a pore scale model of high porosity open cell metal foam". In: *International Journal of Heat and Mass Transfer* 53.11-12, pp. 2539–2550. DOI: 10.1016/j.ijheatmasstransfer.2009.12.067.

Kreitz, Bjarne, Gregor D. Wehinger, and Thomas Turek (2019). "Dynamic simulation of the CO2 methanation in a micro-structured fixed-bed reactor". In: *Chemical Engineering Science* 195, pp. 541–552. DOI: 10.1016/j.ces.2018.09.053.

Kumar, Prashant and Frédéric Topin (2017). "Predicting pressure drop in open-cell foams by adopting Forchheimer number". In: *International Journal of Multiphase Flow* 94, pp. 123–136. DOI: 10.1016/j.ijmultiphaseflow.2017.04.010.

Lacroix, Maxime et al. (2007). "Pressure drop measurements and modeling on SiC foams". In: *Chemical Engineering Science* 62.12, pp. 3259–3267. DOI: 10.1016/j.ces.2007.03.027.

Lefebvre, Jonathan et al. (2015). "Improvement of three-phase methanation reactor performance for steady-state and transient operation". In: *Fuel Processing Technology* 132, pp. 83–90. DOI: 10.1016/j.fuproc.2014.10.040.

Li, Yunhua et al. (2018). "Rational design and preparation of hierarchical monoliths through 3D printing for syngas methanation". In: *Journal of Materials Chemistry A* 6.14, pp. 5695–5702. DOI: 10.1039/c8ta01597j.

Lind, Anna et al. (2020). "Multi-purpose structured catalysts designed and manufactured by 3D printing". In: *Materials and Design* 187, p. 108377. DOI: 10.1016/j.matdes.2019.108377.

Lorenz, Malte et al. (2020). "High-throughput dielectrophoretic filtration of submicron and micro particles in macroscopic porous materials". In: *Analytical and Bioanalytical Chemistry* 412.16, pp. 3903–3914. DOI: 10.1007/s00216-020-02557-0.

Lu, Hongyan et al. (2020). "Numerical and experimental study on convective heat transfer characteristics in foam materials". In: *Energies* 13.2, p. 348. DOI: 10.3390/en13020348.

Lucci, Francesco et al. (2014). "Performance of randomized Kelvin cell structures as catalytic substrates: Mass-transfer based analysis". In: *Chemical Engineering Science* 112, pp. 143–151. DOI: 10.1016/j.ces.2014.03.023.

Lucci, Francesco et al. (2015). "On the catalytic performance of open cell structures versus honeycombs". In: *Chemical Engineering Journal* 264, pp. 514–521. DOI: 10.1016/j.cej.2014.11.080.

Lucci, Francesco et al. (2017). "Comparison of geometrical, momentum and mass transfer characteristics of real foams to Kelvin cell lattices for catalyst applications". In: *International Journal of Heat and Mass Transfer* 108, pp. 341–350. DOI: 10.1016/j.ijheatmasstransfer.2016.11.073.

Meinicke, Sebastian, Thomas Wetzel, and Benjamin Dietrich (2017). "Scale-resolved CFD modelling of single-phase hydrodynamics and conjugate heat transfer in solid sponges". In: *International Journal of Heat and Mass Transfer* 108, pp. 1207–1219. DOI: 10.1016/j.ijheatmasstransfer.2016.12.052.

Meinicke, Sebastian et al. (2017). "Experimental and numerical investigation of single-phase hydrodynamics in glass sponges by means of combined µPIV measurements and CFD simulation". In: *Chemical Engineering Science* 160, pp. 131–143. DOI: 10.1016/j.ces.2016.11.027.

Meinicke, Sebastian et al. (2020). "Characterization of heat transfer in consolidated, highly porous media using a hybrid-scale CFD approach". In: *International Journal of Heat and Mass Transfer* 149, p. 119201. DOI: 10.1016/j.ijheatmasstransfer.2019.119201.

Mey-Cloutier, S. et al. (2016). "Experimental study of ceramic foams used as high temperature volumetric solar absorber". In: *Solar Energy* 136, pp. 226–235. DOI: 10.1016/j.solener.2016.06.066.

Modest, Michael F. (2013). *Radiative Heat Transfer*. 3rd ed. New York, NY : Academic Press. DOI: 10.1016/C2010-0-65874-3.

Montenegro Camacho, Y. S. et al. (2018). "Development of a robust and efficient biogas processor for hydrogen production. Part 2: Experimental campaign". In: *International Journal of Hydrogen Energy* 43.1, pp. 161–177. DOI: 10.1016/j.ijhydene.2017.10.177.

Moreira, E A, M. D.M. Innocentini, and J R Coury (2004). "Permeability of ceramic foams to compressible and incompressible flow". In: *Journal of the European Ceramic Society* 24.10-11, pp. 3209–3218. DOI: 10.1016/j.jeurceramsoc.2003.11.014.

Mutschler, Robin et al. (2020). "Imaging Catalysis: Operando Investigation of the CO2 Hydrogenation Reaction Dynamics by Means of Infrared Thermography". In: *ACS Catalysis* 10.3, pp. 1721–1730. DOI: 10.1021/acscatal.9b04475.

Navarro, Juan C. et al. (2018). "Policies and motivations for the CO2 valorization through the sabatier reaction using structured catalysts. A review of the most recent advances". In: *Catalysts* 8.12, p. 578. DOI: 10.3390/catal8120578.

Nie, Zhengwei, Yuyi Lin, and Qingbin Tong (2017). "Modeling structures of open cell foams". In: *Computational Materials Science* 131, pp. 160–169. DOI: 10.1016/j.commatsci.2017.01.029.

Parra-Cabrera, Cesar et al. (2018). "3D printing in chemical engineering and catalytic technology: Structured catalysts, mixers and reactors". In: *Chemical Society Reviews* 47.1, pp. 209–230. DOI: 10.1039/c7cs00631d.

Parthasarathy, P., P. Habisreuther, and N. Zarzalis (2013). "Evaluation of longitudinal dispersion coefficient in open-cell foams using transient direct pore level simulation". In: *Chemical Engineering Science* 90, pp. 242–249. DOI: 10.1016/j.ces.2012.12.041.

Patcas, Florina Corina, Gerardo Incera Garrido, and Bettina Kraushaar-Czarnetzki (2007). "CO oxidation over structured carriers: A comparison of ceramic foams, honeycombs and beads". In: *Chemical Engineering Science* 62.15, pp. 3984–3990. DOI: 10.1016/j.ces.2007.04.039.

Pedras, Marcos H.J. and Marcelo J.S. De Lemos (2001). "Macroscopic turbulence modeling for incompressible flow through undefromable porous media". In: *International Journal of Heat and Mass Transfer* 44.6, pp. 1081–1093. DOI: 10.1016/S0017-9310(00)00202-7.

Peng, Wenping et al. (2017). "CFD study on thermal transport in open-cell metal foams with and without a washcoat: Effective thermal conductivity and gas-solid interfacial heat transfer". In: *Chemical Engineering Science* 161, pp. 92–108. DOI: 10.1016/j.ces.2016.12.006.

PLM, Siemens (2021). *STAR-CCM+, https://www.plm.automation.siemens.com*.

Poling, B. E., J. M. Prausnitz, and J. P. O'Connell (2001). *The properties of gases and liquids*. 5. ed. int. New York, NY: McGraw-Hill international editions, Chemical engineering series.

Ranut, Paola (2016). "On the effective thermal conductivity of aluminum metal foams: Review and improvement of the available empirical and analytical models". In: *Applied Thermal Engineering* 101, pp. 496–524. DOI: 10.1016/j.applthermaleng.2015.09.094.

Ranut, Paola, Enrico Nobile, and Lucia Mancini (2014). "High resolution microtomography-based CFD simulation of flow and heat transfer in aluminum metal foams". In: *Applied Thermal Engineering* 69.1-2, pp. 230–240. DOI: 10.1016/j.applthermaleng.2013.11.056.

— (2015). "High resolution X-ray microtomography-based CFD simulation for the characterization of flow permeability and effective thermal conductivity of aluminum metal foams". In: *Experimental Thermal and Fluid Science* 67, pp. 30–36. DOI: 10.1016/j.expthermflusci.2014.10.018.

Razza, S. et al. (2016). "Heat transfer performance of structured catalytic reactors packed with metal foam supports: Influence of wall coupling". In: *Catalysis Today* 273, pp. 187–195. DOI: 10.1016/j.cattod.2016.02.058.

Regulski, W et al. (2015). "Pressure drop in flow across ceramic foams-A numerical and experimental study". In: *Chemical Engineering Science* 137, pp. 320–337. DOI: 10.1016/j.ces.2015.06.043.

Reitzmann, Andreas, Florina Corina Patcas, and Bettina Kraushaar-Czarnetzki (2006). "Keramische schwämme - Anwendungspotenzial monolithischer netzstrukturen als katalytische packungen". In: *Chemie-Ingenieur-Technik* 78.7, pp. 885–898. DOI: 10.1002/cite.200600029.

Rezaei, Ehsan et al. (2020). "Pressure Drop and Convective Heat Transfer in Different SiSiC Structures Fabricated by Indirect Additive Manufacturing". In: *Journal of Heat Transfer* 142.3. DOI: 10.1115/1.4045732.

Rickenbach, Jan von et al. (2015). "Effect of washcoat diffusion resistance in foam based catalytic reactors". In: *Chemical Engineering Journal* 276, pp. 388–397. DOI: 10.1016/j.cej.2015.03.132.

Robinius, Martin et al. (2017). "Linking the power and transport sectors - Part 1: The principle of sector coupling". In: *Energies* 10.7, p. 956. DOI: 10.3390/en10070956.

Rönsch, Stefan et al. (2016). "Review on methanation - From fundamentals to current projects". In: *Fuel* 166, pp. 276–296. DOI: 10.1016/j.fuel.2015.10.111. arXiv: NIHMS150003.

Sadeghi, Mehrdad et al. (2020). "Full-field analysis of gas flow within open-cell foams: comparison of micro-computed tomography-based CFD simulations with experimental magnetic resonance flow mapping data". In: *Experiments in Fluids* 61.5, p. 124. DOI: 10.1007/s00348-020-02960-4.

Sahebdelfar, Saeed and Maryam Takht Ravanchi (2015). "Carbon dioxide utilization for methane production: A thermodynamic analysis". In: *Journal of Petroleum Science and Engineering* 134, pp. 14–22. DOI: 10.1016/j.petrol.2015.07.015.

Santoro, Mariarita et al. (2020). "Nickel-based structured catalysts for indirect internal reforming of methane". In: *Applied Sciences (Switzerland)* 10.9, p. 3083. DOI: 10.3390/app10093083.

Saw, Lip Huat et al. (2017). "Computational fluid dynamics simulation on open cell aluminium foams for Li-ion battery cooling system". In: *Applied Energy* 204, pp. 1489–1499. DOI: 10.1016/j.apenergy.2017.04.022.

Schnuelle, Christian et al. (2019). "Socio-technical-economic assessment of power-to-X: Potentials and limitations for an integration into the German energy system". In: *Energy Research and Social Science* 51, pp. 187–197. DOI: 10.1016/j.erss.2019.01.017.

Schwiedernoch, Renate et al. (2003). "Experimental and numerical study on the transient behavior of partial oxidation of methane in a catalytic monolith". In: *Chemical Engineering Science* 58.3-6, pp. 633–642. DOI: 10.1016/S0009-2509(02)00589-4.

Schwieger, Wilhelm et al. (2016). "Hierarchy concepts: Classification and preparation strategies for zeolite containing materials with hierarchical porosity". In: *Chemical Society Reviews* 45.12, pp. 3353–3376. DOI: 10.1039/c5cs00599j.

Semieniuk, Gregor et al. (2021). "Plausible energy demand patterns in a growing global economy with climate policy". In: *Nature Climate Change*. DOI: 10.1038/s41558-020-00975-7.

Shams, A. et al. (2015). "Numerical simulation of nuclear pebble bed configurations". In: *Nuclear Engineering and Design* 290, pp. 51–64. DOI: 10.1016/j.nucengdes.2014.11.002.

Sheng, Min et al. (2011). "Novel catalyst structures with enhanced heat transfer characteristics". In: *Journal of Catalysis* 281.2, pp. 254–262. DOI: 10.1016/j.jcat.2011.05.006.

Sinn, Christoph et al. (2019). "Coupled conjugate heat transfer and heat production in open-cell ceramic foams investigated using CFD". In: *International Journal of Heat and Mass Transfer* 139, pp. 600–612. DOI: 10.1016/j.ijheatmasstransfer.2019.05.042.

Sinn, Christoph et al. (2020a). "CFD Simulations of Radiative Heat Transport in Open-Cell Foam Catalytic Reactors". In: *Catalysts* 10.6, p. 716. DOI: 10.3390/catal10060716.

Sinn, Christoph et al. (2020b). "Influence of Pressure, Velocity and Fluid Material on Heat Transport in Structured Open-Cell Foam Reactors Investigated Using CFD Simulations". In: *ChemEngineering* 4.4, p. 61. DOI: 10.3390/chemengineering4040061.

Sinn, Christoph et al. (2021a). "Heat Transport in Open-Cell Foams: CFD Analysis of Artificial Heat Sources vs Fully Resolved Exothermal Reactions". In: *Industrial and Engineering Chemistry Research* 60, pp. 4542–4551. DOI: 10.1021/acs.iecr.0c05982.

Sinn, Christoph et al. (2021b). "Structure-heat transport analysis of periodic open-cell foams to be used as catalyst carriers". In: *Chemical Engineering Research and Design* 166, pp. 209–219. DOI: 10.1016/j.cherd.2020.12.007.

Skibinski, Jakub et al. (2015). "The influence of pore size variation on the pressure drop in open-cell foams". In: *Materials and Design* 87, pp. 650–655. DOI: 10.1016/j.matdes.2015.08.079.

Sommers, A. et al. (2010). "Ceramics and ceramic matrix composites for heat exchangers in advanced thermal systems-A review". In: *Applied Thermal Engineering* 30.11-12, pp. 1277–1291. DOI: 10.1016/j.applthermaleng.2010.02.018.

Stiegler, Thomas et al. (2019). "Development of a Structured Reactor System for CO2 Methanation under Dynamic Operating Conditions". In: *Energy Technology* 7.6, p. 1900047. DOI: 10.1002/ente.201900047.

Taslicukur, Z., C. Balaban, and N. Kuskonmaz (2007). "Production of ceramic foam filters for molten metal filtration using expanded polystyrene". In: *Journal of the European Ceramic Society* 27.2-3, pp. 637–640. DOI: 10.1016/j.jeurceramsoc.2006.04.129.

Theurich, Steffi, Stefan Rönsch, and Robert Güttel (2020). "Transient Flow Rate Ramps for Methanation of Carbon Dioxide in an Adiabatic Fixed-Bed Recycle Reactor". In: *Energy Technology* 8.3, p. 1901116. DOI: 10.1002/ente.201901116.

Tronconi, Enrico, Gianpiero Groppi, and Carlo Giorgio Visconti (2014). "Structured catalysts for non-adiabatic applications". In: *Current Opinion in Chemical Engineering* 5, pp. 55–67. DOI: 10.1016/j.coche.2014.04.003.

Türks, Daniel et al. (2017). "Methanation of CO2 on Ni/Al2O3 in a structured fixed-bed reactor—A scale-up study". In: *Catalysts* 7.5, p. 152. DOI: 10.3390/catal7050152.

Twigg, Martyn V. and James T. Richardson (2007). "Fundamentals and applications of structured ceramic foam catalysts". In: *Industrial and Engineering Chemistry Research* 46.12, pp. 4166–4177. DOI: 10.1021/ie061122o.

Versteeg, H. K. and W. Malasekera (2007). *An Introduction to Computational Fluid Dynamics: The Finite Volume Method*. 2nd. Harlow, England: Pearson Education Ltd.

Vogt, Charlotte et al. (2019). "The renaissance of the Sabatier reaction and its applications on Earth and in space". In: *Nature Catalysis* 2.3, pp. 188–197. DOI: 10.1038/s41929-019-0244-4.

Von Beyer, Markus (2019). "Hydrodynamische Charakterisierung der Mehrphasenströmung in additiv gefertigten periodisch offenzelligen Strukturen : Optionen zur Prozessintensivierung in einer Hydrodesulfurierungsanlage". PhD thesis. Friedrich-Alexander-University Erlangen-Nuremberg.

Wallenstein, M., M. Kind, and B. Dietrich (2014). "Radial two-phase thermal conductivity and wall heat transfer coefficient of ceramic sponges - Experimental results and correlation". In: *International Journal of Heat and Mass Transfer* 79, pp. 486–495. DOI: 10.1016/j.ijheatmasstransfer.2014.08.003.

Wan, Tan et al. (2021). "Fabrication, properties, and applications of open-cell aluminum foams: A review". In: *Journal of Materials Science and Technology* 62, pp. 11–24. DOI: 10.1016/j.jmst.2020.05.039.

Wehinger, Gregor D. (2016). "Particle-resolved CFD simulations of catalytic flowreactors". PhD thesis. Technical University of Berlin.

— (2019). "Radiation Matters in Fixed-Bed CFD Simulations". In: *Chemie-Ingenieur-Technik* 91.5, pp. 583–591. DOI: 10.1002/cite.201800179.

Wehinger, Gregor D. and Steffen Flaischlen (2019). "Computational Fluid Dynamics Modeling of Radiation in a Steam Methane Reforming Fixed-Bed Reactor". In: *Industrial and Engineering Chemistry Research* 58.31, pp. 14410–14423. DOI: 10.1021/acs.iecr.9b01265.

Wehinger, Gregor D., Helge Heitmann, and Matthias Kraume (2016). "An artificial structure modeler for 3D CFD simulations of catalytic foams". In: *Chemical Engineering Journal* 284, pp. 543–556. DOI: 10.1016/j.cej.2015.09.014.

Wehinger, Gregor D., Felix Klippel, and Matthias Kraume (2017). "Modeling pore processes for particle-resolved CFD simulations of catalytic fixed-bed reactors". In: *Computers and Chemical Engineering* 101, pp. 11–22. DOI: 10.1016/j.compchemeng.2017.02.029.

Wehinger, Gregor D. and Matthias Kraume (2017). "CFD as a Design Tool for Fixed-Bed Reactors with Small Tube-to-Pellet Diameter Ratio: Now or in the Future?" In: *Chemie-Ingenieur-Technik* 89.4, pp. 447–453. DOI: 10.1002/cite.201600155.

Wehinger, Gregor D. et al. (2019). "Modeling fixed-bed reactors from metal-foam pellets with detailed CFD". In: *Chemical Engineering Journal* 373, pp. 709–719. DOI: 10.1016/j.cej.2019.05.067.

Weller, H. G. et al. (1998). "A tensorial approach to computational continuum mechanics using object-oriented techniques". In: *Computers in Physics* 12.6, p. 620. DOI: 10.1063/1.168744.

Wolf, Torsten et al. (2020). "Periodic Open Cellular Raney-Copper Catalysts Fabricated via Selective Electron Beam Melting". In: *Advanced Engineering Materials* 22.5, p. 1901524. DOI: 10.1002/adem.201901524.

Woudberg, S. and J. P. Du Plessis (2016). "An analytical Ergun-type equation for porous foams". In: *Chemical Engineering Science* 148, pp. 44–54. DOI: 10.1016/j.ces.2016.03.013.

Wu, Zhiyong and Zhifeng Wang (2013). "Fully coupled transient modeling of ceramic foam volumetric solar air receiver". In: *Solar Energy* 89, pp. 122–133. DOI: 10.1016/j.solener.2012.12.016.

Wu, Zhiyong et al. (2011). "Numerical simulation of convective heat transfer between air flow and ceramic foams to optimise volumetric solar air receiver performances". In: *International Journal of Heat and Mass Transfer* 54.7-8, pp. 1527–1537. DOI: 10.1016/j.ijheatmasstransfer.2010.11.037.

Xu, Weigang et al. (2008). "Numerical investigation on the flow characteristics and permeability of three-dimensional reticulated foam materials". In: *Chemical Engineering Journal* 140.1-3, pp. 562–569. DOI: 10.1016/j.cej.2007.12.010.

Zafari, Mohammad et al. (2015). "Microtomography-based numerical simulation of fluid flow and heat transfer in open cell metal foams". In: *Applied Thermal Engineering* 80, pp. 347–354. DOI: 10.1016/j.applthermaleng.2015.01.045.

Zhang, Wei et al. (2020). "Computational fluid dynamics simulation of CO2 methanation in a shell-and-tube reactor with multi-region conjugate heat transfer". In: *Chemical Engineering Science* 211, p. 115276. DOI: 10.1016/j.ces.2019.115276.

Zhang, Xiaojin et al. (2017). "Life Cycle Assessment of Power-to-Gas: Approaches, system variations and their environmental implications". In: *Applied Energy* 190, pp. 326–338. DOI: 10.1016/j.apenergy.2016.12.098.

Zhou, Xintong and Chang Jun Liu (2017). "Three-dimensional Printing for Catalytic Applications: Current Status and Perspectives". In: *Advanced Functional Materials* 27.30, p. 1701134. DOI: 10.1002/adfm.201701134.

List of Symbols

Roman

A_k	:	pre-exponential factor of reaktion k, $\mathrm{m\,mol^{-1}\,s^{-1}}$
C_h	:	coefficient for Nusselt correlations, -
C_m	:	coefficient for Sherwood correlations, -
$c_i/c_\mathrm{f}/c_\mathrm{s}$	:	concentration of species i/fluid/solid, $\mathrm{mol\,m^{-3}}$
$c_{\mathrm{p},i}/c_{\mathrm{p,f}}/c_{\mathrm{p,s}}$	:	isobaric heat capacity of species i/ fluid/ solid, $\mathrm{W\,kg^{-1}\,K^{-1}}$
d_c	:	cell diameter, m
d_s	:	strut diameter, m
d_w	:	window diameter, m
d_h	:	hydraulic diameter, m
d_p	:	particle diameter of fixed bed, m
d_char	:	characteristic diameter, m
D	:	diffusion coefficient, $\mathrm{m^2\,s^{-1}}$
$D_{j,i}$	:	binary diffusion coefficient of species j and i, $\mathrm{m^2\,s^{-1}}$
$D_{i,\mathrm{m}}$	:	mixture averaged diffusion coefficient of species i, $\mathrm{m^2\,s^{-1}}$
D_ganc	:	characteristic length for model of Gancarczyk et al., m
E_{a_k}	:	activation energy of reaction k, $\mathrm{J\,mol^{-1}}$
$F_\mathrm{cat/geo}$	:	ratio of catalytic surface to geometrical surface, -
$h_i/h_\mathrm{f}/h_\mathrm{s}$	:	specific enthalpy of species i/fluid/solid, $\mathrm{J\,kg^{-1}}$
h_i^0	:	standard enthalpy of formation of species i, $\mathrm{J\,kg^{-1}}$
I	:	specific radiant intensity, $\mathrm{W\,m^{-2}\,sr^{-1}}$
I_b	:	black body intensity, $\mathrm{W\,m^{-2}\,sr^{-1}}$
$\vec{j}_i$	:	diffusion mass flux vector, $\mathrm{kg\,m^{-2}\,s^{-1}}$
$\vec{j}_q$	:	diffusive energy flux vector, $\mathrm{J\,g\,m^{-2}\,s^{-1}}$
k_k	:	rate constant of reaction k, $\mathrm{s^{-1}}$
k_1	:	permeability coefficient, $\mathrm{m^2}$
k_2	:	Forchheimer coefficient, m
L	:	foam length, m
l_ganc	:	characteristic length for model of Gancarczyk et al., m
M_i	:	molar mass of species i, $\mathrm{kg\,mol^{-1}}$
m	:	exponent for Nusselt correlation, -
M	:	exponent for Sherwood correlation, -
$\vec{n}$	:	normal vector, -
n	:	amount of substance, mol
N_s	:	number of species, -
p	:	pressure, Pa
p_0	:	outlet pressure, Pa
Q	:	heat flow, W
$\dot{q}$	:	specific heat flow, $\mathrm{W\,m^{-2}}$
r	:	position vector, -
R	:	universal gas constant, $8.314\,\mathrm{J\,K^{-1}\,mol^{-1}}$

R_i^{het} : net reaction rate due to heterogeneous reactions of species i, $\mathrm{kg\,m^{-2}\,s^{-1}}$
R_{s} : number of reactions, -
$\dot{s}_i$: surface reaction rate of species i, $\mathrm{mol\,m^{-2}\,s^{-1}}$
S : direction vector, -
S_i : sticking coefficient, -
S_i^0 : initial sticking coefficient, -
S_{v} : specific surface area, $\mathrm{m^{-1}}$
S_{spec} : specific heat source, $\mathrm{W\,m^{-3}}$
S : total heat source, W
t : time, s
t_{sol} : solution time, h
T : temperature, K
T_{in} : inlet temperature, K
T_{f} : fluid temperature, K
T_{s} : solid temperature, K
T_{ref} : reference temperature, K
T_{wall} : wall temperature, K
u : velocity, $\mathrm{m\,s^{-1}}$
v : superficial velocity, $\mathrm{m\,s^{-1}}$
V : volume, $\mathrm{m^3}$
X_i : mole fraction, -
Y_i : mass fraction, -

Greek

α : heat transfer coefficient, $\mathrm{W\,K^{-1}\,m^{-2}}$
α_{ray} : degree of adsorption, -
β_k : temperature exponent in reaction k, -
β : mass transfer coefficient, $\mathrm{m\,s^{-1}}$
γ_{ray} : degree of reflection, -
Γ : surface site density, $\mathrm{mol\,m^{-2}}$
$\Delta_{\text{R}}H^0$: reaction enthalpy, $\mathrm{kJ\,mol^{-1}}$
ε_{o} : open porosity, -
ε_{h} : hydraulic porosity, -
ε_{t} : total porosity, -
ε_{ray} : surface emissivity, -
ε_{i_k} : activation energy adjustment of species i in reaction k, $\mathrm{J\,mol^{-1}}$
κ : adsorption coefficient, $\mathrm{m^{-1}}$
η : effectiveness factor, -
ϕ : arbitrary quantity in conservation equations, -
θ_i : surface coverage of species i, -
λ_{f} : fluid thermal conductivity, $\mathrm{W\,m^{-1}\,K}$
λ_{s} : solid thermal conductivity, $\mathrm{W\,m^{-1}\,K}$
$\lambda^{(\text{eff})}$: effective thermal conductivity, $\mathrm{W\,m^{-1}\,K}$
$\lambda_{\text{ax}}^{(\text{eff})}$: axial effective thermal conductivity, $\mathrm{W\,m^{-1}\,K}$
$\lambda_{\text{r}}^{(\text{eff})}$: radial effective thermal conductivity, $\mathrm{W\,m^{-1}\,K}$
$\lambda_{\text{stg}}^{(\text{eff})}$: stagnant effective thermal conductivity, $\mathrm{W\,m^{-1}\,K}$
$\lambda_{\text{disp,ax}}^{(\text{eff})}$: axial dispersive effective thermal conductivity, $\mathrm{W\,m^{-1}\,K}$
$\lambda_{\text{disp,r}}^{(\text{eff})}$: radial dispersive effective thermal conductivity, $\mathrm{W\,m^{-1}\,K}$
$\lambda_{\text{cond}}^{(\text{eff})}$: conductive effective thermal conductivity, $\mathrm{W\,m^{-1}\,K}$

$\lambda_{\mathrm{rad}}^{(\mathrm{eff})}$	:	radiativeeffective thermal conductivity, $\mathrm{W\,m^{-1}\,K}$
μ_{f}	:	dynamic viscosity of the fluid, $\mathrm{Pa\,s}$
μ_{i_k}	:	reaction order adjustment of species i in reaction k, -
ν_i'	:	stoichiometric coefficient of reactant i, -
$\nu_{i,k}$	:	stoichiometric coefficient of species i in reaction k, -
$\rho/\rho_{\mathrm{f}}/\rho_{\mathrm{s}}$	:	density/fluid density/ solid density, $\mathrm{kg\,m^{-3}}$
σ_i	:	coordination number, -
σ	:	Stefan-Boltzmann constant, $5.67 \times 10^{-8}\,\mathrm{W\,m^{-2}\,K^{-4}}$
τ	:	stress tensor, Pa
τ_{ray}	:	degree of transmission, -
τ_{foam}	:	foam tortuosity, -

List of Student Works Included in this Thesis

- Jonas Wentrup, Master thesis 2019, University of Bremen, *CFD simulation of CO oxidation in open cell foams. Fully resolved exothermic reactions vs. artificial heat sources*
- Felix Kranz, Bachelor thesis 2020, University of Bremen, *Radiation Modeling in Porous Open-Cell Structures via Computational Fluid Dynamics*
- Manuela Romero, Master thesis, 2020 University of Bremen, *Numerical Investigation of Heat Transport in Tubular Reactors: Effect of Contact Area Between Catalytic Foam Segments*

Contribution to Publications

article	concept	modeling/ simulations	visualization/ writing	review/ editing	supervision
Sinn et al., 2019	CS;GP; JT;LK	CS	CS	GP;JT; LK	GP;JT; LK
Sinn et al., 2020a	CS;FK; JW;GP; GW;JT	CS;FK; JW;GW	CS;FK JT	GW;GP;	GP;JT
Sinn et al., 2020b	CS;JW; GP;JT	CS	CS;JW	GP;JT	GP;JT
Sinn et al., 2021b	CS;JW; GP;JT; LK	CS;JW; LK	CS;JW; LK	GP;JT; LK	GP;JT; LK
Sinn et al., 2021a	CS;JW; GP;JT	CS;JW	CS;JW	GP;JT	GP;JT

Abbreviations: CS: Christoph Sinn; LK: Dr.-Ing. Lars Kiewidt; JW: Jonas Wentrup; GP: Dr.-Ing. Georg R. Pesch; FK: Felix Kranz; GW: Prof. Dr.-Ing. Gregor D. Wehinger; JT: Prof. Dr.-Ing. Jorg Thöming.

Colophon

This LaTeX template was downloaded from:
http://www.LaTeXTemplates.com
It is based on a template by:
Steve Gunn (http://users.ecs.soton.ac.uk/srg/softwaretools/document/templates/)
and
Sunil Patel (http://www.sunilpatel.co.uk/thesis-template/).